

**Biochemical and functional characterization of the Pch2/ORC
AAA⁺ assembly in controlling meiotic DNA break formation**

Inaugural-Dissertation
zur
Erlangung des Doktorgrades
Dr. rer. nat.

der Fakultät für Biologie
an der
Universität Duisburg-Essen

vorgelegt von
María Ascensión Villar Fernández
aus Sevilla, Spanien

durchgeführt am
Max-Planck-Institut für molekulare Physiologie
Abteilung für mechanistische Zellbiologie

Dezember 2019

Die der vorliegenden Arbeit zugrunde liegenden Experimente wurden am Max-Planck-Institut für molekulare Physiologie in der Abteilung für mechanistische Zellbiologie durchgeführt.

1. Gutachter: Prof. Dr. Andrea Musacchio

2. Gutachter: Prof. Dr. Dominik Boos

Vorsitzender des Prüfungsausschusses: Prof. Dr. Stefan Westermann

Tag der mündlichen Prüfung: 25. Februar 2020

DuEPublico

Duisburg-Essen Publications online

UNIVERSITÄT
DUISBURG
ESSEN

Offen im Denken

ub | universitäts
bibliothek

Diese Dissertation wird über DuEPublico, dem Dokumenten- und Publikationsserver der Universität Duisburg-Essen, zur Verfügung gestellt und liegt auch als Print-Version vor.

DOI: 10.17185/duepublico/72234

URN: urn:nbn:de:hbz:464-20200722-140752-1

Alle Rechte vorbehalten.

Im Zuge dieser Doktorarbeit wurde der folgende Artikel veröffentlicht:

(In the context of this doctoral work, the following article was published:)

María Ascensión Villar-Fernández, Richard Cardoso da Silva, Dongqing Pan, Elisabeth Weir, Annika Sarembe, Vivek B. Raina, John R. Weir, Gerben Vader. (2019). **A meiosis-specific AAA⁺ assembly reveals repurposing of ORC during budding yeast gametogenesis.** *BioRxiv*, doi: <https://doi.org/10.1101/598128>

Content

List of Figures	VIII
List of Tables	X
List of Abbreviations	XI
1 Introduction	1
1.1 An overview of meiosis	1
1.1.1 Meiotic cell cycle phases	7
1.1.1.1 G1 phase	7
1.1.1.2 S phase	9
1.1.1.3 G2/ Prophase I	11
1.1.1.4 Meiosis I	14
1.1.1.5 Meiosis II	16
1.1.2 Checkpoints	17
1.2 Meiotic recombination	20
1.2.1 DSB formation and inter-homolog repair	20
1.2.2 Non-random spatial distribution of DSBs across the genome	25
1.3 Repetitive elements of the DNA and heterochromatin: the ribosomal DNA (rDNA) as a model of repetitive DNA	29
1.3.1 Repetitive DNA and principles of heterochromatin formation	29
1.3.2 Ribosomal DNA (rDNA)	33
1.3.2.1 Structure, function and silencing of the rDNA	33
1.3.2.2 The integrity of the rDNA and rDNA amplification system	36
1.4 AAA⁺ ATPases	38
1.4.1 Pch2 as a master regulator in meiosis and mitosis	43
1.4.1.1 Pch2 in meiotic G2/prophase.....	43
1.4.1.2 Pch2 ^{TRIP13} in the mitotic checkpoint	52
1.4.2 ORC	54
1.4.2.1 Structural organization of the ORC subunits.....	55
1.4.2.2 ORC in DNA replication	58
1.4.2.2.1 Main principles of ORC as an initiator of DNA replication.....	58
1.4.2.2.2 Origins of replication and insights on ORC structure.	59
1.4.2.2.3 Mechanism of the eukaryotic DNA replication: MCM loading and MCM activation	62
1.4.2.2.4 Control of DNA replication	65
1.4.2.2.5 Role of the chromatin structure in ORC association with origins of replication	67
1.4.2.2.6 Pre-meiotic replication	70
1.4.2.3 Other functions of ORC	71
1.5 Objectives	73

2	Material and Methods	75
2.1	Materials	75
2.1.1	Chemicals and reagents	75
2.1.2	Enzymes and commercial mixes	78
2.1.3	Commercial kits.....	78
2.1.4	Antibiotics	79
2.1.5	Antibodies	79
2.1.6	Buffers and solutions.....	80
2.1.7	Media	83
2.1.8	Synthetic oligonucleotides.....	84
2.1.9	Plasmids.....	85
2.1.10	Competent cells.....	85
2.1.11	Yeast strains.....	85
2.1.12	Laboratory instruments and devices	85
2.1.13	Online tools	89
2.1.14	Software.....	89
2.2	Methods.....	90
2.2.1	Growth and maintenance of <i>Saccharomyces cerevisiae</i>	90
2.2.1.1	Growth conditions of yeast strains	90
2.2.1.2	Meiotic cell cycle synchronization	90
2.2.1.3	Yeast stock maintenance.....	91
2.2.2	Construction of yeast strains.....	91
2.2.2.1	Yeast transformation.....	91
2.2.2.2	Creation of diploid yeast strains	93
2.2.2.3	Sporulation of diploid cells.....	93
2.2.2.4	Preparation and dissection of tetrads	94
2.2.2.5	Determination of phenotype by replica plating	94
2.2.2.6	Determination of mating type.....	95
2.2.3	Yeast two-hybrid system.....	95
2.2.4	Cloning and methods of DNA analysis (Molecular biology methods)..	96
2.2.4.1	Polymerase Chain Reaction (PCR).....	96
2.2.4.2	Cloning using restriction enzymes	98
2.2.4.2.1	Agarose gel electrophoresis	98
2.2.4.2.2	Restriction digestion	99
2.2.4.2.3	DNA extraction and purification.....	99
2.2.4.2.4	Ligation	100
2.2.4.3	Restriction free cloning (Gibson assembly)	100
2.2.4.4	biGBac method	101
2.2.4.5	Site-directed mutagenesis	103
2.2.4.6	Transformation of chemically competent bacterial cells.....	103
2.2.4.7	Isolation of plasmids from bacterial cells.....	104
2.2.4.8	Determination of DNA concentration	104
2.2.4.9	Sequencing.....	104
2.2.4.10	Real time quantitative PCR (qPCR)	105

2.2.4.11	Genomic DNA preparation from yeast for PCR-base genotyping	106
2.2.4.12	Southern Blot	106
2.2.4.12.1	Genomic DNA extraction from meiotic yeast cells ..	107
2.2.4.12.2	Digestion of genomic DNA	108
2.2.4.12.3	Gel electrophoresis	108
2.2.4.12.4	Southern blotting	109
2.2.4.12.5	Probe labelling	110
2.2.4.12.6	Hybridization and washing	110
2.2.4.12.7	Detection by phosphorimaging	111
2.2.4.13	Flow cytometry	111
2.2.5	Methods of protein analysis.....	112
2.2.5.1	Yeast whole cell extract for Western Blot using trichloroacetic acid.....	112
2.2.5.2	Sodium dodecyl sulfate-polyacrylamide gel electrophoresis (SDS-PAGE)	112
2.2.5.3	Coomassie Brilliant Blue staining	113
2.2.5.4	Western Blot	114
2.2.5.5	<i>In vivo</i> Co-Immunoprecipitation.....	114
2.2.5.6	Chromatin immunoprecipitation.....	116
2.2.5.7	Mass spectrometry analysis of purified proteins	118
2.2.6	Expression and purification of recombinant proteins	118
2.2.6.1	Protein expression and purification from bacterial cells	119
2.2.6.1.1	Purification of His-Hop1	119
2.2.6.1.2	Purification of GST-BAH-Orc1	121
2.2.6.1.3	Purification of Flag-Cdc6.....	122
2.2.6.2	Protein purification from yeast cells (CBP-ORC).....	123
2.2.6.3	Protein expression and purification from insect cells.....	124
2.2.6.3.1	Generation of baculovirus and protein expression test in insect cells	124
2.2.6.3.2	Protein purification from insect cells	126
2.2.6.3.2.1	Purification of His-MBP-Pch2 and truncations ...	126
2.2.6.3.2.2	Purification of His-ORC and His- Δ BAH-ORC ...	128
2.2.7	Analytical ultracentrifugation (AUC)	129
2.2.8	Protein quantification methods.....	129
2.2.9	Protein-protein interaction methods	130
2.2.9.1	<i>In vitro</i> pull-down assay	130
2.2.9.2	Analytical size exclusion chromatography (SEC) migration shift assay.....	132
2.2.9.3	Cross-linking mass-spectrometry (XL-MS)	133
3	Results	136
3.1	Pch2 interacts with the ORC complex in meiotic G2/ prophase.....	137
3.1.1	Pch2 interacts with Orc1 in a manner consistent with a stereotypical AAA+: client and/ or adaptor interaction.....	137
3.1.2	Pch2 interacts with the entire ORC in meiotic G2/ prophase.....	139

3.1.3	Pch2-Orc1 function and interaction is independent of DNA replication and Cdc6.....	141
3.2	<i>In vitro</i> reconstitution demonstrates a direct interaction between Pch2 and ORC.....	144
3.2.1	Optimization of Pch2 expression and purification.....	144
3.2.2	Characterization and validation of Pch2 functionality.....	148
3.2.3	Optimization of protein expression and purification of ORC.....	151
3.2.4	Pch2 interacts directly with ORC <i>in vitro</i>	154
3.3	<i>In vitro</i> cross-linking mass-spectrometry (XL-MS) characterization of Pch2-ORC.....	156
3.4	Biochemical delineation of the Pch2-ORC complex formation	162
3.4.1	The NH ₂ -terminal domain (NTD) of Pch2 is necessary for ORC-binding.....	163
3.4.2	Functional dissection of Pch2 interaction with ORC.....	167
3.4.3	Point mutations in the NTD of Pch2 disrupt ORC-binding.....	170
3.5	<i>In vivo</i> analysis of the functional connection between Pch2/ ORC.....	174
3.5.1	Functional depletion of Orc2 and Orc5.....	175
3.5.2	rDNA-associated function of Pch2 is likely independent of Orc2/ Orc5 function.....	177
3.5.3	Orc1 is a central mediator of the interaction between ORC-Pch2	181
3.5.4	Implication of the BAH domain of Orc1 in Pch2/ ORC interaction ..	183
4	Discussion.....	188
4.1	Pch2 interaction with Orc1 is analogous to stereotypical AAA ⁺ ATPases association	189
4.2	Interaction between Orc1 (ORC) and Pch2.....	191
4.2.1	The entire ORC is involved in the interaction with Pch2 <i>in vivo</i>	191
4.2.2	Interaction of Pch2 with ORC is independent of Cdc6.....	192
4.2.3	The interaction between Pch2 and ORC is direct	193
4.2.4	Insights gained through XL-MS suggest a role of Pch2-NTD in the interaction with ORC.....	197
4.3	Delineation of Pch2 reveals a minimum region sufficient for ORC binding. .	203
4.3.1	The NH ₂ -terminal domain (NTD) of Pch2 is necessary for ORC-binding.....	203
4.3.2	Functional dissection of the NTD of Pch2.....	208
4.3.3	Point mutations in the NTD of Pch2 disrupt ORC-binding.....	209
4.4	Orc1 has a prominent role in mediating interaction with Pch2.....	214
4.5	Orc2/Orc5 subunits are dispensable for Pch2-ORC mediated DSB protection at the rDNA.....	217
4.5.1	Efficient depletion of distinct ORC subunits	218
4.5.2	ORC might not need to associate with ARS sequences for its rDNA protective function.....	220
4.5.3	The BAH domain of Orc1 is not necessary for Pch2-ORC binding despite being required for Pch2-ORC functionality at the rDNA	228
5	Summary.....	234

6 Zusammenfassung.....	236
7 Appendices.....	238
8 Bibliography	255
Acknowledgements.....	281
Curriculum Vitae	283
Affidavit	284

List of Figures

Figure 1-1	An overview about the meiotic programme	2
Figure 1-2	Stepwise loss of cohesion in meiosis.....	6
Figure 1-3	Meiotic DSB formation and recombination in G2/prophase.....	13
Figure 1-4	The CO and NCO pathways for meiotic recombination	22
Figure 1-5	Tethered loop-axis model for DSB formation in <i>S. cerevisiae</i>	25
Figure 1-6	Meiotic DSB hotspot designation in <i>S. cerevisiae</i>	27
Figure 1-7	Schematic representation of rDNA structure and rDNA transcriptional silencing.....	35
Figure 1-8	Protection of the budding yeast rDNA against meiotic DSB formation	50
Figure 1-9	Domain organization of the ORC subunits.....	56
Figure 1-10	ORC drives the recruitment of the MCM replicative helicase to initiate DNA replication	66
Figure 3-1	<i>In vivo</i> characterization of Pch2-Orc1	138
Figure 3-2	Pch2 associates with the entire ORC in meiotic G2/prophase	140
Figure 3-3	Pch2-Orc1 function and interaction is independent of DNA replication and Cdc6.....	142
Figure 3-4	Purification strategy of His-MBP-Pch2.....	147
Figure 3-5	Validation of His-MBP-Pch2	149
Figure 3-6	Purification strategy of His-ORC	152
Figure 3-7	Pch2 interacts with ORC directly <i>in vitro</i>	154
Figure 3-8	Cross-linking mass-spectrometric (XL-MS) analysis of Pch2-ORC assembly	158
Figure 3-9	The NH ₂ -terminal domain (NTD) of Pch2 is required for ORC-binding and Pch2 rDNA-associated function	164
Figure 3-10	Dissection of the role of the NTD of Pch2 in ORC association.....	169
Figure 3-11	Point mutations in the NTD of Pch2 disrupt ORC-binding.....	172
Figure 3-12	Functional depletion of Orc2 and Orc5	177
Figure 3-13	rDNA-associated function of Pch2 is likely independent of Orc2/Orc5 function.....	179
Figure 3-14	Orc1 is a central mediator of the interaction between Pch2 and ORC.....	182
Figure 3-15	The BAH domain of Orc1 is not sufficient for Pch2 association.....	184

Figure 3-16	Implications of the BAH domain of Orc1 in Pch2/ORC interaction.....	186
Figure 4-1	<i>In vitro</i> characterization of the interaction between Pch2 and ORC	205
Figure 4-2	Delineation of the Pch2-ORC interaction in terms of rDNA-associated DSB formation.....	212
Figure 4-3	Simplified model of Pch2 and ORC function at the budding yeast ribosomal DNA (rDNA)	215
Figure 4-4	Pch2-ORC function at the rDNA does not necessitate ORC association to origins of replication.....	221
Figure 4-5	Model depicting the origin-independent function of Pch2-Orc1/ORC in local meiotic DSB control	232
Figure 7-1	Expression and purification of GST-tagged Pch2	238
Figure 7-2	Pch2 alignment of the NH ₂ -terminal domain	239
Figure 7-3	Pch2 alignment of the AAA ⁺ ATPase domain of Pch2	240
Figure 7-4	Expression tests of GST- and MBP-tagged Pch2 constructs.....	241
Figure 7-5	Expression test of ORC in insect cells.....	242
Figure 7-6	Biochemical characterization of recombinant Pch2 and ORC	243
Figure 7-7	Tagging of Pch2 with TAP-tag leads to impairment of Pch2 function	244
Figure 7-8	Cross-links identified by XL-MS.	245

List of Tables

Table 2-1	Chemicals and reagents	75
Table 2-2	Enzymes and commercial mixes	78
Table 2-3	Commercial kits.....	79
Table 2-4	Antibiotics.....	79
Table 2-5	Primary antibodies	79
Table 2-6	HRP-conjugated antibodies	80
Table 2-7	Buffers and solutions	80
Table 2-8	Media	84
Table 2-9	Laboratory instruments and devices	86
Table 2-10	Online tools.....	89
Table 2-11	Software.....	89
Table 2-12	Standard composition of a 20 μ L PCR reaction using Taq polymerase.....	97
Table 2-13	Standard composition of a 50 μ L PCR reaction using Q5 polymerase	97
Table 2-14	Standard program for PCR amplification.....	97
Table 2-15	Standard composition for 10 μ L ligation reaction.....	100
Table 2-16	PCR reactions for step-1 assembly of ORC into pBIG1 vectors.....	102
Table 2-17	Composition of a 20 μ L qPCR reaction	106
Table 2-18	qPCR thermocycler program	106
Table 2-19	Composition of SDS-polyacrilamide gels used in this study. Volume (mL) of components required to cast two 1.5 mm gels are shown	113
Table 7-1	Mass spectrometry analysis of purified Pch2 and ORC	246
Table 7-2	Cross-links identified by XL-MS of Pch2-ORC	246
Table 7-3	Cross-links identified by XL-MS analysed by MeroX.....	246
Table 7-4	Comparative analysis of the intra- and inter-ORC cross-links.....	246
Table 7-5	Oligonucleotides used for cloning.....	246
Table 7-6	Oligonucleotides used for the ORC assembly into pLIB vectors (biGBac system).....	247
Table 7-7	Oligonucleotides used for ChIP-qPCR.....	247
Table 7-8	Plasmids used for yeast transformation and protein expression.....	247
Table 7-9	Yeast strains used in this PhD thesis	248

List of Abbreviations

aa	amino acid
AAA+ ATPases	ATPases associated with diverse cellular activities
ABC	Ammonium bicarbonate
Abf1	ARS binding factor 1
ACS	ARS consensus sequence
AD	Activation domain
AGC	Automated gain control
APC/C	Anaphase promoting complex/cyclosome
APS	Ammonium perosulfate
ARS	Autonomous replication sequence
Asn	Asparagine
ATP	Adenosine triphosphate
ATP γ s	Adenosine 5'-[γ -thio]triphosphate
AU	Arbitrary unit
BAH	Bromo-adjacent homology
BD	Binding domain
bp	Base pair
BS3	Bis-sulfosuccinimidyl suberate
BSA	Bovine serum albumin
BYTA medium	Buffered YTA medium
C-Mad2	Closed Mad2
<i>C. elegans</i>	<i>Caenorhabditis elegans</i>
Cam	Chloramphenicol
CBB	Coomassie Blue Staining
CBP	Calmodulin binding peptide
CDKs	Cyclin-dependent kinases
cDNA	Coding DNA
ChIP	Chromatin immunoprecipitation
CL	Clear lysate
Clb	B cyclin
Cln	G1 cyclin
CMG	Cdc45, MCM, GINS

CO	Crossover
Co-IP	Co-immunoprecipitation
CTD	Carboxy-terminal domain
CV	Column Volume
DDK	Dbf4-dependent kinase
DH	Double hexamer
dHJ	double Holliday junction
DMSO	Dimethyl sulfoxide
DSB	DNA double-strand break
DSBU	Disuccinimidyl dibutyric urea
dsDNA	Double-stranded DNA
DTT	Dithiothreitol
DUE	DNA unwinding element
ERCs	Extrachromosomal rDNA circles
FACS	Fluorescence-activated cell sorting
FBS	Fetal bovine serum
FDR	False discovery rate
FKBP12	FK506-binding-protein
FL	Full-length
FRB domain	FKBP12-rapamycin-binding domain
G1 phase	Gap1 phase
G2 phase	Gap2 phase
G418	Geneticin
GECs	Gene expression cassettes
GSH	Glutathione
GST	Glutathione S-transferase
h	hour
HDAC	Histone deacetylase
His	Histidine
HP1	Heterochromatin protein 1
HR	Homologous recombination
HRP	horseradish peroxidase
HTH	Helix-turn-helix
IF	Immunofluorescence

IGS	intergenic spaces
IH bias	Inter-homolog bias
Ime1	Initiator of meiosis 1
IPTG	Isopropyl β - d-1-thiogalactopyranoside
IRB buffer	Isothermal reaction buffer
IS	Intersister
IS repair	Inter-sister repair
ISM	Initiation-specific motif
IT	Injection time
IVS	Intervening sequence
Kan	Kanamycin
kb	kilobase
kDa	kilo Dalton
LB	Luria-Bertani
LN2	Liquid nitrogen
LTR	Long terminal repeat
M phase	Mitosis phase
<i>M. musculus</i>	<i>Mus musculus</i>
MBP	Maltose-binding protein
MCC	Mitotic checkpoint complex
MCM	Minichromosome maintenance
meiS	pre-meiotic S phase
MGF	Mascot generic files
min	minute
MIN plates	Minimal plates
MRX complex	Mre11-Rad50-Xsr2 complex
MS	Mass spectrometry
MWCO	Molecular weight cut-off
NAHR	Non-allelic homologous recombination
NCO	Non-crossover
NDRs	Nucleosome-depleted regions
NFR	Nucleosome free region
NLS	Nuclear localization signal
NoLS	Nucleolar localization signal

NORs	nucleolar organizer regions
NSF	N-ethyl maleimide sensitive factor
NTD	NH2 terminal domain
NTP	Nucleoside triphosphate
NTS	Nontranscribed spacer
O-Mad2	Open Mad2
OCCM complex	ORC-Cdc6-Cdct1-MCM complex
ORC	Origin Recognition Complex
Orc1-BP	Orc1-basic patch
PBS buffer	Phosphate-buffered saline
PBS-T	PBS-Tween
Pch2	Pachytene checkpoint 2
PCR	Polymerase chain reaction
PEG	Polyethylene glycol
pLIB vector	(Plasmid) library vector
PLK	Polo-like kinase
PMSF	Phenylmethylsulfonyl fluoride
PP2A	Protein phosphatase 2A
pre-RC	pre-Replicative complex
qPCR	real time quantitative PCR
rDNA	Ribosomal DNA
RENT	Regulator of nucleolar silencing and telophase
RFB	Replication fork block
RMM complex	Rec114-Mei4-Mer2 complex
RPA	replication protein A
rpm	Revolutions per minute
S phase	Synthesis phase
S-I motif	Sensor 1 motif
S-II motif	Sensor 2 motif
<i>S. cerevisiae</i>	<i>Sacharomyces cerevisiae</i>
SAC	Spindle assembly checkpoint
SC	Synaptonemal complex
SDS	Sodium dodecyl sulfate
SDS-PAGE	Sodium dodecyl sulfate–polyacrylamide gel electrophoresis

SDSA	Synthesis-dependent strand annealing
SE	Sedimentation equilibrium
SEC	Size-exclusion chromatography
SEC-MALS	SEC coupled to multiangle light scattering
Ser	Serine
Sf9	<i>Spodoptera frugiperda</i>
Sgo1	Shugoshin
SIR	Silent information regulator
SMC	Structural Maintenance of Chromosomes
SNAP	Soluble NSF attachment protein
SPB	Spindle pole body
SPO	Sporulation media
SRH	Second region of homology
SSC buffer	Saline-sodium citrate
ssDNA	single stranded DNA
SV-AUC	Sedimentation velocity analytical ultracentrifugation
TCA	Trichloroacetic acid
TCEP	tris(2-carboxyethyl)phosphine
TE	Tris EDTA
TFIIB	Transcription factor IIB
Thr	Threonine
Tnao38 cells	<i>Trichoplusia ni</i> cells
tRNA	Transfer ribonucleic acid
URS	Upstream Regulatory Sequence
USCE	Unequal sister chromatid exchange
WCE	Whole-cell extract
WHD	Winged-helix domain
WT	Wild-type
XL-MS	Cross-linking mass-spectrometry
Y2H	Yeast two-hybrid
YPD	Yeast extract peptone dextrose
YPG	Yeast extract peptone glycerol
YTA medium	Yeast extract, tryptone, potassium acetate/phthalate medium

1 Introduction

Meiosis constitutes the basis of sexual reproduction in eukaryotic organisms. The meiotic programme is a specialized cell division process whose main hallmark is that it enables a diploid progenitor cell to give rise to haploid daughter cells (*i.e.* cells with half the ploidy of the progenitor cell). The final outcome of meiosis is the generation of reproductive cells, known as gametes, which in multicellular organisms are generally referred to as egg (female gamete) and sperm (male gamete), whereas in unicellular organisms are usually called spores. Upon the fusion of two gametes, proper ploidy is restored in the offspring. Therefore, meiosis enables the cell to reduce its genomic content by half, ensuring that ploidy remains stable from one generation to the following, thus avoiding the otherwise inevitable doubling of the genetic material upon fertilization (Hochwagen, 2008; Lee & Amon, 2001; Marston & Amon, 2004b; V. V. Subramanian & Hochwagen, 2014).

Errors that occur during meiosis can lead to deleterious events that can compromise genome integrity, such as aneuploidy, which consist on the presence of an abnormal number of chromosomes in the gametes. In humans, such errors are the basis of spontaneous abortion, congenital birth defects and several genomic diseases (Hassold & Hunt, 2001; Sasaki *et al.*, 2010).

1.1 An overview of meiosis

Meiosis is a modified version of the mitotic cell division cycle. The reduction in ploidy is an essential feature in sexually reproducing organisms and is achieved by coupling a single round of DNA replication (pre-meiotic synthesis (S) phase) to two consecutive chromosome segregation events (meiosis I and meiosis II). In meiosis I, homologous chromosomes (the nearly-identical chromosomes originating from the maternal and paternal organisms) segregate, whereas in meiosis II sister chromatids (the two copies of a single chromosome originated by DNA replication and joined together in a chromosomal region called centromere) segregate (Murakami & Keeney, 2014; Petronczki *et al.*, 2003) (Figure 1-1).

The existence of two successive rounds of cell division without an intervening DNA replication step requires several modifications of the mitotic programme, in which there is a single DNA replication step followed by a single chromosome segregation event, and which ultimately yields two daughter cells with the same chromosome complement (*i.e.* the same

ploidy) as the progenitor cell. Although the basic mechanisms and proteins involved in meiotic progression are conserved among different organisms, in this Ph.D. work we used the budding yeast *Saccharomyces cerevisiae* (*S. cerevisiae*) as a model organism, and we will, therefore, outline in the next sections the main characteristics of the meiotic programme of *S. cerevisiae*, unless otherwise indicated.

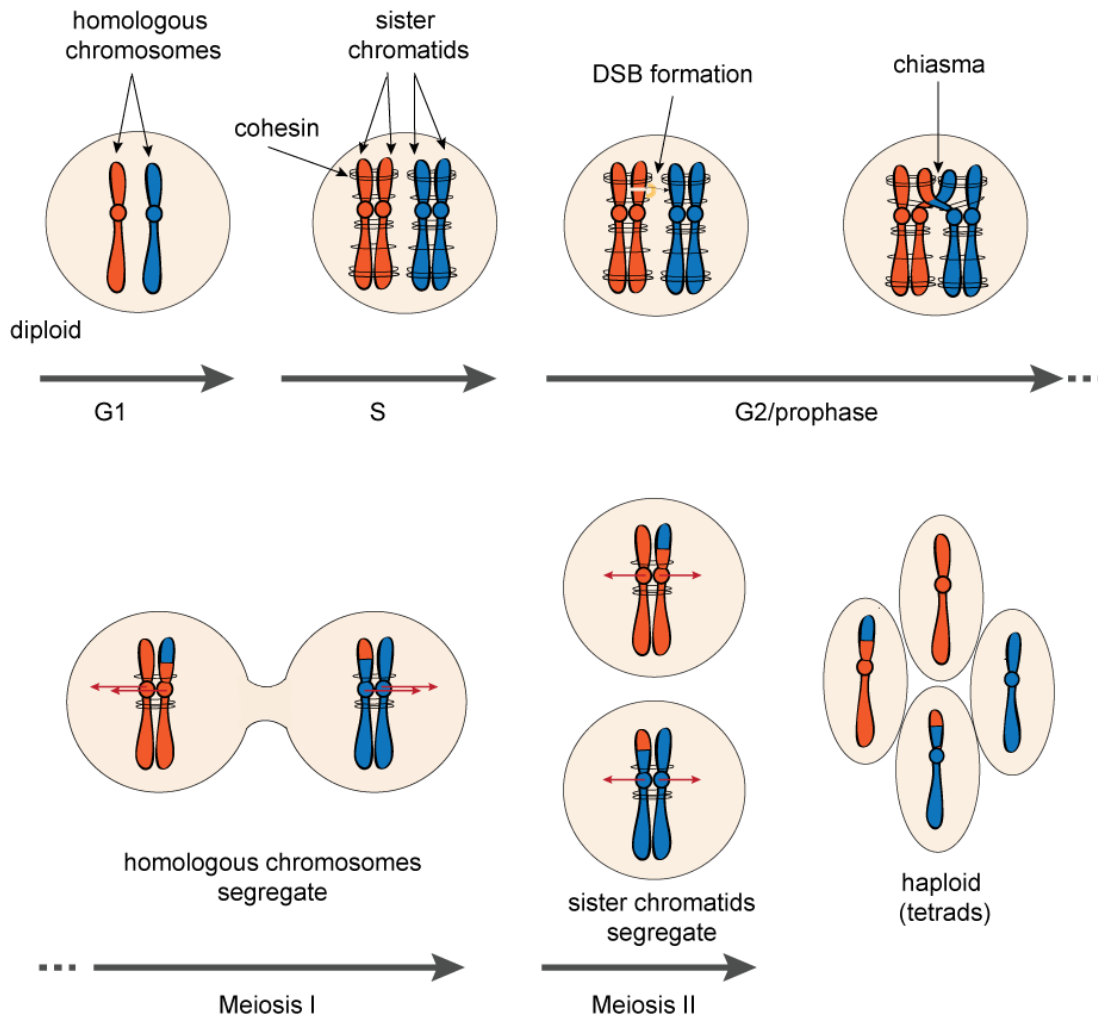


Figure 1-1 An overview about the meiotic programme

A diploid cell contains pairs of chromosomes that are nearly identical in their sequence composition, termed homologous chromosomes (represented in orange and blue). During pre-meiotic S phase (meiS), DNA is replicated. As a result, each homologous chromosome is composed of two identical copies, referred to as sister chromatids. Sister chromatids are linked via ring-shaped protein complexes named cohesin (represented as black rings). Following meiS phase, chromosomes undergo programmed introduction of DNA double-strand breaks (DSBs), depicted in yellow. DSBs repair via crossover recombination establishes linkages between homologous chromosomes (*i.e.* chiasma or chiasmata in plural) in G2/prophase. Chiasmata are essential to enable the proper segregation of chromosomes during meiosis. In the first meiotic division (meiosis I), pulling forces generated by the

Figure 1-1 (Continued)

spindle microtubules allow the segregation of homologous chromosomes (reductional segregation), whereas in the second meiotic division (meiosis II), sister chromatids segregate (equational segregation). Cohesin is removed along the chromosomal arms in meiosis I, but cohesin near the centromere (represented as orange/blue circles) remains associated until meiosis II. The final outcome of meiosis is four haploid, non-identical cells since the maternal and paternal homologous chromosomes have been “reshuffled”. G1: gap1; meiS: pre-meiotic S (synthesis) phase; G2: gap2. Red arrows indicate pulling forces generated by the spindle microtubules.

Budding yeast undergoes meiosis to produce four haploid cells termed spores. As mentioned above, the particular pattern of segregation in meiosis necessitates modifications of the segregation mechanisms that operate during mitosis. In this regard, it is first important to introduce a protein complex that is critical for both cell division programs, called cohesin. Cohesin is a four-member protein complex that functions as a “glue” and holds together sister chromatids of newly replicated chromosomes. This complex is composed of a heterodimer of the SMC (Structural Maintenance of Chromosomes) proteins Smc1 and Smc3 that associates with the non-SMC proteins Scc1 and Scc3. Since cohesin is required to maintain the attachment between sister chromatids, impairment of this complex causes precocious sister chromatid separation. In yeast, cohesin is loaded onto chromatin during DNA replication and in mitosis it remains bound until anaphase, when sister chromatids are separated (Hagstrom & Meyer, 2003; Michaelis *et al.*, 1997; Nasmyth & Haering, 2009). This separation of sister chromatids requires connections between the sister kinetochore (a multiprotein complex assembled at the centromere) and microtubules (long protein fibers that emanate from the centrosome and form a structure called spindle). The linkages between kinetochores and spindle microtubules are unstable unless the pulling forces of microtubules generate tension, which exclusively occurs when sister kinetochores are pulled in opposite directions. Sister chromatid cohesion is critical to maintain the linkage between sister chromatids and to position kinetochores in the correct orientation in the spindle. The meiotic programme presents some particularities with respect to the release of cohesin, outlined below, due to the fact that sister chromatids do not separate until the second meiotic division. Sister chromatid cohesion mostly serves to resist the tendency of microtubules to tear apart the bivalent and to create the tension needed to stabilize correct microtubule-kinetochore attachments (Hochwagen, 2008; Marston, 2014; Marston & Amon, 2004b).

The meiotic cell division incorporates mainly the following modifications of the mitotic cell cycle, further described below:

- 1) Programmed DNA break introduction and homologous meiotic recombination
- 2) Segregation of homologous chromosomes in meiosis I
- 3) Monopolar attachment of sister kinetochores
- 4) Stepwise loss of cohesion

First, homologous chromosomes need to establish physical linkages that enable their separation to opposite poles. Contrary to sister chromatids, which are held together by cohesin protein rings, such a priori connection does not exist in homologous chromosomes. As already mentioned, these physical connections are essential to establish tension on the spindle, so that chromosomes can properly be separated. Proper chromosome segregation in meiosis requires meiotic recombination, initiated by the active introduction of DNA double-strand breaks (DSBs) during meiotic G2/prophase by a conjunction of enzymes of which the endonuclease Spo11 is the catalytic core (see section 1.2 for further details). Subsequent DSB repair via homologous recombination (HR) provides a physical linkage between homologous chromosomes since HR enables the reciprocal DNA exchange between homologs. The mutual DNA exchange is referred to as crossover (CO), and COs mature into a structure known as chiasmata (chiasma in singular). Chiasmata hold chromosomes together and are a prerequisite for faithful meiotic chromosome segregation, and in the absence of meiotic recombination, homologs segregate randomly (Borde & de Massy, 2013; Keeney, 2001; Keeney *et al.*, 1997; Keeney & Neale, 2006; Lam & Keeney, 2015; Murakami & Keeney, 2014). The final outcome of the meiotic programme is four haploid cells that are genetically non-identical due to the exchange of genetic material during inter-homolog recombination (Lee & Amon, 2001; Marston & Amon, 2004b; Nasmyth, 2001). Concomitantly with crossover recombination, homologous chromosomes pair and become attached to a proteinaceous lattice known as synaptonemal complex (SC). Although the immediate role of HR is to facilitate the orientation of homologous chromosomes and their proper segregation in meiosis I, it also generates new allelic combinations, which increases diversity and in turn, can be beneficial for evolution. DSB formation and recombination are further explained in section 1.2.1.

A second key feature of the meiotic division pattern is the segregation of homologs (instead of the sister chromatids, as it is the case in mitosis) to opposite poles during meiosis I. Since a pair of homologous chromosomes consist of two pairs of sister chromatids, which have both the capacity of binding microtubules through their kinetochores, the segregation

pattern in the first meiotic division needs to incorporate specific modifications. The phenomenon by which sister chromatids separate towards the same pole is called monoorientation or monopolar attachment, and is achieved by binding of sister kinetochores to microtubules emanating from the same spindle pole (Figure 1-2). In *S. cerevisiae*, monopolar attachment requires a protein complex called monopolin (composed of the meiosis-specific protein Mam1, two nucleolar proteins (Lrs4 and Csm1) and the casein kinase Hrr25) (Katis *et al.*, 2010; Petronczki *et al.*, 2003; Riedel *et al.*, 2006). The monopolin complex is both necessary and sufficient to link sister kinetochores (or in other words, to allow attachment of sister chromatids of the homologous chromosomes to the same kinetochore) during meiosis I. Studies in budding yeast have pointed towards a role of monopolin in creating a common interface of the two sister kinetochores (by clamping them) to a single microtubule-binding site (Marston, 2014).

Another unique feature of meiosis with respect to mitosis is the so-called stepwise loss of cohesin. In mitosis, cohesion is destroyed in one step at the metaphase-to-anaphase transition, allowing the separation of sister chromatids. However, in meiosis such removal of cohesin should be prevented, since the loss of cohesion in meiosis I would lead to premature separation of sister chromatids. Thus, sister chromatids must remain together during the first meiotic division and separate to opposite poles only in meiosis II (Brar *et al.*, 2006; Buonomo *et al.*, 2000). Whereas sister chromatids are attached to each other via ring-shaped cohesin complexes loaded during DNA replication, physical connections between homologs are established during meiotic crossover recombination by the formation of chiasmata, which enable the establishment of tension necessary for aligning homologs on the spindle and their segregation to opposite poles during meiosis I. Cohesion of sister chromatids near the centromeric region has to be preserved during meiosis I to ensure that sister chromatids do not separate until the second meiotic division (meiosis II). Therefore, the meiotic division pattern has mechanisms that ensure that sister chromatid cohesion is released in a sequential manner: first, along chromosomes arms to segregate homologs (in meiosis I) and then at the centromeric region to separate sister chromatids (in meiosis II) (Figure 1-2) (Hochwagen, 2008; Marston, 2014). The characteristic features of meiosis introduced here are further detailed in the following sections.

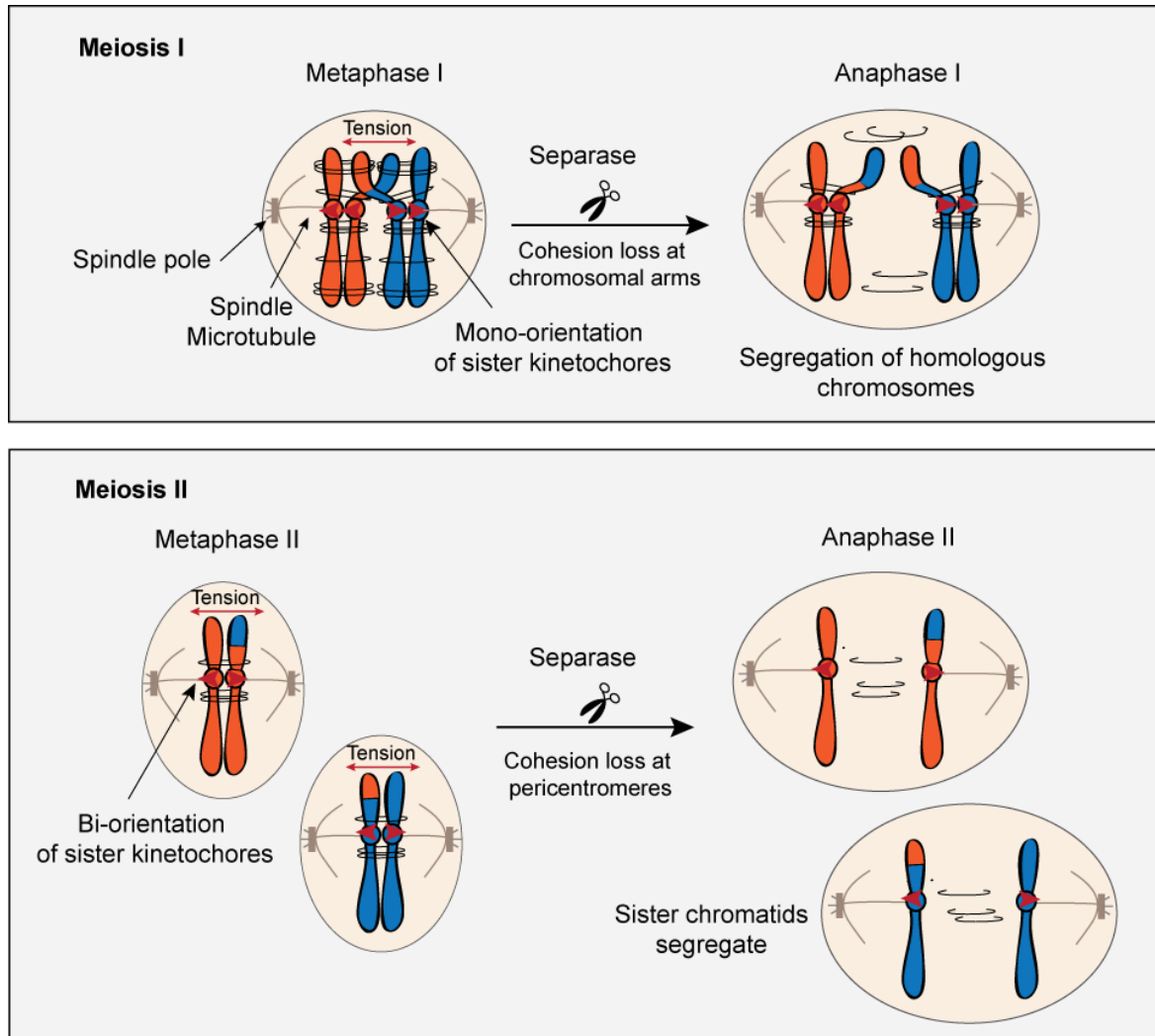


Figure 1-2 Stepwise loss of cohesion in meiosis

The meiotic programme comprises two sequential chromosome segregation events (meiosis I and meiosis II). In meiosis I, homologous chromosomes segregate, whilst in meiosis II, sister chromatids segregate. To enable the segregation of homologous chromosomes during meiosis I, the kinetochores (multi-protein complexes assembled onto defined sequences, named centromeres; represented as orange/blue circles) of sister chromatids must be mono-oriented or co-oriented (*i.e.* sister kinetochores are bound to spindle microtubules emanating from the same spindle pole). Pulling forces exerted by the spindle microtubules towards opposite directions generate tension because homologous chromosomes are physically linked by a chiasma. In meiosis I, cohesin (depicted as black rings) is cleaved by Separase (represented as scissors) along the chromosomal arms, allowing the separation of homologous chromosomes to opposite poles at the onset of anaphase I. Cohesin remains associated at the centromeres and pericentromeres, due to the protection of cohesin at these regions by Sugoshin (Sgo1) (not depicted here). In metaphase II, sister kinetochores are bi-oriented (*i.e.* attached to microtubules from opposite spindle poles). Sgo1 dissociation leaves centromeric and pericentromeric cohesin susceptible to separase-mediated cleavage, triggering the segregation of sister chromatids to

Figure 1-2 (Continued)

opposite poles at the onset of anaphase II. The chromosome segregation pattern in meiosis II is analogous to the mitotic segregation pattern. Red arrows indicate kinetochore orientation. Microtubules are represented as brown lines. Meiotic segregation pattern is reviewed in Marston and Amon, 2004, and Watanabe, 2012.

1.1.1 Meiotic cell cycle phases

Similar to mitosis, the meiotic cell cycle can be divided into discrete phases, namely gap 1 (G1), synthesis (S), gap 2 (G2). In meiosis, these phases are followed by two segregation events (meiosis I and meiosis II), instead of a single division step, as in the mitotic cell cycle. The introduction of a second segregation step in the meiotic programme is the ultimate feature that enables the characteristic halving of the ploidy during meiosis. Both meiotic divisions can also be divided into distinct phases: prophase, metaphase, telophase and anaphase. Once chromosomes segregate, the cytoplasm is also divided into the daughter cells in a process called cytokinesis.

Progression through the meiotic cell cycle is regulated by cyclin-dependent kinases (CDKs) and their regulatory subunits called cyclins (Cln/Clb). In the case of budding yeast, a single CDK named Cdc28 associates with diverse cyclins during the different phases of the meiotic cell cycle. The oscillation of cyclins levels ensures the periodic activation of CDK, which phosphorylates downstream proteins to control distinct cell cycle transitions (Marston & Amon, 2004; Alberts *et al.*, 2008). When errors during meiosis occur, several mechanisms referred to as checkpoints, operate in order to either delay or block the progression of the cell cycle until the previous step is successfully accomplished. In the next sections (1.1.1.1-1.1.1.5) the main events occurring in the different meiotic cell cycle phases are described in more detail.

1.1.1.1 G1 phase

In response to different external stimuli, *S. cerevisiae* can initiate either the mitotic or meiotic cell cycle programme. Laboratory budding yeast strains can exist as haploid or diploid cells. Haploid cells can have two mating types, referred to as ‘a’ and ‘ α ’, that are specified by the cryptic mating locus (*MAT* locus), whereas diploid cells express both *MATa* and *MAT α* genes. In budding yeast, meiosis is coupled to gametogenesis (known as sporulation in yeast), by which the four haploid meiotic products (in yeast termed “spores”) are surrounded by a sac called ascus.

Meiosis and sporulation are coordinated by successive transcriptional cascades, for which the activity of CDK coupled with distinct cyclins is critical. Initiation of meiosis in *S. cerevisiae* requires different signals that promote the activation/repression of several transcription factors that initiate a myriad of responses that culminates with the initiation of the meiotic programme (van Werven & Amon, 2011). Among the signals necessary for meiotic induction in budding yeast are diploid cellular type, nutritional starvation, and respiratory state. First, the cellular mating-type restricts meiotic division to diploid cells (MATa/MAT α) (*i.e.* haploid budding yeast cannot initiate meiosis). Second, nutritional starvation is necessary for the initiation of meiosis. More precisely, meiosis is restricted to cells that are deprived of a nitrogen and glucose source, combined with the presence of a non-fermentable carbon source in the medium (Freese *et al.*, 1982; Mitchell, 1994; Neiman, 2011; H. E. Smith & Mitchell, 1989). This implies that only those yeast cells that are respiratory competent (*i.e.* cells that have functional mitochondria) are able to enter meiosis. The integration of these cues (mating type, nutritional and respiratory state) results in the activation and expression of the transcription factor Ime1 (Initiator or Inducer of meiosis), which is in turn recruited to distinct promoters and provokes the first transcriptional wave by activating the transcription of the so-called ‘early meiotic genes’ (Smith & Mitchell, 1989; Smith *et al.*, 1990).

Among the several targets of Ime1 are two crucial genes (*IME2* and *NDT80*) that are critical for meiotic initiation and progression. Ime2 is a CDK-related protein kinase that phosphorylates the inhibitor of CDK1-Clb5/6 (called Sic1), triggering its degradation. Degradation of Sic1 activates Cdc28-Clb5/6, which induces the entry into pre-meiotic S phase (Chu *et al.*, 1998; Dirick *et al.*, 1998; Irniger, 2011; Marston & Amon, 2004b; Schwob *et al.*, 1994; Stuart & Wittenberg, 1998). Ime1 also influences the expression of *NDT80*, which encodes for a transcription factor of middle-meiosis genes (Kerr *et al.*, 2012; Neiman, 2011; van Werven & Amon, 2011). Activation of Ndt80 results in the transcription of several genes and irreversibly commits cells to the meiotic programme. Ultimately, activation of Ndt80 enables the progression through meiosis, exit of pachytene and spore formation by inducing the transcription of several middle-expressed genes. Among these genes are diverse cyclins that allow progression through meiosis I, due to the increased M-CDK activity that results in SPB (spindle pole body) separation and formation of the metaphase I spindle. Moreover, Ndt80 also activates the polo-like kinase protein Cdc5, which results in the resolution of

crossovers and the disassembly of the SC (Ballew & Lacefield, 2019; Kerr *et al.*, 2012; Neiman, 2011; van Werven & Amon, 2011).

Finally, in order to start the meiotic division, the mitotic programme has to be repressed. This is partially achieved by the activity of CDK bound to different cyclins. Whereas during vegetative growth, CDK-Cln1/2 is required for entry into pre-mitotic S phase, during meiosis this step is promoted by Ime2. CDK-Cln not only promotes budding (*i.e.* vegetative growth), but it also prevents entry into meiosis by actively inhibiting *IME1* expression, making entry into mitosis and meiosis mutually exclusive. Moreover, the early meiotic genes have a regulatory element in their promoters (*URSI*) that is bound to a protein called Ume6. During vegetative growth, Ume6 represses transcription of these genes, but binding of Ime1 to Ume6 is thought to allow transcriptional activation of the early genes (Kerr *et al.*, 2012; Neiman, 2011; van Werven & Amon, 2011).

1.1.1.2 S phase

During pre-meiotic S phase, the DNA of the maternal and paternal chromosomes is replicated, producing a copy known as “sister chromatid” for each homologous chromosome. The basic mechanisms of DNA replication are similar in pre-meiotic and pre-mitotic S phase, and DNA synthesis is catalyzed by the same proteins in both S phases (Collins & Newlon, 1994; Simchen, 1974).

In yeast, DNA replication initiates from specific regions, so-called “origins of replication” distributed along the chromosomes. In the G1 phase of the cell cycle, the Mcm2-7 (minichromosome maintenance 2-7; also known as MCM) replicative helicase is recruited or loaded to these origins. Then, the coordinated activity of CDK and Dbf4-dependent kinase Cdc7 (DDK) triggers the initiation of DNA replication (a process often referred to as “origin firing”) from a subset of these origins, by controlling the recruitment of additional factors needed for DNA replication. Once origins have fired, the DNA replication proteins organize into a structure called replication fork that has DNA unwinding and DNA synthesis activities. The replication fork is a multiprotein complex that progresses along the DNA; the helicases present in the replication fork unwind the double-stranded DNA (dsDNA), while the DNA polymerases copy the DNA. Initiation of replication from origins or origin firing does not occur in all available origins of replication and ‘inactive’ origins are replicated in a passive manner by the replication fork initiating from a nearby origin (Aparicio *et al.*, 1997; Bell &

Kaguni, 2013; Bell & Labib, 2016; Diffley & Labib, 2002) (for a more comprehensive explanation of DNA replication and the proteins involved in this process see section 1.4.2).

Although pre-meiotic and pre-mitotic S phases share the basic principles behind DNA replication (*i.e.* utilize the same proteins for DNA synthesis) there are subtle differences in the regulation of the initiation of this process. During vegetative growth, budding and DNA replication are induced by CDK (Cdc28) and G1 cyclins (Cln1/2/3). However, in order to initiate meiosis, those genes responsible for vegetative growth must be repressed, and nutritional starvation (a prerequisite for meiotic entry) represses the expression of cyclins, inhibiting budding. The fact that DNA replication relies on CDK-Clns implies some modifications in the regulation of the meiotic S phase entry. The CDK-related kinase Ime2 takes over the role of the CDK-Clns to promote DNA replication. Another difference between pre-mitotic and pre-meiotic S phase is that whereas in mitosis DNA replication can occur even if CDK1-Clb5/Clb6 are not present, in the meiotic cell cycle DNA synthesis cannot occur in the absence of those cyclins (Alberts *et al.*, 2008; Dirick *et al.*, 1998; Kerr *et al.*, 2012; Marston, 2014).

Though there has been a general consensus that replication fork progression rates and origin choice is similar in mitosis and meiosis, it is well known that pre-meiotic S phase is 1.5-3 times longer than pre-mitotic S phase (Padmore *et al.*, 1991; Williamson *et al.*, 1983; Zickler & Kleckner, 1999). Previous studies have suggested that the extended pre-meiotic S phase is not due to changes in origin selection. The prolonged length of meiotic S phase has been for a long time attributed to the extensive reorganization of meiotic chromosomes during meiotic prophase, in which chromosomes reorganize into a series of chromatin loops emanating from a central axis (see section 1.1.1.3 for a more thorough explanation). However, a study demonstrated that the extensive chromosome remodelling is not responsible for the extended length of pre-meiotic S phase (Blitzblau *et al.*, 2012). The same study confirmed that origin selection and activation are highly similar in meiosis and mitosis, but also identified several origins of replication whose firing is delayed in meiosis as compared to mitosis. It has been proposed that the extended pre-meiotic S phase could be due to the delay in the initiation of DNA replication in meiosis, probably because of a limiting factor, such as CDK levels. Alternatively, this delay could be accounted for metabolic changes due to the starvation conditions needed to induce the meiotic programme. Another possibility is that the extended pre-meiotic S phase is a reflect of a decreased number of active replication forks; it has been suggested that reduction of active forks could have had an evolutionary advantage,

since slow progression could potentially guarantee that DNA replication occurs in a reliable and accurate manner (*i.e.* with fewer errors), which would be beneficial to avoid that meiotic errors are propagated to the progeny (Blitzblau *et al.*, 2012). Thus, although several hypotheses have the potential to explain the increased length of pre-meiotic S phase, the ultimate cause of the delay of origins in pre-meiotic S phase is not fully understood. For more details on pre-meiotic S phase see section 1.4.2.2.6.

Concomitantly with DNA replication, cohesion between sister chromatids is established by cohesin protein complex (Uhlmann & Nasmyth, 1998). Cohesin molecules are loaded in late G1 by the Scc2/Scc4 loader complex, and as DNA replication occurs, loaded cohesin is converted into functional cohesion that holds sister chromatids together (Ciosk *et al.*, 2000; Haering *et al.*, 2008; Kogut *et al.*, 2009). As mentioned above, sister chromatid cohesion is crucial to ensure proper chromosome segregation during meiosis.

1.1.1.3 G2/ Prophase I

Several important events that lie behind the special features of the meiotic cell programme occur during the prolonged gap phase known as “meiotic prophase I”, including programmed DSB formation, homologous recombination (HR), crossover (CO) formation and synaptonemal complex (SC) assembly. As mentioned earlier, DSBs are actively introduced and their subsequent repair by HR leads to the establishment of physical linkages (chiasmata) that are crucial for proper chromosome segregation during meiosis I. DSB formation and repair are facilitated by changes in chromosome structure that are cytologically observable. These meiosis-specific, higher-order chromosomal arrangements define different stages in meiotic prophase, known as leptotene, zygotene, pachytene and diplotene (Hochwagen & Amon, 2006; Klein *et al.*, 1999; Panizza *et al.*, 2011; Subramanian & Hochwagen, 2014) (Figure 1-3).

In budding yeast, there is no clear separation between pre-meiotic S phase and the start of prophase I (Blitzblau *et al.*, 2012). Concomitantly with DNA replication, proteins required for DSB introduction and axis formation are expressed and assembled onto chromosomes. As prophase progresses, meiotic chromosomes adopt a characteristic arrangement referred to as “loop-axis organization”, which is completed in leptotene. Each pair of sister chromatids (*i.e.* each homologous chromosome) arranges into chromatin loops that emanate from a proteinaceous axis element to which they are anchored at their bases (Blat *et al.*, 2002; Klein

et al., 1999; Lam & Keeney, 2014; Panizza *et al.*, 2011; Storlazzi *et al.*, 2003). The introduction of DSBs occurs at this stage by the DSB-machinery of which the endonuclease Spo11 is the catalytic core. The current model of meiotic DSB formation in budding yeast, supports the idea that the loop-axis organization is critical for DSB introduction. This model, generally referred to as “tethered loop-axis” model, proposes that DSBs are formed in chromatin loops that are transiently tethered to the axis by Spo11-accessory proteins. Spo11 and accessory factors are enriched at the chromosome axes and thus, the transient tethering of chromatin loops could enable the introduction of DSBs (Keeney *et al.*, 2014; Lam & Keeney, 2014, 2015) (see section 1-2 for a detailed explanation of the loop-axis conformation and DSB formation and repair) (Figure 1-3).

In zygotene, DSBs repair is initiated. DSBs can be processed to give two recombination products: non-crossovers (NCOs), where there is no distal DNA exchange between maternal and paternal chromosomes, and crossovers (COs), where there is distal reciprocal DNA exchange between homologs. The NCO/CO decision is tightly controlled to ensure that each homolog pair has at least one CO (“obligate CO”, necessary for physical linkage between homologs and proper alignment in the metaphase spindle of meiosis I) and that COs are distributed apart from each other (a process known as CO interference). Besides enabling DSB formation, the loop-axis chromosomal organization is also necessary for the establishment of inter-homolog (IH) bias, a mechanism by which DSB are preferentially repaired using the homolog as a template (rather than the sister chromatid) and that ultimately leads to the formation of COs (Schwacha & Kleckner, 1997). As mentioned above, resolution of COs ultimately leads to the formation of physical connections between homologs, named chiasmata (Berchowitz & Copenhaver, 2010; Gray & Cohen, 2016; Humphryes & Hochwagen, 2014; V. V. Subramanian & Hochwagen, 2014; Thacker & Keeney, 2009).

As cells progress through zygotene, the axial elements of homologous chromosomes align in a process known as “pairing”. The association of the homologous axes culminates with the assembly of a proteinaceous structure (synaptonemal complex (SC)) along the length of the homologous chromosomes (Page & Hawley, 2004). The SC consists of a “zipper-like” structure that serves as a scaffold between homologous chromosomes (Marston & Amon, 2004b; V. V. Subramanian & Hochwagen, 2014; Zickler & Kleckner, 1999). The SC is a tripartite structure, comprising two lateral elements (*i.e.* one of each homolog) and a central region. The lateral elements consist of the previous axial elements of each homologous chromosome that are arranged in the above-mentioned loop-axis conformation. Axial

elements are defined by the meiosis-specific proteins Red1, Mek1 and Hop1, as well as cohesin complexes (Hollingsworth *et al.*, 1990; Sym *et al.*, 1993). The homologous axial elements align together forming the lateral elements of the SC, which are bridged by transverse filaments. Together with the central element proteins (Ecm11 and Gmc2), these transverse filaments constitute the central region of the SC of which the major component is a protein called Zip1 (Gao & Colaiacovo, 2018; Humphryes *et al.*, 2013).

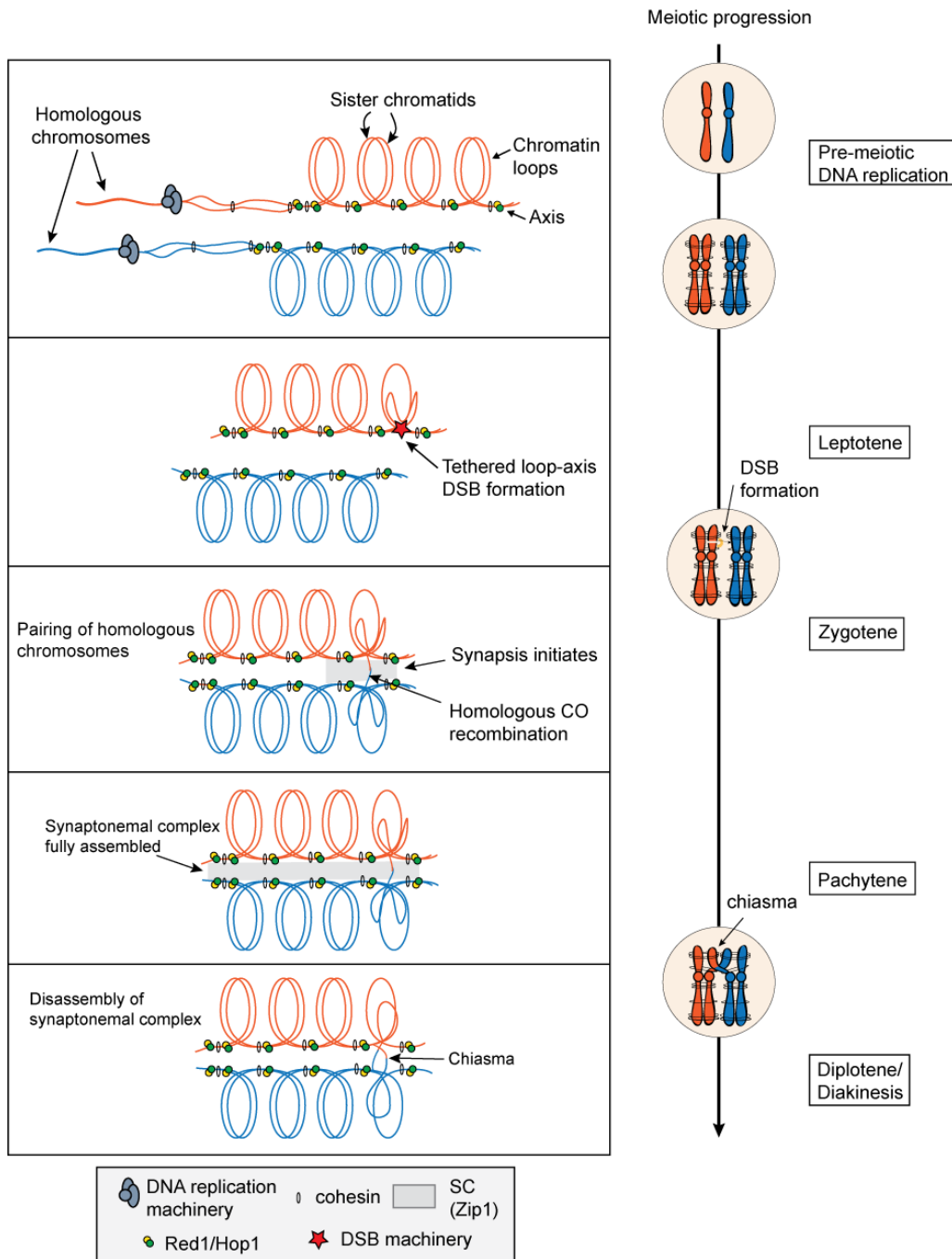


Figure 1-3 Meiotic DSB formation and recombination in G2/prophase

A prerequisite for proper chromosome segregation during meiosis is the establishment of at least one chiasma between homologous chromosomes in G2/prophase I. DSB formation and CO recombination

Figure 1-3 (Continued)

are essential for the formation of chiasmata. DSB formation and repair are facilitated by the formation of higher-order chromosomal arrangements that define different stages in meiotic G2/prophase I, namely leptotene, zygotene, pachytene and diplotene. After pre-meiotic DNA replication (pre-meiotic S phase or meiS), each pair of homologous chromosomes consist of two copies of the original chromosome, termed sister chromatids. Each pair of sister chromatids arrange into chromatin loops that emanate from proteinaceous axes, defined mainly of the meiosis-specific proteins Red1 and Hop1, and cohesin. This “loop-axis” conformation is completed in leptotene. Introduction of DSB occurs at this stage by the DSB machinery. The current model proposes that DSB formation takes place in the chromatin loops that are transiently anchored to the axis by Spo11-accessory proteins (“tethered loop-axis” model; see Figure 1-6). In zygotene, DSB repair initiates and, as cells progress through this stage, the axial elements of homologous chromosomes align, process referred to as “pairing”. Pairing culminates with the assembly of the synaptonemal complex (SC) along the length of the homologous chromosomes. The main component of the SC is a protein called Zip1 (depicted in grey). In the pachytene stage the SC is fully assembled. DSB repair by the CO pathway leads to the formation of a double Holliday junction (dHJ) intermediate. dHJ resolution leads to the formation of physical linkages between homologous chromosomes (chiasma) at the end of pachytene. In diplotene, the SC starts to disassemble and cells prepare to segregate the homologous chromosomes. Adapted from Subramanian and Hochwagen, 2014, and Kuhl, 2018.

In the pachytene stage, homologous chromosomes are fully synapsed and DSB repair is in an intermediate state known as double Holliday junction (dHJ). These dHJs have the potential of giving rise to COs upon resolution of the dHJ by the CO-pathway (see section 1.2). Once all DSBs are repaired, cells exit pachytene. In the next prophase stage, known as diplotene, the SC starts to disassemble and cells prepare to segregate the homologous chromosomes (Hochwagen & Amon, 2006; V. V. Subramanian & Hochwagen, 2014). Diplotene is followed by entry into the first chromosome segregation event driving Meiosis I.

1.1.1.4 Meiosis I

Both meiotic chromosome segregation events (meiosis I and meiosis II) can be divided into the same phases as mitosis, namely prophase, metaphase, anaphase and telophase (Figure 1-2). Meiotic prophase I is significantly different from mitotic prophase and the main events occurring in this stage of meiosis were outlined in the previous section. After prophase I, homologous chromosomes are linked to each other, due to the establishment of chiasmata after CO resolution. In metaphase, homologs become bi-oriented on the metaphase spindle, or in other words, homologs become attached to opposite spindle poles through microtubules

(emanating from the spindle pole body (SPB)) that bind to a multi-protein complex called kinetochore assembled onto constricted chromosomal regions, termed centromeres (Musacchio & Desai, 2017).

In mitosis, microtubules from two opposite spindle poles capture sister kinetochores (*i.e.* kinetochores of sister chromatids), generating “pulling” forces that tend to physically split sister chromatids towards opposite spindle poles. These pulling forces act against the cohesive forces of cohesin molecules that maintain sister chromatids together, resulting in the generation of the so-called tension (Mitchison & Salmon, 1992; Nicklas, 1988; Rieder & Salmon, 1994). The generation of tension facilitates proper alignment of chromosomes on the metaphase plate. In the first meiotic division, the pulling forces from spindle microtubules towards opposite directions result in tension between homologous chromosomes, because these are physically linked by chiasmata. However, the meiotic cells face a challenge during meiosis I derived from the fact that each homolog has two sister chromatids. Unlike the mitotic cell, cells in meiosis must have the sister chromatids of each homolog pair bound to the same pole, or in other words, sister chromatids are mono-oriented. In budding yeast, mono-orientation depends on a group of proteins called monopolin, which is thought to create a single binding unit to spindle microtubules by “fusing” the two sister kinetochores (Marston, 2014; Marston & Amon, 2004b; Tóth *et al.*, 2000; Watanabe, 2012).

In order to establish accurate alignment of homologous chromosomes in the meiotic spindle, homologs must be connected. This linkage is achieved through chiasma only because sister chromatids are topologically linked by cohesin along their arms, distal to the chiasma. Thus, cohesion between sister chromatids is essential for proper chromosome alignment and segregation, and must, therefore, be maintained until metaphase I. In the meiotic programme sister chromatid cohesion must be released so that homologs can segregate to opposite poles in meiosis I, but at the same time cohesion must be partially retained among sister chromatids, so that sisters stay together until meiosis II. As mentioned in the section above, this apparent paradox that arises in the meiotic cell division is solved thanks to the stepwise loss of cohesion, first along the chromosomal arms and then at centromeric regions (Hochwagen, 2008; Marston, 2014).

Sister chromatid cohesion is released by the action of a protease named separase that enables proteolytic cleavage of the cohesin subunit Scc1 or Rec8 during both mitosis and meiosis. Separase remains inactive during most of the cell cycle by binding to an inhibitory

chaperone called securin, which is only removed during metaphase-to-anaphase transition through proteasomal degradation initiated by proteolytic APC/C mediated ubiquitination (Lee & Amon, 2001; Marston & Amon, 2004b; Petronczki *et al.*, 2003). The stepwise loss of cohesion in meiosis is achieved thanks to the incorporation of a meiosis-specific cohesin subunit known as Rec8 (instead of the mitotic Scc1) (Figure 1-2). This cohesin subunit cannot be cleaved unless it is phosphorylated by the polo-like kinase (PLK) Cdc5, together with phosphorylation mediated by the casein-kinase Hrr25 and Dbf4-dependent kinase (DDK). Prior to meiosis I, PLK is activated, which results in phosphorylation of cohesin. Pericentromeric cohesins are protected against phosphorylation by the pericentromeric-specific recruitment of protein phosphatase 2A (PP2A), which is mediated by Shugoshin (Sgo1), leading to a differential pattern of cohesin phosphorylation along chromosomes (higher phosphorylation on chromosomal arms than in the pericentromere). Sgo1-mediated recruitment of PP2A counteracts the phosphorylation by PLK and renders centromeric Rec8 refractory to separase activity. As a result, cleavage of Rec8 by separase triggers the dissociation of cohesin from chromosomal arms (*i.e.* destruction of cohesion) distal to the chiasma, enabling the segregation of homologous chromosomes to opposite poles in anaphase I. However, sister chromatids remain linked by centromeric cohesion until the onset of anaphase II (Brar *et al.*, 2006; Ishiguro *et al.*, 2010; Katis *et al.*, 2010; Kitajima *et al.*, 2006; Riedel *et al.*, 2006). Thus, this protection of centromeric cohesion is essential to hold sister chromatids together and enable bi-orientation and segregation in meiosis II (see section 1.1.1.5). At the end of telophase I, the homologous chromosomes are packaged into two daughter cells. Since the first meiotic division produces cells with half the complement of the progenitor cells (*i.e.* haploid cells), meiosis I is often referred to as “reductional division”.

1.1.1.5 Meiosis II

Homolog segregation during meiosis I is not followed by an additional S phase, but by another chromosome segregation event. The coupling of two consecutive homologous separation steps without an intervening S phase allows Meiosis II to yield cells with the same ploidy as the cells obtained at the end of Meiosis I (as it occurs in mitosis) and thus, meiosis II is also named “equational division” (Figures 1-1 and 1-2).

Meiosis II can, similarly to Meiosis I, be divided into distinct phases (prophase, metaphase, anaphase, and telophase), but in Meiosis II, sister chromatids (rather than homologous chromosomes, as in Meiosis I) segregate. It is important to note that at this stage

sister chromatids are an “amalgam” of the maternal and paternal chromosomes, due to genetic exchange via homolog recombination in prophase I. In metaphase II, sister chromatids align along the equator of the metaphase plate due to the tension originated by centromeric cohesion and pulling forces from the spindle microtubules to which sister kinetochores are attached. Loss of centromeric cohesion (by separase cleavage of Rec8) enables that sister chromatids separate to opposite poles in anaphase II (Marston, 2014; Marston & Amon, 2004b; V. V. Subramanian & Hochwagen, 2014; Watanabe, 2012). By the end of telophase II, haploid cells contain sister chromatids in which the DNA has been reshuffled. In budding yeast, the final product of meiosis II is a tetrad containing four haploid cells named spores.

1.1.2 Checkpoints

Progression through the cell cycle is coordinated and monitored by several surveillance mechanisms termed “checkpoints”. Checkpoint mechanisms operate in both, mitosis and meiosis, and are pathways that detect ongoing cell cycle events and interconnect them with one another. If the execution of a due event is abnormal, these checkpoints halt the cell cycle progression and activate repair responses. Although the term “checkpoint” is usually associated with pathways that respond to aberrant events, here we refer to checkpoint in line with the original definition of cell cycle checkpoints (Hartwell & Weinert, 1989), to describe control mechanisms that create dependent relationships in the cell cycle and ensure the order of cell cycle events. Particularly, in meiosis we refer to meiotic checkpoint mechanisms to describe mechanisms that create dependencies between metabolically independent meiotic processes, as done by others (V. V. Subramanian & Hochwagen, 2014). Thus, these surveillance mechanisms also operate during an unperturbed cell cycle, since they establish certain dependencies of a defined event on the proper execution of the previous one, thus guaranteeing that each cell cycle step is accurately completed before the cell progresses into the next stage. Therefore, checkpoints are crucial for both, coordinating cell cycle events by coupling one process to the previous one and also to monitor anomalous events that endanger the cell cycle.

In general terms, cell cycle regulation in meiosis is similar to the regulation during mitosis, in which there exist three major checkpoints, namely G1 (Gap1) checkpoint, G2 (Gap2) checkpoint and M (Mitotic) checkpoint (Murray, 1994; Weinert, 1998). The G1 checkpoint, also known as “restriction checkpoint” mainly serves to verify that cells have the appropriate cell size and protein content and that there is no DNA damage before the cell

progresses into synthesis (S) phase (where DNA replication occurs). The G2 checkpoint is similar to the G1 checkpoint in that it ensures that cell size and protein reserves are adequate, but it also prevents cell cycle progression when DNA replication is ongoing. Last, the M checkpoint, often referred to as spindle checkpoint or Spindle Assembly Checkpoint (SAC), operates at the metaphase-to-anaphase transition and ensures that kinetochores from all chromosomes are attached to the spindle microtubules before the passage of the cell into anaphase (Musacchio & Salmon, 2007). Although the SAC regulators are mostly conserved in meiosis, the meiotic cell cycle has the unique feature that in the first meiotic division, homologous chromosomes, rather than sister chromatids segregate, which is achieved through the meiosis-specific cohesin subunit Rec8, as explained in section 1.1.1.4.

Despite meiotic cell cycle regulation being analogous to mitotic regulation in many aspects, several distinct surveillance mechanisms operate in the prolonged meiotic prophase I. During this stage, several meiosis-specific processes (*i.e.* DSB formation and repair, CO recombination) occur that must be completed in an accurate manner and thus, need to be controlled. Similarly to mitosis, during the meiotic cell cycle, progression into the next cell stage can be halted until the conditions for progression into the next step are met or until the previous event is accomplished. In *S. cerevisiae*, the meiotic checkpoint mechanisms operating in prophase I usually establish dependencies by phosphorylation of different substrates by the conserved checkpoint sensor serine/threonine kinases Tel1/Mec1 (ATM/ATR homologs), which respond to DNA damage and asynapsis in meiosis (Hochwagen & Amon, 2006; MacQueen & Hochwagen, 2011; V. V. Subramanian & Hochwagen, 2014).

The programmed introduction of meiotic DSBs is an inherent hazardous event for the cell (see section 1-2). Thus, DSBs need to be formed in a discrete-time window and this is achieved through the meiotic replication checkpoint, which prevents the introduction of DSBs when DNA replication is ongoing, guaranteeing that recombination occurs following DNA replication. This checkpoint acts on the expression of Spo11 and the localization and activation of certain components of the DSB machinery (Mer2, Rec114) by DDK. Moreover, as mentioned in section 1.1.2, mechanisms that control DSBs levels operate during meiosis (Keeney, 2001; Murakami & Keeney, 2014)

DSB formation and accumulation of recombination and synapsis intermediates trigger the so-called “recombination checkpoint”, often referred to as “pachytene checkpoint” or

“G2/prophase checkpoint”. This checkpoint prevents progression through meiosis when cells fail to complete recombination or chromosome synapsis. The presence of unrepaired Spo11-induced DSBs delays meiotic progression in order to provide cells with extra time for repair. Persistent breaks are mostly sensed by Tel1/Mec1 and the 9-1-1 complex. In budding yeast, the recombination checkpoint inhibits meiotic transcription of Ndt80, a key protein that controls the expression of genes necessary for later meiotic events (MacQueen & Hochwagen, 2011; Roeder & Bailis, 2000; V. V. Subramanian & Hochwagen, 2014).

Several surveillance mechanisms at the level of DSB repair can be involved in the recombination checkpoint, which ultimately blocks entry in metaphase I if recombination is not efficiently executed, and many of these mechanisms share proteins operating in the DNA damage checkpoint. First, during meiosis mechanisms exist to establish a recombination bias towards repair with the homologous chromosome rather than the sister chromatid, a process known as “inter-homolog bias” (IH bias) (Hollingsworth, 2010; Lao & Hunter, 2010). IH bias is mediated by Tel1/Mec1 kinases (ATM/ATR in higher organisms), which promote the homologous chromosome as the preferred template for DSB repair by phosphorylating the HORMA-domain protein Hop1 at multiple sites. Phosphorylation of this substrate leads to the recruitment, dimerization, and activation of Mek1, which in turn leads to phosphorylation and inactivation of Rad54. Rad54 is an ATPase that normally stimulates Rad51-recombinase activity enabling the repair using the sister chromatid as a template. Therefore, by Tel1/Mec1-mediated inactivation of Rad54, DSB repair during meiosis is biased to use the homolog as the repair template, rather than the sister chromatid, which is the preferred repair template in mitosis. Moreover, similarly to mitosis, Tel1/Mec1 dependent phosphorylation of Sae2 (a DSB resection protein) is important to promote homologous recombination (Carballo *et al.*, 2008, 2013; Garcia *et al.*, 2015; Hollingsworth, 2010; Lao & Hunter, 2010). Second, non-allelic (ectopic) recombination is suppressed in meiosis, possibly via the 9-1-1 complex. Third, there are mechanisms that ensure that each homolog pair receives at least one CO (obligate CO) and that COs are not randomly placed with respect to each other along chromosomes. This last process, known as “CO interference”, refers to the fact that the occurrence of one CO interferes with the coincident occurrence of another CO in the same place at the homologous chromosome. CO interference ensures that COs are spaced and also involves the action of Tel1/Mec1. Furthermore, Mec1-dependent phosphorylation of a protein called Rfa2 controls CO distribution and is involved as well in the preferential use of a non-sister chromatid (chromatid of another homolog) rather than a sister chromatid (Berchowitz &

Copenhaver, 2010; Bishop & Zickler, 2004; Gray & Cohen, 2016; M. Shinohara *et al.*, 2015; Subramanian & Hochwagen, 2014).

Last, the synapsis checkpoint responds to defects in the chromosome axes formation or to aberrant SC, which can also result in a delay in meiotic progression. In budding yeast and other organisms, a meiosis-specific AAA⁺ ATPase named Pch2 (Pachytene checkpoint 2) is necessary for cell cycle arrest in mutants that show defects on the SC assembly. Cells lacking Zip1, the central element of the SC, show a Pch2-dependent arrest (San-Segundo & Roeder, 1999). Additionally, Pch2 acts in the recombination checkpoint, in combination with Xrs2 and Tel1, in response to unprocessed DSBs. Here, Pch2 also collaborates with Tel1, promoting IH bias (Ho & Burgess, 2011; Wu & Burgess, 2006; Zanders & Alani, 2009; Zanders *et al.*, 2011). Pch2 also regulates the chromosomal distribution of Hop1 (protein necessary for DSB introduction). More precisely, Pch2 removes Hop1 from the regions where chromosome synapsis initiate, therefore linking formation of DSBs with synapsis (see section 1.4 for a detail description of Pch2 and Pch2 functions) (Börner *et al.*, 2008; Joshi *et al.*, 2009; Wojtasz *et al.*, 2009).

Briefly, the meiotic cell cycle is subjected to a tight regulation that coordinates different meiotic events with one another and that ensures their proper execution. Besides control mechanisms sharing similarities with the checkpoints operating during vegetative growth, meiosis incorporates a complex network of surveillance mechanisms to regulate distinct meiotic processes occurring during prophase I and that utilize a series of meiosis-specific proteins.

1.2 Meiotic recombination

Meiotic recombination consists of the reshuffling of maternal and paternal chromosomes and it is initiated by the programmed introduction of DSBs. Homologous meiotic recombination not only allows the formation of physical linkages among homologous chromosomes but also increases genetic diversity in the progeny (Lam & Keeney, 2014). In sections 1.2.1 and 1.2.2, we detail several processes underlying DSB formation, different pathways of DSB repair and DSB distribution and control across the genome.

1.2.1 DSB formation and inter-homolog repair

DSBs are catalyzed by the evolutionary conserved topoisomerase-like protein Spo11 (Keeney *et al.*, 1997). In *S. cerevisiae*, there are 9 additional proteins required for DSB

formation that functionally act with Spo11, constituting the DSB machinery. These proteins act in four interacting subgroups: Spo11-Ski8, Rec102-Rec104, Rec114-Mei4-Mer2 (RMM complex) and Mre11-Rad50-Xrs2 (MRX complex). Null mutants of any of the above-mentioned proteins fail in DSB formation and show reduced sporulation and spore viability (Keeney, 2001; Keeney & Neale, 2006; Lam & Keeney, 2014).

The creation of a DSB is achieved by the coordinated creation of nicks on both DNA strands in a manner similar to topoisomerase function, which has led to the hypothesis that Spo11 is able to dimerize. Many of the steps in the DSB formation and recombination pathways are still not entirely clear, but the current model is stated below. DSBs are thought to be created by Spo11 dimers and after cleavage, each Spo11 monomers remain covalently linked via its active tyrosine residues to the 5' termini of each side of the break (Keeney & Kleckner, 1995). These Spo11-DNA complexes are then processed by endonucleolytic cleavage, likely by the nuclease Mre11, releasing the Spo11 monomers bound to a short oligonucleotide. Subsequently, the DNA ends undergo 5' to 3' resection by Exo1 to expose 3' single-stranded DNA (ssDNA) ends. The bacterial-related RecA strand-exchange proteins Rad51 and Dmc1 (which is meiosis-specific) associate with the ssDNA forming a helical nucleoprotein filament that invades the unbroken chromosome, creating a heteroduplex DNA, and priming DNA synthesis (Bishop *et al.*, 1992; Lam & Keeney, 2014; A. Shinohara *et al.*, 1992) (Figure 1-3).

Subsequently, the second ssDNA tail invades the unbroken homolog duplex. This nascent invasion is unstable and it is at this step where the decision between different DSB repair pathways, that ultimately yield different recombination products, is made. If after invasion of the ssDNA tail, the interaction between the DNA tails and the intact homologous DNA duplex is stabilized, a single-end invasion (SEI) intermediate is formed. Annealing of the second end of the break with the displaced strand of the SEI intermediate leads to the formation of an intermediate structure referred to as DNA double-Holliday junction (dHJ) (Schwacha & Kleckner, 1995). In the dHJ pathway, inter-homolog repair of the DSB and resolution of dHJs leads to the formation of COs, in which there is a reciprocal exchange of chromosomal DNA flanking the sites of the DSB (Storlazzi *et al.*, 1995). If the invading ssDNA tail dissociates from the DNA duplex, the DSB is repaired by the synthesis-dependent strand annealing (SDSA) pathway, in which the ssDNA end is extended by DNA synthesis and, after displacement, captures the complementary ssDNA tail of the other side of the DSB. This pathway leads to the formation of a non-crossover (NCO), in which there is no distal

DNA exchange between homologs. However, in the NCO recombination pathway there is a minimal DNA exchange (known as gene conversion) near the sites of the DSB due to the DNA synthesis using the homolog as a repair template before the ejection of the DNA tail (Carpenter, 1987; Fink & Petes, 1984; Lam & Keeney, 2014).

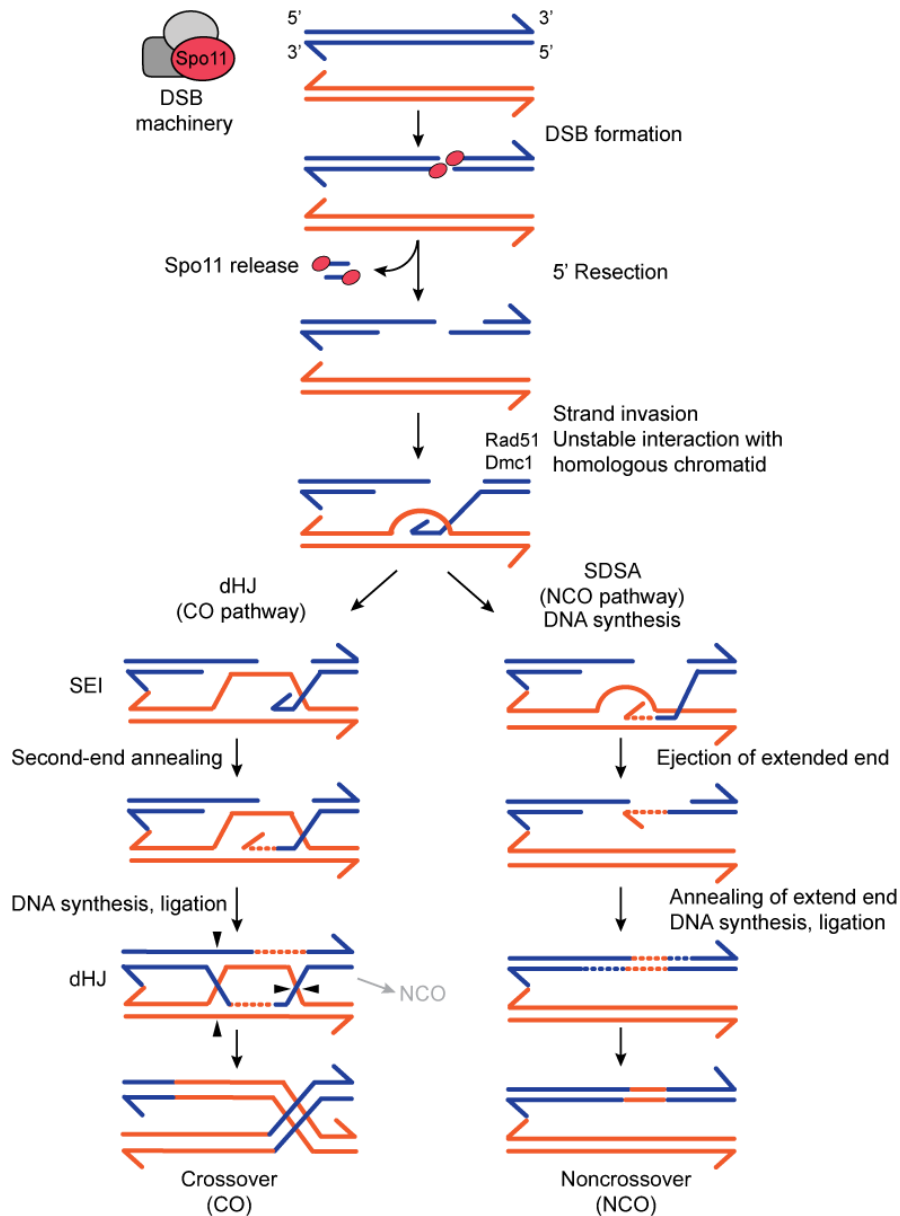


Figure 1-4 The CO and NCO pathways for meiotic recombination

Meiotic recombination initiates with the programmed introduction of DNA double-strand breaks (DSBs). DSB formation is mediated by the DSB machinery, of which the topoisomerase-like protein Spo11 is the catalytic core (represented in red). Besides Spo11, the DSB machinery is composed of 9 additional proteins (Ski8, Rec102-Rec104, Rec114-Mei4-Mer2, Mre11-Rad50-Xrs2). After DNA cleavage, Spo11 monomers remain covalently linked to short oligonucleotides. Spo11 release is

Figure 1-4 (Continued)

followed by 5' resection yielding single-stranded DNA (ssDNA). The proteins Rad51 and Dmcl1 associate with the ssDNA and mediate the strand invasion of the intact homologous chromatid. Interaction of the resected ssDNA tail with the repair template is unstable and at this step, the decision to follow the crossover (CO) or NCO (non-crossover) pathway is made. In the CO pathway, stabilization of this initial interaction leads to the formation of a single-end invasion (SEI). After annealing of the second-end, DNA synthesis and subsequent ligation of the extended end enables the formation of a double Holliday junction (dHJ). Resolution of dHJ gives rise to a CO (only one cleavage pattern is represented here as black arrowheads). The CO pathway depicted here only includes the class I crossover (mediated by the ZMM proteins), which correspond to the majority of CO in yeast. On the contrary, in the NCO pathway (also referred to as synthesis-dependent strand annealing -SDSA- pathway) the ssDNA tail that invades the homolog is displaced after initial DNA synthesis. The extended end re-anneals to the other end of the DSB, followed by DNA synthesis, nick repair and ligation. The result of the SSDA pathway is the formation of NCO recombinant products. Note that whereas in the CO pathway there is distal DNA exchange, in the NCO pathway there is a minimal DNA exchange (derived from the DNA synthesis using the intact homolog as a repair template). Note also that only one of the possible resolutions of the dHJ is depicted here for clarity, and that dHJ resolution can also give rise to a NCO. Adapted from Lam and Keeney, 2001, Marston and Amon, 2004, Baudat and De Massy, 2007.

COs lead to formation of chiasmata, which are necessary for proper alignment in the meiotic I spindle and faithful chromosome segregation. Indeed, the absence of COs leads to defects such as random segregation of chromosomes and gamete aneuploidy. Thus, as mentioned in section 1.1, there is a tight regulation to ensure that each homolog pair receives at least one CO (obligate CO), as well as mechanisms that guarantee that COs are not placed close to each other (a phenomenon known as “crossover interference”). In addition, the choice between NCO and CO outcomes is tightly controlled (Bishop & Zickler, 2004; Gray & Cohen, 2016; Serrentino & Borde, 2012).

Homolog DSB repair is based on the annealing to DNA that is homologous to the sequence where the DSB was formed. Thus, a DSB could be potentially repaired either by the homologous chromosome or the sister chromatid of the same homolog. However, as explained in section 1.1.2, there are mechanisms in meiosis that establish a bias towards repair with the homologous chromosome rather than the sister chromatid (IH bias) (Hollingsworth, 2010; Lao & Hunter, 2010; Schwacha & Kleckner, 1997). IH bias is achieved by Tel1/Mec1-mediated phosphorylation of Hop1, which ultimately blocks the inter-sister

repair of DSBs. Besides IH bias, Tel1/Mec1 are regulating other meiotic processes that are essential for faithful progression through meiotic prophase I (see section 1.1.2 and 1.4.1.1 for further details).

DSB introduction and meiotic recombination occur concomitantly with the development of higher-order chromosomal structures and these processes are functionally linked (Lam & Keeney, 2014; Zickler & Kleckner, 1999). As mentioned in section 1.1.1.3, in prophase I the sister chromatids of each homolog pair start arranging into protruding chromatin loops that are anchored at their bases to a proteinaceous axis, which in zygotene align to form the lateral elements of the SC. The resulting loop-axis conformation is essential for DSB formation. Meiotic recombination initiates in the axes since in this structure there is an enrichment of the proteins that constitute the DSB machinery. However, DSBs form within the chromatin loops that extend out of the axes, which implies that the chromatin loops must be close to the axes in order for Spo11 to cleave the DNA. This apparent contradiction is explained by the “tethered loop-axis model”, which conciliates the DSB formation in the chromatin loops with the fact that the DSB machinery is in the axes by proposing that the chromatin loops are transiently tethered to the axis by Spo11-accessory proteins (Keeney, 2001; Keeney & Neale, 2006; Lam & Keeney, 2014) (Figure 1-5). This is thought to happen through sequential steps. First, Mer2 is initially recruited to the axes by the axial proteins Red1 and Hop1 (Panizza *et al.*, 2011). Then, Mer2 is phosphorylated by the S-phase cyclin-dependent kinase (Cdc28-Cln5/6, also named CDK-S), which primes additional phosphorylation by DDK. Phosphorylation by these two kinases is essential for DSB formation and regulation of DSBs levels. Moreover, phosphorylation of Mer2 by CDK-S is critical for coordinating replication and DSB formation. Mer2 phosphorylation leads to recruitment of the Rec114, Mei4 and Xrs2, and possibly subsequently other DSB proteins (Rec102, Rec104, Ski8, Spo11, Mre11 and Rad50) (K. A. Henderson *et al.*, 2006; Sasanuma *et al.*, 2008; Wan *et al.*, 2008). Since Mre11 requires all the proteins of the DSB machinery (except Rad50) to associate with DSB sites, the MRX (Mre11-Rad50-Xrs2) complex might be recruited last, and its recruitment is thought to be mediated by the interaction between Mer2 and Xrs2. Mer2 is also able to bind Spp1, which recognizes and binds H3K4 me2/me3 on chromatin loops (chromatin modification enriched at *S. cerevisiae* DSBs “hotspots”) (Acquaviva *et al.*, 2016; De Massy, 2013; Sommermeyer *et al.*, 2013). Ultimately, the tethered-loop axis model proposes that binding of Mer2 to both, Xrs2 and Spp1, tethers the

chromatin loop to the axis, enabling the accessibility of Spo11 to the chromatin loop for cleavage (Lam & Keeney, 2014) (Figure 1-5)

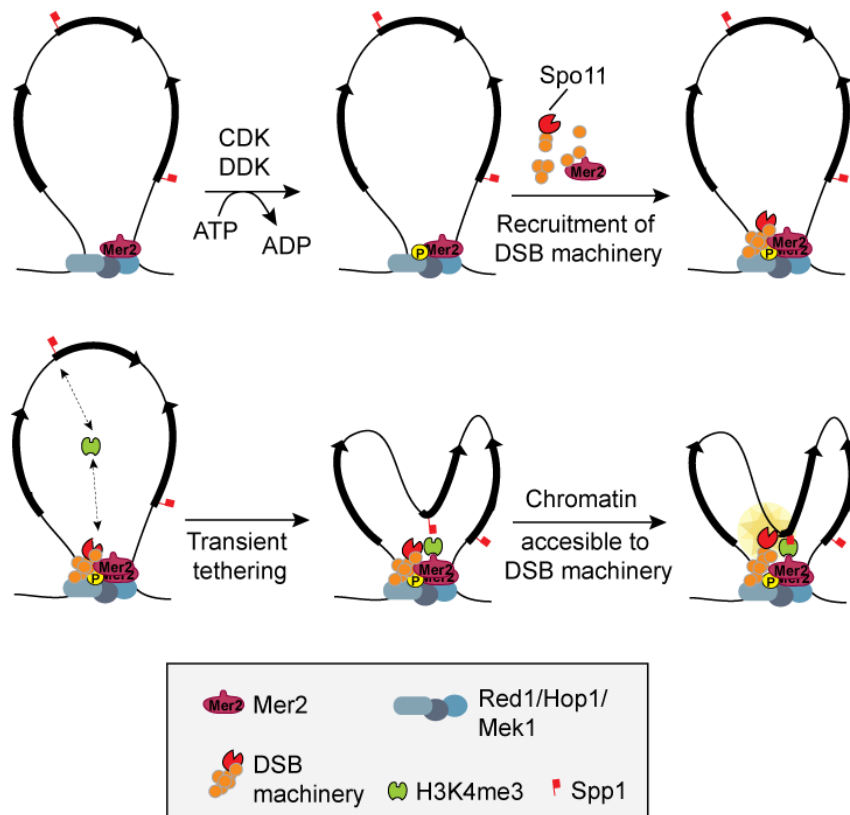


Figure 1-5 Tethered loop-axis model for DSB formation in *S. cerevisiae*

Model integrating DSB formation with loop-axis chromosomal structure (only one sister chromatid is represented for clarity). Mer2 (red) is localized to chromosome axes, together with the axial element proteins Red1, Hop1 and Rec8 (blue ovals). After CDK phosphorylation and further DDK-mediated phosphorylation, Mer2 is enriched at the axes. Mer2 associated to the axes interacts with Spp1 (light green), which binds H3K4me3 (red squares), transiently anchoring the chromatin loop to the axes in the so-called “tethered loop-axis” conformation. Tethering the loop makes the nucleosome-depleted promoter near the tethered loop accessible to the rest of components of the DSB machinery (represented in orange; the catalytic core of the DSB machinery (Spo11) is represented in red), located at the chromosome axes. Transiently tethering the chromatin loops enables the introduction of DSBs. Gray arrows on the chromatin loop represent gene open reading frames. P stands for phosphorylation. Modified from Keeney, 2001.

1.2.2 Non-random spatial distribution of DSBs across the genome

Meiotic DSBs are not randomly distributed across the genome. DSB formation is an inherently dangerous, yet necessary process for establishing physical linkages between homologous chromosomes, and as such, proper location of DSBs must be tightly controlled in

order to preserve genome integrity (Lichten & Goldman, 1995; J. Pan *et al.*, 2011; Petes, 2001).

Recent studies have shown that DSB patterns are shaped at multiple levels that regulate not only the number of DSBs introduced per cell, but also that those DSBs are spatially regulated. DSBs are preferentially formed in discrete regions (typically <250 bp) termed “hotspots”. In budding yeast, there are around ~3600 hotspots (1 hotspot/3.4kb) that consist of clusters of approximately 200 bp, in which the Spo11 machinery cleaves preferentially (Lam & Keeney, 2014; Pan *et al.*, 2011). In *S. cerevisiae* these hotspots are designated by a simultaneous combination of several factors that enable the “unlocking” of a region for DSB introduction and recombination. Most of the hotspots in budding yeast are influenced by chromatin structure, being most of them nucleosome-depleted regions (NDRs), a feature associated with gene promoters. However, the presence of an NDR is not *per se* sufficient to designate a region with high DSB activity and the final DSB patterning is a result of several layers of regulation (Figure 1-6). The introduction of DSBs is more frequent in the GC-rich chromatin loops than in the AT-rich DNA of the axis and thus, meiotic hotspots fall predominantly in chromatin loops. Some studies in budding yeast have associated trimethylation of lysine 4 at histone H3 (H3K4me3) to the designation of DSB sites, which is supported by the observation that deletion of Set1 (methyltransferase responsible for this modification) shows reduced DSB frequency in several hotspots (Acquaviva *et al.*, 2016; Cooper *et al.*, 2016; Pan *et al.*, 2011; Sommermeyer *et al.*, 2013). However, there is a weak correlation genome-wide between H3K4me3 and DSBs levels. It is worth mentioning that this chromatin modification (H3K4me3) is commonly associated with the transcriptional activation of nearby genes, offering a link between the designation of hotspots and transcriptional activity (Tischfield & Keeney, 2012). In striking contrast to budding yeast, within some mammals (*Homo sapiens* – *H. sapiens*– and *Mus musculus*), a single protein named PRDM9 has emerged as the main determinant of hotspots (Baudat *et al.*, 2010; Cooper *et al.*, 2016; Lam & Keeney, 2014, 2015). PRDM9 binds to consensus sequences determined by its zinc finger motif and enables the introduction of DSBs by trimethylating lysine 4 of histone H3 (H3K4me3) and potentially recruiting the Spo11 machinery to those sites, again highlighting the connection between H3K4me3 and DSB formation.

Besides spatial regulation, there are mechanisms that regulate DSBs levels. In *S. cerevisiae*, approximately ~150-200 DSBs formed per cell (Pan *et al.*, 2011). Regulation of DSBs levels occurs both *in cis* and *in trans* by the coordinated action of Tel1/Mec1, and the meiotic chromosomal organization in chromatin loops appears to be critical for this regulation. *In cis*, the presence of a strong hotspot suppresses DSBs in the same chromatid, probably to avoid coincident DSBs in the same chromatin loop. Regulation *in trans* guarantees that when DSBs are formed in a chromosome, DSBs on the sister chromatid and/or homolog are suppressed, ensuring the existence of an intact repair template.

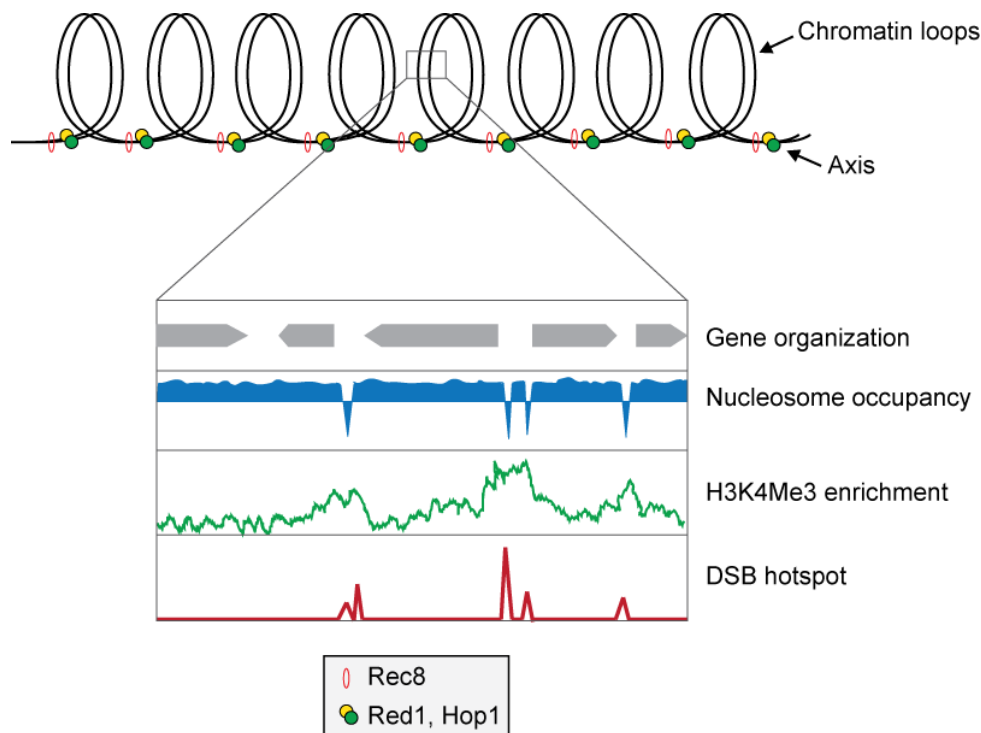


Figure 1-6 Meiotic DSB hotspot designation in *S. cerevisiae*

Model representing the layers that influence the DSB hotspot designation in *S. cerevisiae*. In budding yeast, chromosomes undergo structural changes and arrange into loops (depicted in black) that are anchored at their bases to a proteinaceous axis, which is mainly defined by Red1, Hop1 and cohesin (Rec8) (yellow, green and red circles, respectively). DSB formation and recombination is dependent on the chromatin organization, being more frequent in chromatin loops than in the axis. Meiotic DSB hotspots (red lines) in this organism are designated by a combination of factors. Most of the hotspots are influenced by chromatin structure and usually occurred in nucleosome-depleted regions (NDRs), a feature associated with gene promoters (nucleosome occupancy is represented in blue; genes are represented in grey). Besides the presence of an NDR, the DSB patterning is influenced by other factors, such as the trimethylation of lysine 4 at histone H3 (H3K4me3; represented in green), which seems to influence the designation of DSB sites. Adapted from Cooper *et al.*, 2016.

The regulation of DSBs *in cis* and *in trans* is often referred to as “DSB interference” and it is critical to ensure that DSB formation and recombination events are evenly distributed, having implications as well in the DSB levels. However, the mechanisms of DSB interference are not fully understood. Tel1 mediates DSB interference over domains of ~70-100 kb, which is likely modulated by the organization of meiotic chromosomes. In the absence of Tel1, DSBs occur independently of each other over mid-long distances (>20-100 kb), whereas over short distances (<20 kb), loss of Tel1 activity leads to the formation of DSB in individual hotspots at a higher frequency than expected by random expectation. It has been proposed that tethering of chromatin loops to the chromosomal axes could pre-activate those loops for DSB formation. DSB formation at a hotspot probably activates a Tel1-suppressive effect, repressing DSB formation at adjacent hotspots in the same loop and neighboring regions. The effect of Tel1 deletion over short distances suggests that Tel1 normally suppresses the tendency of Spo11 to generate clusters of chromatin loops within domains where DSB form. Thus, Tel1 negatively regulates meiotic DSB levels and this has been shown to influence the DSB “landscape” at a population level (Keeney *et al.*, 2014). The mechanisms of trans-interference are less clear, but both Tel1 and Mec1 have been implicated in DSB regulation *in trans* (Cooper *et al.*, 2016; Garcia *et al.*, 2015).

Another aspect of DSB formation that needs to be controlled is the time in which these breaks are formed. In budding yeast, DSB introduction is restricted to a narrow window of opportunity in prophase I and occurs once DNA has been replicated (~1-1.5 h after pre-meiotic DNA replication) (Borde *et al.*, 2000; Murakami *et al.*, 2003). The coordinated action of CDK-S and DDK in both origins of replication firing and DSB formation ensures that DNA replication precedes DSB formation. The requirement of CDK-S and DDK activities are higher for DSB formation than for origin firing, and such levels of both kinases activities are achieved at a later time point. However, besides the linkage of DNA replication and DSB formation, the latest can occur in absence of pre-meiotic replication. In addition, passage through pachytene I finalises the window for Spo11 cleavage.

As mentioned above, mechanisms have evolved to protect certain genomic regions from DSB formation, due to the fact that the introduction of DSBs and recombination in such regions can have deleterious, downstream effects, threatening genome stability. These regions that receive less DSBs are referred to as “coldspots”. These coldspots include, among others, pericentric and subtelomeric zones (where DSBs are 2-3 and 3.5 fold below genome average, respectively) (Blitzblau *et al.*, 2007; Gerton *et al.*, 2000; Petes, 2001). COs at centromeric

regions can be deleterious since they can cause precocious disjunction of sister chromatids in meiosis I, which in yeast results in aneuploidy and spore unviability. In addition, repetitive regions such as the ribosomal DNA –rDNA– of budding yeast also endanger genome stability, since DSB introduction in repetitive DNA sequences and their repair by non-allelic homologous recombination (NAHR) can lead to genome rearrangements (Gottlieb & Esposito, 1989; Vader *et al.*, 2011).

1.3 Repetitive elements of the DNA and heterochromatin: the ribosomal DNA (rDNA) as a model of repetitive DNA

1.3.1 Repetitive DNA and principles of heterochromatin formation

Repetitive elements of the DNA are a shared feature of the genome of many eukaryotes and consist of identical or nearly identical DNA sequences, which depending on the organism, are present in (sub-) telomeric and (peri-) centromeric regions, micro and macrosatellites, transposable elements and the ribosomal DNA (rDNA). As mentioned earlier, these repetitive elements present a high risk for genome integrity, since DSB formation in these regions and subsequent repair by NAHR can lead to aberrant loss or gain of DNA. In humans, NAHR occurring in the germline is a major cause of chromosomal alterations that are linked to infertility and several genetic disorders (Sasaki *et al.*, 2010). As such, these regions necessitate mechanisms to protect them from inherently dangerous events, like DSB formation and recombination.

Repetitive regions are often transcriptionally repressed regions, also referred to as “silenced regions”, which constitute the heterochromatic portion of the genome. Heterochromatin, in contrast to euchromatin, is more tightly packaged throughout the cell cycle and in most eukaryotes is present in telomeres, pericentromeric regions and the rDNA loci. The main feature of heterochromatin in *S. pombe* and other eukaryotes is the presence of heterochromatin proteins, such as a H3-K9 methyltransferase and the chromodomain-containing protein HP1 (heterochromatin protein 1), which are absent in *S. cerevisiae* (Hickman *et al.*, 2011). In budding yeast heterochromatin has a distinct molecular composition and thus, the concept of heterochromatin in this organism differs from the typical heterochromatin definition in most eukaryotes (mostly characterized by HP1). Budding yeast heterochromatin is generally characterized as repressive chromatin defined by hypoacetylation mediated by silencer proteins (see below) (Hickman *et al.*, 2011). However, the budding yeast heterochromatin shares a common feature with the canonical

heterochromatin, which is its arrangement into a more compacted structure. In budding yeast there are three heterochromatic regions: the rDNA, telomeres and the *HM* mating-type loci. Although silencing in these regions is driven by similar basic principles and involves the action of a protein family known as “Silent Information Regulators” (SIR), there are several distinct features in the establishment of the silencing among them. In *S. cerevisiae*, silent chromatin contains histone octamers usually lacking most of the acetylation and methylation modifications and binds SIR proteins (Sir1, Sir2, Sir3 and Sir4) (Kueng *et al.*, 2013). Silent chromatin in the HM mating-type loci and telomeres is fundamentally similar and requires the action of all four SIR proteins, whereas the rDNA array requires the histone deacetylase (HDAC) Sir2, but not Sir1/3/4 (Imai *et al.*, 2000). The most accepted view is that the SIR complex silences the specialized chromatin structure assembled by blocking the access of transcription factors to DNA-promoters. Ultimately, the SIR complex influences transcription in genes located within or close to the silenced domains, potentially allowing small factors to bind, but obstructing the access of RNA polymerase II (PolII) (Gartenberg & Smith, 2016; Hickman *et al.*, 2011; Rusche *et al.*, 2003).

In budding yeast, the best-characterized system of heterochromatin assembly is the silencing of the mating-type genes at the *HM* mating loci. These loci comprise pairs of genes, the “a” genes at *HMR* (*HMRa*) and the “ α ” genes at *HML* (*HML α*), that enable mating-type switching, but that need to be silenced in order to maintain haploid mating-type identity and the capacity to mate. The establishment of silencing normally comprises two phases, known as nucleation and spreading (Gartenberg & Smith, 2016). Silencing is initiated at defined DNA regions, termed silencers. Both *HMRa* and *HML α* are flanked by silencers (namely, *E* – essential– and *I*–important–), which have binding sites for silencing proteins (Origin Recognition Complex (ORC) and the transcription factors Rap1 and/or Abf1). The Orc1 subunit of ORC recruits Sir1 to the *HM* silencers in the mating-loci (Foss *et al.*, 1993; Fox *et al.*, 1997, 1995; Hou *et al.*, 2005; Oppikofer *et al.*, 2013). Although the core SIR proteins cannot recognize these specific DNA sequence motifs (silencers), they are recruited through protein-protein interactions with several silencer-binding factors (ORC, Abf1 and Rap1) in a sequence-specific manner (Gartenberg & Smith, 2016; Triolo & Sternglanz, 1996). At telomeres, the silencer role is fulfilled by the telomeric TG₁₋₃ (Thymine-Guanine) repeats, since the SIR proteins are directed to these repeats through interactions with Rap1. In addition, subtelomeric repeats contain elements called “protosilencers” that do not have

silencing function on their own, but that cooperate with silencers over a distance to maintain the silenced state.

In the mating loci and telomeres of *S. cerevisiae*, the principles of heterochromatin formation are as follows: in the first nucleation step, Sir1 associates to the silencer regions through interaction with silencer-binding factors. Subsequently, Sir1 leads to the sequence-specific recruitment of other Sir proteins (Sir2/3/4 (SIR) complex), thus acting as an adaptor between silencer-associated proteins and the SIR complex and functioning as a silent chromatin nucleator. Sir2 NAD⁺-dependent deacetylase activity deacetylates the N-terminal tails of neighboring H3 and H4 histones, creating new high-affinity binding sites for Sir3 and Sir4, which in turn, recruit additional Sir2. Sir3 and Sir4 also associate with Rap1 and bind preferentially to deacetylated H3 and H4 histones. In addition, Sir4 associates to ORC-bound Sir1 and Sir2, and thus serves as a scaffold, linking Sir2 to silencer-bound proteins. The NAD⁺-dependent histone deacetylase activity of Sir2 is essential for the SIR protein silencing and spreading. Ultimately, sequential rounds of histone deacetylation in closeby nucleosomes leads to the spreading of the silencing until either a barrier is reached or until the pool of free SIR proteins is below a threshold (Bell *et al.*, 1995; Gartenberg & Smith, 2016; Kueng *et al.*, 2013; Oppikofer *et al.*, 2011)

In budding yeast, SIR complexes can spread a few kilobases (kb). However, close to the silenced domains there are essential genes (such as genes necessary for yeast growth) that might be threatened by the transcriptional silencing that spreads from adjacent silencing regions. Thus, silenced regions need boundary elements (also referred to as insulators) that regulate the spread of the silencing in order to protect nearby genes. Although the mechanisms of heterochromatin boundary formation are still poorly characterized, this is thought to arise either from specific DNA elements or from competition between acetylated and deacetylated histones.

So far, in budding yeast there have been several elements linked to either the establishment of boundaries to the SIR complex spreading or that influence, up to a certain extent, boundary formation in the different heterochromatic regions. There are five different kinds of transposons in *S. cerevisiae* (Ty1-Ty5) that, together with LTR (long terminal repeat) sequences, tend to flank silenced regions (*HMR* and telomeres) and that influence boundary formation, linking transposons and silencing. The right boundary at the *HML* locus is established by the unidirectional spreading of silencing towards the mating-type genes from

the *HML-I* silencer. Although there is no clear boundary flanking this locus, there is an *UAS_{rrg}* (upstream activation sequence of ribosome protein genes) that binds the protein Rap1 and that can function as a boundary element by forming a gap between nucleosomes, therefore halting propagation of the SIR complex (Gartenberg & Smith, 2016; Sun *et al.*, 2011). By contrast, *HMR* silencing spreads bidirectionally from the silencers sequences and its boundary elements are better defined than in the *HML* locus. Besides the Ty1-LTR and the Ty5-LTR that are flanking the *HMR* locus and that contribute to boundary function, there are other elements involved in controlling the spreading of the SIR proteins. The right flank of this locus is more efficient than the left boundary. Propagation at the right flank of *HMR* is halted by a tDNA boundary (tRNA^{Thr} gene) (Donze & Kamakaka, 2001; Sun *et al.*, 2011). The antisilencing property of this class of barrier elements has been linked to RNA PolIII transcription of tRNAs, which begins with the assembly of the TFIIC transcription factor at the box A and box B promoter elements, followed by recruitment of TFIIB and RNA PolIII. tRNA^{Thr} binds TFIIC and tRNA-bound PolIII transcription factors help to create a histone-depleted region around this tRNA. Another pathway to establish a SIR barrier is the competition between histone acetyltransferases (for instance, Sas2) and Sir2 histone deacetylases, in such a manner that acetylated nucleosomes block the spreading of deacetylated nucleosomes by the SIR complex. At the *HMR* left boundary, spreading is stopped from the *HMR-E* silencer, but the mechanisms by which this occur are not fully understood (Donze *et al.*, 1999; Sun *et al.*, 2011; Thurtle-Schmidt *et al.*, 2016).

In *S. cerevisiae*, boundaries at telomeric regions are established by opposite activities of Sir2 and Sas2, which deacetylate and acetylate lysine 16 in histone H4 (H4K16), respectively. Sas2 acts thus as a boundary by competing with Sir2 deacetylation and, as a consequence, restricts SIR spreading when H4 is acetylated at K16 in the adjacent chromatin. In addition to competition between Sir2 and Sas2, methylation of H3K79 by the histone methyltransferase protein Dot1 also contributes to antisilencing (Sun *et al.*, 2011; Van Leeuwen *et al.*, 2002). Thus, the main mechanism by which silencing barriers are established in the telomeric regions is by competition between different chromatin modifications. Silencing at the rDNA locus is governed by the same deacetylation principle, but is mechanistically distinct from silencing at the *HM* loci and telomeres (Gartenberg & Smith, 2016; Hickman *et al.*, 2011). Additionally, the establishment of boundaries for silencing spreading presents unique characteristics. Silencing and SIR spreading at the rDNA are further detailed in section 1.3.2.

1.3.2 Ribosomal DNA (rDNA)

1.3.2.1 Structure, function and silencing of the rDNA

Genes that encode for RNA products, such as the transfer RNA (tRNA) genes and the ribosomal DNA (rDNA) are characterized for not having an expression increase achieved by the amplification step during protein translation. Hence, cells normally harbor many copies of these genes. Such is the case of the rDNA, which is transcribed to produce the ribosomal RNA subunits that are crucial for the assembly of the ribosomes, the protein factories of the cell. The product of the rDNA (ribosomal RNA, rRNA) accounts for approximately 60% of the total RNA of the cell and, in most eukaryotes, these genes are present in high copy and are transcribed at a high rate to cope with the high demand of ribosomes required for protein synthesis (Ganley & Kobayashi, 2014; Ide *et al.*, 2010; Kobayashi & Sasaki, 2017).

In humans, each rDNA repeat is ~43 kb and is distributed into five acrocentric autosomal chromosomes (Chrm. 13, 14, 15, 21 and 22) (Henderson *et al.*, 1973). The human rDNA is contained in nucleolar organizer regions (NORs), composed of 300-400 copies per haploid genome. In contrast, in budding yeast, the rDNA locus comprises a single tandem array of ~150-200 repeats of 9.1 kb each, located in the long arm of chromosome *XII* and packed into a distinct membraneless structure, the nucleolus, localized at the periphery of the nucleus (Petes, 1979) (Figure 1-7). Each 9.1 kb repeat is composed of a region encoding the 35S ribosomal RNA precursor (transcribed by RNA polymerase I), that is spliced into three mature rRNAs (25S, 18S and 5.8S), and the small 5S precursor (transcribed by RNA polymerase III), separated by two intergenic spaces (*IGS1* and *IGS2*), sometimes referred to as “non-transcribed spacers” (*NTS1* and *NTS2*) or “intervening sequences” (*IVS*) (Granneman & Baserga, 2005; Srivastava *et al.*, 2016). *NTS1* contains the Pol I-termination sequences and a RFB (Replication Fork Barrier) sequence, where a protein called Fob1 binds to prevent collision of the transcription and replication machinery. In addition, *NTS1* harbors a bi-directional RNA polymerase II promoter (E-pro), which is normally silenced. *NTS2* encompasses the Pol I promoter and an autonomous replication sequence (*ARS*), critical for DNA replication (see section 1.4.2.2). The mature 18S, 5.8S, 25S and 5S rRNAs, together with ribosomal proteins, constitute the ribosomes, which translate mRNA into proteins and are thus crucial for gene expression.

Although the rDNA is transcribed at a high rate, RNA polymerase II-driven transcription in this locus is hindered by a mechanism that resembles silencing at the *HM* loci

and telomeres, but that requires only Sir2 (Gartenberg & Smith, 2016; Gottlieb & Esposito, 1989). The fact that a mechanism exists at the rDNA to silence Pol II-dependent transcription when this locus is transcribed to rRNA by Pol I and Pol III came initially as a paradox. However, later studies showed that PolIII transcription from the bi-directional E-pro promoter at the *NTS1* region destabilizes the rDNA and must be therefore normally suppressed by Sir2 (Kobayashi & Sasaki, 2017). The most accepted model of how E-pro transcription originates rDNA instability is linked to cohesion at the rDNA. Cohesin binds to the *NTS* regions and it is thought to maintain the integrity of the rDNA repeats. Fob1 binding to the RFB site to pause the replication fork yields DSBs that induce repair by rDNA recombination. Here, cohesin-mediated cohesion of the rDNA helps in promoting equal sister chromatid exchange during recombination, maintaining the integrity of the repeats. Thus, Sir2-mediated rDNA silencing serves to control rDNA stability by regulating PolIII transcription at the intergenic spacers (Gartenberg & Smith, 2016; Srivastava *et al.*, 2016).

rDNA transcriptional silencing occurs more strongly within the *NTS1* and *NTS2* regions and involves the action of the RENT (regulator of nucleolar silencing and telophase) complex, which is composed of Sir2, Cdc14 and Net1, and specifically silences Pol II-transcription within the rDNA through the histone deacetylase activity of Sir2 (Shou *et al.*, 1999; Straight *et al.*, 1999). In the budding yeast rDNA, Sir2-dependent silencing occurs as follows: Sir2 (as part of the RENT complex) is recruited to *NTS1* via interaction with Fob1, which binds to the RFB sites (Ter1 and Ter2), whilst recruitment of the RENT complex to *NTS2* occurs via Net1 tethering to RNA PolII at the 35S rDNA promoter. At *NTS1* and *NTS2*, RENT recruitment further recruits Sir2 to the chromatin, and Sir2 deacetylation hinders PolIII activity. Binding of the RENT complex nucleates a Sir2-dependent chromatin structure that spreads in a form analogous to the Sir2/3/4 spreading mechanism at the HM loci and telomeres (Buck *et al.*, 2002; Gartenberg & Smith, 2016; Huang & Moazed, 2003).

Spreading of the rDNA silencing occurs unidirectionally towards the centromere-proximal (right) region of the rDNA, but not towards the telomere-proximal (right) flank of the rDNA. rDNA spreading occurs in the direction of PolIII transcription (leftward within the rDNA repeat) and requires transcription by PolII (Gartenberg & Smith, 2016; Srivastava *et al.*, 2016). The unique sequence flanking the first rDNA repeat (*RDNI*) is a gene free region that spans ~2.4 kb, until a LTR, a tRNA gene and a small gene encoding a subunit of RNase H. All these elements precede the nearest essential gene (*ACS2*), which encodes for acetyl-CoA synthetase required to provide acetyl-CoA for histone acetylation. Impairment of this gene

results in histone deacetylation and impacts global transcription (Biswas *et al.*, 2009; Laloraya *et al.*, 2000). Thus, there should exist protective mechanisms to avoid propagation of the rDNA silencing, so that it does not encroach this essential gene.

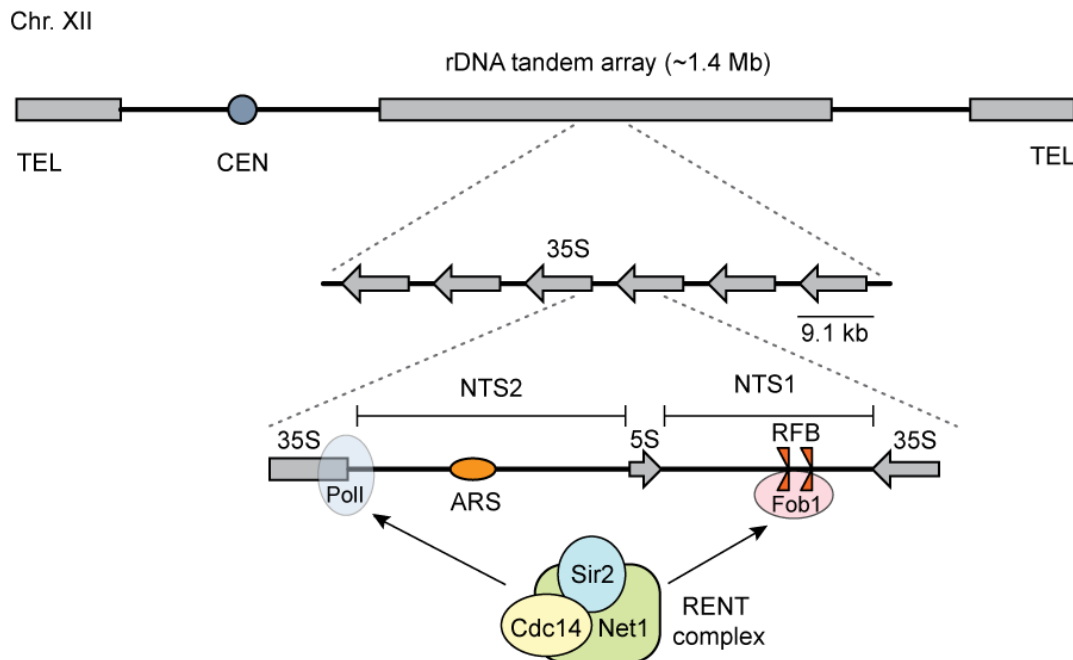


Figure 1-7 Schematic representation of rDNA structure and rDNA transcriptional silencing

The budding yeast ribosomal DNA (rDNA) consist of 150-200 tandem copies of a 9.1 kb repeat on the right arm of chromosome *XII* that assembles into the nucleolus, at the periphery of the nucleus. Each repeat encodes a copy of the Pol I-transcribed 35S precursor ribosomal RNA (rRNA) (that gives rise to the mature 25S, 18S and 5.8S mRNAs) and a copy of the small 5S RNA (transcribed by Pol III), separated from each other by non-transcribed spacers (*NTS1* and *NTS2*). *NTS2* contains the Pol I promoter and an origin of replication or autonomous replication sequence (ARS), and *NTS1* contains a replication fork block (RFB; formed by the Ter1 and Ter2 sites, orange triangles), where a protein called Fob1 binds. The RENT complex is constituted of Sir2, Cdc14 and Net1. Sir2-dependent transcriptional silencing at the rDNA occurs via recruitment of Sir2 (as part of the RENT complex) to *NTS1* via interaction with Fob1. Recruitment of RENT is also mediated via Net1 tethering to RNA Pol I at the rDNA 35S promoter in *NTS2*. Recruitment of the RENT complex nucleates a Sir2-dependent silent chromatin structure that spreads via Sir2-mediated histone deacetylation. Position of centromere (CEN) and telomere (TEL) on chromosome *XII* are indicated. Adapted from Buck *et al.*, 2016.

The left edge of the rDNA tandem array ends at the Ter2 within the RFB of the terminal *NTS1* element. The Ter1 site at the boundary between the leftmost rDNA repeat and the unique chromosome *XII* sequence is truncated and inactive. Therefore, at the leftmost

boundary, silencing is suboptimal due to the reduced recruitment of the RENT complex. However, binding of RENT to Ter2 is able to nucleate Sir2-silencing and moderately spread into the left adjacent chromatin. In conditions of normal levels of Sir2, silencing spreading is then blocked by this genetically defined barrier of the rDNA, which occurs between 300 and 600 bp away from the left flank of the array (Buck *et al.*, 2016, 2002; Gartenberg & Smith, 2016). When the nucleolar levels of Sir2 are upregulated (for instance, when silencing at telomeric regions is impaired or when there is a decrease of rDNA repeats) distinct mechanisms operate to halt the silencing spreading arising from the rDNA. Until recently, it was unclear how this spreading of the silencing was limited at the rDNA locus, but recent studies have demonstrated that a 427 bp fragment upstream of *RDNI* blocks silencing and acts as a functional barrier. This fragment is located approximately 2.4 kb to the left rDNA boundary and harbors a gene encoding tRNA^{Gln} and a Ty1-LTR sequence, and has a strong silencing barrier activity. Sir2 overexpression leads to silencing spreading up to ~2.4 kb until the tRNA^{Gln} boundary element (Biswas *et al.*, 2009; Gartenberg & Smith, 2016). This barrier function needs the Sas2 and Gcn5 histone acetyltransferases. The fact that Sas2 acetylates H4K16, the same residue that is deacetylated by Sir2, raises the possibility that barrier elements recruit Sas2 to counteract deacetylation by Sir2. The barrier activity of the tRNA^{Gln} also depends on the Smc1 cohesin subunit, similar to what occurs at the *HMR* locus. Interestingly, near the left rDNA flank, there is a prominent cohesin-binding site (*CARL2*, cohesin-associated region L2) (Laloraya *et al.*, 2000). Thus, the centromere-proximal (left) region of the rDNA repetitive locus is controlled by the tRNA^{Gln} gene, which acts as a silencing boundary, and is also influenced by the Sir2 protein levels (Biswas *et al.*, 2009; Sun *et al.*, 2011).

1.3.2.2 The integrity of the rDNA and rDNA amplification system

A remarkable aspect of the budding yeast rDNA is that, besides having ~150-200 tandem repeats of the rDNA genes, only around half of these copies are transcribed (Ide *et al.*, 2010; Salim *et al.*, 2017). The role of these “extra” (non-transcribed) copies has been the focus of extensive research. It has been shown that strains with fewer rDNA copies present higher sensitivity to DNA damage. This phenomenon is due to the heavy transcription of *Poll* that occurs to compensate for the lower copy number of rDNA genes and, which compromises rDNA replication and recombination repair (Iida & Kobayashi, 2019; Kobayashi *et al.*, 1998). Due to its repetitive nature and high transcriptional rates, the rDNA is essentially unstable and is the main target for homologous (mitotic) recombination

(Gottlieb & Esposito, 1989; Petes, 1980; Petes & Botstein, 1977). Homologous recombination at the rDNA normally takes place by repairing DSBs (that arise from exposure to external DNA damage agents or as a consequence of stalled replication forks) with the nearest sister chromatid and is a crucial process to rescue stalled replication forks and preserve rDNA repeats. When transcription is up-regulated, repair of DSBs with the nearest sister chromatid is compromised, which can lead to aberrant recombination and DSB repair by unequal sister chromatid exchange (USCE). This subsequently leads to rDNA array expansion or contraction, causing changes in the number of rDNA repeats (Ide *et al.*, 2010; Kobayashi *et al.*, 1998). Therefore, since an intrinsic feature of repetitive genes is the tendency to lose copies during homologous recombination and this is the main cause for genomic instability within the rDNA, *S. cerevisiae* counts with a so-called “rDNA amplification system”, in which PolIII-transcription from E-pro (normally repressed by Sir2) and cohesin play a critical role. The rDNA amplification system ensures the maintenance of multiple copies of rDNA above a certain threshold, so that rDNA transcription rates can remain low and replication-coupled recombination repair can occur efficiently by repairing the DSBs originated at RFB with the sister chromatid (Ganley & Kobayashi, 2014; Kobayashi, 2014). The establishment of this rDNA amplification system might have been an evolutionary mechanism: cells from higher organisms might have necessitated more ribosomes and thus, more rDNA transcription. An increase in transcription rates would have been deleterious for cells due to an increased sensitivity to DNA damage. Therefore, there would have been a selection for the prevalence of multiple rDNA copies, leading to the establishment of the rDNA amplification system (Ide *et al.*, 2010; Kobayashi, 2006; Kobayashi *et al.*, 1998). Another phenomenon derived from a higher USCE, is the formation of extrachromosomal rDNA circles (ERCs) that replicate in each S phase, but are not properly segregated into the daughter cells due to the lack of centromere (Sinclair & Guarente, 1997). These ERCs have been linked to cell senescence in budding yeast, and since they arise from recombination at the rDNA (which is up-regulated in cells lacking Sir2), Sir2 heterochromatin has been extensively studied as a determinant of cell life span (Ganley & Kobayashi, 2014; Kobayashi, 2006, 2014; Kobayashi & Sasaki, 2017; Rusche *et al.*, 2003).

As stated in section 1.1.2, DSBs within repetitive regions are hazardous for the cell, since they can be repaired by NAHR. Moreover, DSBs adjacent to repetitive DNA can also trigger NAHR and can equally compromise genome integrity. As mentioned earlier, the budding yeast rDNA consists of approximately 150-200 copies tandemly arrayed into a single

locus and Sir2 is required for suppressing mitotic and meiotic DSBs and recombination within the rDNA repeats (Gottlieb & Esposito, 1989; Petes, 1979). Meiotic recombination at this region is estimated to be 50-fold less frequent than recombination in non-ribosomal nuclear DNA and this suppression of meiotic recombination at the rDNA is essential, since unequal crossover recombination events among repeats can lead to large deletions or duplications of rDNA copies (Petes & Botstein, 1977). It has been shown that the meiosis-specific AAA⁺ ATPase (ATPases associated with diverse cellular activities) Pch2 (Pachytene checkpoint 2) is also involved in repressing meiotic inter-homolog recombination at the rDNA (San-Segundo & Roeder, 1999). Remarkably, although previous studies have shown that DSBs are almost absent from the rDNA cluster (Petes, 1980; Petes & Botstein, 1977), the edges of this region present a high risk of genome rearrangement and DSBs, which necessitates special DSB protection (Vader *et al.*, 2011). Strikingly, Vader *et al.* demonstrated that, even if Sir2 suppresses DSBs within the rDNA, Sir2-dependent heterochromatin promotes meiotic DSB formation at the boundaries of the rDNA. This localized Sir2-DSB-promoting effect at the rDNA borders needs an rDNA-boundary specific system that minimizes Spo11-dependent DSBs formation. This protective mechanism involves the AAA⁺ ATPases Pch2 and the origin recognition complex subunit Orc1 (San-Segundo & Roeder, 1999; Vader *et al.*, 2011). In the absence of this ‘anti-break’ system, strong DSBs occur at the rDNA boundaries, leading to unequal recombination within the first ~10 rDNA repeats. Moreover, the localization of Pch2 to the nucleolus (where the rDNA assembles) is dependent on both Sir2 and Orc1, and an Orc1 temperature-sensitive mutant (*orc1-161*) phenocopies *PCH2* deletion (*i.e.* increased DSB formation and recombination at the right rDNA flank; see section 1.4.1.1) (Vader *et al.*, 2011). Therefore, Pch2 and Orc1 counteract the Sir2-DSB promoting activity and collaborate in order to suppress meiotic DSB introduction and recombination at the rDNA boundaries. However, the mechanism and characteristics of this “anti-DSB” system have remained unknown so far.

1.4 AAA⁺ ATPases

AAA⁺ ATPases (ATPases associated with various cellular activities) constitute a subfamily of the Walker-type nucleoside triphosphate (NTP) binding proteins, also known as Walker-type NTPases, referring to the presence of specific motifs (Walker A and B; see below) first reported by Walker and co-workers (Hanson & Whiteheart, 2005; Ogura & Wilkinson, 2001; Walker *et al.*, 1982). The AAA⁺ ATPase family is a large and functionally diverse group of proteins that transforms chemical energy into conformational changes to a

wide range of substrates. The hallmark of AAA⁺ ATPases is a structurally conserved ATP-binding domain consisting of approximately 200-250 amino acids, referred to as “AAA⁺ domain”, “AAA⁺ module” or “AAA⁺ cassette”, which is able to oligomerize to form assemblies that constitute the active form of the AAA⁺ ATPases. In these oligomeric protein complexes, the functional nucleotide-binding site (also referred to as ATP-binding site) is constituted by shared regions within pairs of subunits that associate (see below). Upon ATP binding and/or hydrolysis, AAA⁺ ATPases undergo conformational changes that are communicated to their substrate proteins and are ultimately responsible for their function (Gates & Martin, 2019; Hanson & Whiteheart, 2005; Ogura & Wilkinson, 2001).

AAA⁺ proteins are molecular engines that participate in a vast diversity of cellular processes, such as protein degradation, protein refolding, protein aggregate disassembly, DNA helicase activity, DNA replication initiation and intracellular transport (Hanson & Whiteheart, 2005; Ogura & Wilkinson, 2001; Tucker & Sallai, 2007). The functional diversity of the members of the AAA⁺ superfamily is given by the ability of these proteins to engage and interact with many distinct substrates. In addition, this functional heterogeneity derives from the heterogeneity of the amino acid residues that constitute the nucleotide-binding motifs, which influences different aspects, such as nucleotide-binding and hydrolysis rates, stability of the oligomers, specificity for the substrates and the mechanism by which conformational changes are coupled among subunits (Erzberger & Berger, 2006).

The classification of the different AAA⁺ proteins that belong to this superfamily is essentially challenging. A recent review of the literature on this topic established a classification of the members of the AAA⁺ superfamily in seven clades of proteins, based on sequence alignments and structural information, and attending mostly to the insertion of secondary structural elements at specific positions within or around the AAA⁺ module (reviewed in Erzberger & Berger, 2006). Although, most of the AAA⁺ ATPases assemble into hexameric (closed) rings with a central channel, proteins from some clades (1 and 2) comprise proteins that form “open-ring” assemblies, such as the heteropentameric clamp loader that have spiral arrangement or the bacterial replication initiator DnaA, which forms helical filaments (Erzberger & Berger, 2006; Yao & Donnell, 2012).

Though there are structural disparities among the different members of the AAA⁺ superfamily, here we focus on the “classic AAA⁺ ATPases”, which share a typical organizational structure of the AAA⁺ domain. This AAA⁺ domain comprises two subdomains

that are more conserved in terms of structure than in their sequence: an N-terminal α/β Rossman fold subdomain (which contains the nucleotide-binding pocket) and a C-terminal α -helical subdomain. The topology of the N-terminal α/β Rossman fold subdomain consists of a β -pleated sheet of parallel strands, which are connected through insertions of α helices. The number and position of these α helices confer diversity to the AAA⁺ modules and is one of the main differences among AAA⁺ proteins of distinct subfamilies (reviewed in Hanson & Whiteheart, 2005; Tucker & Sallai, 2007). The most NH₂-terminal part of this region harbors a conserved sequence motif known as “N-linker”, which has a sequence containing either glycine-glycine residues or a glycine preceded by another hydrophobic residue. The N-linker contributes to the ATP-binding pocket and it helps to connect one AAA⁺ domain to other non-AAA⁺ domain. Moreover, due to its flexibility, this linker can propagate nucleotide-dependent changes to other regions of the protein.

Another consensus motifs in the AAA⁺ module are the Walker A and Walker B motifs, which are critical parts of the ATP-binding site (Hanson & Whiteheart, 2005; Walker *et al.*, 1982). The mechanism of ATP hydrolysis of an AAA⁺ protein involves a nucleophilic attack of a water molecule on the γ -phosphate of the ATP. The Walker A motif contains highly conserved residues that form a P-loop that interacts directly with the phosphates of the ATP. This P-loop consists of a GXXXXGK(T/S) consensus sequence, where X represents any amino acid residue. The lysine (K) residue in this consensus sequence has a crucial function and mutation of this amino acid typically impairs nucleotide binding. The Walker B motif harbors an hhhhDE consensus sequence (where h represents any hydrophobic amino acid) and also interacts with the bound nucleotide. The aspartate (D) residue is involved in coordinating the Mg²⁺ required for ATP hydrolysis, whereas the glutamate (E) is likely activating the water for the hydrolysis reaction. When this glutamate residue is mutated, the nucleotides can still bind, but hydrolysis is abolished. Since ATP is needed for substrate binding in many, if not all ATPases, this amino acid substitution has been commonly used to generate “substrate-trapping mutants”, which are particularly useful to identify target proteins of AAA⁺ enzymes, since they can bind, but not release substrates (Babst *et al.*, 1998; Weibezahn *et al.*, 2003; Whiteheart *et al.*, 1994).

The “classical” family members also contain another motif, referred to as SRH (for second region of homology) situated C-terminally to the Walker B motif. This SRH has two characteristic structural elements: Sensor 1 (S-I) and one or two arginine residues, often known as “arginine fingers”. The S-I contains polar residues (usually asparagine (N)), but can

also be serine (S), threonine (T) or histidine (H)) and it probably acts in concert with the second acidic residue of the Walker B motif to orient the water molecule enabling the nucleophilic attack on the γ -phosphate of the ATP molecule (Hanson & Whiteheart, 2005; Tucker & Sallai, 2007). By inserting themselves, the arginine fingers from one subunit form part of the nucleotide-binding site of the adjacent subunit and are therefore critical to coordinate ATP hydrolysis and conformational changes between the subunits of the AAA⁺ oligomeric assemblies (Augustin *et al.*, 2009; Ogura *et al.*, 2004). Substitutions of these arginine fingers can thus affect nucleotide hydrolysis and propagation of hydrolysis-dependent structural changes. In addition, AAA⁺ ATPases contain a Sensor 2 (S-II) region near the C-terminal end of the AAA⁺ domain that also participates in nucleotide binding. The C-terminal α -helical subdomain is composed of several α -helices that arrange to form a partial lid over the nucleotide-binding site (Hanson & Whiteheart, 2005).

As mentioned earlier, AAA⁺ ATPases function by linking nucleotide binding and/or hydrolysis to conformational changes within the oligomeric assembly, which are propagated to domains linked to the AAA⁺ modules and transduced to target substrates. The typical arrangement of hexameric AAA⁺ ATPase assemblies has a number of implications. First, different subunits of the hexamer are intercoupled in such a manner that the arginine fingers of one subunit form part of the ATP-binding pocket of the adjacent one. Thus, the ATP-binding pocket is usually located at the interface between pairs of subunits of the hexameric assembly and each AAA⁺ module contributes to create this bipartite ATP-binding site. Second, ATP binding and hydrolysis at the interface of neighboring subunits can then be propagated, driving coordinated structural changes within the AAA⁺ assembly that can direct translocation or remodeling of target substrates. ATP binding and hydrolysis function as a switch between at least two distinct conformational states defined by ATP binding, ATP hydrolysis, and subsequent ADP release. Upon cycles of nucleotide-binding and release, the structural changes are propagated due to the conformational coupling by the arginine fingers shared within neighbouring AAA modules. Third, hexameric AAA⁺ enzymes have a central cavity or pore that is often used to thread DNA or protein substrates through, inducing conformational changes, as it is the case of AAA⁺ ATPases involved in protein unfolding (Hanson & Whiteheart, 2005; Wendler *et al.*, 2012a).

The ATP hydrolysis mechanism in AAA⁺ proteins that assemble into open-rings (see above) appear to function in a switch-like fashion. This is typical for assemblies in which ATP binding and hydrolysis are slow and which seem to function as bimodal switches, being

active upon nucleotide binding and resetting after hydrolysis and ADP release. On the other hand, AAA⁺ modules can also continuously coordinate cycles of nucleotide-binding and release, being like processive molecular motors (Erzberger & Berger, 2006). In AAA⁺ ATPases that form closed hexameric rings, structural rearrangements among the six subunits induced by ATP hydrolysis could occur by different proposed mechanisms, referred to as synchronized, rotational and sequential (Ogura & Wilkinson, 2001). In the synchronized model, ATP binds to and is hydrolysed in a concerted manner (six simultaneous ATP binding and hydrolysis events), probably leading to paddle-like movements. In the rotational model, only three of the subunits are active as ATPases and function in independent cycles of ATP binding and hydrolysis around the hexameric assembly; in this model, the three active subunits are always at different stages of the cycle (bound to ATP/ADP or with the nucleotide-binding site free). The sequential model proposes a mechanism derived from the rotational model, but in which all subunits are active; pairs of subunits on opposite sides of the ring are in the same state with one another (bound to ATP/ADP), but out of phase with the remaining subunits.

Since the classic AAA⁺ ATPases share a similar ATPase core, the functional diversity within this vast group of enzymes is generally determined by elements outside the AAA⁺ module. These proteins can interact with a wide variety of cofactors that can be functional partners (if they contribute to the catalytic activity of the assembly) or adaptor proteins (if they mediate substrate recognition). One of the best-studied cases of AAA⁺ ATPases with a wide range of cellular activities is Cdc48 (also known as p97 or N-ethylmaleimide sensitive fusion protein, NSF) (Meyer, 2012; Meyer & Wehl, 2014). Cdc48's ability to mediate a number of distinct cellular processes is determined by its NH₂-terminal domain (NTD), which is involved in substrate and/or cofactor recognition. Cdc48 is composed of an NTD, two tandem AAA⁺ domains (D1 and D2) and a flexible C-terminal tail (DeLaBarre & Brunger, 2003). The AAA domains arrange into two stacked rings with a central pore, critical to move substrates through the double ring. The D1 domain was thought to lack significant ATPase activity and was often referred to as hexamerization domain. However, recent studies showed that both AAA⁺ domains have ATPase activity, although their roles in processing substrates seem to be different (Bodnar & Rapoport, 2017; Ye *et al.*, 2003). Cdc48 functions unfolding ubiquitinated substrates by translocation through its central cavity, and ATP binding in D1 and D2, but only ATP hydrolysis in D2, are needed for substrate unfolding, whereas ATPase hydrolysis in the D1 rings is important for substrate release and to reset the NTD

conformation (Bodnar & Rapoport, 2017). Cdc48 serves as a classical example of AAA⁺ since changes in the nucleotide-bound state extensively vary the position of its NTD with respect to the AAA⁺ cassettes.

It is worth mentioning that there are a number of AAA⁺ modules that have degenerated into proteins that lack significant ATP binding and/or hydrolysis activity, such as Orc4 and Orc5 (both members of the ORC assembly). These degenerated AAA⁺ modules typically function as modulators or amplifiers between the active AAA⁺ subunits within the oligomeric assembly (Erzberger & Berger, 2006). Altogether, although there are significant molecular differences within the large AAA⁺ superfamily, AAA⁺ proteins share a number of commonalities in their structure and the basic mechanisms by which energy derived from ATP binding and hydrolysis are used to induce conformational changes onto their substrates.

1.4.1 Pch2 as a master regulator in meiosis and mitosis

Pch2 (Pachytene checkpoint 2) is a widely conserved member of the AAA⁺ ATPase family that controls multiple events during meiosis in budding yeast, whereas Pch2 homologs in several other species (such as the mammalian TRIP13) are also involved in the proper execution of the mitotic cell cycle (Bhalla & Dernburg, 2005; Joshi *et al.*, 2009; Nelson *et al.*, 2015; Roig *et al.*, 2010; Vader, 2014; Wu & Burgess, 2006; Zanders & Alani, 2009; Zanders *et al.*, 2011). In sections 1.4.1.1 and 1.4.1.2, we focus on the main aspects of Pch2 (and its homologs) and the processes that they influence during meiosis and mitosis, respectively.

1.4.1.1 Pch2 in meiotic G2/prophase

In *S. cerevisiae*, Pch2 is a meiosis-specific AAA⁺ ATPase involved in a myriad of processes during G2/prophase of the meiotic cell cycle. Pch2 was initially identified as a factor that influences chromosome synapsis in budding yeast (San-Segundo & Roeder, 1999). Homologs of Pch2 have been identified in multiple organisms, such as fruit flies, nematodes and mammals, and have both shared and unique functions. In budding yeast, in the absence of Zip1 (the central component of the SC), chromosomes fail to synapse leading to the accumulation of recombination intermediates, which ultimately results in a checkpoint-mediated arrest at the pachytene stage of meiotic prophase I. Pch2 deletion bypasses this Zip1 arrest, since *pch2Δzip1Δ* cells progress through meiosis. Although *pch2Δzip1Δ* cells have sporulation frequencies similar to wild type (WT) cells, spore viability in this double mutant is severely reduced (~37% of WT), indicating that in *pch2Δzip1Δ*, defects in chromosome

segregation due to the lack of Zip1 remain, and cells proceed through meiosis with unsynapsed chromosomes (San-Segundo & Roeder, 1999). Therefore, Pch2 is a meiotic checkpoint factor responsible for the pachytene arrest due to defects in chromosomal pairing and synapsis in budding yeast.

In *S. cerevisiae*, Pch2 expression is induced before cells undergo meiosis I (*i.e.* in G2/prophase), reaching its maximal expression at the pachytene stage and decreasing as meiosis and sporulation progress (San-Segundo & Roeder, 1999). In line with Pch2 being expressed in the early meiotic stages, the promoter region of Pch2 contains two elements that are characteristic of early meiotic genes (Mitchell, 1994): a sequence analogous to the URS1 (Upstream Regulatory Sequence) element (TGGGCGGCA, at position -97 to -89 relative to the ATG codon) and a T4C element (TTTTTCATCG, at position -181 to -173). In *zip1* Δ cells, Pch2 levels remain high at later time points, and show a Pch2-dependent arrest, indicative of an essential function of Pch2 for pachytene arrest (commonly referred to as pachytene checkpoint) in response to synapsis defects.

In *Caenorhabditis elegans* (*C. elegans*) the homolog of Pch2 (PCH-2) is required for apoptosis due to synaptic failures, indicating a role of PCH-2 in the synapsis checkpoint. Whilst in *S. cerevisiae* and *C. elegans* Pch2-dependent checkpoint seems to respond to synapsis defects, several mutants in *Drosophila* manifest Pch2-dependent delays without obvious defects in synapsis. Moreover, removing the central element (C(3)G) of the SC in *Drosophila* does not cause Pch2-dependent delays (Bhalla & Dernburg, 2005; Joyce & McKim, 2009). In this regard, several studies in *Drosophila* have proposed that in this organism the pachytene checkpoint is not monitoring synapsis *per se*, but rather responds to synapsis-dependent changes in the chromosomal axes structure that are required for crossover formation. In this organism, the pachytene checkpoint may function to promote an optimal number of crossovers by increasing the chance of DSBs becoming crossovers. Consistent with this, synapsis mutants in budding yeast and nematodes have defects in crossover production. Thus, it could be that the Pch2-dependent checkpoint is triggered by the effects of failures on proper synapsis on the crossover pathways. Importantly, although defects in chromosome synapsis lead to activation of Pch2-mediated pathways in many organisms, the ultimate consequence differs among organisms: whereas Pch2-dependent checkpoint results in a pachytene arrest in flies and budding yeast, in nematodes it leads to apoptosis of those oocytes with unsynapsed chromosomes. Therefore, Pch2 responds to synapsis failures and/or disruption in chromosome axis in several organisms, suggesting that Pch2-dependent

surveillance mechanism operating in the meiotic pachytene stage is widely conserved (Bhalla & Dernburg, 2005; Joyce & Mckim, 2010; Joyce & McKim, 2009).

In addition, budding yeast Pch2 is involved in a recombination checkpoint in response to unrepaired DSBs, which are monitored by DNA damage checkpoint proteins, such as Mec1, Rad17, Rad24, Tel1 and the MRX (Mre11-Rad50-Xrs2) complex (Vader, 2014). Different damages activate distinct checkpoint pathways; for instance, the presence of unresected (blunt-ended) DSBs trigger a checkpoint that requires Tel1 (ATM homolog), while unrepaired but resected DSBs activate a Mec1 (ATR homolog) pathway. The second pathway that responds to ssDNA, requires Mec1 and Rad17, whereas the former, responding to unresected DNA, requires Tel1 and Pch2. In addition to Tel1 and Pch2, the recombination checkpoint that responds to blunt-ended DSBs involves the MRX-complex protein Xrs2. It has been shown that Pch2 interacts with the N-terminal region of Xrs2 and this interaction is required for Pch2 function in the recombination checkpoint (Ho & Burgess, 2011; Wu & Burgess, 2006). Therefore, Pch2, Tel1 and Xrs2 collaborate in the same epistasis pathways to activate the recombination checkpoint when unprocessed DSBs remain. The ultimate consequence of both pathways that respond to unrepaired DSBs (Rad17/Mec1- or Pch2-Tel1-Xrs2-mediated pathways) is the phosphorylation of an axis protein named Hop1, which in turn promotes dimerization and activation of the Mek1 kinase. Mek1 plays dual roles; on one hand, it promotes inter-homolog (IH) bias and on the other hand, it is involved in checkpoint signaling in the presence of recombination intermediates (see below) (Hollingsworth, 2010; Lao & Hunter, 2010). Deletion of the N-terminal domain of Xrs2 partially suppresses *zip1Δ* delay, suggesting that interaction of Xrs2 and Pch2 might be important not only to mediate a recombination checkpoint in the presence of unprocessed DSBs, but also in the synapsis checkpoint. Hence, Pch2 is involved in two checkpoints during meiotic G2/prophase: one that responds to defects in synapsis/chromosome axes structure failures and one that is activated by defects in DSB processing (Ho & Burgess, 2011; Wu & Burgess, 2006). In addition to its roles in checkpoint surveillance during defective meiosis, in the last decade a number of studies have elucidated a wide-range of Pch2 functions in wild type meiosis, such as CO control and recombination. Some of these roles appear to be conserved among different organisms, as it is the case with recombination in yeast and mouse (Roig *et al.*, 2010).

There are several mechanisms that operate to ensure disjunction of homologous chromosomes in meiosis I; first, the obligate CO formation, which refers to the mechanism that ensures that each homolog pair receives at least one CO; second, CO interference, which

guarantees the non-random, evenly distribution of COs; and third, CO homeostasis, which operates to safeguard that COs levels are maintained even when DSB frequencies decrease (Gray & Cohen, 2016). Research with *pch2Δ* mutants revealed a delay in the timely progression of CO and NCO pathways in such yeast strains, and also an increased CO formation on medium and large chromosomes, suggesting a role of Pch2 in CO interference. Pch2 seems to mediate CO interference by increasing the proportion of DSBs that are repaired as COs, rather than NCOs. This Pch2 function is related to chromosome axes structure. In budding yeast, Pch2 mediates the assembly of a structural normal SC, by controlling the domain-like association of the axis component Hop1 and the central element Zip1 along meiotic chromosomes. Interestingly, Pch2 foci colocalize with Zip3, a protein that marks future CO sites. In WT pachytene stage, Hop1 appears as discrete foci, whereas in *pch2Δ*, Hop1 forms extended structures (Joshi *et al.*, 2009). Thus, Pch2 controls Hop1 association to designated CO sites by controlling the levels and localization pattern of Hop1 in meiotic chromosomes. Pch2 facilitates that COs are uniformly spaced within the genome by suppressing COs in adjacent chromosomal regions and also limits the total number of COs (Börner *et al.*, 2008).

A mechanism interconnected to CO formation is the process of IH bias. As mentioned earlier, during vegetative growth, DSBs are preferentially repaired using the sister chromatid as a repair template, which requires the Rad51 recombinase and its partner Rad54 to mediate the strand exchange with the sister chromatid. However, during meiosis, DSBs engage in the IH pathway preferentially allowing their repair using the homologous chromosome, rather than the sister chromatid (Humphryes & Hochwagen, 2014). As mentioned in section 1.1.1.3, IH repair is essential for establishing physical linkages that enable faithful chromosome segregation in meiosis I and the formation of viable gametes (Petronczki *et al.*, 2003). In budding yeast, when IH is lost (*i.e.* in the absence of Red1, Hop1 or Mek1, see below), DSBs are repaired via the Rad51/Rad54-dependent strand exchange pathway using the sister chromatid as a template, yielding unviable spores. IH bias is achieved by phosphorylation of Hop1 by the Tel1/Mec1 kinases. The role of Tel1 and Mec1 in IH bias was inferred from strains carrying Hop1 versions mutated at presumed Tel1/Mec1 phosphorylation sites, which show a lack of CO formation (Carballo *et al.*, 2008; Joshi *et al.*, 2015). Briefly, phosphorylation of this axial element leads to autophosphorylation, dimerization and activation of Mek1, which in turn phosphorylates Rad54. This last phosphorylation step in Rad54 inhibits its interaction with Rad51 and thus, intersister (IS) repair. In addition, the

meiosis-specific protein Hed1 contributes to IH bias by competing with Rad54 for Rad51 binding, thus preventing the formation of the Rad54/Rad51 complex.

The role of Pch2 in IH bias was deduced by various research groups (Börner *et al.*, 2008; Ho & Burgess, 2011; Roig *et al.*, 2010; Zanders *et al.*, 2011). Strains carrying a deletion of *PCH2* show an increased IS repair and it was proposed that Pch2 controls IH bias redundantly with Rad17 by activating Mek1 (Wu & Burgess, 2006; Zanders *et al.*, 2011). Joshi *et al.* demonstrated that during WT meiosis there are two pathways controlling IH bias: one involving Tel1 and another dependent on Mec1 (Joshi *et al.*, 2015). *tell1Δ* has similar effects on IH bias as *pch2Δ*, suggesting that Tel1 and Pch2 function in the same IH recombination pathway. Tel1/Pch2- and Mec1-pathways are sequentially activated and seem to respond to different levels of DSBs. Upon low levels of DSBs during early meiosis, DSB resection and partner choice are dependent on Tel1 and Pch2, whereas, above a DSB threshold, a Mec1-dependent pathway is activated (Ho & Burgess, 2011; Wu & Burgess, 2006). Thus, the Tel1/Pch2-pathway is active at all DSB levels, whilst the Mec1-mediated pathway becomes prominent once the levels of DSBs increase, complementing Tel1/Pch2 functions. Therefore, in budding yeast meiosis there are two largely redundant pathways operating to ensure maximum IH bias, and Pch2 modulates meiotic DSB repair to favor recombination between homologs.

For all the above-mentioned Pch2-mediated processes, the meiosis-specific protein Hop1 is involved. Hop1 is a HORMA-domain-containing protein (Aravind & Koonin, 1998), which is associated with dimerization/oligomerization. The HORMA-domain makes reference to three proteins in *S. cerevisiae* in which this domain was initially identified through sequence similarity (Hop1, Rev7 and Mad2, HORMA). This domain consists of ~200 aa and its organizational structure is best understood based on work on Mad2; the HORMA domain comprises two regions: the core, of about 150 aa and the C-terminal “safety belt” region. The core is composed of three α -helices (α -A, α -B and α -C) and three stranded- β -sheets (β 4, β 5 and β 6), usually with two additional β -strands (β 2 and β 3 hairpin) on the backside of the α -helices. The safety-belt region can fold itself against the HORMA-domain core in two conformations, referred to as “open” or “closed” state. In the open conformer, the safety belt region folds into two β -strands (β 7 and β 8) that extend towards the core β -sheet, whereas in the closed state the safety belt forms two new β -strands (β 8' and β 8'') that wrap entirely on the opposite side of the HORMA-domain core region. The close conformer allows a short peptide from a binding partner to interact with the core of the HORMA-domain, which

holds the peptide as the safety belt wraps around the domain (Muniyappa *et al.*, 2014; Rosenberg & Corbett, 2015).

Besides the HORMA domain, Hop1 contains a zinc finger domain and (S/T)Q motifs that can be phosphorylated by Tel1/Mec1 in response to DSBs. Hop1 constitutes, together with Red1, the axial component of the SC and thus, Hop1 is required for chromosomal organization and pairing during meiosis. In addition, Hop1 is necessary for meiotic DSB formation and IH repair (Börner *et al.*, 2008; Carballo *et al.*, 2013; Hollingsworth *et al.*, 1990; Panizza *et al.*, 2011). As mentioned earlier, in order to perform their functions, the assembly of an oligo-hexameric ring is typically required for AAA⁺ ATPases. Consistently, *in vitro* studies have shown that budding yeast Pch2 assembles into homo-hexameric rings with a central pore in a nucleotide-dependent manner and uses its enzymatic activity to remodel clients (Chen *et al.*, 2014).

Recent work has provided useful insights that help in understanding the relation of Pch2/TRIP13 with other members of the AAA⁺ ATPase superfamily. Pch2/TRIP13 contains an NH₂-terminal domain (NTD) responsible for substrate recognition, which is similar to the NTD of the “classic remodeler” family (Cdc48/p97/NSF), and an AAA⁺ ATPase domain that typically assembles into hexameric rings and the mechanism of which is related to the bacterial unfoldase ClpX (Ye *et al.*, 2015). The AAA⁺ ATPase domain of Pch2 comprises two domains, named small and large. Like many other AAA⁺ ATPases, Pch2 hexamerization depends on interactions between each subunit large domain and the small AAA⁺ domain of the adjacent subunit, and the interfaces between these subunits constitute the ATP binding sites. Pch2 also shares the characteristic motifs of other AAA⁺ ATPases, such as the Walker A and Walker B motifs, the Sensor 1 region and arginine finger motifs, situated in the large AAA⁺ domain, and that cooperate to bind/hydrolyze nucleotides (Erzberger & Berger, 2006; Ogura & Wilkinson, 2001). Contrary to Cdc48/p97/NSF proteins, which seem to lack a Sensor 2 motif, Pch2/TRIP13 has a single arginine finger that serves as a Sensor 2 motif (see section 1.4). Thus, despite having an NTD organization similar to the classic remodeler family, the mechanism by which nucleotide-dependent conformational changes occur in Pch2/TRIP13 may be more similar to other AAA⁺ ATPases (such as ClpX) (Ye *et al.*, 2015).

Although Pch2 and homologs typically oligomerizes into hexamers, there are slight differences among them with respect to the manner that this occurs. Whereas budding yeast Pch2 has been shown to assemble into hexamers upon the presence of nucleotides, *C. elegans* PCH-2 forms stable hexamers in both presence and absence of nucleotides. *Mus musculus* (*M.*

musculus) TRIP13 assembles into different oligomers, ranging from monomers to hexamers (Ye *et al.*, 2015). Assembly into hexameric conformers enables Pch2/TRIP13 to couple ATP hydrolysis with conformational changes that are transmitted to clients to typically remodel unfolding. HORMA-domain-containing proteins are confirmed clients of Pch2 (and its mammalian homolog TRIP13; see section 1.4.1.2) and both Pch2 and TRIP13 seem to act through HORMA-domain proteins (see below) (Chen *et al.*, 2014; Ye *et al.*, 2017).

At the leptotene stage of meiosis, Hop1 is present in chromosomes in a punctate (discontinuous) manner and there are few Zip1 foci, whereas at zygotene Hop1 and Zip1 acquire a domain-like organization that becomes even clearer at pachytene stage when the SC is fully formed (Börner *et al.*, 2008; San-Segundo & Roeder, 1999). Pch2 is involved in the active removal of Hop1 from chromosomes in meiotic G2/prophase, and this removal correlates with chromosome synapsis (Börner *et al.*, 2008; Subramanian *et al.*, 2016; Wojtasz *et al.*, 2009). As mentioned earlier, Hop1 is a phosphosubstrate of Tel1/Mec1, key proteins in the establishment of IH bias, and Pch2 facilitates this process (Carballo *et al.*, 2008; Niu *et al.*, 2009; Vader, 2014; Zanders *et al.*, 2011). In addition, Hop1 is necessary for DSB formation and Pch2 also influences DSB formation at the rDNA locus in budding yeast (Carballo *et al.*, 2013; Hollingsworth *et al.*, 1990; Mao-Draayer *et al.*, 1996; San-Segundo & Roeder, 1999; Vader *et al.*, 2011) (see below). Thus, many of the functions of Pch2, if not all, can be explained by the Pch2 activity towards a HORMA-domain protein (Hop1) and as such, Pch2 can be considered a modulator of Hop1. *In vivo* data has been reinforced with *in vitro* studies that have revealed that recombinant Pch2 can bind Hop1 *in vitro* and displace it from DNA substrates. Both ATP binding and hydrolysis appear to be required for Pch2-Hop1 transactions (Chen *et al.*, 2014). These data support a model in which Pch2 uses its enzymatic activity via ATP binding/hydrolysis to remodel Hop1, which in turn might restrict localization of Hop1 to specific regions, promoting the establishment of a chromosomal organization that favors IH DSB repair and designation of CO sites (Herruzo *et al.*, 2016).

In addition to the roles ascribed to Pch2 in G2/prophase, Pch2 is needed to prevent inappropriate DSB formation and recombination within the tandem repetitive ribosomal (rDNA) array of *S. cerevisiae*. Pch2 is enriched at the nucleolus, the nuclear membraneless organelle where the rDNA resides (San-Segundo & Roeder, 1999; Vader *et al.*, 2011). In addition to the nucleolar pool of Pch2, some Pch2 foci are localized on chromosomes in a punctate pattern that overlaps with Zip1. In the rDNA of budding yeast, DSB formation is repressed partially by Sir2-dependent heterochromatin formation (Fritze *et al.*, 1997; Gottlieb

& Esposito, 1989; San-Segundo & Roeder, 1999; J. S. Smith & Boeke, 1997) (see section 1.3). The Sir2-deacetylase is required to suppress sister chromatid recombination in the rDNA during both, mitosis and meiosis, and for localization of Pch2 in the nucleolus (Gotta *et al.*, 1997; Gottlieb & Esposito, 1989; Herruzo *et al.*, 2016; Mieczkowski *et al.*, 2007; Petes, 1980; San-Segundo & Roeder, 1999). Thus, mutation of Sir2 increases the frequency of IH recombination, a phenotype that is also shared by deletion of Pch2. Moreover, whereas in a wild-type situation, Hop1 is excluded from the nucleolar region, in *sir2Δ* and *pch2Δ* strains, Hop1 is localized in the nucleolus (Herruzo *et al.*, 2016; San-Segundo & Roeder, 1999). Therefore, the way by which DSB formation at the rDNA array could be prevented is by recruiting Pch2 to the nucleolus, which in turn excludes Hop1 from this region. Even though the bulk of the rDNA array is protected against DSB formation by the establishment of a specialized Sir2-dependent heterochromatin, Vader and co-workers showed that the edges of the rDNA are highly susceptible to meiotic DSBs (Vader *et al.*, 2011). This localized DSB susceptibility is counteracted by an rDNA-boundary specific system that minimizes Spo11-dependent DSBs formation. This protective mechanism involves two AAA⁺ ATPases: Pch2 and the ORC subunit Orc1 (Figure 1-8).

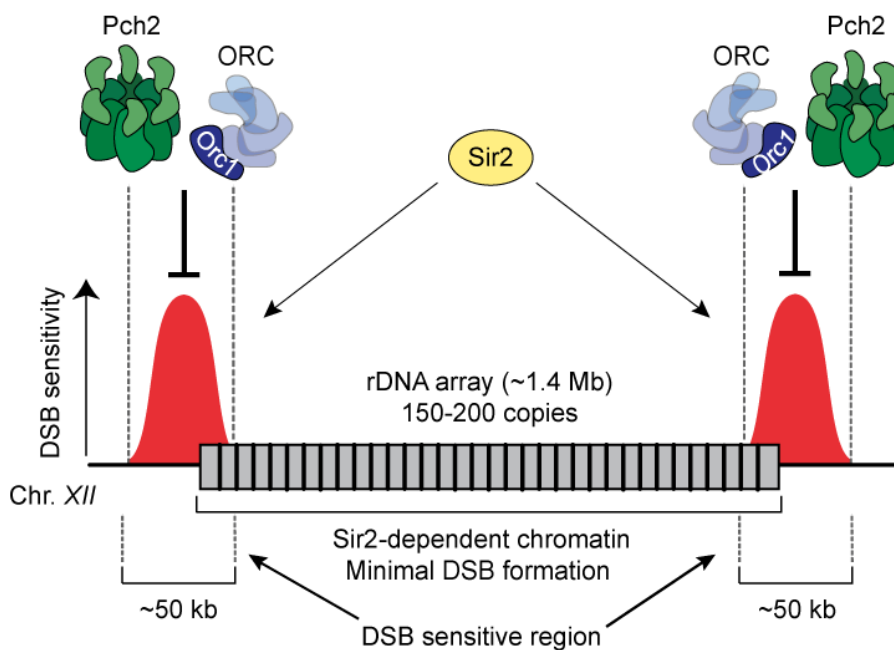


Figure 1-8 Protection of the budding yeast rDNA against meiotic DSB formation

rDNA copies are arranged into a single highly repetitive tandem locus. DNA double-strand breaks (DSBs) within and adjacent to repetitive DNA can be repaired by non-allelic homologous repair (NAHR), which have the potential to endanger genome integrity. Meiotic DSBs are almost absent from the budding yeast rDNA cluster due to the Sir2-dependent heterochromatin present at this locus. However, Sir2 promotes meiotic DSB formation at the rDNA boundaries. This localized Sir2-

Figure 1-8 (Continued)

dependent DSB promoting effect is counteracted by a protective mechanism that involves the meiosis-specific AAA⁺ ATPase Pch2 and the Orc1 subunit of the Origin recognition complex (ORC). Upon disruption of this anti-DSB mechanism, there is increased DSB formation (depicted in red) leading to unequal recombination (NAHR) within the ~1-10 first rDNA repeats and ~50 kb of single copy flanking sequences.

In the absence of this ‘anti-break’ system, strong DSBs occur specifically at the rDNA boundaries, leading to unequal recombination (NAHR) within the first ~10 rDNA repeats and rDNA instability. This study demonstrated that the Sir2-dependent heterochromatin accounts for the induction of DSBs at the rDNA edges in *pch2Δ*. Loss of Sir2 or its deacetylase activity eliminates DSB formation in the outermost region of the rDNA in *pch2Δ* mutants (Vader *et al.*, 2011). Hence, Pch2 functions to repress NAHR at the rDNA by preventing DSB formation, but in a manner distinct than Sir2. Therefore, although Sir2 prevents meiotic DSBs within the rDNA, it creates a highly permissive environment for DSB formation at the borders between heterochromatin and euchromatin. The rDNA flanking regions constitute regions with a high risk of meiotic NAHR and Pch2 seems to act here by suppressing the recruitment of DSB factors.

Vader *et al.* identified a fragment containing the AAA⁺ ATPase of Orc1, a member of ORC, as an interactor of Pch2. Impairing Orc1 protein levels by a temperature-sensitive mutant (*orc1-161*) triggers DSB formation at the rDNA boundaries, analogously to *pch2Δ*. A mutant lacking the N-terminal Bromo-adjacent homology (BAH) domain of Orc1, which is required for the chromatin-silencing role of Orc1 (see section 1.4.2) but dispensable for DNA replication, also shows increased DSBs levels close to the rDNA flank, indicating that the functions of Orc1 in DSB formation and DNA replication are separable. Pch2 recruitment to the nucleolus depends on Sir2 (Bell *et al.*, 1995; San-Segundo & Roeder, 1999; Vader *et al.*, 2011); moreover, in an *orc1-161* mutant, Pch2 also fails to localize in the nucleolus, indicating that recruitment of Pch2 to the nucleolar region depends also on Orc1. In addition, the ATPase activity of Pch2 is required for suppression of rDNA-proximal DSBs. The main role of Orc1 seems to be the nucleolar recruitment of Pch2, but this ORC subunit might also have a function in the activation of Pch2 to prevent local DSB formation at the rDNA borders. The highly-susceptibility of these rDNA boundaries to NAHR necessitates a special protection mechanism that counteracts the DSB-promoting activity of Sir2. This anti-DSB system involves the collaboration of the AAA⁺ ATPases Pch2 and Orc1 (Vader *et al.*, 2011).

However, up to date the basis underlying the functioning of the Pch2/Orc1 protective mechanism has remained elusive.

1.4.1.2 Pch2^{TRIP13} in the mitotic checkpoint

Although in budding yeast Pch2 is exclusively expressed during the meiotic cell cycle, Pch2 homologs in many other organisms, such as *C. elegans* PCH-2 or mammalian TRIP13, are also expressed during the mitotic cell cycle. In this section, we focus on the function of Pch2/TRIP13 in the mitotic checkpoint, since structural work of TRIP13 in the last decade has provided useful insights on the functioning of this AAA⁺ ATPase towards HORMA-domain proteins (see below).

The expression of TRIP13 is similar to known mitotic regulators and TRIP13 is a key regulator of the spindle assembly checkpoint (SAC), which monitors kinetochore-microtubule attachments (Nelson *et al.*, 2015; Tipton *et al.*, 2012; Vader, 2014). The SAC serves as a quality control to ensure that all chromosomes are properly attached to spindle microtubules before they are segregated in anaphase, and that operates through the MCC (mitotic checkpoint complex), composed of Mad2 (a HORMA-domain-containing protein), Cdc20, BubR1 and Bub3 (Corbett, 2017; Musacchio & Salmon, 2007; Sun & Kim, 2012; Vader, 2014). As mentioned earlier, the main feature of HORMA-domains is that they form complexes through a so-called “safety belt” interaction, in which the C-terminus of the safety-belt region completely wraps around a region of the binding partner (Musacchio & Salmon, 2007; Rosenberg & Corbett, 2015; Vader, 2014). These safety belt conformational changes define the two conformations that Mad2 can adopt, referred to as “closed” (C-Mad2) and “open” (O-Mad2). In its closed conformation, Mad2 has its C-terminal safety belt region wrapped around its interacting or closure motif and this constitutes the “active” form of Mad2. In its open conformation, the safety-belt of Mad2 is folded back on the closure motif, thus preventing binding with partners and constituting the “inactive” state of Mad2. Upon the presence of unattached kinetochores, C-Mad2 together with BubR1 and Bub3 binds to a protein called Cdc20 through a safety belt interaction, inhibiting it. Once the kinetochores of all chromosomes are attached to spindle microtubules, the SAC is inactivated. Another HORMA-domain protein called p31 (comet), which shares the Mad2-binding interface with BubR1, specifically binds to C-Mad2, competing with BubR1 for Mad2 association and displacing BubR1 from C-Mad2/Cdc20. Upon dissociation of Cdc20 from C-Mad2, Cdc20 can bind the Anaphase promoting complex/cyclosome (APC/C), an E3 ubiquitin ligase that

drives anaphase-onset, thus promoting anaphase transition. The p31(comet)-dependent release of Cdc20 requires the transformation of C-Mad2 to O-Mad2 and this is achieved through TRIP13-driven conformational changes. Therefore, p31(comet) is an adaptor that recognizes C-Mad2 and releases it to TRIP13, which catalyzes the conformational change from C-Mad2 to O-Mad2, necessary for the dissociation of Cdc20 (Corbett, 2017; Musacchio & Salmon, 2007; Vader, 2014).

Recent biochemical and structural work with Pch2/TRIP13 from *M. musculus*, *C. elegans* and *H. sapiens* has revealed important insights into the mechanisms by which TRIP13 recognizes its substrates and operates to inactivate the SAC (Alfieri *et al.*, 2018; Ye *et al.*, 2017a, 2015). The NTD of TRIP13 mediates the initial recognition of p31(comet), which is associated with Mad2. Association of p31(comet) with TRIP13 likely promotes the rotation of TRIP13 NTD, which might then “flip-up” upon p31(comet) binding and which in turn, would enable that the TRIP13 pore loops engage the disordered Mad2 N-terminus. Engagement of the Mad2 N-terminal tail by the TRIP13 pore loops appears to be coupled to TRIP13 ATPase activity, which is stimulated upon Mad2-association. Subsequently, TRIP13 unfolds a stretch of Mad2 N-terminus (at least 106 residues of Mad2), enabling the conformational conversion between C-Mad2 (“active”) and O-Mad2 (“inactive”). Contrary to several members of the AAA⁺ ATPase family, TRIP13 does not trigger the complete unfolding of its substrate (*i.e.* Mad2), but rather a partial conformational change in the safety belt region of Mad2, triggering a conversion of topology (Ye *et al.*, 2017a).

The structural research on TRIP13 in the SAC has also served to better understand the mechanism of action of HORMA proteins during meiosis. As mentioned above, several meiotic processes are regulated by HORMA-domain-containing proteins (HORMADs). In early prophase, meiotic HORMADs localized along the entire length of chromosomes and facilitate DSB formation. After DSB introduction, HORMADs suppress recombination with the sister chromatid by IH bias. In both yeast and mammals, HORMADs are involved in recombination and CO formation by a feedback mechanism that ensures proper recombination levels. This feedback mechanism is achieved by removing HORMADs from the chromosome axis upon enough COs number and this removal is mediated by Pch2/TRIP13 (Börner *et al.*, 2008; Joshi *et al.*, 2009; Roig *et al.*, 2010; San-Segundo & Roeder, 1999; Wojtasz *et al.*, 2009). Therefore, HORMADs removal correlates with chromosome synapsis. In *C. elegans* there are four HORMAD proteins (HIM-3, HTP-1/2/3) and work from the Corbett laboratory has shown that these proteins contain closure motifs in

their COOH terminal unstructured “tail”. HORMADs form complexes through HORMA domain-closure motif interactions, and such interactions are required for SC assembly and CO formation in this organism. Although the mechanism of HORMADs localization to the meiotic chromosome axis is unclear, the current model proposes that HORMADs might localize to the axis by initial recruitment mediated through binding of the HORMA domain to closure motifs present in cohesin or other axis protein. Indeed, biochemical work has demonstrated that Hop1 binds the closure motif present in the axis protein Red1 (West *et al.*, 2018). This initial Hop1 recruitment to chromosomes would be followed by self-association of HORMADs in a head-to-tail pattern to mediate the assembly of HORMAD complexes on chromosomes, which likely promotes DSB and CO formation. Upon progression through meiosis, HORMADs are removed from the chromosome axis in a Pch2/TRIP13 dependent manner (Kim *et al.*, 2014; Rosenberg & Corbett, 2015).

Since TRIP13 regulates conformational changes of Mad2 (which is also an HORMA-domain-containing protein) in mitosis, it has been proposed that Pch2/TRIP13 could use a common mechanism on both clients. Studies with *M. musculus* have shown that the N-terminal of HORMAD1 (Mad2-related HORMAD protein) is needed for the function of TRIP13 towards this HORMA-domain protein (*i.e.* truncation of HORMAD1 N-terminus affects its TRIP13-driven removal upon chromosome synapsis, although it does not affect the initial recruitment of HORMAD1) (Ye *et al.*, 2017b). Thus, the N-terminal region of HORMAD1 seems to be key for Pch2/TRIP13 activity, similarly to what is observed in the Mad2 N-terminus (see above). Therefore, although more research is needed in this area, the current understanding suggests that Pch2/TRIP13 mediates meiotic HORMADs removal from chromosomes using a mechanism analogous to the TRIP13-mediated conformational change of Mad2.

1.4.2 ORC

In each cell cycle, parental genomes must be faithfully copied. Genome duplication is carried out by DNA polymerases, but a combination of proteins that assembles at specific chromosomal regions, known as origins of replication or autonomously replicative sequences (ARSs), is crucial to initiate DNA replication (Bell & Labib, 2016; Bell & Stillman, 1992; Deegan & Diffley, 2016). In order for DNA replication to occur, the double DNA helix has to be separated into its two strands and this unwinding process is driven by the hetero-hexameric

AAA⁺ ATPase called MCM helicase (minichromosome maintenance), also referred to as Mcm2-7 (Deegan & Diffley, 2016; Remus & Diffley, 2009).

The six-subunit ORC assembly orchestrates the loading of the MCM to distinct locations (*i.e.* origins of replication) and acts as a platform to recruit several other accessory proteins needed for DNA replication (Bell & Stillman, 1992; Deegan & Diffley, 2016; Diffley *et al.*, 1995; Diffley & Labib, 2002). DNA replication is a highly regulated event that is subjected to a tight control to ensure that the genome is duplicated only once per cell cycle. This regulation is mediated by phosphorylation of different targets by the kinases CDK and DDK and is further described in section 1.4.2.2.4 (Bell & Labib, 2016; Diffley, 2011; Yeeles *et al.*, 2015). Although ORC is primarily known by its function in DNA replication, other roles have been ascribed to ORC (or ORC subunits), such as transcriptional silencing at the mating-type locus and telomeres. In addition, there are different lines of emerging evidence that involve ORC in other processes, such as sister-chromatid cohesion and rDNA protection in budding yeast, and polar body extrusion in mouse, which are further detailed in section 1.4.2.3 (Bell *et al.*, 1995; Dillin & Rine, 1995; Foss *et al.*, 1993; Fox *et al.*, 1995; Hickman & Rusche, 2010; Nguyen *et al.*, 2015; Popova *et al.*, 2018; Shimada & Gasser, 2007; Suter *et al.*, 2004).

1.4.2.1 Structural organization of the ORC subunits

ORC is a hetero-hexameric complex that constitutes the eukaryotic DNA replication initiator and that is conserved throughout evolution. ORC is composed of the Orc1, Orc2, Orc3, Orc4, Orc5 and Orc6 subunits, which were initially identified in budding yeast and named according to their apparent molecular masses, being Orc1 the largest (~120 kDa) and Orc6 the smallest (~50 kDa) (Duncker *et al.*, 2009; Li & Stillman, 2012). Although Orc1 through Orc5 contain a predicted AAA⁺ or AAA⁺-like module, only Orc1, Orc4 and Orc5 contain functional ATPase related motifs that are able to bind ATP. The ORC assembly belongs to the AAA⁺ ATPase family and the major source of ATPase activity within this complex is provided by the Orc1 subunit and requires a conserved arginine residue from Orc4 for its catalytic activity (Duncker *et al.*, 2009; Li & Stillman, 2012; Speck *et al.*, 2005). As mentioned earlier, the insertion of arginine fingers of one AAA⁺ module into an adjacent one is critical for ATPase activity and constitutes a hallmark of AAA⁺ ATPases (Gates & Martin, 2019; Hanson & Whiteheart, 2005; Ogura *et al.*, 2004; Ogura & Wilkinson, 2001; Wendler *et al.*, 2012b) (Figure 1-9).

In addition, the Orc1-Orc5 subunits contain winged-helix domains (WHDs) near their C-terminal region that are thought to contribute to DNA binding. Orc6 does not contain either an AAA⁺-like domain or a WHD and shows no structural similarity with the rest of ORC components. Instead, Orc6 is composed of tandem cyclin-box folds similar to transcription factor IIB (TFIIB) and a carboxy-terminal domain (CTD) (Duncker *et al.*, 2009; Yuan *et al.*, 2017). Structural work in *Drosophila* and *S. cerevisiae* has shown that the Orc1-5 subunits are arranged into an open ring-shaped complex, in which the Orc6 subunit is situated distal to the ORC central channel, although this subunit interacts with Orc2, Orc3 and Orc5 (Bleichert *et al.*, 2015; Li *et al.*, 2018; Sun *et al.*, 2014; Yuan *et al.*, 2017). Moreover, whilst Orc1-5 are essential for DNA binding, Orc6 is not involved in recognition of origins, although this subunit is necessary for DNA replication and its role in the assembly of ORC around DNA origins appears to differ among organisms (Duncker *et al.*, 2009). For instance, recent structural work has implicated the Orc6 subunit of *S. cerevisiae* in interacting with certain elements of the ARS sequences through its TFIIB domain (Li *et al.*, 2018).

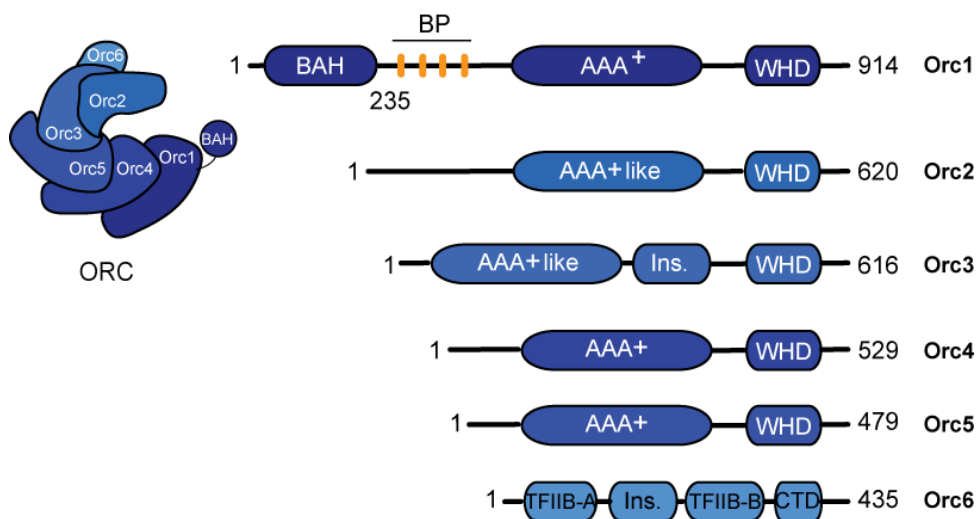


Figure 1-9 Domain organization of the ORC subunits

Schematic organization of the hetero-hexameric ORC, composed of the Orc1-Orc6 subunits. The Orc1-Orc5 subunits each harbor an AAA⁺ ATPase domain (AAA⁺) or AAA⁺-like domain (AAA⁺ like) and a winged-helix domain (WHD). In addition, the Orc1 subunit harbors an NH₂-terminal Bromo-adjacent homology (BAH) domain and unstructured basic patch (BP). For clarity, the BAH domain of Orc1 is depicted here as an “extension” of the Orc1 subunit, indicative from the flexibility of this domain. The Orc6 subunit bears little resemblance to the other ORC members and contains transcription factor II B-like domains (TFIIB-A and TFIIB-B) and a carboxy-terminal domain (CTD). Ins. stands for insertion domains. Protein lengths (amino acids) are indicated. Adapted from Li *et al.*, 2018, and Yuan *et al.*, 2017.

Besides Orc6, which as mentioned earlier, bears little resemblance to the other ORC members, the Orc1 subunit is also unique with respect to other ORC components, because it harbors an additional N-terminal Bromo-adjacent homology domain (BAH) of ~235 residues (Duncker *et al.*, 2009; Li & Stillman, 2012). BAH domains are chromatin-binding modules and in budding yeast, the BAH domain of Orc1 is necessary for the function of ORC in transcriptional silencing at the mating-type loci and telomeres, as described in section 1.3 (Hickman & Rusche, 2010; Srivastava *et al.*, 2016; Triolo & Sternglanz, 1996; Yang & Xu, 2013). Although the BAH domain of Orc1 is not essential for DNA replication, it influences origin binding specificity (Müller *et al.*, 2010a). A comprehensive explanation of this aspect of the BAH domain is provided in section 1.4.2.2.5. Interestingly, Orc1 is a paralog of Sir3, a crucial protein for transcriptionally silencing in *S. cerevisiae*. Sir3 arose via gene duplication and functional specialization throughout evolution (Hanner & Rusche, 2017). Sir3 plays a key role in silencing spreading, which is thought to occur due to the ability of its BAH domain (and a second C-terminal histone binding domain) to interact with histones (Connelly *et al.*, 2006; Gartenberg & Smith, 2016; Hickman & Rusche, 2010; Wang *et al.*, 2004). However, besides Orc1 and Sir3 sharing a similar organizational domain, the AAA⁺ ATPase domain of Sir3 does not have ATPase activity (contrary to Orc1-AAA⁺ module) (Li & Stillman, 2012).

Recent high-resolution structures that include ORC, such as the OCCM (ORC-Cdc6-Cdt1-Mcm2-7) structure or trimmed regions of ORC in *Drosophila* and human, have provided useful insights on the ORC architecture (Bleichert *et al.*, 2015; Tocilj *et al.*, 2017; Yuan *et al.*, 2017). In addition, a recent study has unveiled the structure of ORC bound to DNA replication origin, which has made a valuable contribution in understanding the mechanism by which ORC binds to origin DNA sequences (Li *et al.*, 2018) (see section 1.4.2.2.2 for further details). Current literature about ORC organization in *S. cerevisiae* has shown that the Orc1-Orc5 subunits assemble to encircle DNA through both, canonical interactions between AAA⁺ modules of distinct ORC subunits and “domain-swapping” interactions between the WHDs and AAA⁺ domains of neighboring subunits (Li *et al.*, 2018). The Orc1-Orc5 subunits form a ring-shaped complex with a gap between Orc1 and Orc2, in which another AAA⁺ protein called Cdc6 is transiently inserted in G1 phase, enabling ORC to function in helicase loading. Thus, the interface between Orc1 and Orc2 appears to be dynamic, as it serves as a DNA entry and as an “anchor” for Cdc6. Besides having high sequence similarity to Sir3, Orc1 is also related to Cdc6 and phylogenetic analyses of several species have suggested that Cdc6 and Orc1 may be paralogs (Duncker *et al.*, 2009).

Moreover, Cdc6 seems to act as an additional ORC subunit, since it bridges the space between Orc1 and Orc2 and completes the ring-shaped complex. In addition, binding of Cdc6 to ORC induces a conformational change that re-orientates the BAH domain of Orc1, thus increasing specificity for DNA binding (Sun *et al.*, 2012). In the next section, a more detailed explanation of the current ORC structure is given, with a special focus on how recognition of origin DNA occurs and how ORC contributes to the initiation of DNA replication.

1.4.2.2 ORC in DNA replication

1.4.2.2.1 Main principles of ORC as an initiator of DNA replication

The identification of short, well-characterized chromosomal DNA sequences that act as origins of DNA replication in *S. cerevisiae* made it a useful organism to study the early steps of eukaryotic DNA replication (Bell & Stillman, 1992; Stinchcomb *et al.*, 1979). Indeed, most of the current knowledge of how DNA replication occurs derives from work with this organism.

ORC was initially identified as a six-subunit assemblage in budding yeast that promoted the initiation of DNA replication and that presented DNA-binding specificity to origin sites (Bell & Stillman, 1992). Since then, a growing body of research has extensively investigated the function of ORC and additional factors in driving the initiation of DNA replication. Literature in the field is still providing novel insights about the earliest steps that drive the recruitment of the replicative helicase that unwinds DNA and about accessory proteins involved in the initiation of DNA replication (Bell, 2002, 2017; Bell & Labib, 2016; Boos *et al.*, 2012; Remus & Diffley, 2009). In addition, in recent years there has been a considerable focus on structural work with ORC, which has elucidated important cues on the structure and biochemistry of this complex and on how this assembly specifically recognizes origins of DNA replication (Bleichert, 2019; Bleichert *et al.*, 2015; Li *et al.*, 2018; Sun *et al.*, 2014, 2012; Tocilj *et al.*, 2017; Yuan *et al.*, 2017).

The initiation of DNA replication occurs at multiple genomic loci called origins of replication (Lucas & Raghuraman, 2003; Newlon, 1988; Stinchcomb *et al.*, 1979). In eukaryotic organisms, an origin of replication is a DNA sequence where ORC binds and subsequently recruits additional factors that together form the pre-replicative complex (pre-RC) (see below) (Deegan & Diffley, 2016; Diffley & Labib, 2002; Tsakraklides & Bell, 2010). These origins of replication are dispersed along the genome enabling that DNA

duplication occurs in a timely manner. Upon entry into S phase, the activities of two kinases, CDK and DDK, trigger the initiation of DNA replication from a subset of these potential origins, and the remaining non-activated origins are replicated in a passive manner by replication forks derived from closeby origins. The likelihood of utilization of origins of replication modulates the length of S phase and, although there are substantial differences in the timing at which origins initiate DNA replication between cells, at the population level there exists a robust replication timing program (Eaton *et al.*, 2010; Yoshida *et al.*, 2013).

1.4.2.2.2 Origins of replication and insights on ORC structure

The selectivity of ORC for distinct DNA sequences significantly differs between organisms and there is little consensus among eukaryotes regarding origins. In this regard, *S. cerevisiae* represents the exception to the rule, since in this organism, ORC binds to genetically defined origins that share common features, although here there is also a certain degree of variation in the consensus sequences (Eaton *et al.*, 2010; Li & Stillman, 2012; Loo *et al.*, 1995; Lucas & Raghuraman, 2003). Although in budding yeast the DNA sequence plays a determinant role in defining origins of replication, in *S.pombe* and metazoans, origins are predominantly determined by chromatin structure and, specifically, the presence of a nucleosome-free region (NFR). Both DNA sequence and chromatin environment play a role in the definition of origins, although their prevalence differs among organisms (Eaton *et al.*, 2010; Lipford & Bell, 2001; Yoshida *et al.*, 2013).

In *S. cerevisiae*, replication origins were initially identified as short stretches of DNA sufficient for maintenance of episomes (accessory DNA elements similar to plasmids) (Stinchcomb *et al.*, 1979). These origins of replication are autonomously replicating sequences (ARSs) of approximately 100-150 base pairs (bp) that contain several elements termed “A” and “B”. The core, essential A element is defined by the ARS consensus sequence (ACS), which is composed of an AT-rich 11-to-17 bp DNA stretch that is necessary but not sufficient for origin activity. Comparison of several ARSs identified the $\overset{A}{T}TTTA\overset{C}{T}A\overset{A}{G}TTT\overset{A}{T}$ sequence as the ACS (Lucas & Raghuraman, 2003; Newlon, 1988). Although this 11-to-17 bp sequence is considered a hallmark of ARSs, there is a certain degree of flexibility in the matching degree of this sequence among different ARSs (Brewer & Fangman, 1987; Dubey *et al.*, 1991; Huberman, 1987; H. Li & Stillman, 2012; Lucas & Raghuraman, 2003; Yoshida *et al.*, 2013). In addition to the A element, ARSs harbor two or three B elements (B1, B2 and, in certain origins, also B3) that lie 3’ of the ACS and that

contribute to ARS function (Marahrens & Stillman, 1992). Unlike the A element, B elements are poorly defined and have minimal conservation of sequence or spacing between different origins. The B1 element, similarly to the ACS, contributes to the DNA-binding specificity of ORC, whereas the B2 element contains the DNA unwinding element (DUE), a region that is considered to promote unwinding of the DNA for the initiation of DNA replication, and that is required for loading the MCM (R. Y. Huang & Kowalski, 1993; H. Li & Stillman, 2012; Lucas & Raghuraman, 2003). Some origins have an auxiliary B element (B3). Such is the case of *ARS1*, in which the B3 element acts as a binding site for the transcriptional activator/repressor ARS binding factor 1 (Abf1). *In vitro* and *in vivo* studies have demonstrated that the role of the ACS, together with the nearest B element, is to nucleate the assembly of the DNA replication initiation complex by serving as a binding site for ORC, which in turn acts as a landing pad for the association of accessory proteins required for origin firing (H. Li & Stillman, 2012; Lucas & Raghuraman, 2003). Among these additional proteins are Cdc6, Cdt1 and MCM (Mcm2-7), which together constitute the OCCM (ORC-Cdc6-Cdct1-MCM) complex (see below).

ORC recognition and binding to origin DNA occurs in an ATP-dependent manner (Bell, 2002; Bell & Stillman, 1992; Speck *et al.*, 2005). Recent work has yielded a high-resolution structure of *S. cerevisiae* ORC bound to a stretch of DNA that contains an ACS and the B1 element and has provided important insights about how ORC facilitates origin selection and helicase loading in eukaryotes (Li *et al.*, 2018). As stated above, budding yeast Orc1-5 form a breached ring assembly around DNA, in which the subunits are arranged in the following order: Orc1-Orc2-Orc3-Orc5-Orc4, with a gap present between the Orc1 and Orc2 subunits. Similar to other ORC structures in *Drosophila* and human, in budding yeast ORC oligomerization between the Orc1-5 subunits occurs through canonical interactions among the AAA⁺ domains and domain-swapping interactions between the AAA⁺ core and WHDs tiers of adjacent subunits (Bleichert *et al.*, 2015; Li *et al.*, 2018; Tocilj *et al.*, 2017; Yuan *et al.*, 2017). In the archaeal initiator Orc1 (which is related to eukaryotic Orc1), origin DNA recognition takes place by using three main modules: an initiation-specific motif (ISM) from the AAA⁺ domain, a β -hairpin and a helix-turn-helix (HTH) motif present in the WHD (Erzberger *et al.*, 2006; Gaudier *et al.*, 2007). Although their roles in binding DNA differ, these recognition modules are highly preserved in the Orc1-5 subunits in eukaryotes and enable the establishment of non-specific interactions between ORC and the DNA backbone (Li *et al.*, 2018).

As mentioned earlier, budding yeast specifically recognizes the ACS and this specificity is possible due to the acquisition of new elements besides the DNA binding modules conserved among different organisms. Structural analysis has identified motifs within Orc1, Orc2 and Orc4 that are determinant for the specific binding to origin DNA in *S. cerevisiae* (Li *et al.*, 2018). Specifically, a basic patch in Orc1 (residues 358-371, Orc1-BP), situated between the AAA⁺ core and the BAH domain; an initiation-specific motif (ISM) in Orc2, which facilitates the insertion of Orc1-BP into the minor groove of the ACS; and an α -helix inserted in the β -hairpin of Orc4-WHD, which is likely involved in the recognition of the T-rich DNA stretch present in the ACS. Remarkably, this insertion is absent in metazoans and thus, it is possible that in these organisms the major or sole determinant for DNA recognition would be the Orc1-BP, which could account for the different sequence specificity of ORC for origin DNA among species (*i.e.* the more “relaxed” sequence specificity of ORC in metazoans) (Eaton *et al.*, 2010; Kumar & Remus, 2016; Li *et al.*, 2018). Insights gained through recent structural work have led to the hypothesis that in eukaryotes, ORC binding sites are determined by several factors, including the BAH domain and Orc1-BPs subunit.

The Orc1-BAH domain of yeast, plant and human is able to interact with nucleosomes adjacent to replication origins and both the Orc1-BAH domain and Orc1-BPs are likely involved in the initial recognition and binding of ORC to the replication initiation site (Kawakami *et al.*, 2015; Kuo *et al.*, 2012; Li *et al.*, 2018; Müller *et al.*, 2010a). ORC binding to DNA origins is probably facilitated by the association of the Orc1-BAH domain to juxtaposed nucleosomes and the searching of Orc1-BPs for the ACS. Thus, in budding yeast, positioning of ORC at the ACS seems to be achieved by interactions between Orc1-BP and Orc4-insertion helix with the ACS. Interactions between various ORC subunits and the major and minor DNA grooves by ORC base-specific recognition motifs induces DNA curving or bending at successive points of the ACS and B1 element, which in turn positions the bent DNA at the interface between Mcm2 and Mcm5 subunits (known as Mcm2/Mcm5 gate) of the MCM replicative helicase ring. It has been proposed that DNA straightening may be coordinated with opening of the Mcm2/Mcm5 gate to form the stable OCCM complex and that double-stranded DNA (dsDNA) enters the MCM ring via this gate. An additional consequence of DNA bending could be that the TFIIB module of Orc6 could establish contact with origin DNA beyond the B1 element, which could account for the function of ORC-origin DNA in organizing chromatin and particularly, on providing an NFR for replication initiation (Deegan & Diffley, 2016; Li *et al.*, 2018).

1.4.2.2.3 Mechanism of the eukaryotic DNA replication: MCM loading and MCM activation

As mentioned in the previous section, DNA replication involves multiple replication proteins, named initiators, that recognize and/or bind replication origins and ultimately lead to the formation of replication forks, which are structures formed during replication by helicases that unwind the double-stranded (dsDNA) and provide two branches of single-stranded DNA (ssDNA) used as replication templates for the leading and lagging strands. Subsequently, several additional factors (such as polymerases and topoisomerase II) are recruited to the replication fork and convert it into a “replisome” that is capable of driving the elongation step of DNA replication (Coster & Diffley, 2017; Deegan & Diffley, 2016; Gai *et al.*, 2010; Yeeles *et al.*, 2015). There are two key events necessary to accomplish DNA replication initiation, named origin melting and DNA unwinding. Origin melting refers to the initial separation of dsDNA into ssDNA, which is achieved by the initiators that assemble into origin DNA. DNA unwinding refers to the process by which the MCM replicative helicase travels along the replication fork and opens (*i.e.* unwinds) the double DNA helix to provide the template needed for the DNA polymerase.

The eukaryotic DNA replication cycle proceeds via two main steps, usually referred to as “helicase loading” and “helicase activation”, that are highly regulated throughout the cell cycle (Bell & Kaguni, 2013; Boos *et al.*, 2012; Deegan & Diffley, 2016). This regulation enables genome duplication to occur only once per cell cycle and is achieved by phosphorylation events driven by CDK and DDK, which ensure that both steps (MCM loading and activation) are separated into two temporally discrete events (see section 1.4.2.2.4). Moreover, DNA replication is controlled by ATP binding and hydrolysis of several of the proteins involved in origin firing (Bell & Labib, 2016; Coster *et al.*, 2014; Diffley, 2011; Speck *et al.*, 2005).

The helicase loading step occurs in G1 phase and consists of the binding or loading of the replicative helicase MCM onto origins of replication (Bell & Kaguni, 2013). Besides ORC, the loading of the MCM onto DNA requires two additional proteins, Cdc6 and Cdt1. As already mentioned, helicase loading is initiated by the recognition and binding of ORC to ARSs. Association of ORC to the ARS subsequently helps in the step-wise assembly of additional proteins (“origin licensing”) required for the initiation of DNA replication or, as it is more commonly referred, “origin firing”. After initial binding of ORC to an ARS, Cdc6 is

recruited, which in turn leads to the recruitment of Cdt1-bound MCM. The assembly of these proteins constitutes the so-called OCCM complex (ORC, Cdc6, Cdt1, MCM) or pre-RC. Loading of MCM by ORC, Cdc6 and Cdt1, and thus “origin licensing” for DNA replication is controlled by several ATPase-dependent events (Bell & Labib, 2016; Deegan & Diffley, 2016; Frigola *et al.*, 2013; Remus & Diffley, 2009). As mentioned earlier, ORC binding to origins depends on ATP and Cdc6 recruitment depends on ORC and ATP (Coster *et al.*, 2014; Speck *et al.*, 2005; Tsakraklides & Bell, 2010). *In vitro* studies have proposed that initial recruitment of MCM-Cdt1 is achieved by the interaction between the C-terminus of the MCM subunit Mcm3 and ORC-Cdc6. Moreover, such studies demonstrated that binding of the C-terminus of Mcm3 to ORC-Cdc6 stimulates the ATPase activity of ORC-Cdc6 and that this binding is able to induce multiple rounds of ATP binding and hydrolysis by ORC-Cdc6. It has been suggested that binding of Mcm3 triggers conformational movements in ORC-Cdc6, presumably by bringing arginine fingers in contact with ATP binding sites in adjacent subunits, as it is typical of AAA⁺ ATPases (Frigola *et al.*, 2017, 2013).

DNA replication occurs bidirectionally from eukaryotic DNA replication origins and is achieved by the loading of two MCM helicases around DNA in opposite orientations, in a conformation of an inactive head-to-head double hexamer (DH) (Coster & Diffley, 2017; Deegan & Diffley, 2016; Ticau *et al.*, 2015). ORC, together with Cdc6, orchestrates the MCM recruitment of the first hexamer, for which ATP binding by ORC, Cdc6 and MCM is required. In the OCCM complex, the C-terminus of Mcm3 is proximal to Cdc6, which is in line with observations showing that interaction between the C-terminus of Mcm3 and Cdc6-bound ORC mediates the recruitment of MCM (Frigola *et al.*, 2013). During the loading step, MCM undergoes a series of conformational changes; first, the MCM ring must open and then close to capture DNA and second, two MCM-Cdt1 have to be converted into a DNA-bound DH in which the two MCM complexes interact via their N-termini. ATP binding and hydrolysis by MCM is critical for MCM loading. Indeed, ATP-driven conformational changes in MCM are required for the assembly of the DH. Thus, the replicative MCM helicase presents inherent plasticity, and ATP binding and hydrolysis can regulate transitions between the open and closed states of MCM, as well as different conformational states, which in turn enables MCM loading, origin melting and DNA unwinding at replication forks (Coster & Diffley, 2017; Deegan & Diffley, 2016).

The formation of MCM DH implies that both MCM molecules must be able to bind to ORC/Cdc6 that are associated to ORC binding sites. However, yeast origins usually contain a

single high-affinity ORC site located in an NFR. Recruitment of the second MCM hexamer in order to drive bidirectional replication has been a focus of extensive research. However, not until recently *in vitro* studies have started providing cues on how the second MCM is recruited to form the DH necessary to initiate DNA unwinding. Single-molecule studies have proposed a model in which loading of the MCM-DH occurs via a sequential mechanism, in which the loading of the first MCM drives the recruitment of the second MCM hexamer (Ticau *et al.*, 2017). By contrast, biochemical data have demonstrated that the loading of the MCM hexamers occurs via the same ORC-dependent mechanism, proposing a “concerted loading” model (Coster & Diffley, 2017; Remus *et al.*, 2009). This latest model proposes that MCM loading requires two ORC molecules, which is possible because budding yeast origins contain multiple, degenerated ORC binding sites near the high-affinity site. Loading of MCM seems to be achieved by two ORC binding events, one at the high-affinity ORC binding site and an additional non-specific ORC binding event in an adjacent, lower affinity site. Remarkably, the distance between high- and low-affinity sites is not important for origin function and indeed, the distance between high affinity and secondary sites within natural origins diverges. Although the distance between these sites does not affect ORC binding or MCM recruitment *in vitro*, the orientation of these sites must be in a head-to-head orientation (*i.e.* opposite orientation) and such an orientation has been also proven to generate functional origins *in vivo* (Coster & Diffley, 2017). The fact that two ORC binding steps promote efficient MCM loading, but the high-affinity and degenerated ORC sites are spaced, suggests that MCM hexamers might translocate along DNA to form the MCM DH. It has been proposed that MCM translocation could occur merely by passive sliding along the DNA, but since ATP hydrolysis by both MCM hexamers is necessary for MCM loading, a more plausible hypothesis is that translocation is an active process (Coster & Diffley, 2017; Coster *et al.*, 2014; Kang *et al.*, 2014). Although each MCM hexamer that constitutes an MCM DH is loaded by the same mechanism that requires ORC, Cdc6 and Cdt1, whether loading of both MCM hexamers occurs in a sequential or concerted manner is still under debate. Nonetheless, a recent study has provided insights into the loading of the MCM-DH that seem to reconcile both aforementioned models. This study has shown that both MCM rings are recruited onto origins of replication via two ORC assemblies and via the same OCCM mechanism (concerted model), but also that the loading of the first MCM hexamer promotes the loading of the second MCM (sequential and coordinated model) (Miller *et al.*, 2019). The efficient loading of MCM in budding yeast requires a high-affinity ORC binding site and several lower affinity sites arranged in the opposite orientation, and this arrangement has been termed

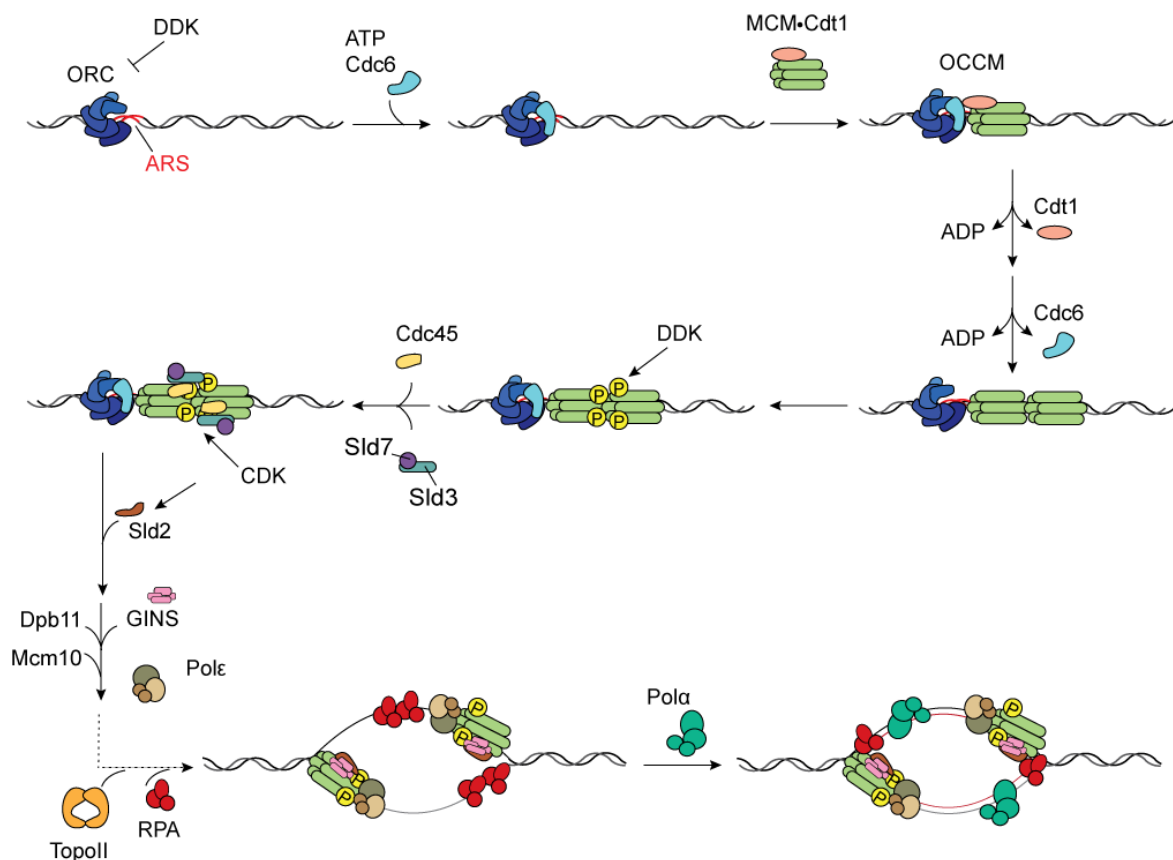
“quasi-symmetrical” (Coster & Diffley, 2017). Remarkably, archaeal origins of replication have similar head-to-head affinity ORC binding sites and *in vivo* work with fission yeast has revealed the requirement for two ORC binding sites for MCM loading (Robinson *et al.*, 2004). Therefore, it is feasible that even if in higher eukaryotes replication origins have low sequence specificity, the mechanism by which MCMs are loaded onto DNA is similar to budding yeast, involving two ORC binding sites.

Both MCM hexamers that are loaded onto DNA are inactive and their activation is necessary for initiation of DNA replication or “origin firing”. Helicase activation requires the combined action of CDK and DDK, as well as a set of “firing factors” that include Sld3/7, Dpb11, Sld2, Cdc45, Mcm10 and DNA polymerase ϵ (Deegan & Diffley, 2016; Diffley & Labib, 2002; Yeeles *et al.*, 2015). The coordinated action of these proteins leads to the conversion of the MCM-DH into two active CMG (Cdc45, MCM, GINS) helicases. In order for the inactive MCM-DH to be remodeled into two active CMG, several steps must take place: *i*) Origin DNA melting to produce ssDNA, *ii*) each MCM ring has to be opened and re-closed to encircle the DNA template, *iii*) Cdc45 and GINS must stably associate with MCM, *iv*) the DH has to separate to produce two CMG complexes, and *v*) activation of the ATPase activity of MCM to allow DNA unwinding, as CMG translocates. The CMG helicase encircles ssDNA and translocates away from origins with a 3'-to-5' directionality on the leading strand.

1.4.2.2.4 Control of DNA replication

As mentioned earlier, DNA replication is regulated throughout the cell cycle by CDK and DDK, which act via several phosphorylation steps of various firing factors, ensuring that the events enabling DNA replication origin firing occur in a temporally controlled manner. CDK has a dual effect since it inhibits MCM loading by phosphorylating ORC and it promotes GMC formation. Therefore, CDK-mediated phosphorylation ensures that MCM loading exclusively occurs during G1 phase (when CDK activity is low) and that helicase activation and consequently, origin firing, can only occur after G1 phase, when CDK levels rise. On the other hand, DDK promotes DNA replication by phosphorylation of MCM and within MCM, Mcm4 and Mcm6 subunits are the DDK key substrates (Diffley, 2011; Remus & Diffley, 2009; Sclafani & Holzen, 2007; Yoshida *et al.*, 2013).

Biochemical work has been able to reconstitute origin firing with purified proteins and has provided insights about the protein kinase regulation in DNA replication origin firing (Yeeles *et al.*, 2015). The eukaryotic DNA replication cycle is inhibited outside G1 phase by phosphorylation of ORC. Phosphorylation of MCM by DDK promotes replication, and Sld3/7 and Cdc45 are recruited to MCM in a DDK-dependent manner, whereas the remaining firing factors (Sld2, Dpb11, GINS, DNA polymerase ϵ and Mcm10) are recruited in a CDK- and DDK-dependent manner. Phosphorylation of the firing factors Sld2 and Sld3 by CDK, promotes their binding to Dpb11, subsequent recruitment of GINS and formation of the CMG



helicase (Figure 1-10).

Figure 1-10 ORC drives the recruitment of the MCM replicative helicase to initiate DNA replication

DNA replication is regulated by the coordinated activities of the CDK and DDK kinases. CDK has a dual effect, as it inhibits MCM loading by phosphorylating ORC and it also promotes helicase activation, ensuring that origin firing only occurs after G1 phase. ARS-associated ORC (bound to Cdc6) mediates the loading of the hetero-hexameric MCM replicative helicase (associated with Cdt1). Main subsequent events driving the initiation of DNA replication, as well as firing factors needed are represented (see section 1.4.2.2.3 for further details). P stands for phosphorylation. The dotted line

Figure 1-10 (Continued)

represents intermediate steps. The dark red line represents newly synthesized DNA. ARS is indicated in red. Modified from Yeeles *et al.*, 2016.

These factors are sufficient to recruit the replication protein A (RPA), a protein that binds to ssDNA and that is necessary to prevent that unwound DNA winds back or forms secondary structures. RPA recruitment is likely induced by the generation of ssDNA by Topoisomerase II, and Mcm10 is as well required for RPA recruitment (Yeeles *et al.*, 2015). Association of all these factors leads to the stable DNA unwinding and the formation of a replication fork. DNA synthesis initiates once that the DNA template is unwound and DNA polymerase α generates primers for DNA synthesis. Though the DNA polymerase ϵ is needed to form CMG, to our knowledge, it remains unclear whether it also contributes to DNA synthesis (Coster & Diffley, 2017; Deegan & Diffley, 2016).

Contrary to what has been described in several metazoans, budding yeast ORC remains associated to chromatin throughout the cell cycle (DePamphilis, 2005; Diffley *et al.*, 1995; Liang & Stillman, 1997). Thus, a long-standing question has been how re-replication (*i.e.* successive DNA replication events) is prevented. In *S. cerevisiae*, re-replication is prevented by several CDK-mediated, overlapping mechanisms that comprise phosphorylation of ORC, nuclear exclusion of the MCM helicase and down-regulation of Cdc6 activity (DePamphilis, 2005; V. Q. Nguyen *et al.*, 2001). Although CDK phosphorylation of Cdc6 and MCM-Cdt1 prevents re-replication *in vivo*, phosphorylation of these proteins does not prevent the loading of MCM *in vitro*. Indeed, *in vitro* research has shown that Sld3/7 and Sld2 are the only CDK substrates necessary for DNA replication initiation (Yeeles *et al.*, 2015). *In vivo* inhibition of re-replication is likely to involve CDK-mediated inhibition of Cdc6 function by promoting its degradation, and CDK inhibition of MCM-Cdt1 by promoting its nuclear exclusion. Re-replication is also avoided by phosphorylation of Orc6 and Orc2 by CDK, since it blocks the ability of ORC to load MCM (Arias & Walter, 2007; Elsasser *et al.*, 1999; V. Q. Nguyen *et al.*, 2001). Thus, CDK levels and activity are critical to ensure that replication occurs once and only once per cell cycle.

1.4.2.2.5 Role of the chromatin structure in ORC association with origins of replication

In other eukaryotic organisms the origin sequence pattern is not as well defined as in budding yeast, except for the fact that they are usually AT-rich sequences. Determinants that

define replication origins have been proposed, such as the local chromatin structure (and particularly, nucleosome positioning), chromatin modifications or transcription regulation (Bell & Labib, 2016; Lucas & Raghuraman, 2003). Even in budding yeast, the presence of an ORC-binding site is necessary but not sufficient for origin function. Indeed, in *S. cerevisiae*, accessory elements of the ACS, such as the B2 element or the B3 element enhance or influence origin activity. Moreover, in both yeast and higher organisms, origins are normally in NFR or nucleosome depleted regions (NDRs). In fact, budding yeast ARSs usually map to intergenic regions and those ARSs that fall within genes might be inefficient or inactive as origins (Kumar & Remus, 2016; Lucas & Raghuraman, 2003; Yoshida *et al.*, 2013).

Early studies led to an estimate of ~200-400 origins of replication in the budding yeast genome, but the database from the *S. cerevisiae* origins (OriDB) identifies >600 origins (“confirmed” or “likely” origins), of which only a subset initiate replication (Bell & Labib, 2016; Lucas & Raghuraman, 2003; Siow *et al.*, 2012). There are different aspects that influence origin choice and origin efficiency and timing. Origin efficiency refers to the frequency in which a defined origin is used in each cell cycle (*i.e.* an origin efficiency can be low or high depending on how frequently is the same origin used in the cell cycles). Low origin efficiency likely accounts for the low competence of a due origin to assemble the pre-RC. For instance, in the budding yeast rDNA (in which each repeat harbors an ARS) ARSs seem to have low firing efficiency and it is estimated that only ~5-7 origins are used on average. Replication timing refers to the moment in which an origin is duplicated, either by active or passive replication (Bell & Labib, 2016; Lucas & Raghuraman, 2003; Yoshida *et al.*, 2013). It is worth mentioning that replication origins do not fire simultaneously at the G1/S transition. Instead, origin activation occurs sequentially throughout S phase and each origin presents a characteristic timing at a population level. Some origins fire early in S phase and other origins fire in late S phase, and origin timing seems to be determined by architectural features present in the chromosomes (Méchali *et al.*, 2013; Yoshida *et al.*, 2013). An example of how the chromosome context influences origin timing comes from the knowledge that the state of histone acetylation is a key determinant of replication timing. In this line, it has been shown that in budding yeast, tethering the Gcn5 histone acetyltransferase closeby a near origin partially advances its initiation time. Moreover, the HDAC Sir2 represses initiation at the origins of the rDNA array (Vogelauer *et al.*, 2002; Yoshida *et al.*, 2014, 2013).

In recent years, it has become more evident that, also in budding yeast, origin timing and efficiency is influenced by the local chromatin structure and particularly, by the

positioning of nucleosomes. ORC binding sites are usually situated in NDRs and ORC contributes to shape the pattern of nucleosome positioning around the ACS; nucleosome positioning in turn, can influence origin function and timing. It is believed that those origins that are more accessible (*i.e.* few nucleosomes in the adjacent regions) fire earlier in S phase. Although origin sequences are sufficient to maintain an NDR, it has been shown that ORC is required to position the nucleosomes flanking the origin in an asymmetric pattern (Eaton *et al.*, 2010). In budding yeast, the characteristic nucleosome positioning pattern is generated in two steps; first, an NDR is established in a sequence-specific manner (determined by ACS matches) and second, ORC bound at origins positions the upstream (-1) and downstream (+1) flanking nucleosomes and establishes the typical nucleosomal patterning seen at origins of replication. Those nucleosomes positioned by ORC are important for pre-RC formation, as disruption of ORC-directed arrangement of nucleosomes interferes with replication initiation. Indeed, ORC is key in the nucleosomal arrangement of yeast origins both *in vivo* and *in vitro*, and nucleosomes adjacent to origins have a positive role in replication since they stimulate initiation of DNA replication by helping in the formation of the pre-RC (Eaton *et al.*, 2010; Lipford & Bell, 2001). Thus, nucleosome organization is an additional determinant of origins (also in budding yeast) and that chromatin-associated features, such as histone modifications, might control the efficiency and timing of DNA replication.

The BAH domain of the Orc1 subunit plays a determinant role in origin selection (Müller *et al.*, 2010a). As mentioned earlier, BAH domains are chromatin-binding modules and the Orc1-BAH domain has been mostly known for its crucial function in the process of transcriptional silencing via interaction with the silencing protein Sir1 (Gartenberg & Smith, 2016; Hickman & Rusche, 2010; N. Yang & Xu, 2013). Nonetheless, this domain is dispensable for cell viability (*i.e.* is not essential for DNA replication), because in *orc1bahΔ* yeast strains most replication origins remain partially or fully functional (Bell *et al.*, 1995). However, Müller and co-workers have shown that the BAH domain of Orc1 contributes to ORC association with most origins and that there is a subset of origins especially sensitive to the deletion of this domain (named *orc1bahΔ*-sensitive origins). Orc1-BAH domain contributes differently to the association of ORC to origins, such that origins vary from being highly dependent on this domain (*orc1bahΔ*-sensitive) to independent (*orc1bahΔ*-resistant). It has been proposed that in the *orc1bahΔ*-sensitive origins, ORC recognizes both a consensus sequence and nearby nucleosomes. Nucleosome positioning has been involved in the regulation of origin activity, but normally nucleosomes are associated with inhibition, rather

than with enhancement of origin activity. The *orc1bah Δ* -sensitive origins present a distinct nucleosome organization in which the NFRs are smaller and in this class of origins, the BAH domain of Orc1 could interact with the nucleosome positioned 5' of the NFR, promoting ORC-origin association (Müller *et al.*, 2010a). Therefore, although yeast ORC clearly recognizes and binds specific DNA sequences, a subset of yeast origins might function more similar to metazoan origins, in which other factors besides DNA sequence, such as chromatin structure, are determinant of origin recognition by ORC, suggesting the existence of evolutionarily conserved mechanisms for origin selection.

1.4.2.2.6 Pre-meiotic replication

Budding yeast pre-meiotic S phase (meiS) has been estimated to last 1.5 to 3 times more than pre-mitotic S phase. The increased length of meiS has been attributed to the extensive chromosome re-organization that occurs during meiotic prophase (*i.e.* organization of chromosomes into chromatin loops that emanate from a central axis) (Padmore *et al.*, 1991; Williamson *et al.*, 1983; Zickler & Kleckner, 1999). Nevertheless, pre-meiotic DNA replication and meiotic chromosome axis formation are not strictly coupled; preventing the formation of recombination structures does not bypass delays in pre-meiotic DNA replication and cells with unreplicated DNA are able to initiate meiotic recombination (Blitzblau *et al.*, 2012). Thus, the longer duration of pre-meiotic S phase cannot be explained by the formation of meiotic recombination intermediates. Instead, it has been proposed that the extended meiS could be theoretically due to reduced efficiency of the initiation of DNA replication (either from all or from a subset of origins), to reduced replication fork rates, or a combination of both.

Genome-wide analysis of the MCM replicative helicase subunit Mcm2 has revealed that the majority of origins equally load MCM during pre-meiotic and pre-mitotic DNA replication, supporting the idea that the mechanism by which origins are selected is similar. ORC mapping analyses have tended to focus on revealing ORC binding sites in mitosis rather than meiosis. Since ORC serves as a loading pad for MCM recruitment, Mcm2 mapping in meiosis can be plausibly used as a proxy for ORC binding, and such an assumption would imply that not only MCM but also ORC binding sites are mostly conserved in mitosis and meiosis. Nonetheless, there are some differences in MCM binding (as judged per Mcm2 association to origins) and subsets of origins have been found to be either mitosis- or meiosis-specific (Blitzblau *et al.*, 2012).

In addition, it has been shown that most origins are active in *meiS* and pre-mitotic S phase, although the replication timing in both S phases differs. Particularly, the majority of origins evaluated in the aforementioned study are delayed in the meiotic cell cycle, as seen by comparing replication profiles from meiotic and mitotic cells. Such origins initiate replication later in pre-meiotic cells and thus, the extended length of *meiS* could be attributed to delayed initiation of DNA replication or to slow fork progression rates. Studies focusing on Mcm2 genome-wide analysis support a model of delayed initiation of replication. The reduced replication initiation could be due to a limiting activating factor, such as CDK activity levels. Another plausible explanation for the slow pre-meiotic DNA replication could be that dNTP levels are reduced during *meiS*, due to the starvation conditions needed to initiate the meiotic program in budding yeast. These lowered nucleotide amounts could cause a delay in initiation of replication and also decrease replication fork progression rates. It is worth mentioning that not all origins in *meiS* seem to be equally delayed. In fact, origins close to centromeric regions replicate efficiently, also in pre-meiotic S phase and these sites have been shown to be critical in defining the timing of the replication program (Blitzblau *et al.*, 2012).

Altogether, pre-meiotic replication is driven by the same mechanisms than replication in vegetative growing cells (Simchen, 1974). The main difference between the replication program prior to meiosis and mitosis in budding yeast appears to be the replication timing since *meiS* is longer than pre-mitotic S phase. However, this discrepancy is not due to changes in origin selection or origin activation, which are highly similar in *meiS* and pre-mitotic S phase (Collins & Newlon, 1994).

1.4.2.3 Other functions of ORC

Beyond the essential, well-defined role of ORC in initiation of DNA replication, this complex performs other functions in *S. cerevisiae*, such as transcriptional silencing, sister chromatid cohesion and protection of rDNA-associated DSB formation (reviewed in Popova *et al.*, 2018; Suter *et al.*, 2004).

As mentioned in section 1.3.1, unlike the expressed *MAT* locus, mating-type genes need to be transcriptionally silenced in the budding yeast mating-type loci (*HMR/HMR*). Silencing initiates in specific DNA sequences known as “silencers”, in which silencer-binding proteins associate to subsequently recruit a set of silencing proteins (Sir proteins) that enable the formation of specialized, repressed chromatin. The primary role of ORC in silencing is to

act as a silencer-binding protein, as it recruits the silencing protein Sir1 through direct protein-protein interactions in which the BAH domain of Orc1 is involved (Foss *et al.*, 1993; Fox *et al.*, 1995; Hickman & Rusche, 2010; Hou *et al.*, 2005; Loo *et al.*, 1995; Triolo & Sternglanz, 1996). Interaction between ORC and Sir1 in turn nucleates the assembly of silent chromatin domains by recruitment of other Sir proteins (Sir2, Sir3 and Sir4) and Sir2-mediated histone deacetylation (Bell *et al.*, 1995; Foss *et al.*, 1993; Gartenberg & Smith, 2016; Hou *et al.*, 2005) (For more details on transcriptional silencing, see section 1.3).

ORC has also been implicated in sister chromatid cohesion in budding yeast mitosis, which is essential for the equal segregation of duplicated chromosomes into daughter cells. This cohesion is achieved by the ring-shaped complex cohesin, which ensures the linkage of sister chromatids so that they resist pulling forces from the microtubules until metaphase-to-anaphase transition (Haering *et al.*, 2008; Nasmyth & Haering, 2009; Uhlmann & Nasmyth, 1998). Conditional depletion of the Orc2 subunit by a glucose repression system in an *orc2-1(ts)* background showed that, although DNA replication is not impaired, progression through mitosis is significantly delayed. Specifically, a Mad2-spindle checkpoint is activated upon Orc2 depletion and cells undergo a transient delay in G2/M (Shimada & Gasser, 2007). This cell cycle delay has been accounted for the impairment of sister chromatid cohesion seen in Orc2-depleted cells. In fact, sister chromatid cohesion is compromised by Orc2 depletion, although cohesin is properly loaded onto chromatin. It has been suggested that ORC promotes cohesion between replicated sister chromatids in parallel to cohesin, possibly by forming a bridge between sisters that is independent of the cohesin ring. Nevertheless, the exact mechanism by which ORC mediates cohesion between sister chromatids remains unknown (Popova *et al.*, 2018; Shimada & Gasser, 2007; Suter *et al.*, 2004).

Centrosomes serve as the main organizer of microtubules in animal cells and they contain a pair of centrioles, and Orc1 has been implicated in controlling copy number of centrosomes and centrioles in human cells by regulating Cyclin E-dependent duplication of these structures (Hemerly *et al.*, 2009). In addition, the Orc1 subunit represses Cyclin E (*CCNE1*) transcription. Cyclin E together with Cdc6 promotes DNA replication, and Orc1 and Cdc6 have opposite effects on the control of the Cyclin E levels. The fact that Cdc6 counteracts the effects of Orc1 and reactivates *CCNE1* appears to be critical for the cell commitment to either DNA replication or cell division (Hossain & Stillman, 2016).

It is worth mentioning, that Shibata and co-workers have revealed that human cells that lack two components of ORC, Orc1 and Orc2, are viable without significant effects on DNA replication or cell survival. However, in conditions of Orc1 or Orc2 depletion, cells replicate with reduced MCM loading and became more dependent on the Cdc6 protein to survive and divide (Shibata *et al.*, 2016). This contrasts with *S. cerevisiae*, in which all the ORC subunits are needed for cell viability.

Recently, a subunit of ORC, Orc4, has been found to associate with the extrusion of the polar body in mice (Nguyen *et al.*, 2015). A polar body is a byproduct of female meiosis that forms concomitantly with the female gamete (the egg), in which genomic material is discarded and that does not have the ability to be fertilized. In mouse, the association of Orc4 with the polar body chromatin appears to be independent of other ORC subunits, which suggests that Orc4 functions separately from other ORC members.

In addition to its functions in DNA replication, transcriptional silencing and sister chromatid cohesion, budding yeast ORC has also been implicated in a meiosis-specific process. Particularly, the Orc1 subunit has been associated to the rDNA protection against DSBs in meiosis. As mentioned in section 1.4.1.1, this function is achieved in collaboration with the AAA⁺ ATPase Pch2. The Orc1 subunit seems to be driving the recruitment of Pch2 to the nucleolus, where the rDNA assembles, and impairment of either Orc1 (via a ts mutant, *orc1-161*) or Pch2 (via deletion, *pch2Δ*) leads to increased meiotic recombination in the rDNA boundaries (Vader *et al.*, 2011). However, the role of Orc1/ORC in protecting the rDNA of *S. cerevisiae* has remained mostly unexplored.

1.5 Objectives

Controlled DSB formation is an essential feature for the proper execution of the meiotic programme. However, DSB introduction within repetitive DNA elements and subsequent DSB repair can lead to genome destabilization. Thus, DSB formation within or nearby repetitive sequences should be minimized to avoid genome instability. In this Ph.D. work, we used the repetitive ribosomal DNA (rDNA) of budding yeast to better characterize how the rDNA boundaries, which are also at high risk of non-allelic homologous recombination (NAHR), are protected against DSB formation. Although it is known that the AAA⁺ ATPases Pch2 and Orc1 are involved in the suppression of DSBs at the rDNA edges, the molecular basis by which the Pch2-Orc1(ORC) anti-DSB system operates remain unclear. Therefore, this Ph.D. thesis aims to:

- 1) Characterize the interaction between Pch2 and Orc1 *in vivo*
- 2) Understand whether other ORC subunits, besides Orc1, are involved in the interaction with Pch2

If other subunits of ORC are involved in the interaction between Pch2 and Orc1, we aim to:

- 3) Define whether the interaction between Pch2 and ORC is direct
- 4) Test whether other ORC subunits also play a role together with Pch2 in the protection of the rDNA borders
- 5) Reconstitute the Pch2-ORC assembly and characterize the interaction of this complex *in vitro*
- 6) Investigate whether the function of Pch2 at the rDNA depends on ORC association to its canonical sites (*i.e.* origins of replication)

To shed light on the interaction mode and functionality of these AAA⁺ ATPases, we employed a combination of *in vivo* studies and biochemical *in vitro* assays.

2 Material and Methods

2.1 Materials

2.1.1 Chemicals and reagents

All chemicals and reagents used in this study are listed in Table 2-1.

Table 2-1 Chemicals and reagents

Chemicals and reagents	Supplier
Acetic acid	Sigma-Aldrich
Acid-washed glass beads	Sigma-Aldrich
Acrylamide/bis-acrylamide solution 30% (29:1)	Carl Roth
Adenosine triphosphate (ATP)	Sigma-Aldrich
Adenosine 5-(3-thiotriphosphate) tetralithium salt (ATP- γ -S)	Merck Millipore
Agar	Becton Dickinson
Agarose standard	Carl Roth
Alpha-factor	MPI Dortmund
Ammonium bicarbonate (ABC), Fluka	Thermo Fisher Scientific
Ammoniumperoxosulfate (APS)	Serva Electrophoresis
Amylose beads	New England BioLabs
Bacto-peptone	Becton Dickinson
Bacto-tryptone	Becton Dickinson
Benzonase	Sigma-Aldrich
Bradford solution	Bio-Rad Laboratories
Boric acid	Gerbu Biotechnik
Bromophenol blue	Sigma-Aldrich
Chloroacetamide (CAA)	Sigma-Aldrich
Chloramphenicol	Sigma-Aldrich
cOmplete™ Mini, EDTA-free protease inhibitor	Roche
Coomassie G250	Serva Electrophoresis
[α - ³² P]dCTP (6000 Ci/mmol, 20 mCi/ mL Easy)	Perkin Elmer
Deoxyribonucleic acid sodium salt from salmon testes	Sigma-Aldrich

Table 2-1 Chemicals and reagents (Continued)

Chemicals and reagents	Supplier
Dextran sulfate sodium salt	Sigma-Aldrich
Difco yeast nitrogen base without AA and AS	Becton Dickinson
Dimethylsulfoxide (DMSO)	Serva Electrophoresis
Disuccinimidyl dibutyric urea (DSBU)	Alinda Chemical Limited
Dithiothreitol (DTT)	Serva Electrophoresis/GERBU
DNA ladder GeneRuler™ 1kb	Fermentas
Dynabeads™ Protein G	Invitrogen, Thermo Fisher Scientific
ECL Prime/ECL Select Western Blotting Detection Reagent™	GE Healthcare
EGTA	Thermo Fisher Scientific
Empore C18 47mm discs, 3M	Thermo Fisher Scientific
Ethylenediaminetetraacetic acid (EDTA)	Gerbu Biotechnik
Ethanol (EtOH)	Carl Roth
Fetal Bovine Serum (FBS)	Thermo Fisher Scientific
Formaldehyde, 10%, methanol free, Ultra Pure	Polysciences
FuGENE® HD Transfection Reagent	Promega
D-Galactose	Sigma-Aldrich
Gel filtration standard	Bio-Rad
Glycerol	Gerbu Biotechnik
Glycine	Carl Roth
HEPES	Sigma-Aldrich
Hydrochloric acid (HCl)	Fisher Scientific
Imidazole	Merck Millipore
IPTG	Carl Roth
Isopropanol	J.T.Baker Chemicals
Lysyl Endopeptidase	WAKO
Lithium acetate dihydrate (LiAc)	Sigma-Aldrich
Magnesium chloride (MgCl ₂)	J.T.Baker Chemicals
β-Mercaptoethanol	Serva Electrophoresis
Methanol	Sigma-Aldrich

Table 2-1 Chemicals and reagents (Continued)

Chemicals and reagents	Supplier
Midori Green Advanced DNA stain	Nippon Genetics Europe GmbH
Milk powder blocking grade	Carl Roth
4–15% /10% Mini-PROTEAN® TGX™ Precast Protein gels	Bio-Rad Laboratories
PerfeCTa® SYBR® Green FastMix®	Quantabio
Phenylmethylsulfonyl fluoride (PMSF)	Serva Electrophoresis
Phenol/Chloroform/Isopropanol (25:24:1)	Carl Roth
Polyethylene glycol (PEG) 3350	Sigma-Aldrich
Ponceau S solution	PanReac AppliChem
Potassium acetate (KOAc)	Carl Roth
Potassium dihydrogen phosphate (KH ₂ PO ₄)	Merck Millipore
Potassium chloride (KCl)	J.T.Baker Chemicals
Potassium phthalate	Merck Millipore
Precision Plus Protein™ Dual Color Standards	Bio-Rad Laboratories
Proteinase K	Amresco
Proteinase K-PCR grade	Roche Diagnostics
RedSafe™ Nucleic acid staining solution	Intron Biotechnology
Rapamycin	LC Laboratories
RNase A, 50 µg/mL	Sigma-Aldrich
SeaKem® LE Agarose	Lonza
Serva protease-inhibitor mix	Serva Electrophoresis
Sheared salmon sperm DNA	Invitrogen
Sodium chloride (NaCl)	VWR chemicals
Sodium dodecyl sulfate (SDS)	Carl Roth
Sodium hydroxide (NaOH)	VWR chemicals
Sodium orthovanadate	Sigma-Aldrich
D-Sorbitol	Sigma-Aldrich
SYTOX® Green nucleic acid stain	Life Technologies
N, N, N', N'- Tetramethylethylenediamine (TEMED)	Serva Electrophoresis
Trifluoroacetic acid (TFA)	Sigma-Aldrich

Table 2-1 Chemicals and reagents (Continued)

Chemicals and reagents	Supplier
Tris-(hydroxymethyl)-aminomethane (Tris)	Carl Roth
Triton X-100	Thermo Fisher Scientific
Trypsin, recombinant, proteomics grade	Sigma-Aldrich
Tween-20	AppliChem
Urea	Sigma-Aldrich
Zymolyase® 100T from <i>Arthrobacter luteus</i>	Amsbio
Yeast extract	Becton Dickinson

2.1.2 Enzymes and commercial mixes

Enzymes and commercial prepared mixes used in this study are listed in Table 2-2.

Table 2-2 Enzymes and commercial mixes

Enzyme type	Name	Supplier
Exonuclease	T5 Exonuclease	Epicentre
Ligase	T4 DNA Ligase	New England BioLabs
	Gibson Assembly® Master Mix	
Polymerase	TaKaRa Ex Taq®	TaKaRa Bio
	Q5 High-Fidelity® 2x Master Mix	New England BioLabs
	VWR Taq	VWR Life Science
	PerfeCTa®SYBR® Green FastMix®	Quantabio
	Phusion HF DNA Polymerase	Thermo Scientific
Restriction endonuclease	<i>Sall High Fidelity (HF)</i>	New England BioLabs
	<i>EcoRI</i>	
	<i>StuI</i>	
	<i>XbaI</i>	
	<i>DpnI</i>	
	<i>BamHI</i>	
	<i>HindIII</i>	
	<i>SwaI</i>	
<i>ApalI</i>		
Yeast lytic enzyme (Lyticase)	Zymolyase® T100	AMS Biotechnology

2.1.3 Commercial kits

Commercial kits used in this study are listed in Table 2-3.

Table 2-3 Commercial kits

Kits	Supplier
Prime-It RmT Random Primer labeling Kit	Agilent Technologies
QIAquick Gel Extraction Kit	Qiagen
QIAquick PCR purification Kit	
QIAprep Spin Miniprep Kit	
Rapid DNA Ligation Kit	Thermo Fisher Scientific
Wizard® SV Gel and PCR Clean-Up system	Promega

2.1.4 Antibiotics

Antibiotics added to the bacterial cultures in this study are indicated in Table 2-4 at the corresponding concentrations.

Table 2-4 Antibiotics

Antibiotic	Concentration	Supplier
Ampicillin	100 µg/ml	Serva Electrophoresis
Gentamycin	50 µg/ml	Sigma-Aldrich
Kanamycin	10 µg/ml	Gerbu Biotechnik
Tetracyclin	7 µg/ml	Sigma-Aldrich

2.1.5 Antibodies

Primary and secondary (HRP-conjugated) antibodies used in this study are listed in Tables 2-5 and 2-6.

Table 2-5 Primary antibodies

Immunogen	Source	Dilution	Supplier
α-Flag	Mouse monoclonal	1:1000	Sigma-Aldrich
α-HA	Mouse monoclonal	1:1000	BioLegend
α-MBP	Mouse monoclonal	1:10000	New England BioLabs
α-ORC	Rabbit	1:1000	Stephen Bell Laboratory
α-Orc2	Mouse monoclonal	1:1000	Abcam
α-Pgk1	Mouse monoclonal	1:5000	Life Technologies
α-TAP	Rabbit polyclonal	1:2500	Thermo Fisher Scientific
α-V5	Mouse monoclonal	NA*	Invitrogen

Dilutions indicated are for use of the antibodies for Western blot analysis.

*NA (not applicable): antibody used for Co-Immunoprecipitation (Co-IP) assays. The amounts of antibody are indicated in the Method section.

Table 2-6 HRP-conjugated antibodies

Immunogen	Source	Dilution	Supplier
Anti-mouse IgG	Sheep	1:5000	GE Healthcare
Anti-rabbit IgG	Donkey	1:5000	GE Healthcare

2.1.6 Buffers and solutions

Frequent buffers and solutions used in this study with the corresponded method are summarized in Table 2-7. Buffers used for protein purification are specifically detailed within the section Methods for each protein.

Table 2-7 Buffers and solutions

Method	Buffer/Solution	Composition	Final concentration
Agarose gel electrophoresis	10x DNA Loading buffer	EDTA Bromophenol blue Xylencyanoblue Glycerol	1 mM 0.25% (w/v) 0.25% (w/v) 50% (v/v)
	10x TAE buffer	Tris-base Glacial acetic acid EDTA	400 mM 200 mM 10 mM
	5x TBE buffer	Tris-base Boric acid EDTA	445 mM 445 mM 10 mM

Table 2-7 Buffers and solutions (Continued)

Method	Buffer/Solution	Composition	Final concentration
Chromatin Immunoprecipitation (ChIP)	TAP ChIP buffer	Tris-HCl pH 8.0 NaCl NP-40 EDTA pH 8.0	25 mM 150 mM 0.1% 1 mM
	10x Tris Buffered Saline (TBS)	Tris-base NaCl KCl	25 mM 150 mM 2mM
	Tris-EDTA (TE) buffer	Tris-HCl pH 7.5/8 EDTA pH 8.0	10 mM 1 mM
	TE-SDS buffer	Tris-HCl pH 8 EDTA pH 8.0 SDS	10 mM 1 mM 1% (w/v)
Co-Immunoprecipitation (Co-IP)	IP buffer	Tris-HCl pH 7.5 NaCl Triton X-100 EDTA pH 8.0	50 mM 150 mM 1% (v/v) 1 mM
	TCA resuspension buffer	Tris-HCl 7.5 Urea	50 mM 6 M
Genomic DNA extraction from meiotic yeast cells	DNA Breakage buffer	Triton X-100 SDS NaCl Tris pH 8.0 EDTA	2% (v/v) 1% (w/v) 100 mM 10 mM 1 mM
	Lysing buffer	Tris (pH 8) EDTA	1M 500 mM
	Spheroplasting buffer	Sorbitol K ₂ HPO ₄ KH ₂ PO ₄ EDTA	1M 42 mM 8 mM 5 mM

	Spheroplasting solution	β -Mercaptoethanol Zymolyase in Spheroplasting buffer	1% (v/v) 2.5% (v/v)
Gibson cloning (biGBac)	5x isothermal reaction buffer (IRB)	PEG-8000 Tris-HCl pH 7.5 MgCl ₂ DTT dNTPs (dATP, dGTP, dCTP, and dTTP) NAD	25% 500mM 50mM 50mM 1mM of each 5mM
Hybridization, neutralization and washing for Southern blots	High stringency wash buffer	SDS in 0.1x SSC	0.1% (w/v)
	Hybridization buffer	Sodium phosphate pH 7.2	250 mM
		NaCl	250 mM
		EDTA	1mM
	SDS	7% (w/v)	
Dextran sulphate	5% (w/v)		
Low stringency wash buffer	SDS in 2x SSC	0.1% (w/v)	
Sodium phosphate buffer pH 7.2	Na ₂ HPO ₄ NaH ₂ PO ₄	1M 1M	
20x SSC	NaCl Na ₃ Citrate	3 M 300 mM	
Protein staining	Coomassie Brilliant Blue staining solution	Acetic acid Coomassie G-250 EtOH	7.5% (v/v) 0.2% (w/v) 50% (v/v)
SDS-PAGE	5x SDS Loading Buffer	Tris-HCl pH 6.8 β -Mercaptoethanol Glycerol SDS Bromophenol blue	50 mM 1% (v/v) 10% (v/v) 4% (w/v) 0.02% (w/v)

	10x SDS Running Buffer	Tris-base Glycine SDS	25mM 192mM 0.1% (w/v)
Western blot	1x Phosphate Buffered Saline (PBS)	NaCl KCl Na ₂ HPO ₄ KH ₂ PO ₄	137 mM 2.7 mM 8 mM 2 mM
	1x PBS-T	Tween-20 in 1x PBS	0.05% (v/v)
	10x Western transfer buffer	TRIZMA base Glycine SDS	3% (w/v) 14.4% (w/v) 0.2% (w/v)
	Blocking Buffer	Milk powder in 1x PBS- T	4% (w/v)
Yeast whole-cell extract for Western Blot using TCA	Protein breakage buffer	Tris pH 7.5 EDTA DTT	50 mM 1 mM 2.75 mM

2.1.7 Media

Media used for yeast and bacteria are summarized in Table 2-8. For solid media, the media listed below was supplemented with 2% (w/v) agar for yeast plates or 1.5% (w/v) agar for bacteria plates. For selection of auxotrophic yeast strains, minimal (MIN) medium supplemented with various nutrients (amino acids such as tryptophan, histidine, leucine, arginine and lysine, and nucleotide precursors, such as uracil and adenine). All amino acids and nucleotide precursors were purchased from Sigma-Aldrich. For yeast two-hybrid (Y2H) assays, MIN medium was supplemented with all amino acids and nucleotide precursors except from Ura and Leu (for control plates) or Ura, Leu and His (for selection plates). For selection of drug-resistant mutants and cell growth assays with the anchor-away yeast strains, the drug rapamycin was added to a final concentration of 1 µg/mL to yeast extract peptone dextrose (YPD). For plasmid selection in bacteria, usually Ampicilin (100 µg/ml) was added to Luria-Bertani (LB) medium. For selection of bacmids used for insect cells protein expression, LB was supplemented with 10 g/mL gentamycin, 7 g/mL tetracycline, 50 g/mL kanamycin, 40 g/mL IPTG and 100 g/mL X-Gal. For insect cells culture, Sf-900™ III SFM (Thermo Fisher Scientific) was used.

Table 2-8 Media

Medium	Microorganism	Composition	Final concentration
Buffered YTA (BYTA)	<i>S. cerevisiae</i>	Yeast extract Bactotryptone KAc Potassium phthalate	1% (w/v) 2% (w/v) 1% (w/v) 50mM
Luria-Bertani (LB)	<i>E. coli</i>	Tryptone Yeast extract NaCl	0.5% (w/v) 1% (w/v) 0.5% (w/v)
Minimal (MIN)	<i>S. cerevisiae</i>	Difco yeast nitrogen without AA and AS Ammonium sulfate Inositol D-Glucose	0.15% (w/v) 0.5% (w/v) 2 mM 2% (w/v)
Sporulation (SPO)	<i>S. cerevisiae</i>	KAc Acetic acid	0.3% (w/v) 5% (v/v)
Yeast extract peptone dextrose (YPD)	<i>S. cerevisiae</i>	Bactopeptone Yeast extract L-Tryptophan D-Glucose	2% (w/v) 1% (w/v) 0.015% (w/v) 2% or 4 % (w/v)
Yeast peptone glycerol (YPG)	<i>S. cerevisiae</i>	Bactopeptone Yeast extract L-Tryptophan Glycerol	2% (w/v) 1% (w/v) 0.015% (w/v) 3% (v/v)

2.1.8 Synthetic oligonucleotides

Synthetic oligonucleotides were used for Polymerase Chain Reaction (PCR), real-time quantitative PCR (qPCR), cloning (by restriction ligation and Gibson assembly) and sequencing. All synthetic oligonucleotides were purchased from Sigma-Aldrich. A list of synthetic oligonucleotides used for qPCR and cloning can be found in Table 7-5, 7-6 and 7-7 (Appendix).

2.1.9 Plasmids

Plasmids used for yeast two-hybrid (Y2H) assays were majorly cloned by restriction digestion with *EcoRI* and *Sall* restriction enzymes. Plasmids used for expression of TAP- and Flag-tagged constructs were majorly cloned by Gibson assembly and integrated at the budding yeast *TRIP1* locus after digestion with *PmlI*. Plasmids used for protein expression in insect cells were mostly cloned by Gibson assembly. A detailed list with plasmids employed in this study can be found in Table 7-8 (Appendix). Plasmid containing *Spodoptera frugiperda* (*Sf9*) codon optimized sequences were acquired from GeneArt/Gene Synthesis. Plasmid containing 3xFlag-6xGly-tag was purchased from Life Technologies (Thermo Fisher Scientific).

2.1.10 Competent cells

For bacterial transformation *E. coli* OmniMax chemically competent cells (kindly provided by the Dormund Protein Facility (DPF), MPI Dortmund) were used in most of the cases. Alternatively, Top10 chemically competent cells (Thermo Fisher Scientific) were used. For expression of constructs employed for bacterial protein expression BL21(DE), BL21-CodonPlus (DE3)-RIPL, C41 (D43) and RosettaTM (D43) competent cells were used. For transformation of constructs for protein expression in insect cells, MAX EfficiencyTM DH10 BacTM cells (EMBacY cells) (Thermo Fisher Scientific) were employed.

2.1.11 Yeast strains

Yeast strains used in this study are listed in Table 7-9 (Appendix).

2.1.12 Laboratory instruments and devices

Laboratory instruments and devices used in this study are listed in Table 2-9.

Table 2-9 Laboratory instruments and devices

Application/ Method	Instruments and supplies	Supplier
Agarose gel electrophoresis	Agarose gel electrophoresis system	Carl Roth
	Owl™ A2-BP large gel system	Thermo Fisher Scientific
Cell density measurement	BioPhotometer®	Eppendorf
Cell lysis	Branson Sonifier 450	Branson Ultrasonics Corporation
	Bioruptor®-Plus	Diagenode
	FastPrep®-24 machine	MP Biomedicals
	IKA® VXR basic Vibrax	IKA®-Werke
	Microfluidizer M-110S	Microfluidics Corporation
Centrifuge	Optima XL-A analytical ultracentrifuge	Beckman Coulter
	Allegra® X-15R centrifuge	
	Avanti J-30I centrifuge	
	Optima XL-A ultracentrifuge	
	Avanti JXN-30 centrifuge	Eppendorf
	Centrifuge 5810 R	
	Centrifuge 5424	
	Centrifuge 5424 R	Thermo Scientific
	Sorvall RC 3BP+ centrifuge	
Co-Immunoprecipitation (Co-IP)	DynaMag™-2 Magnet	Thermo Fisher Scientific
Cross-link mass-spectrometry (XL-MS)	Superdex Peptide 3.2/ 300 column	GE Healthcare
	Ultimate 3000 RSLC nanosystem and a Q-Exactive Plus mass spectrometer	Thermo Fisher Scientific
Flow cytometry	BD Accuri™ C6 Flow Cytometer	BD Biosciences
Incubators	Heratherm™ microbiological incubator	Thermo Fisher Scientific
	Kelvitron® Thermo Scientific	
	Heraeus® incubator	

Table 2-9 Laboratory instruments and devices

Application/ Method	Instruments and supplies	Supplier
Mass spectrometry	Thermo Scientific™ EASY-nLC 1000 HPLC system	Thermo Fisher Scientific
	Q Exactive™ mass spectrometer	
Microscopy/ Tetrad dissection	Tetrad dissection Microscope Nikon Eclipse Ci	Schuett-biotec
Mixer/ Shaker/ Rotator	Stuart™ Scientific roller mixer SRT6	Bibby Scientific
	Thermomixer comfort 5436	Eppendorf
	Minitron	Infors HT
	Multitron® shaker	
	Rotator L29	Labinco
	Test-tube rotator	
	Innova™ 2000 platform shaker	New Brunswick Scientific
	RS-TR 05 tube roller	Phoenix Instruments
	See-saw rocker SSL4	Stuart® See-saw rockers Cole Parmer
	Labquake shaker rotisserie	Thermo Scientific
Nucleic acid hybridization	HB-1000 Hybridizer Hybridization Oven	Analytik Jena AG
pH measurement	pH-Meter 766 Calimatic	Knick
Phosphorimaging	LB 122 Contamination monitor equipment	Berthold Technologies
	Storage Phosphor Screen BAS-IP MS 2040	GE Healthcare
	Typhoon Trio+ scanner	
	X-ray cassette (35x43cm)	Kisker Biotech GmbH & Co. KG

Table 2-9 Laboratory instruments and devices (Continued)

Application/ Method	Instruments and supplies	Supplier
Polymerase chain reaction (PCR)	7500 FAST Real-Time PCR machine	Applied Biosystems
	T3000 Thermocycler	Biometra
	UV light transilluminator	BLstar 16, Biometra
	96-well plate	Kisker Biotech GmbH & Co. KG
	PCR ultra-clear adhesive	
Power supply (WB, SB)	Power Source 300V	VWR International
Protein purification and Size Exclusion Chromatography (SEC)	TALON column	GE Healthcare
	HiTrap Heparin 16/10	
	HiLoad 16/600 Superdex 200 column	
	Superdex S200 10/ 300 column	
	Superose 6 Increase 10/300 GL	
	Superdex 200 5/150 GL	
	Superose 6 5/150 GL column	
	ÄKTA prime	
	ÄKTA protein purifier system	Merck Millipore
	ÄKTAmicro FLPC system	
	30K Amicon-Ultra-4 centrifugal filter	
	30K Amicon-Ultra-15 centrifugal filter	
	Amylose resin	New England BioLabs
	cOmplete His-Tag Purification Resin	Roche
	MegaBlock® 96 Well	Sarstedt
	Microtest plate 96 well	
GSH-beads	Thermo Scientific	
Pierce™ centrifuge column		
SDS-PAGE/ Western blot	BioTrace™ NT nitrocellulose transfer membrane	Pall Corporation
	Mini-PROTEAN® II Cell	Bio-Rad
	ChemiDoc™ MP Imaging System	

Application/ Method	Instruments and supplies	Supplier
Southern blot	Amersham Hybond™-XL membrane	GE Healthcare
	illustra ProbeQuant G-50 Micro Column	

2.1.13 Online tools

Online tools used in this study are listed in Table 2-10.

Table 2-10 Online tools

Online tool	Website
Blast2seq	https://blast.ncbi.nlm.nih.gov/Blast.cgi
NEBcloner® Restriction Enzyme Double Digestion tool	https://nebcloner.neb.com/#!/redigest
PSIPRED	http://bioinf.cs.ucl.ac.uk/psipred/
Reverse complement	http://www.bioinformatics.org/sms/rev_comp.html
Saccharomyces genome database (SGD)	http://www.yeastgenome.org
t-test calculator	https://www.graphpad.com/quickcalcs/ttest1.cfm
xVis	https://xvis.genzentrum.lmu.de

2.1.14 Software

Software used in this study is listed in Table 2-11.

Table 2-11 Software

Software	Supplier
Adobe® Illustrator® CS4 v14.0.0	Adobe
Adobe® Photoshop® CS4 Extended v11.0	
ApE-A plasmid editor v2.0.47	M. Wayne Davis
EnzymeX v3.1	Mek&Tosj, The Netherlands Cancer Institute
Excel v14.4.5	Microsoft®
FlowJo™ v10.2	FlowJo LLC
GUSSI	Chad A. Brautigam (UT Southwestern)
ImageJ v2.0.0	National Institutes of Health (NIH), Rockville
MeroX v1.6.6.6	www.StavroX.com

Table 2-11 Software (Continued)

Software	Supplier
SnapGene® Viewer v2.7.3	SnapGene
SEDFIT	Peter Schuck (NIH/NIBIB)
SEDNTERP	John Philo (Alliance Protein Laboratories)

2.2 Methods

2.2.1 Growth and maintenance of *Saccharomyces cerevisiae*

2.2.1.1 Growth conditions of yeast strains

Yeast strains were grown on liquid media or solid agar plates, depending on the experimental procedure. To grow yeast in liquid media, cells were resuspended in the desired medium in Erlenmeyer flasks. In order to ensure good aeration, the medium was kept no more than one-tenth of the total flask volume. To grow yeast on solid plates, 2% agar was added to the media. Typically, strains were grown on YPD (yeast extract, peptone, dextrose) medium under non-selective conditions. Prior to long-term storage, yeast strains were grown on a non-fermentable carbon source media, YPG (yeast extract, peptone, glycerol) agar plates, to ensure the maintenance of mitochondria.

Strains used in yeast two-hybrid analysis (detailed in section 2.2.3), were grown in media lacking those amino acids for which the bait and prey plasmids confer prototrophy, to avoid plasmid loss. Diploid yeast cells were sporulated in liquid sporulation medium (SPO), consisting of a nitrogen-deficient medium supplemented with a non-fermentable carbon source (acetate). Further information about liquid medium and plates used in this study is detailed in Table 2-8. Yeast was grown on solid agar plates in a Heratherm™ incubator (Thermo Fisher Scientific), whereas liquid yeast cultures were grown in a Multitron® shaker (Infors HT) or Innova™ 2000 (New Brunswick Scientific) platform shaker with shaking at 180 rpm. Both liquid cultures and yeast solid plates were grown at 30°C, unless otherwise indicated.

2.2.1.2 Meiotic cell cycle synchronization

Yeast cells were patched from glycerol stocks onto YPG plates and grown overnight at 30°C in a Heratherm™ incubator (Thermo Scientific). Patched cells were transferred to 4% YPD plates and further grown overnight at 30°C. On the following day, 20-50 mL of YPD

liquid culture was inoculated and grown to saturation for 24 h at 180 rpm at room temperature. The next day, cultures were diluted at a cell optical density at 600nm (OD_{600}) of 0.3 into pre-sporulation media (BYTA; buffered YTA medium: 1% yeast extract, 2% bacto-tryptone, 1% potassium acetate, 50 mM potassium phthalate) and grown at 30 °C for 16-18 h in a Multitron® incubator (Infors HT). OD_{600} was determined by using a spectrophotometer (BioPhotometer, Eppendorf). Cells were then washed twice with distilled water and resuspended in sporulation media (SPO; 0.3% KAc) at OD_{600} 1.9 to induce meiosis. Sporulation cultures were grown at 30°C (except for experiments involving temperature-sensitive (ts) strains, where cells were grown at the permissive temperature (23°C)).

For time courses in which the anchor-away system was used, rapamycin (1 µg/mL) was added at time point 0 hour (in SPO). Time courses were conducted and samples for Western Blots, flow cytometry (or fluorescence-activated cell sorting, FACS) and Southern Blots analyses were taken at the desired time points. For Western Blots, samples were taken after 0, 3 and 4 or 5 h, whereas for FACS and Southern Blots, samples were typically taken after 0, 3, 5 and 8 h, unless otherwise indicated.

2.2.1.3 Yeast stock maintenance

Yeast cells were grown on a YPG plate overnight at 30°C in a Heratherm™ incubator (Thermo Scientific), scraped with a sterile toothpick and then resuspended in 1 mL of sterile 15% glycerol in a screw cap microcentrifuge tube. The content of the microfuge tube was mixed by inversion to thoroughly disperse the cells. Cells were immediately frozen at -80°C for long-term storage.

2.2.2 Construction of yeast strains

2.2.2.1 Yeast transformation

Yeast transformation was based on the protocol described in Agatep *et al.*, 1998. Prior to yeast transformation with plasmids or a PCR-amplified DNA fragment, yeast cells were treated with Lithium acetate (LiAc) in order to make them competent. In this method cells are prepared and suspended in a LiAc solution, along with the DNA to be transformed and an excess of carrier DNA. Polyethylene glycol (PEG) is added and the yeast cells are then incubated at 30°C, followed by a heat-shock that allows the DNA to enter the cells.

Competent yeast cells were prepared as follows: Cells were first grown on a YPD plate overnight at 30°C and scrapped out with a sterile glass pipette next morning to prepare a yeast pre-culture of 50 mL YPD. The culture was then grown overnight at 30°C with 180 rpm shaking in a Multitron® shaker (Infors HT). The following morning, yeast from the pre-culture was diluted at OD₆₀₀ 0.15 in a total volume of 50 mL of fresh YPD and grown 4 h at 30°C with 180 rpm shaking.

Cells were harvested in a falcon tube and spun down 5 min at 3000 rpm (Centrifuge 5810 R, Eppendorf). Cell pellet was resuspended in 1 mL of 0.1 M LiAc, transferred to a 1.5 mL microfuge tube and spun down 2 min at 3000 rpm in a tabletop centrifuge (Centrifuge 5424, Eppendorf). Supernatant was discarded and the cell pellet was resuspended in 4 volumes of 0.1 M LiAc.

Once yeast cells were competent, a transformation mix was prepared in a microfuge tube. The transformation mix consisted of 240 µL (PEG3350; 50% w/v), 36 µL of 1 M LiAc, 10 µL of single-stranded DNA carrier (previously boiled for 5 min at 95 °C and quenched on ice), 25 µL of DNA amplified by PCR (100 µL reaction precipitated and dissolved in 25 µL water) or 10 µL of plasmid from a heat-inactivated digestion mix, and distilled water up to a total volume of 360 µL.

As a single-stranded DNA carrier, salmon sperm DNA (Deoxyribonucleic acid sodium salt from salmon testes, Sigma Aldrich) was used after preparing as follows: first, the DNA string was cut and dissolved in sterile TE pH 7.6 at 10 mg/mL overnight with gentle stirring. Salmon sperm DNA was then sonicated twice for 30 sec (Branson Sonifier 450) in order to yield DNA fragments of approximately 3000 bp, and boiled to sterilize. Salmon sperm DNA was distributed into aliquots that were kept at -20°C until used for the yeast transformation protocol.

The transformation mix was vortexed and 50 µL of the competent cells suspension was added and vortexed vigorously. After an incubation of 30 min at a 30°C rotating rack (Labquake shaker rotisserie, Thermo Scientific), cells were heat-shocked at 42°C for 15 min in a heating block (Thermomixer 5436, Eppendorf). Cells were pelleted at 3000 rpm for 2 min in a benchtop centrifuge, supernatant was removed and cells resuspended in 300 µL of sterile water. Cell resuspension was plated onto the appropriate selective medium and the plates

grown 2 to 4 days at 30°C. The colonies grown were then tested by PCR for positive transformants.

2.2.2.2 Creation of diploid yeast strains

Diploid yeast strains were generated by mating two haploid strains of the opposite mating type (*MATa* and *MATα*) on the surface of agar plates. Briefly, cells from the two haploids were scraped with a sterile toothpick from a YPD plate (more cells from the *MATa* mating-type than *MATα* were patched, to allow further selection of diploids by alpha-factor) and mated on solid YPD medium overnight at 30°C. Next day, this mating mixture was streaked onto a fresh YPD plate containing alpha-factor (10 µg/ml). By this method, diploid and haploid yeast cells from the *MATα* mating type are selected. After two days at 30°C, single shiny colonies were scraped and streaked onto a fresh YPD plate and grown overnight at 30°C. Diploid strains were selected from haploid cells by replica plating onto minimal (MIN) agar plates. Yeast cells were replica-plated onto MIN plates and MIN plates in which 600 µL of liquid YPD medium plus a scraped patch of *MATa/ MATα* yeast cells (tester strains) were evenly spread. Plates were grown overnight at 30°C. This approach is based on the ability of the tester strains (which contain a single auxotrophic marker) to complement the nutritional requirements of strains of the opposite mating type. This nutritional deficiency is complemented by the uncharacterized strains, which usually cannot grow on MIN plates due to auxotrophy. Diploid strains are distinguished then by their inability of growing in any of the MIN/ MIN+tester strain plates (unless the resultant diploid strain contains all the markers that confer auxotrophy).

2.2.2.3 Sporulation of diploid cells

Meiosis and spore formation can be induced by starvation of diploid yeast cells for nitrogen and carbon sources. The two consecutive meiotic divisions yield four spore products (known as tetrad) that are held together in a sac, ascus.

The sporulation process was induced in liquid SPO medium. After growing the diploid yeast strain overnight at 30°C, cells were inoculated in 5 ml of SPO in a glass tube and incubated overnight at room temperature in a rotating wheel (Rotator L29, Labinco). This sporulation culture was used immediately or kept at 4°C until used for dissection (see section 2.2.2.4).

2.2.2.4 Preparation and dissection of tetrads

Tetrads obtained as described in section 2.2.2.3, were prepared for dissection as follows: Between 150 and 200 μL of the sporulation culture was transferred to a 1.5 mL microfuge tube and treated with the same amount of Zymolyase 100T (10 mg/ml), in order to break the ascus cell wall. After 20-30 min incubation at 37°C, 300-400 μL of distilled water were added.

Around 70 μL of the diluted culture were placed in a line across a YPD plate and dissected using a dissection microscope (Nikon Eclipse Ci, Schuett-biotec). The dissection microscope is a modified light microscope equipped with a movable stage in which it is possible to mount an inverted petri dish. This microscope also counts with a micromanipulator that holds and moves a fine needle, used to pick up the tetrads.

The YPD plate with the dissected tetrads was incubated at 30°C (23°C for *ts* strains) for two days until the growth of single colonies. Tetrads were picked and patched with a sterile toothpick onto a fresh YPD plate and grown overnight at 30°C (23°C for *ts* strains). The genotype of each dissected cell was then determined by replica plating and PCR analysis, as described in sections 2.2.2.5 and 2.2.4.1, respectively.

2.2.2.5 Determination of phenotype by replica plating

In order to determine the phenotype of the tetrads dissected or of a given strain, yeast cells were replica-plated onto MIN agar plates supplemented with specific nutrients. Most of the used yeast strains carry at least one nutritional marker allowing for selection of yeast transformants plated on MIN medium lacking that specific nutrient (*i.e.* amino acids). Alternatively, some yeast strains that carry a drug resistance marker (*i.e.* KAN, which confers resistance to the antibiotic geneticin, also known as G418) were selected by growth on YPD medium containing antibiotics. By replica plating onto MIN plates lacking for a specific amino acid or containing an antibiotic, yeast cells can be tested for their nutritional requirements and for their resistance to the specific antibiotic. Sterile velvets are placed onto a replica plating metal block and a master plate containing the strain/s of interest is printed onto a velvet. This impression is then copied by transferring to plates with all the relevant selective media. For analysis of temperature-sensitive strains, a copy of the master plate is made onto a YPD plate and incubated at 37°C, keeping a permissive (*i.e.* 23°C) plate as a control for the transfer of the yeast cells. By analyzing the growth of the uncharacterized strain on different

plates lacking a certain nutrient (or containing an antibiotic) it is possible to determine its phenotype. When the analysis by replica plating was unclear, additional PCR analysis (section 2.2.4.1) of a given locus was used to determine the genotype of the yeast strains.

2.2.2.6 Determination of mating type

For testing the mating type of yeast strains, MIN plates were used, together with specific mating test strains (known as *MATa* and *MAT α*). In order to know which is the mating type of an uncharacterized strain, yeast cells were replica-plated onto MIN plates uncovered or evenly covered by *MATa* or *MAT α* . Growth on minimal plates supplemented with *MATa* tester strain indicated that the uncharacterized strain was *MAT α* , whereas growth on a minimal plate covered with the *MAT α* tester strain indicated that the uncharacterized strain was *MATa*. This method is based on the auxotrophic requirements of the tester strains and is further detailed in section 2.2.2.5.

2.2.3 Yeast two-hybrid system

The yeast two-hybrid (Y2H) technique is used to detect protein-protein interactions. This assay is based on the activation of a reporter gene (*LacZ*) by the binding of a transcription factor (Gal4, involved in galactose processing) onto an upstream activating sequence. In this system, the transcription factor is split into two fragments, known as DNA-binding domain (BD) and activating domain (AD), where BD is responsible for binding to the upstream activating sequence, whereas the AD is capable of activating the transcription of a reporter gene. The basic premise of the Y2H assay is that the binding and activating domains are modular and can function in close proximity without direct binding.

The Y2H technique employs two different vectors; first, a yeast two-hybrid “bait” vector, which consists of the GAL4 DNA binding domain (BD) fused to the gene coding for one of the proteins whose interaction we want to test; second, a “prey” plasmid, used for fusing the gene coding for the other protein to the GAL4 activating domain (AD). Only when there is a direct interaction between the two proteins fused to the AD and BD, these two domains will be in proximity and lead to the transcription of the reporter gene. The “bait” and “prey” vectors are introduced into a yeast strain in which the biosynthesis of a specific nutrient (*i.e.* amino acid) is lacking. Therefore, when grown on media that lacks this nutrient, yeast does not survive. Only when the two proteins fused to the AD and BD, respectively, bind to each other, transcription of the reporter gene (involved in the biosynthesis of the nutrient that the

strain is deficient for) takes place and yeast can grow. Thus, the interaction between two proteins can be read in terms of growth/ non-growth of yeast cells in agar plates lacking specific amino acids.

For the yeast two-hybrid assays in this study, Pch2 (full length and different truncations/mutants), and Orc1-4 and Orc6 were cloned in the pGBDU-C1 or pGAD-C1 vectors. The resulting “bait” and “prey” plasmids were transformed into a yeast two-hybrid reporter strain (yGV864). Y2H strains (detailed in Table 7-9, Appendix) were grown on -Ura-Leu agar plates overnight at 30°C. The following day, a 15-20 mL culture was grown overnight at 30°C in -Ura-Leu liquid medium. Next morning, cultures were diluted to an OD₆₀₀ of 0.5. Y2H spot assay was performed by spotting 5-10 µL of the diluted cultures onto -Ura-Leu plates (control medium) and -Ura-Leu-His plates (selective medium) and grown for 2-4 days. Pictures were acquired with an Epson Perfection V550 Photo scanner (Epson).

2.2.4 Cloning and methods of DNA analysis (Molecular biology methods)

2.2.4.1 Polymerase Chain Reaction (PCR)

PCR is a molecular biology technique that allows the amplification of a specific sequence of nucleic acid by using pairs of oligonucleotides (or primers) that align specifically to the nucleic acid of interest and a DNA polymerase. In this study, PCR was used to amplify regions of plasmids or genomic DNA for cloning the desired DNA fragment into a vector by restriction cloning, Gibson cloning or the biGBac method (detailed in sections 2.2.4.4). In addition, PCR was used for transformation in *S. cerevisiae* and for genotyping yeast strains (sections 2.2.2.5).

In this study, two different polymerases were used: Taq polymerase (ExTaq®, TaKaRa) and Q5 DNA polymerase (Q5® High-Fidelity 2x Master Mix, New England BioLabs). Taq polymerase was used for confirming results after cloning and yeast transformation, whereas Q5 polymerase was used for amplification of genes for cloning, due to its higher fidelity. PCRs were performed in a T3000 Thermocycler (Biometra).

A standard PCR reaction and PCR program used for PCR amplification are shown in Tables 2-12, 2-13 and 2-14.

Table 2-12 Standard composition of a 20 μ L PCR reaction using Taq polymerase

Component	Volume (20 μ L reaction)
DNA template	1 μ L
20 μ M forward primer	1 μ L
20 μ M reverse primer	1 μ L
dNTPs	1.6 μ L
10x ExTaq buffer	2 μ L
ExTaq (TaKaRa ExTaq®)	0.16 μ L
Sterile water	13.24 μ L

Table 2-13 Standard composition of a 50 μ L PCR reaction using Q5 polymerase

Component	Volume (50 μ L reaction)
Q5® High-Fidelity 2x Master Mix	25 μ L
20 μ M forward primer	1.25 μ L
20 μ M reverse primer	1.25 μ L
DNA template	1 ng-1 μ g (genomic DNA) 1 pg-10 ng (plasmid)
Sterile water	to 50 μ L

Table 2-14 Standard program for PCR amplification

Step	Temperature	Time	
Initial denaturation	94°C	2 min	
Denaturation	94°C	1 min	2 x 30
Primer annealing	50°C *	30 sec	
Elongation	72°C *	2 min 30 sec	
Final elongation	72°C	10 min	
Hold	4°C	∞	

*Primer annealing and elongation steps were adapted depending on the melting temperature of primers and the length of the DNA product to amplify, respectively.

A variant of PCR, known as “nested PCR” was employed to produce the probes used for Southern Blot analysis (detailed in 2.2.4.12). Nested PCR is a variation of standard PCR

that enhances the specificity and yield of DNA by using two successive rounds of amplification with two sets of primers. The first pair of primers (outer primers) flanks DNA containing the region of interest, while the second pair of primers (nested primers) amplifies a precise region of DNA using as template the product from the first PCR round. This approach limits non-specific amplicons and allows to obtain a sufficient yield of the desired target from a limited amount of DNA template.

For probe amplification, PCRs were performed with ExTaq (TaKaRa ExTaq®) polymerase, as indicated in Table 2-12, with the exception that the final volume was 200 μ L. After the first PCR round, amplified DNA was purified as described in sections 2.2.4.2.1 and 2.2.4.2.2, and 1 μ L of the purified DNA (previously diluted 1:100) was used as a template for the second PCR round.

Oligonucleotide sequences are detailed in Tables 7-5, 7-6 and 7-7.

2.2.4.2 Cloning using restriction enzymes

Traditional cloning involves the amplification of a DNA fragment by PCR, followed by restriction digestion with the appropriate enzyme. These enzymes recognise specific sites and cut the target DNA. After treatment of the vector with the same restriction enzymes, the DNA fragment is ligated, producing the desired plasmid with the DNA inserted into a specific site. A more detailed explanation of restriction cloning is described in the following sections.

2.2.4.2.1 Agarose gel electrophoresis

Agarose gel electrophoresis was used to separate DNA molecules according to their molecular size. This step was performed routinely to check the size of a PCR-amplified DNA fragment and after restriction digestion. Depending on the expected molecular size, DNA was loaded onto 0.8%-1.2% agarose (Agarose standard, Carl Roth GmbH & Co. KG) gels. Prior to loading of the samples, 10x DNA loading dye was added. As a reference for molecular weight, GeneRuler™ 1kb Plus DNA Ladder (Thermo Fisher Scientific) was used. Samples were separated at 120 V in an agarose gel system (Carl Roth) containing 1x TAE buffer and 1:25000 Midori Green Advanced DNA stain (Nippon Genetics Europe GmbH). DNA samples were visualised either by UV light transilluminator (BLstar 16, Biometra) or using ChemiDoc™ MP Imaging System (Bio-Rad).

2.2.4.2 .2 Restriction digestion

After PCR amplification of the insert and purification using a PCR purification kit (QIAquick® PCR purification kit, Qiagen), both insert and vector were digested with the same restriction enzymes. In order to clone a DNA insert into a plasmid, both DNAs were treated with the same restriction enzymes to create compatible ends (in this work, enzymes used yielded “sticky ends”). Restriction digestion was performed in the appropriate buffer (provided by New England BioLabs (NEB)) that guarantees effective cut for the enzymes that digest both ends of the insert and/or vector. Alternatively, if one of the enzymes was not efficient in the commercially available buffer of the other restriction enzyme, the digestions were performed sequentially.

Y2H plasmids with Pch2 constructs were digested with *Sall High Fidelity* (*Sall HF*, New England BioLabs) and *EcoRI* (New England BioLabs) in 10x NEBuffer 3.1 (New England BioLabs). The same enzymes and buffer were used for cloning into pGEX vector for Pch2 production in bacteria. pFG vectors for Pch2 and Pch2 constructs expressions were cloned by digestion with *StuI* and *XbaI* in 10x CutSmart® buffer (New England BioLabs). Compatibility of the restriction enzymes with the restriction buffer was assessed with the NEBcloner® Restriction Enzyme Double Digestion tool from New England BioLabs (<https://nebcloner.neb.com/#!/redigest>). Typically, 1 µg of DNA was digested with 1 µL of restriction enzyme and the digestion was performed for 3-4 h at 37°C. To avoid self-ligation of the digested vector, 2 µL of alkaline phosphatase was added one hour prior to the end of the digestion. After successful restriction of the insert and vector, both were loaded onto agarose gels and extracted from the gel, as explained in sections 2.2.4.2.1 and 2.2.4.2.2. Additionally, restriction ligation was used to check positive recombinant plasmids before verifying by sequencing (described in section 2.2.4.9).

2.2.4.2 .3 DNA extraction and purification

DNA fragments were extracted from the agarose gels and purified using a gel extraction kit, according to the manufacturer’s instructions. In this study, two gel extraction kits were used: QIAquick Gel Extraction Kit (Qiagen) and Wizard® SV Gel and PCR Clean-Up system (Promega).

2.2.4.2 .4 Ligation

Digested and purified inserts and vectors were ligated using a Rapid DNA Ligation Kit (Thermo Fisher Scientific). Typically, a 3:1 molar excess of insert DNA over vector was used. An example of ligation reaction is illustrated in Table 2-15.

Table 2-15 Standard composition for 10 μ L ligation reaction

Component	Volume (10 μ L)
Linearized vector DNA: insert DNA	1:3
5x Rapid Ligation Buffer	2 μ L
T4 DNA Ligase	0.5 μ L
Sterile water	to 10 μ L

After vortexing briefly, the ligation reaction was incubated at room temperature for 15 min. Next, the ligation mix was transformed into *E. coli* OmniMax and the recombinant plasmid isolated, as described in sections 2.2.4.6 and 2.2.4.7. All constructs were verified by sequencing as detailed in section 2.2.4.9.

2.2.4.3 Restriction free cloning (Gibson assembly)

Alternatively to the traditional restriction digestion cloning, restriction-digest free cloning was used to originate plasmids for recombinant expression of proteins (pLIB-MBP/pLIB-GST derived vectors) and for vectors that were further used for yeast transformation (TAP-tagged and Flag-tagged derived constructs).

Restriction-digest free cloning was performed as described by Gibson *et al.* 2009. Gibson assembly is a powerful one-step technique that allows the assembly of multiple overlapping DNA fragments by the combined action of a 5' exonuclease, a DNA polymerase and a DNA ligase. The first step in Gibson assembly consists of resecting DNA fragments by using 5' T5 exonuclease, which yields single-stranded DNA 3' overhangs. These 3' overhangs specifically anneal and subsequently are extended by the Phusion polymerase. This step is followed by the action of the DNA ligase that seals the remaining nicks.

Following DNA amplification by PCR and purification, DNA was treated with *DpnI* (New England Biolabs) for 1 h at 37°C to cut the methylated plasmid. Next, 5 μ L of the

purified DNA template was mixed with 15 μ L of Gibson Assembly® Master Mix (New England Biolabs) and incubated 1 hour at 50°C. The Gibson assembly mix was further used for bacterial transformation and constructs were verified by sequencing.

For the Flag-tagged yeast constructs of Pch2, we used Gibson cloning in order to add a 3xFlag-6xGly-tag (amplified from a synthesized plasmid containing 500 bp of the promoter of Pch2 and the 3xFlag-6xGly-tag, provided by Life Technologies (Thermo Fisher Scientific) to the Pch2 sequence (or truncations of Pch2). The plasmid obtained was then transformed into *S. cerevisiae*. For full-length Pch2 and Pch2 truncations used for protein expression in insect cells, we used a *Spodoptera frugiperda* (Sf9)-codon-optimized sequence of Pch2, provided by GeneArt Gene Synthesis. See Table 7-8 for plasmid and primers details.

2.2.4.4 biGBac method

The biGBac method (Weissmann *et al.*, 2016) is a powerful technique based on Gibson cloning that enables the assembly of multiple genes into a single baculoviral expression vector. Therefore, this approach is especially useful for expression of multisubunit protein complexes in insect cells. In this study, the biGBac method was used to clone the different ORC subunits into two vectors for protein expression and production in insect cells. In this technique, initially, cDNAs or genes encoding for the protein or proteins of interest are cloned using Gibson assembly (or alternatively, traditional cloning) into library vectors (pLIB vectors; vectors that contain an expression cassette and a polyhedrin promoter that enables protein expression in insect cells). From these pLIB vectors, expression cassettes are amplified by PCR using a predefined set of primers that flank the DNA ends and that contain linker sequences. By performing multiple assembly steps (rounds of PCR amplification in which specific linker sequences are introduced, and further assembly of these PCR products into vectors) the biGBac method allows to clone up to 25 cDNAs into a single vector.

The different ORC subunits were cloned into two plasmids that were further used to express this protein complex in insect cells. pLIB vectors of the individual ORC subunits were cloned by PCR, producing six pLIB vectors with the coding sequences of Orc1 to Orc6. Of note is that the pLIB vector used to clone the Orc1 subunit was modified to contain an N-terminal His-tag, whereas the pLIB vectors used to clone the other ORC subunits did not contain any tag. These vectors were then used in an assembly step to produce two pBIG1 vectors: one containing His-Orc1, Orc2 and Orc3 and another containing Orc4, Orc5 and

Orc6. These pBIG1 vectors were then used to express and purify ORC from Tnao38 insect cells. The biGBac method to produce ORC was performed according to Weissmann *et al.* Briefly, the pLIB vector was linearized by digestion with *Bam*HI and *Hind*III and the linearized vector was gel purified (section 2.2.4.2.3).

Gene coding sequences were amplified by PCR using a forward primer that carried the sequence overhang 5'-CCACCATCGGGCGCGGATCC (followed by the start codon and gene-specific sequences) and a reverse primer that carried the sequence overhang 5'-TCCTCTAGTACTTCTCGACAAGCTT (followed by the reverse complement of stop codon and gene-specific sequences. See Table 7-6 for more details). The PCR product was purified by gel extraction. Gibson assembly was used to fuse the homologous ends of the linearized pLIB vector (100 ng) and the insert, mixed at a molar ratio of 1:5. To assemble the generated pLIB vectors, 10 µg of the step-1 vectors (pBIG1a and pBIG1b) were digested with 1 µl *Swa*I (New England Biolabs) in NEBuffer 3.1 at 25°C for 16 h. To ensure complete digestion (and avoid colonies derived from empty step-1 vectors), an additional 2 µl of *Swa*I were added and the vectors incubated for further 2 h. *Swa*I was heat-inactivated at 65°C for 20 min and the linearized vectors were purified using the QIAquick PCR purification kit (Qiagen). Gene expression cassettes (GECs) were generated by PCR with Q5 polymerase (see section 2.2.4.1) using the respective library vector (coding for Orc1, Orc2, Orc3, Orc4, Orc5 or Orc6) as a template and one of the predefined primer sets that contain DNA linker sequences. Specifically, the following PCR reactions were performed:

Table 2-16 PCR reactions for step-1 assembly of ORC into pBIG1 vectors

PCR	Vector	Primers
1	pLIB-His-Orc1	α + Ir
2	pLIB- Orc2	IIIf + IIr
3	pLIB- Orc3	IIIIf + Ω r
4	pLIB- Orc4	α + Ir
5	pLIB- Orc5	IIIf + IIr
6	pLIB- Orc6	IIIIf + Ω r

For more details of primers used, see List 7-6.

PCR products were verified by agarose gel electrophoresis (see 2.2.4.2.1) and gel-purified (section 2.2.4.2.3), eluting in 30 µL. To perform the step-1 assembly reaction, 50 ng of the previously linearized pBIG1a vector was mixed with the PCR derived products of the PCR

reactions 1-3 (See Table 2-16) at a 5-fold molar excess of each GEC over the vector. Similarly, the linearized pBIG1b vector was mixed with the PCR products derived from PCR reaction 4-6 (See Table 2-16) at a 5-fold molar excess PCR over vector.

The Gibson assembly reactions were carried out in a final volume of 20 μ L, composed of the DNA fragments to be assembled, 4 μ L 5x isothermal reaction buffer (5xIRB: 25% PEG-8000, 500mM Tris-HCl pH 7.5, 50mM MgCl₂, 50mM DTT, 1mM each of the four dNTPs, 5mM NAD) (Gibson *et al.*, 2009), 2 μ L Taq DNA Ligase (New England Biolabs), 0.25 μ L Phusion HF DNA Polymerase (Thermo Scientific), 0.25 μ L T5 Exonuclease (Epicentre) (pre-diluted 1:30 in 1xIRB). This reaction was mixed on ice and immediately transferred to a 50°C preheated thermocycler (T3000 Thermocycler, Biometra) and incubated for 60 min.

After Gibson assembly, 5 μ l of the assembly reactions were transformed (See section 2.2.4.6 for detailed transformation protocol) into 50 μ l of chemically competent *E. coli* OmniMax cells, with the exception of an extended recovery time (1 h) in LB medium at 37°C. Cells were plated onto LB agar plates containing 50 μ g/mL spectinomycin. The following day, single colonies were picked and grown at 37°C for 14-16 h in 5 mL LB medium supplemented with 50 μ g/mL spectinomycin. Next, plasmid DNA was purified using the QIAprep Spin Miniprep Kit (Qiagen). Positive colonies were tested by restriction digestion with *Swa*I to release the individual GECs and those clones that showed a correct restriction pattern were further verified by DNA sequencing.

2.2.4.5 Site-directed mutagenesis

Site-directed mutagenesis was used to substitute single or multiple DNA bases to obtain mutations in the amino acid sequence of the desired constructs. This base substitution was achieved by using specific primers that already harbour the substituted base. By performing PCR with these primers, the base/s is changed and the point mutation is introduced in the corresponding constructs.

2.2.4.6 Transformation of chemically competent bacterial cells

DNA derived from restriction cloning and Gibson assembly was transformed into competent *E. coli* OmniMax cells by a heat-shock method. Briefly, 5 μ L of the mix obtained after ligation or 10 μ L of the Gibson assembly mix were added to 50 μ L of competent cells.

This mixture was incubated on ice for 20 min, followed by a heat-shock for 45 sec at 42°C in a heating block (Thermomixer 5436, Eppendorf) and incubation on ice for 2 min. Afterwards, 700 µL of LB medium were added and cells were incubated for 30 min at 37°C with shaking at 500 rpm in a Thermomixer comfort heat-block (Eppendorf). Cells were subsequently pelleted 3 min at 4000 rpm in a benchtop centrifuge (Centrifuge 5424, Eppendorf) and ~500 µL of the supernatant were removed. Pelleted cells were resuspended in the remaining volume and 150-200 µL of the resuspension was plated onto LB agar plate containing the appropriate antibiotic for selection and incubated overnight at 37 °C in a Kelvitron® Thermo Scientific Heraeus® incubator.

2.2.4.7 Isolation of plasmids from bacterial cells

A single colony from an LB plate was used to inoculate a 5 mL LB culture, containing the appropriate antibody, and grown overnight at 37°C and 180 rpm shaking in a Minitron incubator shaker (Infors HT). The following day, the plasmid was isolated by the alkaline lysis principle, using a QIAprep® Spin Miniprep Kit (Qiagen), according to the manufacturer's instructions.

2.2.4.8 Determination of DNA concentration

Concentration of nucleic acids was determined by measuring absorbance at 260 nm using a NanoDrop2000 spectrophotometer (Thermo Fisher Scientific). A $260_{\text{nm}}/280_{\text{nm}}$ ratio was used to assess the purity of the DNA. A ratio of ~ 1.8 is normally accepted as “pure” DNA. A higher 260/280 ratio usually indicates contamination with RNA and a considerably lower ratio indicates the presence of protein. An additional measure of nucleic acid purity is the 260/230 ratio, which should be 1.8-2.2.

2.2.4.9 Sequencing

All plasmids obtained by restriction cloning, Gibson assembly and biGBac method were submitted for Sanger sequencing to the company GENEWIZ to verify their DNA sequences. Sets of primers covering the whole fragment were designed and provided..

2.2.4.10 Real-time quantitative PCR (qPCR)

Samples obtained from chromatin immunoprecipitation (ChIP) experiments (described in 2.2.5.5) were used to perform analysis by real-time quantitative PCR (qPCR). qPCR allows the detection and quantification of nucleic acids for different purposes. Typically, in qPCR a fluorescent dye is used to label the amplified DNA molecules as the PCR progresses. This dye intercalates to double-stranded DNA (dsDNA) and the fluorescence is measured during each PCR cycle. Therefore, fluorescence signal increases in a manner proportional to the amount of amplified DNA, hence allowing monitoring of the DNA quantity in “real-time”.

In this study, a master mix (PerfeCTa® SYBR® Green FastMix®, Quantabio) containing all components (the fluorescent dye SYBR Green, MgCl₂ and dNTPs), except primers and DNA template, was used. Both ChIP and Input samples were quantified by qPCR on a 7500 FAST Real-Time PCR machine (Applied Biosystems). The percentage of ChIP relative to input was calculated for the target loci as well as for the negative controls. The enrichment was calculated using the threshold cycle (ΔC_t) method: $1/(2^{[C_t - C_{tcontrol}]})$ (Goni *et al.*, 2009).

The set of primers used to amplify a region within *PPRI* (control locus, coordinates chromosome XII; 174,237-174,354), and a region adjacent to *ARS1116* (coordinates chromosome XI, 516,725-516,892) (See Table 7-7 for primer details). Prior to qPCR analysis of ChIP samples, oligos were tested by performing conventional PCR (20-25 cycles, $t_m = 60^\circ\text{C}$). Amplicons were run on a 2% agarose gel to ensure the presence of a single PCR band. Oligo efficiencies were determined by performing a standard curve control with serial dilutions of genomic DNA (100-0.01 ng) and calculated using standard procedures. The efficiencies of the primers used in this study were: *PPRI*=1.998, *ARS1116*=1.991. Statistical significance indicated in Figure 3-13 D was determined using an unpaired t-test (<https://www.graphpad.com/quickcalcs/ttest1.cfm>). The composition of a 20 μL qPCR reaction mix and the cycling program used are shown in Tables 2-17 and 2-18, respectively. qPCR was set up on ice in a 96-well plate (Kisker Biotech GmbH & Co. KG). The plate was covered with a PCR ultra-clear adhesive (Kisker Biotech GmbH & Co. KG), vortexed and briefly spun down in an Allegra® X-15R centrifuge (Beckman Coulter). The 96-well plate was kept on ice and protected from light until running the qPCR.

Table 2-17 Composition of a 20 μ L qPCR reaction

Component	Volume (20 μ L reaction)
2x PerfeCTa® SYBR® Green FastMix®	10 μ L
20 μ M forward primer	0.25 μ L
20 μ M reverse primer	0.25 μ L
DNA template	5 μ L
Sterile water	4.5 μ L

Table 2-18 qPCR thermocycler program

Step	Temperature	Time
Initial denaturation	95°C	30 sec
PCR cycling (30 cycles)	95°C	5 sec
Collect data after extension step	60°C	30 sec

2.2.4.11 Genomic DNA preparation from yeast for PCR-base genotyping

Genomic DNA isolation was performed routinely in order to genotype yeast strains by PCR. A toothpick worth of cells was scrapped from a fresh YPD plate and resuspended in 500 μ L of TE in a 2 mL microfuge tube. Cells were briefly spun down in a tabletop centrifuge (Centrifuge 5424, Eppendorf) and the supernatant was removed. Next, 200 μ L of DNA breakage buffer, approximately 0.3 g of acid-washed glass beads (Sigma Aldrich) and 200 μ L of phenol: chloroform: isoamylalcohol (Carl Roth GmbH) were added. Lysis was achieved by vortexing vigorously in a IKA® Vibrax VXR basic (IKA®-Werke) for 6 min at 1500 rpm. The mixture was then centrifuged at 14000 rpm for 5 min in a pre-chilled table-top centrifuge (Centrifuge 5424 R, Eppendorf) for phase separation. Then, 100 μ L of the upper aqueous layer was transferred to 1 mL of absolute, cold ethanol and mixed by inversion. Samples were then centrifuged at 14000 rpm for 5 min, supernatant was discarded and pellet air-dried for 10-15 min at room temperature. DNA-pellet was then resuspended in 50 μ L of water or TE buffer.

2.2.4.12 Southern Blot

Southern Blot is a technique used to detect specific DNA sequences within the whole cell genome. This method involves separation of DNA fragments based on size via

electrophoresis, followed by a transfer to a membrane, hybridization with a labelled sequence-specific probe and detection of the labelled DNA. In this study, Southern Blot was used to detect formation of DNA double-strand breaks (DSBs) at specific chromosomal loci in meiotic yeast samples. Southern blot analysis was performed according to the method described in Vader *et al.*, 2011, detailed in the following sections.

2.2.4.12.1 Genomic DNA extraction from meiotic yeast cells

Samples for Southern blotting were harvested at time points 0, 3, 5 and 8 h after induction of synchronous meiosis. 10 ml of meiotic cultures were harvested by centrifugation in a tabletop centrifuge (Centrifuge 5424 R, Eppendorf) 3 min at 3000 rpm at 4°C and stored at -20°C. Genomic DNA from meiotic cells samples was prepared as follows: cells were thawed on ice, resuspended in 1 mL of pre-chilled TE buffer, transferred to 1.5 mL microfuge tube and briefly spun in a tabletop centrifuge at 7000 rpm at 4°C. Cell pellets were resuspended in 500 µL of fresh spheroplasting solution (spheroplasting buffer, 1/100 volume β-mercaptoethanol, 1/40 zymolyase stock) and incubated 45 min at 37°C on a rotating rack until spheroplasting was complete. The spheroplasts were then lysed by adding 100 µL of lysing buffer and 15 µL of PCR-grade proteinase K (Roche Diagnostics) and incubated for 2 h at 65°C with occasional mixing by inverting the tubes. Lysis was further facilitated by addition of 150 µL of 5 M KOAc and subsequent incubation at 4°C for approximately 30 min, until the content became semi-solid. Lysed cells were centrifuged in a tabletop centrifuge at 15000 rpm at 4°C for 20 min and 650 µL of the supernatant transferred to a clean 2 mL microfuge tube containing 750 µL of absolute ethanol. Tube content was mixed a few times by inversion and incubated on ice for 10 min. Precipitated DNA was centrifuged 10 min at 15000 rpm at 4 °C and the supernatant removed. Pelleted DNA was dissolved in 750 µL of freshly prepared TE/RNase A buffer (TE buffer supplemented with 1:600 of RNase A, 50 µg/mL Sigma Aldrich) and incubated at 37°C for 40 min, until the pellet was dissolved. Samples were stored at 4°C overnight.

The following day, 500 µL of phenol: chloroform: isopropanol solution (Carl Roth GmbH) was added to the samples, which were vigorously mixed ~60 times. After letting the tubes sit for a few min, samples were further inverted ~60 times and centrifuged for 10 min at 15000 rpm at 4°C for phase separation. Samples were then processed in sets of four, while the rest remained spinning down in a tabletop centrifuge. 600 µL of the upper phase was added to a fresh tube containing 750 µL of isopropanol, the content was mixed by inversion 10 times

and incubated on ice for 10 min. Next, samples were centrifuged for 10 min at 15000 rpm at 4°C, the DNA pellet was washed with 1 mL of 70% ethanol and further centrifuged 5 min at 15000 rpm at 4°C. Residual ethanol was removed and the DNA was dissolved in 125 µL of TE and incubated at 4°C overnight. The following morning, the content of the tube was mixed by gently tapping the microfuge tubes 3-4 times.

2.2.4.12.2 Digestion of genomic DNA

For Southern Blot analysis, the isolated genomic DNA from meiotic yeast cells was digested with the appropriate restriction enzyme (*HindIII* to detect DSBs at the control *YCR047C* hotspot or *ApaLI* to monitor DSBs in the region of interest -right rDNA flank-*YLR164W*). Digestion was carried out in a final volume of 300 µL (35 µL of genomic DNA, 10x NEB buffer- NEB 2.1 buffer for *HindIII* digestion; NEB CutSmart buffer for *ApaLI* digestion-, 2.5 µL of restriction enzyme and sterile, distilled water) and incubated 4 h at 37°C. After digestion, fragmented DNA was precipitated by adding 25 µL of 3 M sodium acetate pH 5.5 and 650 µL of absolute ethanol, and incubating at -20°C for at least 1 hour. Precipitated DNA was recovered by spinning down for 10 min at 15000 rpm at 4°C in a benchtop centrifuge. Supernatant was removed, samples air-dried for 15 min to eliminate any traces of ethanol and DNA pellet dissolved in 15 µL of TE for 20 min. Prior to agarose gel electrophoresis, 5 µL of loading buffer (1 mL of Southern Blot loading buffer contains 600 µL of 10x DNA loading buffer and 400 µL of NEB3 restriction buffer; extra salt prevents the sample from coming out of the well) was added and the samples briefly mixed and spun down.

2.2.4.12.3 Gel electrophoresis

Restricted genomic DNA was separated on a 6% SeaKem® LE agarose (Lonza) gel for 16-17 h at 70 V in an Owl™ A2-BP large gel system (Thermo Fisher Scientific) containing 1x TBE buffer. 20 µL of GeneRuler™ 1 kb Plus DNA Ladder was loaded in the agarose gel (leaving one empty well between the marker and the first sample) to monitor the molecular size of the digested DNA. The gel was stained in a bath of RedSafe™ (1 mL RedSafe™/1 L H₂O; iNtRON Biotechnology) for 30 min at room temperature at 35 rpm on an Innova® 2000 platform shaker (New Brunswick Scientific) and digested DNA was visualized by UV light (ChemiDoc™ MP Imaging System (Bio-Rad)).

2.2.4.12.4 Southern blotting

The aim of the blotting step is to transfer the DNA fragments to a positively charged nylon membrane that can be treated with a radiolabeled probe to detect the hybridization signal. Prior to blotting, the agarose gel was first soaked with 0.25 M hydrochloric acid (HCl) in a clean plastic dish with gentle shaking for 40 min, in order to depurinate the DNA and achieve a more efficient transfer of larger DNA fragments. After pouring off the HCl, the gel was briefly rinsed with distilled water, inverted and further treated with 0.4 M sodium hydroxide (NaOH) for 35 min with gentle shaking. The treatment with an alkaline solution denatures the double-stranded DNA, yielding single DNA strands that can then bind to the membrane and hybridize to the probe in the following steps.

For the following blotting, a piece of Whatman filter paper wick (20 x 35 cm) was placed on an inverted tray Owl™ A2-BP large gel system (Thermo Fisher Scientific) and wetted with a solution consisting of 0.4 M NaOH and 0.6 M NaCl. This solution was poured into the gel apparatus to create a reservoir. One at a time, two gel-size pieces of Whatman paper were placed on top of the wick and soaked in 0.4 M NaOH/ 0.6 M NaCl solution. The agarose gel was then laid on top of the wetted Whatman paper and covered by a gel-size piece of Amersham Hybond™-XL membrane (GE Healthcare), previously soaked in distilled water. Two additional pieces of Whatman paper were soaked in water and placed on top of the membrane. In each blotting step, a glass tube was carefully and firmly rolled over the wick and the Whatman paper in order to prevent the formation of any air bubbles.

To ensure a proper contact between the gel and the membrane, pressure was applied evenly on top of the gel by placing a stack of paper towels and a glass plate on top of which a small weight (typically 1 L bottle) was placed. In order to isolate the paper towels from the reservoir, the Whatman paper and the paper towels were separated by placing a strip of parafilm on each side of the inverted tray. Blotting of DNA was done by upward-transfer overnight. The following day, the blot was deconstructed and the membrane immediately neutralized by incubation with 1 L of 50 mM sodium phosphate, pH 7.2 with gentle shaking for at least 30 min. Excess buffer was drained and the membrane carefully wrapped in Saran wrap and stored at -20°C until further hybridization.

2.2.4.12.5 Probe labelling

DNA probes specific for *YCR047C* (Chromosome III; 209,361 – 201,030) or *YLR164W* (Chromosome XII; 493,432 – 493,932) (for detection of DSBs in hotspot control region or rDNA, respectively) were prepared by nested PCR (described in section 2.2.4.1) followed by [α - 32 P]dCTP labeling. PCR-amplified probes were labelled with [α - 32 P]dCTP (6000 Ci/mmol, 20 mCi/mL Easy; Perkin Elmer) using the Prime-It RmT Random Primer labeling Kit (Agilent Technologies) according to the manufacturer's protocol. Labeled probes were then purified from unincorporated nucleotides using spin-column chromatography (illustra ProbeQuant G-50 Micro Column; GE Healthcare) and further used for hybridization.

2.2.4.12.6 Hybridization and washing

Prior to hybridization, Southern Blot membranes were thawed on 50 mM sodium phosphate, pH 7.2 bath at room temperature. Blots were carefully rolled up with the help of a cloth mesh placed underneath, introduced in pre-warmed glass bottles and unrolled so that the DNA inner side of the membrane remained wet with 20 mL of pre-warmed (65°C) hybridization buffer. 300 μ L of sheared salmon sperm DNA (Invitrogen, Thermo Fisher Scientific) was denatured by heating in a 95°C block for 5 min, followed by quenching on ice, and finally added to the glass bottle to block the membranes. The blots were promptly returned to a 65°C oven and pre-hybridized for at least 30 min. In the meantime, probes specific for *YCR047C* or *YLR164W* were labeled as detailed in section 2.2.4.12.5. Labeled probes were denatured in a 95°C heating block for 2 min, immediately quenched on ice and added to 5 mL pre-warmed hybridization buffer. Probe solution was subsequently poured into the hybridization bottle and the Southern Blot membranes were hybridized overnight in the 65°C oven.

The following morning, the hybridization mix was poured off and the membranes washed twice with 120 mL pre-heated (65°C) low-stringency solution (2x SSC) for 15 min at 65 °C. After the last low-stringency wash, membranes were washed with 120 mL of pre-warmed high-stringency (0.1x SSC) buffer for at least 30 min at 65°C. High-stringency wash was repeated once. The solution was drained off and the blots were carefully covered with Saran wrap.

2.2.4.12.7 Detection by phosphorimaging

The wrapped membranes were placed in an X-ray cassette (Kisker Biotech GmbH & Co. KG) and exposed to a phosphorimager film (Storage Phosphor Screen, BAS-IP MS 2040; GE Healthcare) for one week at room temperature. DSB signals were detected by developing the X-ray film using a Typhoon Trio scanner (GE Healthcare) and the signal intensity of the obtained images adapted by Adobe® Photoshop® CS4 Extended version 11.0.

2.2.4.13 Flow cytometry

Flow cytometry is a laser-based technique used to analyse and/or measure characteristics of a population of cells or particles. Typically, a sample containing fluorescent-labelled cells or particles suspended in a fluid is passed through a laser beam of flow cytometer instrument and fluorescence levels of each cell or particle are quantitated. The scatter of the light is characteristic to the particles being analysed and can be used to define cell components, identify different populations present in a heterogeneous sample, analyse cell size and volume and assess a particular cell status.

In this study, flow cytometry was used to assess the synchronous passage of yeast cells through the meiotic program (as judged by duplication of the genomic content), and was performed as described in Vader *et al.*, 2011. Briefly, 150 μL of sporulation culture at defined time points (typically 0, 3, 5 and 8 h after meiotic synchronization) were taken and fixed with 350 μL of absolute ethanol at least two h to overnight at 4°C. Fixed samples were spun down at 7000 rpm for 2 min in a benchtop centrifuge (Centrifuge 5424, Eppendorf) and ethanol poured off. Cells were resuspended in 500 μL of 50 mM sodium citrate supplemented with 0.7 μL RNase A (30mg/mL, Sigma Aldrich) and incubated at 50 °C (INCU-Line, VWR) for 2 h to overnight. To remove contamination of proteins, 10 μL of proteinase K (20 mg/mL, VWR) were added and samples incubated for further 2 h at 50°C. The DNA was stained with 500 μL of sodium citrate with 1/2500 (v/v) of SYTOX® green (Life Technologies). Samples were vortexed and sonicated 10 sec at the lowest output power (Branson Sonifier 450) prior to analysis using a BD Accuri™ C6 (BD Biosciences) flow cytometer. DNA histograms were analysed by FlowJo 10.2 software (FlowJo LLC). For analysis of rapamycin-induced phenotype, mitotic cultures were grown to saturation and diluted to OD₆₀₀ 1.0, and rapamycin (1 $\mu\text{g}/\text{mL}$) was added. Samples were taken at the indicated time points and processed as detailed above.

2.2.5 Methods of protein analysis

2.2.5.1 Yeast whole-cell extract for Western Blot using trichloroacetic acid

For the preparation of protein extracts from yeast, 5 mL of meiotic culture were harvested at different time points (usually time points 0, 3 and 4 h) and spun down for 3 min at 3000 rpm at 4°C in a tabletop centrifuge (Centrifuge 5424 R, Eppendorf). Supernatant was removed and the pellet was kept at -20°C until further processing.

Pellet was thawed at 4°C, resuspended in 5 mL of ice-cold 5% trichloroacetic acid (TCA) solution and incubated on ice for 10 min. Precipitated proteins were then recovered by spinning down for 3 min at 3000 rpm at 4°C. Pellets were washed with 800 µL of acetone and transferred to a screw-cap microcentrifuge tube. After a quick spin, pellets were air-dried overnight in the fume hood. Next day, the pellet was resuspended in 100 µL of protein breakage buffer (4 mL of TE (50 mM Tris pH 7.5, 1 mM EDTA), 11 µL of DTT). One volume of acid-washed glass beads (Sigma Aldrich) was added and cells were disrupted using a FastPrep®-24 machine (MP Biomedicals) twice at speed 6 for 45 sec. Samples were kept on ice in-between runs. 50 µL of 5x SDS loading buffer were added and samples were boiled at 95°C for 5 min before loading on a gel. Proteins were separated by SDS-PAGE and analysed by Western Blot (described in sections 2.2.5.2 and 2.2.5.4, respectively).

2.2.5.2 Sodium dodecyl sulfate-polyacrylamide gel electrophoresis (SDS-PAGE)

SDS-PAGE is an electrophoresis method that allows the separation of a mixture of proteins in base of their mass. It involves the use of sodium dodecyl sulfate (SDS), a detergent that confers a negative charge to the proteins. Prior to sample loading in polyacrylamide gels, 50 µL of 5x SDS loading buffer was added and samples were boiled 5 min at 95°C. By heating the samples, secondary and tertiary protein structure is disrupted and SDS covers the proteins with a negative charge proportional to their molecular weight. After boiling, samples were briefly spun down and loaded onto a gel of polyacrylamide (see details in Table 2-19). Protein samples were run onto an electrophoresis chamber (Carl Roth) at 100-120 V in 1x SDS buffer, as electrolyte. For SDS-PAGE of purified protein (*i.e.* pull-downs) samples were usually run at 70 V.

The negatively charged proteins migrate through the gel in the direction of the positively charged anode and molecules are separated according to their molecular size. Larger

molecules migrate more slowly through the pores of the gel than lower molecular weight proteins. Separated proteins were further analysed by gel staining with Coomassie Brilliant Blue (CBB) or by Western Blot (see section 2.2.5.3 and 2.2.5.4).

Table 2-19. Composition of SDS-polyacrilamide gels used in this study. Volume (mL) of components required to cast two 1.5 mm gels are shown.

Component	Volume 20 mL		Volume 6 mL
	Running gel (10%)	Running gel (8%)	Stacking gel (5%)
Sterile water	7.9 mL	9.3 mL	4.1 mL
30% acrylamide mix	6.7 mL	5.3 mL	1 mL
1.5 M Tris pH 8.8	5 mL	5 mL	----
1 M Tris pH 6.8	-----	----	0.75 mL
10% SDS	0.2 mL	0.2 mL	0.06 mL
10% APS	0.2 mL	0.2 mL	0.06 mL
TEMED	0.008 mL	0.012 mL	0.006 mL

Alternatively, precast 4-15% gradient gels (Bio-Rad) or precast 10% gels (Bio-Rad) were used for some purposes (protein purification and SEC experiments involving His-ORC, and purification of His-MBP-Pch2 and constructs, respectively).

2.2.5.3 Coomassie Brilliant Blue staining

Coomassie blue staining is one of the most common methods used to visualize proteins after SDS-PAGE. Coomassie blue allows the detection of proteins in a polyacrylamide gel by binding to proteins through interactions between positive protein amine groups and sulfonic acid groups present in the dye.

After electrophoresis, polyacrylamide gels were rinsed with deionized water and subsequently stained with Coomassie Brilliant Blue (CBB) staining solution (0.2% Coomassie Brilliant Blue, 7.5% acetic acid, 50% EtOH) by heating in a microwave for 10 sec at power settings 700 W. Gels were stained for 10 min to overnight at room temperature with gentle shaking. After incubation, staining solution was discarded and gels were destained by performing several washes with deionized water. Washes with water were repeated until removal of background. Gels were imaged using a ChemiDoc™ MP Imaging System (Bio-Rad).

2.2.5.4 Western Blot

Western Blot is a technique used to detect specific proteins within a sample. It involves the electrophoretic separation of proteins and their transfer onto a membrane that can be probed with antibodies specific to the target protein. For immunodetection of proteins by Western Blot, proteins were first separated according to their molecular weight by SDS-PAGE (section 2.2.5.2). After electrophoresis, resolved proteins were then transferred onto BioTrace™ NT nitrocellulose transfer membrane (Pall Corporation) in a blotting apparatus (Mini-PROTEAN® II Cell (Bio-Rad)) at 100 V-120 V for 90 min at 4°C. In order to control the transfer, the membrane was stained with PonceauS staining solution (PanReac AppliChem ITW Reagents), which reversibly detects proteins. PonceauS staining was removed by washing the membrane with 1x PBS supplemented with 0.05% Tween-20 (PBS-T) and the membrane was blocked with 5% (w/v) powdered milk (Carl Roth) in PBS-T buffer for 30-45 min at room temperature on a rocking platform See-saw SSL4 (Stuart® See-saw rockers, Cole Parmer). After blocking, the membrane was incubated with the corresponding primary antibodies (α -Pgk1, α -Flag, α -ORC, α -TAP, α -HA, α -Orc2, α -MBP) diluted in 5% (w/v) milk powder/PBS-T overnight at 4°C. For a detail description of antibodies and dilutions used, see Table 2-5.

The following day, the membrane was washed three times with PBS-T buffer for 10-20 min at room temperature on a rocking platform and then incubated for 1 h at room temperature with the appropriate secondary HRP-conjugated antibody diluted in 5% (w/v) milk powder/PBS-T. Following incubation with the secondary antibody, the membrane was washed with PBS-T (3x10-20 min) and proteins visualized by adding ECL Prime (or ECL Select) Western Blotting Detection Reagent™ (GE Healthcare), according to manufacturer's instructions. Images were acquired with ChemiDoc™ MP Imaging System (Bio-Rad).

2.2.5.5 *In vivo* Co-Immunoprecipitation

Co-Immunoprecipitation (Co-IP) is a technique that allows the detection of protein-protein interactions. Co-IP experiments use an antibody that targets a known protein that is believed to interact with other protein or protein complex. If the interaction between these two proteins/ protein complexes is strong enough, it is possible to detect the interaction partners of the known protein by pulling it down with its specific antibody. For Co-IP assays, 100 mL of synchronized meiotic cultures at OD₆₀₀ 1.9 were grown and

harvested after 4.5 h (unless otherwise indicated) in two 50 mL falcon tubes. Cell pellets were washed with ice-cold H₂O and cells originating from the same sporulation culture were transferred to a screw-cap microfuge tube, snap-frozen in liquid nitrogen (LN₂) and stored at -80°C.

Acid-washed glass beads (Sigma Aldrich) were then added, together with 500 µL of ice-cold IP buffer (50 mM Tris-HCl pH 7.5, 150 mM NaCl, 1% Triton X-100, 1 mM EDTA pH 8.0) supplemented with protease inhibitors (per 10 mL of IP buffer, 1 tablet of cOmplete™ Mini, EDTA-free, protease inhibitors (Roche), 20 µL of Serva inhibitor (Serva), 1 mM PMSF). Cells were then broken with a Fastprep disruptor (FastPrep®-24, MP Biomedicals) by two 45 sec cycles on speed 6. Samples were kept on ice in-between runs. The lysate was subsequently spun down for 30 sec at 500 rpm at 4°C, and the supernatant transferred to a falcon tube. The lysate was next sonicated by 25 cycles (30 sec on/30 sec off), high power range, using a Bioruptor sonication device (Bioruptor®-Plus, Diagenode). Alternatively, the lysate was sonicated twice for 15 sec at a constant setting, intensity 2 using a sonicator device (Branson Sonifier 450). After sonication, lysates were spun down for 20 min at 15000 rpm in a tabletop centrifuge (Centrifuge 5810 R, Eppendorf) at 4°C. Supernatant was transferred to a new microfuge tube and 50 µL of input was taken into a separate microfuge tube.

For α-Flag/HA- based IPs, 1 µL of antibody (α-Flag-M2 antibody/α-HA) was added to the lysate and rotated for 3 h. For α-TAP co-IPs, 2 µL of antibody (α-TAP antibody) was added. After the incubation step, 25 µL of previously washed and equilibrated Dynabeads protein G (Invitrogen, Thermo Fisher Scientific) was added and rotated overnight at 4°C. For α-Orc2-based IPs, lysate was pre-cleared with 10 µL of Dynabeads protein G for 1 h at 4°C. Lysate was then incubated with 2 µL of α-V5 (IgG isotype control) or 11 µL of α-Orc2 for 3 h at 4°C, followed by 3 h incubation with 25 µL of Dynabeads protein G. The reactions were washed 4 times with ~ 500 µL of ice-cold IP buffer. In the last wash, beads were transferred to a new microfuge tube. 55 µL of 2x SDS loading buffer was added and samples were boiled at 95°C for 5 min. Supernatant was transferred to a new microfuge tube and stored at 4°C until samples were used for SDS-PAGE. The inputs followed a trichloroacetic acid (TCA) precipitation step. Briefly, 10% TCA was added and input samples were incubated for 30 min on ice. Inputs were spun down for 15 min at maximum speed at 4°C. Pellets were then washed once with ice-cold

acetone and spun down for 5 min at 15000 rpm. Supernatant was removed and the pellet was further resuspended in 50 μ L of TCA resuspension buffer (50 mM Tris-HCl 7.5, 6 M Urea), vortexed and incubated overnight at 4°C. Next morning, pellets were vigorously vortexed before adding 20 μ L of 2.5x SDS loading buffer. Samples were subsequently boiled at 95°C for 5 min and run onto an SDS-PAGE gel together with the IP samples. Immunoprecipitated proteins were then visualized by Western Blot (described in section 2.2.5.4).

2.2.5.6 Chromatin immunoprecipitation

Chromatin immunoprecipitation (ChIP) is a technique used to identify interactions of defined proteins with specific genomic regions. ChIP involves an initial step in which cells are fixed by formaldehyde, allowing the formation of reversible cross-links between DNA and associated proteins. Following the fixation step, the chromatin is sheared and DNA fragments bound to the target protein are immunoprecipitated by using a protein-specific antibody (coupled to beads), followed by reverting of the cross-links. The combination of ChIP with different techniques (*i.e.* qPCR or DNA sequencing) provides information about the enrichment of specific DNA sequences, which ultimately represent those genome regions that the protein is bound to *in vivo*.

In this study, ChIP experiments were performed for TAP-tagged proteins. Cells from 100 mL sporulation cultures were harvested at 4 h after meiosis induction in two falcon tubes and cross-linked with 1% formaldehyde for 15 min at room temperature. Samples were mixed by inversion several times, followed by quenching of the crosslinking reaction by adding glycine to a final concentration of 125 mM. After quenching, cells were spun down for 3 min at 3000 rpm at 4°C in a centrifuge 5810 R (Eppendorf) and cell pellets were washed with ice-cold 1x TBS. Cells proceeding from the same sporulation cultures were pooled together and transferred to 2 mL screw-cap microfuge tubes and centrifuged for 30 sec at 13000 rpm at 4°C in a table-top centrifuge (Centrifuge 5424 R (Eppendorf)). Cell pellets were snap-frozen in LN₂ and store at -80°C.

Cells were thawed on ice and resuspended in 600 μ L of ice-cold TAP ChIP buffer (25 mM Tris-HCl pH 8, 150 mM NaCl, 0.1% NP-40, 1 mM EDTA pH 8) supplemented with cComplete™ Mini, EDTA-free protease inhibitor (Roche), 1 mM PMSF, 1 mM sodium orthovanadate and 1x Serva protease-inhibitor mix (Serva). An equal volume of acid-washed

glass beads (Sigma Aldrich) was added and cells were lysed on a Fastprep disruptor (FastPrep®-24, MP Biomedicals) by two 60 sec cycles on speed 6. Samples were kept on ice in-between cycles and through the ChIP protocol to avoid protein degradation. After the breakage of cells, samples were centrifuged for 30 sec at 500 rpm at 4°C and the eluate on top of the glass beads was transferred to a pre-chilled 15 mL falcon tube.

Chromatin was then sheared using a Bioruptor sonication device (Bioruptor®-Plus, Diagenode) with the following settings: 25 cycles (30 sec on/30 sec off) and high power range. After chromatin shearing, samples were briefly spun down and content was transferred to a pre-chilled 1.5 mL microfuge tube. Cell debris was then pelleted by spinning down for 10 min at 13000 rpm at 4°C. Supernatant was transferred to a new 1.5 mL microfuge tube and 50 µL from this crude lysate was taken into a fresh tube and stored at -20°C until further use. For immunoprecipitation, 5 µL of α -TAP antibody (Thermo Fisher Scientific) were added to the crude lysate and incubated for 3 h in a rotating rack at 4°C. After incubation, 30 µL of Dynabeads protein G (Invitrogen, Thermo Fisher Scientific), previously washed with TAP ChIP buffer without protease inhibitors, were added to the lysate and samples were incubated overnight at 4°C in a rotating rack.

Following a 17-18 h of incubation step, beads were washed four times with ice-cold TAP ChIP buffer by rotating 2 min at 4°C. Dynabeads were subsequently washed once with ice-cold TE buffer. Supernatant was removed and beads resuspended in 200 µL of ice-cold TE and transferred to a new microcentrifuge tube. After removing the supernatant using a magnetic rack (Invitrogen), crosslinking was reversed by adding 100 µL of TE-SDS (10 mM Tris-HCl pH 8, 1 mM EDTA, 1% SDS) to the IP samples and incubating samples at 65°C for 30 min with shaking at 1200 rpm, followed by overnight incubation at 65°C with shaking at 600 rpm. Input samples kept at -20°C followed the same treatment (5 µL of the input was added to 95 µL of TE-SDS buffer and incubated at 65°C overnight).

The following day, samples were vortexed for 1 min and incubated for further 20 min at 65°C. IP samples were then centrifuged for 2 min at 15000 rpm at 4°C and supernatant was transferred to a new tube. Next, 150 µL of proteinase K mix (5% Proteinase K, 2.5% glycogen, TE buffer) was added to the IP and input samples, followed by incubation at 37°C for 3 h with gentle shaking (400 rpm). Following the proteinase K mix treatment, 300 µL of phenol: chlorophorm: isoamylalcohol (Carl Roth) was added and samples were mixed by vortexing 30 sec, before spinning down for 5 min at 13000 g at 4°C. Afterwards, 35 µL of 3

M LiCl and 1 mL of ice-cold 100% ethanol were added and DNA was precipitated by storing samples overnight at -20°C. The DNA of both input and IP samples was pelleted by centrifugation at 15000 rpm for 40 min in a pre-chilled centrifuge. Pelleted DNA was then washed with 1 mL of 75% ethanol and further centrifuged 15 min at 4°C. Supernatant was removed and pellets were air-dried at 4°C for 15 min. DNA pellets were finally resuspended in 80 µL of RNase A mix (3% RNase A, in TE) and incubated for 30 min at 37°C with gentle shaking. ChIP experiments were coupled to real time quantitative PCR (qPCR), described in section 2.2.4.10.

2.2.5.7 Mass spectrometry analysis of purified proteins

For mass spectrometry of His-MBP-Pch2 and His-ORC (His-Orc1-Orc6) purified from insect cells, samples were processed similarly as in Breit *et al.*, 2015. Briefly, protein samples were denatured with 8 M urea, reduced with DTT (1 mM) for 30 min, alkylated with chloroacetamide (5.5 mM) for 20 min and diluted to final urea concentration of 4M in 20 mM ammonium bicarbonate (ABC). Samples were digested with LysC/Trypsin (0,5 µg LysC/10 µg protein sample) for 3 h at room temperature, diluted to 2M urea in ABC and digested with 1 µg trypsin/10 µg protein sample, overnight at room temperature. Digestion was stopped by adding trifluoroacetic acid (TFA) to a final concentration of 2%. Samples were desalted/concentrated on C18 reversed-phase stage tips (activation: methanol; equilibration: buffer A (2% ACN, 0,1% TFA in H₂O); wash: buffer A (0,5% acetic acid, 2% ACN)). Peptide samples were eluted in buffer B (60 % ACN, 0,1 % TFA in H₂O) and subsequently evaporated. Samples were then separated on a Thermo Fisher Scientific™ EASY-nLC 1000 HPLC system using a two hour gradient from 5%–60% with 0.1% formic acid and directly sprayed via a nanoelectrospray ion source (Proxeon Biosystems, now Thermo Fisher Scientific) in a quadrupole Orbitrap mass spectrometer (Q Exactive™, Thermo Fisher Scientific). The Q Exactive™ was operated in a data-dependent mode acquiring one survey scan and subsequently ten MS/MS scans. Data were analysed as previously described (Breit *et al.*, 2015).

2.2.6 Expression and purification of recombinant proteins

High amounts of protein are usually required to perform biochemistry studies aiming to mechanistically analyse the function of the proteins of interest. Such big quantities are not sufficient from the natural source and, moreover, the proteins have to be tagged to enable

their further purification. Recombinant proteins are encoded by recombinant DNA (usually cDNA) that has been cloned in a system that supports the expression of the gene and translation of mRNA. This DNA is normally under the control of a promoter that allows high-levels of protein expression in a certain host cell and/ or an inducible promoter (*i.e.* in the case of bacteria, usually protein production is induced by IPTG). There are several expression systems used for recombinant protein expression, with different applications and characteristics. In this study, bacteria cells, yeast cells and baculovirus expression system (insect cells) were used to produce different proteins.

After expression, proteins have to undergo several purification steps to finally yield a pure product that will be further used in different applications. These purification steps involve one or several initial steps in which proteins are separated by an affinity method by the N- or C-terminally tag that they have fused to the cDNA. All the recombinant proteins purified in this study underwent as a final step a size exclusion chromatography (SEC) (also known as gel filtration chromatography). SEC is used to separate molecules according to their molecular size and shape as they pass through a column that contains a porous matrix with different properties (See Table 2-9 for details on chromatographic columns used). Those proteins that have a lower molecular weight will be trapped in this porous bed and will be therefore delayed. Higher molecular weight particles do not enter the matrix as easily as smaller molecules and are then eluted earlier. For a more detailed description of SEC, see section 2.2.9.2. The different purification methods employed in this study are detailed below.

2.2.6.1 Protein expression and purification from bacterial cells

2.2.6.1.1 Purification of His-Hop1

Hop1 was purified from bacterial cells. Briefly, the coding sequence of Hop1 was sub-cloned into a pET28a vector for expression of recombinant NH₂-terminally polyhistidine-tagged Hop1 (6xHis-Hop1). For protein expression, BL21-CodonPlus (DE3)-RIPL cells were transformed with 1 μ L of the resulting vector, plated onto an LB agar plate supplemented with kanamycin (Kan) and chloramphenicol (Cam) (10 μ /ml and 100 μ /ml, respectively) and incubated overnight at 37°C. The following afternoon, one colony was picked and used to inoculate a preculture of 1-2 L of LB media supplemented with Kan and Cam. This preculture was grown overnight at 37°C with shaking at 180 rpm in a Multitron® shaker (Infors HT). The following morning, the preculture was used to

further inoculate 11 L of LB media (supplemented with the appropriate antibiotics) at an OD₆₀₀ of 0.1. Cultures were grown at 37°C with vigorous shaking until OD₆₀₀ reached 0.6-0.8.

Protein expression was induced by the addition of 0.25 mM IPTG overnight at 18-20°C. Next morning, cells were harvested by centrifugation at 4500 rpm for 15 min at room temperature in a Sorvall RC 3BP+ centrifuge (Thermo Scientific). The pellet was washed with ~ 400 mL of 1x PBS and immediately snap-frozen in LN₂ and stored at -80°C until purification step. For protein purification, cell pellets were resuspended in 150 mL of lysis buffer (50 mM Hepes pH 7.5, 300 mM NaCl, 5 mM Imidazole, 10 % Glycerol, 0.05% Tween-20, 5 mM β-mercaptoethanol, 1:100000 benzonase, 1 mM PMSF and 1x Serva protease inhibitor mix (Serva)). Cells were lysed using a microfluidizer (Microfluidizer M-110S, Microfluidics Corporation), previously equilibrated in buffer A (50 mM Hepes pH 7.5, 300 mM NaCl, 5 mM Imidazole, 10% Glycerol, 0.05% Tween-20, 5 mM β-mercaptoethanol). Lysed cells were centrifuged at 30000 rpm for 1h at 4°C and the lysate filtered.

The clear lysate was first passed through a previously equilibrated 5 mL TALON column (GE Healthcare) at a flow rate of 0.5 mL/min. The column was then washed firstly with buffer A until UV₂₈₀ signal was back at basal level, followed by a washing step with wash buffer (50 mM Hepes pH 7.5, 1 M NaCl, 5 mM Imidazole, 10% Glycerol, 0.05% Tween-20, 5 mM β-mercaptoethanol, 5 mM MgCl₂, 1 mM ATP) and an additional wash with buffer A. Protein was eluted with an imidazole gradient between buffer A and buffer B (buffer A supplemented with 400 mM imidazole) (gradient length: 100 mL, target B: 100%, fraction size: 3 mL, flow rate: 5 mL/min). Eluate was pooled, diluted 2:1 in buffer A without NaCl, Tween-20 and imidazole, and subsequently loaded onto a Heparin column (HiTrap Heparin 16/10, GE Healthcare), previously equilibrated with buffer C (20 mM Hepes pH 7.5, 150 mM NaCl, 5 mM MgCl₂, 10% Glycerol, 5 mM β-mercaptoethanol). Protein was further eluted in a gradient between buffer C and D (buffer C with 1 M NaCl) with the following parameters: gradient length: 300 mL, target B: 100%, fraction size: 5 mL. Fractions were pooled and concentrated using a 30K Amicon-Ultra-15 centrifugal filter (Merck Millipore), previously washed and equilibrated. Concentrated protein was spun down at 15000 rpm for 15 min in a benchtop centrifuge (Centrifuge 5810 R, Eppendorf) at 4°C down to ~1 mL and immediately loaded onto a HiLoad 16/600 Superdex 200 column (GE Healthcare), pre-equilibrated in gel filtration

buffer consisting of 20 mM HEPES pH 7.5, 300 mM NaCl, 5 mM MgCl₂, 5% glycerol and 2 mM β -mercaptoethanol. Protein was run over the column overnight at a flow rate of 1.5 mL/min and fractions of 500 μ L were collected in a 96-well plate (MegaBlock® 96 Well; Sarstedt). Next morning, fractions were analyzed by SDS-PAGE and those fractions containing 6xHis-Hop1 were concentrated with an Amicon-Ultra-15 concentrator (MWCO 30 kDa), snap-frozen in aliquots and kept at -80°C until further use.

2.2.6.1.2 Purification of GST-BAH-Orc1

The Bromo Adjacent Homology (BAH) domain of Orc1 was purified from bacterial cells. The coding sequence of BAH-Orc1 was clone into a pGEX vector by Gibson cloning (see primers in Table 7-5) to yield a GST-BAH-Orc1 construct. The resulting plasmid was transformed into BL21-CodonPlus (DE3)-RIPL competent cells and plated onto LB plates supplemented with ampicillin (Amp, 100 μ /ml) and chloramphenicol (Cam, 10 μ /ml) that were grown overnight at 37°C. Colonies from this LB plates were picked and used to inoculate a 2 L LB culture (containing Amp and Cam). Cultures were grown at 25°C with shaking in a Multitron® shaker (Infors HT). Once OD₆₀₀ reached 0.6, protein expression was induced overnight by adding 100 μ M IPTG and the temperature was reduced to 20°C.

Next morning, the cultures were harvested at 4000 rpm for 15 min in a Sorvall RC 3BP+ centrifuge (Thermo Scientific). Pellets were washed with 1x PBS, re-centrifuged at 2500 rpm and the cells were immediately resuspended in buffer A (50 mM Hepes pH 8.5, 300 mM NaCl, 5% glycerol, 5 mM MgCl₂, 2 mM TCEP) supplemented with 1x Serva protease inhibitor (Serva). Resuspended cells were lysed twice using a microfluidizer (Microfluidizer M-110S, Microfluidics Corporation), previously washed with buffer A. Lysed cells were spun down for 45 min at 30000 rpm in a cooled centrifuge (Avanti J-30I or Avanti JXN-30 centrifuge –depending on availability–, Beckman Coulter). After filtering, the clear lysate was loaded onto 5 mL of GSH-beads, previously equilibrated in buffer A. Clear lysate was incubated for 2 h rotating at 4°C and next washed with 5 column volumes (CV) of buffer A. Protein was eluted by adding 5x 1 mL of buffer A supplemented with 30 mM glutathione. Eluted protein was concentrated in a 30 kDa Amicon concentrator (Merck Millipore) at 4000 rpm in a pre-chilled centrifuge until volume was 400-500 μ L. Concentrated protein was spun down 15 min at 15000 rpm in a benchtop centrifuge (4°C) and immediately injected onto a Superdex S200 10/ 300 column (GE Healthcare). Collected fractions were analyzed by SDS-PAGE, followed by CBB staining. Those fractions containing the protein of interest were

pooled and further concentrated with an Amicon-Ultra-15 centrifugal filter (MWCO 30kDa) (Merck Millipore). Protein aliquots were snap-frozen before storing at -80°C .

2.2.6.1.3 Purification of Flag-Cdc6

Flag-Cdc6 was purified from bacterial cells. Briefly, the coding sequence of Cdc6 was sub-cloned into pGEX-6P-3 for expression of recombinant NH_2 -terminally GST-Flag-Cdc6 (with a PreScission protease cleaving site between the GST and the Flag tags). For protein expression, BL21-CodonPlus (DE3)-RIPL competent cells were transformed with 1 μL of the resulting vector, plated onto an LB agar plate supplemented with kanamycin (Kan) and chloramphenicol (Cam) and incubated overnight at 37°C . Next afternoon, a 2 L preculture of LB supplemented with Kan and Cam was grown overnight at 37°C with 180 rpm shaking in a Multitron® shaker (Infors HT). The following morning, the preculture was diluted to an OD_{600} of 0.1 and further used to inoculate 10 L of LB media (supplemented with the appropriate antibiotics). Cultures were grown at 37°C with vigorous shaking until OD_{600} reached 0.6 and protein expression was then induced by addition of 100 μM of IPTG. Next morning, cells were harvested for 15 min at 4500 rpm at room temperature in a Sorvall RC 3BP+ centrifuge (Thermo Scientific). Cell pellet was washed once with ~ 400 mL of 1x PBS and spun down for 20 min at 4000 rpm at 4°C . Pellets were immediately snap-frozen in LN_2 in falcon tubes and stored at -80°C until purification step.

For protein purification, cell pellets were resuspended in 280 mL of lysis buffer (50 mM Hepes pH 7, 400 mM NaCl, 5% glycerol, 10 mM EDTA, 2 mM TCEP, 1x Serva protease inhibitors (Serva), 1:100000 benzonase, cOmplete™ Mini, EDTA-free, protease inhibitors (Roche)). Cells were lysed twice using a microfluidizer (Microfluidizer M-110S, Microfluidics Corporation), previously equilibrated in buffer A (lysis buffer without protease inhibitors). Lysed cells were centrifuged at 30000 rpm for 1 h at 4°C in an Avanti J-30I (Beckman Coulter) centrifuge and the lysate filtered. Clear lysate was then distributed into 50 mL falcon tubes and incubated with 4 mL of GSH beads, previously equilibrated in buffer A, for 2 h at 4°C in a rotating device (RS-TR 05 tube roller; Phoenix Instruments). After the incubation period, GSH beads were washed with 5 column volumes (CV) of buffer A. Protein was eluted by sequentially adding 1 mL of buffer A supplemented with 10 mM glutathione. This step was repeated five times and protein concentration in the eluted fractions was monitored by $\text{UV}_{280\text{nm}}$. Those fractions with a protein concentration > 0.1 mg/ mL and a ratio $\text{UV}_{260}/\text{UV}_{280} < 0.7$ (indicative of protein purity) were pooled.

Pooled fractions were diluted with 2.5 volumes of buffer A and cleaved with the appropriate amount of GST PreScission protease, rotating overnight at 4°C. In order to separate the cleaved GST tag and the PreScission protease from Flag-Cdc6 the fractions were incubated for 30 min at 4°C with gentle rotation after overnight cleavage. Fractions were then passed to a flow-through column (Pierce™ centrifuge column; Thermo Scientific) and the flow-through containing Flag-Cdc6 was collected. Protein was subsequently concentrated using a 30 kDa Amicon concentrator (Merck Millipore) to approximately 400 µL. After spinning down at 15000 rpm for 15 min in a pre-chilled centrifuge (Centrifuge 5810, Eppendorf), the concentrated protein was injected onto a Superdex 200 10/300 column (GE Healthcare), connected to an ÄKTA protein purifier system (GE Healthcare). Fractions were collected in a 96 well plate and checked by SDS-PAGE and CBB. Those fractions containing Flag-Cdc6 protein were pooled and concentrated using a 30 kDa Amicon centrifugal filter. After concentrating the protein, working aliquots were made, snap frozen in LN₂ and stored at -80°C until further use.

2.2.6.2 Protein purification from yeast cells (CBP-ORC)

CBP-ORC was purified as described previously (Frigola *et al.*, 2013). ORC overexpression in yeast (ySD-ORC; codon-optimized ORC; strain was a kind gift of C. Kurat, John's Diffley laboratory, Francis Crick Institute, United Kingdom) was driven by the Gal1,10 promoter and induced by galactose. Briefly, yeast cultures were grown overnight in YPD until saturation. Next morning, cells were diluted into YP medium supplemented with 2% raffinose and further grown overnight. Next morning, 50 ng/µL of alpha-factor was added and after 2-3 hours (when cells have formed “shmoo” shape), 2% galactose was added to the medium. Cells were harvested after 3 hours at 4700 rpm for 10-20 minutes. Cell pellets were resuspended in the remaining medium and centrifuged at 4000 rpm for 5-10 min. Pellets were further resuspended in lysis buffer (25 mM HEPES-KOH pH 7.6, 0.05% np-40, 10% glycerol, 0.3 M KCl, 2 mM β-mercaptoethanol) supplemented with protease inhibitors. Cells were frozen as droplets in LN₂ and store at -80°C. Cells were disrupted by using a freezer mill and the powder dissolved in lysis buffer and spun in Ti45 tubes at 45000 rpm for 45 min at 4°C. Lysate was added to previously-equilibrated calmodulin beads, 2 mM CaCl₂ was added and lysate was incubated 2 hours. Next, beads were washed with binding buffer (lysis buffer supplemented with 2 mM CaCl₂). Protein was eluted with elution buffer (lysis buffer supplemented with 2 mM EGTA and 2mM EDTA). Fractions were evaluated by SDS-PAGE and CBB staining, and those fractions containing the protein were concentrated and loaded

onto a Superdex 6 10/300 GL column. Relevant fractions were concentrated, frozen in LN₂ and stored at -80°C until needed.

2.2.6.3 Protein expression and purification from insect cells

2.2.6.3.1 Generation of baculovirus and protein expression test in insect cells

Full-length Pch2 and its truncated versions, as well as ORC, were purified from insect cells. Specifically, fragments containing the coding sequences of Pch2 or its truncations, derived from codon-optimized cDNA were sub-cloned into pLIB MultiBAC His-MBP/ GST vectors and confirmed by sequencing. pLIB plasmids contain an expression cassette with a polyhedrin promoter, which enables expression of the gene of interest in insect cells. In this study, modified pLIB vectors (kind gift of Andrea Musacchio), which allow the protein of interest to be tagged with a His-tag, His-MBP-tag or GST-tag, were used. Sequences coding for the different subunits of the ORC complex (Orc1-Orc6) were cloned using the biGBac method (described in 2.2.4.4) and verified by sequencing. Vectors containing the gene/s of interest were further employed for protein production using a baculovirus protein expression system.

Baculovirus protein expression system was performed as described in Trowitzsch *et al.*, 2010. Briefly, recombinant DNA was further integrated into EMBacY DH10 cells following a standard transformation protocol, with the exception of a longer (~6 h) recovery time at 37°C. Bacterial cells were plated on LB agar plates supplemented with 10 g/mL gentamycin, 7 g/mL tetracycline, 50 g/mL kanamycin, 40 g/mL IPTG and 100 g/mL X-Gal, and incubated at 37°C for two days until colonies appeared. The MultiBAC baculovirus expression system is based on an engineered version of the *Autographa californica* multiple nuclear polyhedrosis virus (AcMPV). In the MultiBAC vectors, the gene of interest is flanked by Tn7R and Tn7L sequences of the Tn7 transposon system, and its expression is driven by the polyhedrin promoter. The EMBacY cells harbor a BAC containing the baculoviral genome with an attachment site for the bacterial transposon Tn7 and a segment of the lacZ gene (lacZ α). The EMBacY cells also contain a helper plasmid that harbors the Tn7 transposase under an IPTG inducible promoter.

After induction with IPTG, the Tn7 transposon enzyme allows the integration of the gene of interest from the MultiBAC vector to the baculoviral DNA. If the integration of expression cassettes via Tn7 transposition is successful, the lacZ α gene is disrupted and cells

are unable to process the X-gal substrate present in the agar plates, leading to the growth of white colonies. In the case of unsuccessful transposition, the *lacZ α* gene remains intact and colonies are blue (due to the ability of β -galactosidase to process the X-gal substrate present in the agar plates). Thus, recombinant BACs harboring our gene of interest can be easily identified by blue/white screening. After the recombination step, one white colony was grown on 5 mL of LB medium (supplemented with 10 g/mL gentamycin, 7 g/mL tetracycline and 50 g/mL kanamycin) overnight at 37°C.

BAC DNA was purified by using a QIAprep Spin Miniprep Kit (Qiagen) with slight modifications. Briefly, the overnight culture was centrifuged 3 min at 8600 rpm in a microfuge tube. Pellet was resuspended in 300 μ L of P1 buffer, followed by addition of 300 μ L of P2 buffer. Samples were mixed by inversion and 300 μ L of N3 buffer were added, and further inverted. Samples were incubated on ice 30 min and then centrifuged at 15000 rpm for 15 min in a pre-chilled benchtop centrifuge (Centrifuge 5424 R, Eppendorf). The supernatant was transferred to a new microfuge tube containing 850 μ L of cold isopropyl and DNA was precipitated by incubation at -20°C from overnight to several days. After precipitation, DNA was pelleted by centrifugation at 15000 rpm for 15 min at 4°C and the pellet was washed with 1 mL of 70% ethanol. Followed by centrifugation at 15000 rpm for 5 min at 4°C, ethanol was removed under sterile conditions and pellet was resuspended in 40 μ L of sterile TE buffer.

For virus production, the bacmid-DNA was transfected into *Spodoptera frugiperda* cells (Sf9 cells) using FuGENE® HD Transfection Reagent (Promega). Briefly, 2 mL of 1×10^6 cells/mL were seeded in 6 well plate and incubated at 27°C for 30 min. In the meantime, a transfection mix consisting of 250 μ L of Sf-900III medium, 20 μ L of bacmid-DNA and 5 μ L of FuGENE® was prepared and incubated during 20-30 min. After the incubation time, the transfection mix was added to the seeded Sf9 cells and the 6 well dish was incubated at 27°C for 4 days in a Multitron® shaker (Infors HT). Next, the supernatant of the transfection was added to a 10 cm dish containing 1×10^6 cells/ mL and incubated 4 days at 27°C for virus amplification. After 96 h, cells were harvested at 2500 rpm for 5 min, supernatant was sterile filtered and 5-10 % FBS was added. This was stored at 4°C as the virus 0 (V0) and further used to amplify the virus by adding 1:100 of the V0 to 50 mL of Sf9 cells at 1×10^6 cells/mL. After 4 days incubation period at 27°C at 110 rpm, the 50 mL cell suspension was harvested similarly as described above and stored as the V1. Similarly, a second round of virus amplification was performed using the V1 (1:100) to infect a 50 mL Sf9 culture. After 4 days at 27°C, the V2 was harvested and further used to either do

expression tests or for large-scale expression of proteins in *Trichoplusia ni* (Tnao38) cells. For protein expression tests of GST-Pch2 and His-MBP-Pch2 (and derived constructs), 50 mL of Sf-900 medium was inoculated with 1×10^6 Tnao38 cells/mL and different dilutions of V2 were added (typically 1:100, 1:10, 1:50), and incubated at 27°C at 110 rpm for 4 days. 1 mL samples were taken at different time points (48 h and 72 h, unless otherwise indicated), washed twice in 1x PBS and resuspended in the same fresh buffer. After adding 5x SDS loading buffer to the samples and boiling at 95°C, samples were loaded onto SDS-PAGE gels and stained with CBB.

For ORC expression tests in insect cells, 50 mL of Sf-900 medium was inoculated with 1×10^6 Tnao38 cells/mL and infected at different ratios (1:100/ 1:10; 1:40/ 1:40; 1:10/ 1:100) of the two V2 baculoviruses coding from His-Orc1-3 and Orc4-6, respectively. Samples were harvested after 48, 72 and 96 h, cell pellets washed 2 times with 1x PBS, snap-frozen in LN₂ and stored at -80°C. Pellets were then resuspended in lysis buffer (50 mM HEPES pH 8, 300 mM NaCl, 5 mM imidazole, 5% glycerol, 5 mM β-mercaptoethanol, 1 mM MgCl₂, 1:100000 benzonase and 1x Serva protease inhibitor mix (Serva)) and sonicated 3 times for 30 sec using a Branson sonifier 450 device at 50% amplitude and outcome 7. At this step, whole-cell extract (WCE) sample was taken. Lysate was then harvested by centrifugation at 29000 rpm for 1 h at 4°C and filtered. After centrifugation, a clear lysate (CL) sample was taken. Filtered lysate was then incubated with His-beads (cComplete His-Tag Purification Resin; Roche) during 1 h at 4°C. Afterwards, beads were washed 3 times with buffer A (lysis buffer without protease inhibitors) and protein was eluted in 3 consecutive 1 mL elution steps with elution buffer (50 mM HEPES pH 8, 300 mM NaCl, 400 mM imidazole, 5% glycerol, 5 mM β-mercaptoethanol). Samples were loaded onto SDS-PAGE and gels stained with either CBB or blot with α-ORC antibody (kind gift of Stephen Bell; MIT, Cambridge, USA).

2.2.6.3.2 Protein purification from insect cells

2.2.6.3.2.1 Purification of His-MBP-Pch2 and truncations

Full-length Pch2 and its truncated versions were expressed in Tnao38 insect cells by inoculating the corresponding baculovirus (V2) at a titer of 1:10 (virus to culture). Cells from 2 L cultures were grown for 48 h at 27°C in a Multitron® shaker (Infors HT). After two-days incubation period, cells were harvested by centrifugation at 1000 g for 15 min at 17°C in a

Sorvall RC 3BP+ centrifuge (Thermo Scientific). Cell pellets were washed with 1x PBS and the cell suspension was then transferred to 50 mL falcons, spun down for 20 min at 1000-1500 g in a centrifuge 5810 R (Eppendorf) at 4°C and snap-frozen. Pellets were stored at -80°C until further purification step.

Pellets from 2 L culture were resuspended in lysis buffer (50 mM HEPES pH 8, 300 mM NaCl, 5 mM imidazole, 5% glycerol, 5 mM β -mercaptoethanol, 1 mM MgCl₂, 1: 100000 benzonase, supplemented with 1x Serva protease inhibitor mix (Serva) and cOmplete™ mini, EDTA-free protease inhibitor cocktail tablets (Sigma Aldrich)) and lysed by sonication (Branson Sonifier 450) 4 times for 30 sec, duty cycle 50%, output control 7. Sonicated cells were cleared by centrifugation 1 h at 30000 rpm (4°C) and the supernatant filtered. Clear lysate was immediately passed through a 5 mL TALON™ Superflow cartridge (Takara Bio) at a flow rate of 5 mL/min. Afterwards the TALON column was extensively washed with buffer A (50 mM HEPES pH 8.0, 300 mM NaCl, 5 mM imidazole, 5% glycerol, 5 mM β -mercaptoethanol, 1 mM MgCl₂) until the UV_{280nm} signal was at basal level. Following the buffer A wash, the column was washed with wash buffer (50 mM HEPES pH 8.0, 1 M NaCl, 5 mM imidazole, 5% glycerol, 5 mM β -mercaptoethanol, 1 mM MgCl₂) until the conductivity (concentration of NaCl) level stabilized. The high salt wash step helped to reduce the presence of contaminants in the Pch2 (and mutants) protein. After an additional wash with buffer A (until conductivity reading reached the basal level), protein was eluted with a gradient between buffer A and buffer B (50 mM HEPES pH 8, 300 mM NaCl, 400 mM imidazole, 5% glycerol, 5 mM β -mercaptoethanol, 1 mM MgCl₂) with the following parameters: length of the gradient: 100 mL; flow rate: 5 mL/min; target: 100% B. 3 mL fractions were collected and the presence of protein was monitored by UV_{280nm}. Those fractions containing the protein of interest were pooled together and distributed in two closed gravity flow columns (Pierce™ centrifuge column; Thermo Scientific) and incubated 30 min at 4°C with pre-equilibrated amylose resin (New England BioLabs) in a rotating rack (RS-TR 05 tube roller; Phoenix Instruments). Then, the amylose resin was washed with 5 CV of buffer without imidazole, followed by protein elution with elution buffer (30 mM HEPES pH 8, 500 mM NaCl, 3% glycerol, 2 mM TCEP, 1 mM MgCl₂, and 20 mM maltose). Sequential elutions of 1 mL were collected in microfuge tubes and the presence of protein was monitored by UV_{280nm}. Those eluted fractions containing protein and a ratio 260 nm/ 280 nm \leq 0.6 were pooled together.

The eluted protein was concentrated using an Amicon-Ultra-15 centrifugal filter (MWCO 30kDa) (Merck Millipore) by spinning down at 4°C until volume was approximately 400 μ L. Concentrated protein was then transferred to a 1.5 mL microfuge tube and spun down for 15 min in a refrigerated benchtop centrifuge 5424 R (Eppendorf), to pellet any possible aggregates. Protein was subsequently purified by size-exclusion chromatography (SEC), by loading onto a Superose 6 Increase 10/300 GL (GE Healthcare) previously equilibrated in gel filtration buffer (30 mM HEPES pH 8.0, 500 mM NaCl, 3% glycerol, 2mM TCEP, 1 mM $MgCl_2$). A flow rate of 0.5 mL/min was used and 500 μ L fractions were collected in a 96-well plate (MegaBlock® 96 Well; Sarstedt). The peak fractions were analyzed by SDS-PAGE and those fractions corresponding to the protein of interest were collected and concentrated using a 30K Amicon-Ultra-4 centrifugal filter (in the presence of protease inhibitors). The concentrated protein was snap-frozen in LN_2 and stored at -80°C until further use. Note that for purification of His-MBP-Pch2-243-564, buffers were adjusted to pH 7.6 instead of pH 8.

2.2.6.3.2.2 Purification of His-ORC and His- Δ BAH-ORC

The His-tagged ORC complex was purified from insect cells. The multiple subunits of the ORC complex were expressed using two baculoviruses (coding from His-Orc1-3 and Orc4-6, respectively) as described in section 2.2.4.4. A 3-liter culture of Tnao38 cells was co-infected with the two baculoviruses (V2) at a 1:40 titer (virus: culture) and incubated for 2 days at 27°C with 110 rpm shaking in a Multitron® shaker (Infors HT). 48 h post-infection, cells were harvested by centrifugation for 15 min at 1000g in a Sorvall RC 3BP+ centrifuge (Thermo Scientific) at 17°C. Cell pellets were washed once with 1x PBS, snap-frozen and stored at -80°C. Cell pellets were resuspended in lysis buffer (50 mM HEPES 7.5, 300 mM KCl, 1 mM $MgCl_2$, 10% glycerol, 5 mM β -mercaptoethanol, 5 mM imidazole, 1:100000 benzonase, 1x Serva protease inhibitor (Serva) and cOmplete™ mini, EDTA-free protease inhibitor cocktail (Roche)) and lysed by sonication 4 times for 30 sec, duty cycle 50%, output control 7.

Lysed cells were harvested by ultracentrifugation for 1 h at 30000 rpm in a pre-chilled (4°C) centrifuge (Avanti J-30I Centrifuge, Beckman Coulter) and the supernatant was filtered. Cleared lysate was precipitated with 20% $(NH_4)_2SO_4$ on ice for ~45 min and re-centrifuged for 30 min at 30000 rpm. Clear lysate was affinity-purified by incubating it with cOmplete His-Tag purification resin (Roche) for 2 h in a rotating rack at 4°C. After incubation, His-Tag

resin was extensively washed with a gradient from 5 mM to 15 mM imidazole in buffer A (50 mM HEPES-KOH 7.5, 300 mM KCl, 1 mM MgCl₂, 10% glycerol, 5 mM β -mercaptoethanol). Subsequently, the protein was eluted with elution buffer (buffer A supplemented with 300 mM imidazole) by sequential elutions of 1 mL. The Presence of protein was monitored by absorbance at UV_{280nm}. The fractions containing protein and a ratio $260/280 \leq 0.6$ were pooled together.

The eluted protein complex was concentrated using a 30K Amicon-Ultra-15 centrifugal filter (previously equilibrated) by spinning down at 4000 rpm in a refrigerated centrifuge (Centrifuge 5810 R, Eppendorf) until volume was 350-500 μ L. Concentrated protein was transferred to a microcentrifuge tube and spun down for 15 min at 15000 rpm in a benchtop centrifuge (4°C) to eliminate aggregates. Protein was then loaded onto a Superose 6 Increase 10/300 GL column (GE Healthcare), previously equilibrated in gel filtration buffer (30 mM HEPES pH 7.5, 300 mM KCl, 5% glycerol, 1 mM MgCl₂, 2 mM TCEP). Using a flow rate of 0.5 mL/min, 500 μ L fractions were collected in a 96-well plate. Fractions were analyzed by SDS-PAGE and those fractions containing His-ORC were concentrated using a 30 kDa MWCO concentrator and flash frozen in LN₂.

2.2.7 Analytical ultracentrifugation (AUC)

Sedimentation velocity analytical ultracentrifugation (SV-AUC) experiments were performed in an Optima XL-A analytical ultracentrifuge (Beckman Coulter). Purified His-MBP-Pch2 protein samples (at a concentration ranging from 1 μ M to 0.3 μ M) in 20 mM Tris-HCl, 150 mM NaCl and 1 mM TCEP were loaded in double-standard Epon-charcoal centrepieces and samples were centrifuged at 42.000 rpm at 20 °C. The cells were scanned at 280 nm and a total of 500 radial absorbance scans were collected with a time interval of 1 min. Data was analysed using the module for sedimentation coefficient distribution $c(s)$ model implemented in the SEDFIT program (Schuck, 2000). In order to calculate partial specific volume, buffer density and buffer viscosity, SEDNTERP software was used (www.rasmb.org/sednterp). Figures were generated using the software GUSSE (Brautigam, 2015).

2.2.8 Protein quantification methods

Concentration of proteins used in this study was determined by measuring absorbance at 280 nm using a NanoDrop2000 spectrophotometer (Thermo Fisher Scientific). This method

is based on the absorbance of aromatic residues (tryptophan, tyrosin) or Cys-Cys disulphide bonds. Different options are available for determining the concentration of purified proteins. In this study, two of these options were used: the general absorbance and the molar extinction coefficient/molecular weight method. An estimated concentration of the protein can be obtained by measuring the UV_{280nm} taking as a general reference a protein sample of 1 mg/mL giving an absorbance at 280 nm of 1 A. However, for more accurate measurements, UV_{280nm} was measured providing user-entered values for the mass extinction coefficient ($M^{-1}cm^{-1}$) and the molecular weight in kilo Daltons (kDa). Since these two parameters are specific to each protein/protein complex, this value results normally is a more precise measurement. For protein samples, a ratio $260_{nm}/280_{nm}$ of ~ 0.6 was usually considered as indicative of protein purity. Alternatively, proteins were quantified by performing a BSA standard curve. For this purpose, samples with defined concentrations of BSA were prepared and loaded onto an SDS-PAGE gel together with the protein sample of unknown concentration. After staining the gel with CBB, protein concentration was determined by using ImageJ software.

2.2.9 Protein-protein interaction methods

2.2.9.1 *In vitro* pull-down assay

The pull-down assay is an *in vitro* technique used to detect physical interactions between two or more proteins, and it is a useful tool for identifying novel protein-protein interactions or confirming interactions predicted by other techniques. Pull-down assays involve an affinity binding step, several washes and an elution step, followed by a method to detect the interacting partners (such as SDS-PAGE followed by CBB or by Western Blot). In the affinity step, the “bait” protein is bound specifically to an immobilized ligand for the tag that is fused to the protein. This provides a platform for purifying other proteins that interact with the bait. After several washes to eliminate the unbound bait protein, the bait is incubated with either a cell lysate that contains putative “prey” proteins or a purified protein, depending on whether the aim of the pull-down is to identify unknown interacting partners or to confirm a suspected protein-protein interaction, respectively. Following several washes to eliminate unspecific binding proteins, the complex is eluted by different methods (such as adding reducing loading buffer or competitive substances). In this study, *in vitro* pull-down experiments were performed in order to confirm a protein-protein interaction predicted by other techniques (*i.e.* co-immunoprecipitation) or to confirm the functionality of purified proteins. Pull-down protocols used in this work are detailed below.

To test the interaction between His-MBP-Pch2 and His-Hop1, His-MBP-Pch2 was pulled down. For that 7.5 μ L of amylose beads (New England BioLabs), pre-blocked with 5% BSA, were incubated with 6 μ M His-MBP or 1 μ M His-MBP-Pch2 (assuming an hexamer of Pch2) for 1 h on ice in a final volume of 30 μ L of pull-down buffer (50 mM Tris pH 7.5, 50 mM NaCl, 10 mM imidazole, 10 mM β -mercaptoethanol, 0.1% Tween-20, 1 mM $MgCl_2$) in a 0.5 mL microfuge tube. Beads were then washed once with 100 μ L of pull-down buffer, and 6 μ M Hop1 was added. As input, 6% of the final volume was taken and then diluted in pull-down buffer up to 10 μ L. The pull-down reaction was incubated for 90 min on ice, and next washed once with wash buffer (50 mM Tris pH 7.5, 200 mM NaCl, 10 mM imidazole, 10 mM β -mercaptoethanol, 0.5% Triton X-100, 1 mM $MgCl_2$). To elute bound proteins, 20 μ L of 2.5x SDS loading buffer was added, samples were boiled 5 min at 95°C, and the supernatant transferred to a new microfuge tube. To inputs, 5x SDS loading buffer was added and samples were boiled similarly to the pull-down samples. Samples of both, inputs and pull-downs, were resolved by SDS-PAGE and stained with CBB.

For testing the interaction between His-MBP-Pch2 and His-ORC, pull-downs were performed as follows: 5 μ L of 5 % BSA pre-blocked amylose beads (New England BioLabs) were incubated with 6 μ M His-MBP or 1 μ M His-MBP-Pch2 (assuming Pch2 as a hexamer) for 1 h on ice in a 30 μ L final volume of pull-down buffer (30 mM HEPES pH 7.5, 150 mM NaCl, 10 mM imidazole, 10 mM β -mercaptoethanol, 0.1% Tween-20, 10 mM $MgCl_2$). The pull-down reactions were washed twice with 200 μ L of pull-down buffer, briefly spun down and supernatant removed. Then, 1 μ M ORC was added. At this step, 10% of the final volume was taken as input. The pull-down reaction was incubated for 90 min on ice and washed twice with 200 μ L of wash buffer (30 mM HEPES pH 7.5, 200 mM NaCl, 10 mM imidazole, 10 mM β -mercaptoethanol, 10% TritonX-100, 10 mM $MgCl_2$).

Inputs were diluted with pull-down buffer up to 10 μ L and then 5x SDS loading buffer was added. For the pull-down reactions, 20 μ L of 2.5x SDS loading buffer was added. Samples were boiled at 95°C, and supernatant from pull-down reactions transferred to a new 0.5 mL microfuge tube. Samples were resolved by SDS-PAGE and stained with CBB. Alternatively, the input/pull-down samples were analyzed by Western blotting, as follows: half of the input/pull-down reactions were run on an SDS-PAGE gel, transferred to a nitrocellulose membrane at 300 mA for 90 min and probed overnight with α -MBP (1:10000, New England BioLabs) or α -ORC (1:1000, a kind gift of Stephen Bell; MIT, Cambridge, USA). Membranes were then incubated with the corresponding secondary antibodies and

subsequently developed. Pull-down assay of Δ bah-ORC and His-MBP-Pch2 was performed similarly as pull-down with full-length ORC and His-MBP-Pch2.

Pull-down experiments with Pch2 fragments (His-MBP-Pch2-2-144/His-MBP-Pch2-243-564) were performed similarly, except that 6 μ M of His-MBP-Pch2-2-144 was used (due to formation of monomer instead of hexamer in this fragment). Note that for pull-down with His-MBP-Pch2-2-144 and ORC analysed by Western blot, we used a 2-fold excess of His-MBP-Pch2-2-144 fragment as compared with the pull-down analysed by CBB staining. Western blotting was performed similarly as detailed above, probing with α -MBP or α -ORC. Pull-down assay with the BAH domain of Orc1 alone (GST-BAH) and His-MBP-Pch2 were performed similarly to pull-down experiments with ORC and His-MBP-Pch2, except that buffers were adjusted to pH 8.0. For such pull-downs, the following protein concentrations were used: 1 μ M His-MBP-Pch2 (considering hexameric formation), 3 μ M GST-BAH; 3 μ M GST and 6 μ M of MBP-His (as negative controls).

To detect the interaction between Cdc6 (purified from bacteria) and ORC pull-down experiments via the His-tag in ORC were performed. ORC (1 μ M, considering hexamer) was immobilized in His-beads (cOmplete His-Tag Purification Resin, Roche) and further incubated with Cdc6 (6 μ M/18 μ M). His-beads were used as a negative control. Pull-down assay was performed similarly as previous pull-down assays with His-MBP-Pch2 and ORC, and inputs and pull-down samples were analysed by SDS-PAGE and CBB staining.

2.2.9.2 Analytical size exclusion chromatography (SEC) migration shift assay

Analytical size-exclusion chromatography (analytical SEC) is used to separate proteins or protein complexes based on their molecular size. This technique is based on the principle that smaller proteins enter the pores of a column matrix (stationary phase) more easily than larger molecules. Therefore, larger proteins pass through the column faster than lower size molecules and elute earlier. In contrast, smaller molecules get trapped in the porous bed and elute later. The stationary phase consists of a tightly packed column with different polymer beads of a particular size depending on the column type. In this study, columns with Superose and Superdex matrices were used (see below).

This method is a useful technique to detect protein-protein interactions in solution. By comparing the elution profile of individual proteins and mixed proteins that flow in the column, it is possible to detect binding between the proteins present in the mixture sample.

An earlier elution with respect to the individual proteins is indicative of the formation of a bigger complex and thus, of an interaction between them.

In this study, analytical SEC was performed on a Superose 6 5/150 GL column (GE Healthcare) connected to an ÄKTAmicro FLPC system (GE Healthcare). Proteins (1 μM His-MBP-Pch2, 3 μM His-ORC) were mixed in a total volume of 50 μL , incubated 2 h on ice and spun down for 15 min at 15000 rpm in a benchtop centrifuge (4°C) before injection. All samples were eluted under isocratic conditions at 4°C in SEC buffer containing 30 mM HEPES pH 7.5, 150 mM NaCl, 3% glycerol, 1 mM MgCl_2 , and 2 mM TCEP, at a flow rate of 0.1 mL/min. Fractions (100 μL) were collected in a microplate (Microtest plate 96 well, R; Sarstedt) and 20 μL of the eluates were separated by SDS-PAGE, followed by CBB staining. For SEC profiles represented in Figures 3-5, 3-6, 3-9 and 3-10, the purified proteins were run as described above. Briefly, purified His-MBP-Pch2 (2 μM), His-MBP-Pch2-2-144 (6 μM), His-MBP-Pch2-243-564 (2 μM) or His-ORC (6 μM) were diluted in SEC buffer (30 mM HEPES pH 7.5, 150 mM NaCl, 3% glycerol, 2 mM TCEP, 1 mM MgCl_2) up to a volume of 50 μL , spun down 15 min at 15000 rpm (4°C) and immediately loaded onto a Superose 6 Increase 5/150 GL column (for His-MBP-Pch2 and His-ORC) or onto a Superdex 200 5/150 GL (for His-MBP-Pch2-2-144).

2.2.9.3 Cross-linking mass-spectrometry (XL-MS)

Chemical cross-linking coupled to mass spectrometry (XL-MS) is an approach to identify and map protein-protein interactions. XL-MS can provide information on inter- and intramolecular interactions that can yield useful insights into assembly principles of complex protein samples. The general XL-MS workflow involves an initial cross-linking reaction in which a cross-linking reagent physically tethers amino acid residues that are spatially proximal in the mixed protein sample. The cross-linked proteins are then enzymatically digested and the resulting peptides are purified and enriched by size exclusion chromatography. These peptides are subsequently analysed by tandem mass spectrometry (MS/MS).

XL-MS was performed as described by Pan *et al.*, 2018. Briefly, 0.75 μM of His-MBP-Pch2 was mixed with 1.5 μM of His-ORC complex in 200 μL of buffer (30 mM HEPES pH 7.5, 150 mM NaCl, 2 mM TCEP) and incubated at 4°C for 90 min. Next, a MS-cleavable chemical crosslinker (DSBU, disuccinimidyl dibutyric urea - also known as BuUrBu-, Alinda

Chemical Limited) was added to a final concentration of 3 mM and incubated at 25°C for 1 h. The reaction was stopped by adding Tris-HCl pH 8.0 to a final concentration of 100 mM and incubated at 25°C for an additional 30 min. 10 μ L of protein sample was taken, before and after adding the cross-linker, for analysis by SDS-PAGE. SDS-PAGE gel was stained with CBB. Cross-linked protein complexes were precipitated by adding 4 volumes of cold acetone and kept at -20°C overnight. Next, sample was centrifuged 5 min at 15000 rpm and the pellet was dried at room temperature. Protein pellets obtained after acetone precipitation were denatured in 25 μ L of denaturation-reduction solution (8 M urea, 1 mM DTT) for 30 min at 25°C. Cysteine residues were alkylated by adding 5.5 mM chloroacetamide and incubating for 20 min at 25°C. ABC buffer (20 mM ammonium bicarbonate pH 8.0) was added to reduce the final concentration of urea to 4 M. Sample was digested by Lys-C (2 μ g) at 25°C for 3h, followed by overnight Trypsin (1 μ g) digestion in buffer containing 100 mM Tris-HCl pH 8.5 and 1 mM CaCl₂ at 25°C. The digestion was stopped by adding trifluoroacetic acid (TFA) to a final concentration of 0.2 %.

Resulting peptides after digestion were run in three independent size-exclusion chromatography (SEC) runs on a Superdex Peptide 3.2/ 300 column (GE Healthcare) connected to an ÄKTAmicro FPLC system (GE Healthcare). SEC runs were performed at a flow rate of 0.1 mL/min in buffer containing 30% acetonitrile and 0.1% formic acid. 100 μ L fractions were collected and the same fractions from the three SEC runs were pooled, dried and submitted to LC-MS/MS analysis. LC-MS/MS analysis was performed as previously reported (Pan *et al.*, 2018) using an Ultimate 3000 RSLC nano system and a Q-Exactive Plus mass spectrometer (Thermo Fisher Scientific). Peptides were dissolved in water containing 0.1% TFA and were separated on the Ultimate 3000 RSLC nano system (precolumn: C18, Acclaim PepMap, 300 μ m \times 5 mm, 5 μ m, 100 Å, separation column: C18, Acclaim PepMap, 75 μ m \times 500 mm, 2 μ m, 100 Å; Thermo Fisher Scientific). After loading the sample on the precolumn, a multistep gradient from 5–40% B (90 min), 40–60% B (5 min), and 60–95% B (5 min) was used with a flow rate of 300 nL/min; solvent A: water + 0.1% formic acid; solvent B: acetonitrile + 0.1% formic acid.

Data were acquired using the Q-Exactive Plus mass spectrometer in data-dependent MS/MS mode. For full scan MS, we used a mass range of m/z 300–1800, resolution of $R = 140000$ at m/z 200, one microscan using an automated gain control (AGC) target of $3e6$ and maximum injection time (IT) of 50 ms. Then, we acquired up to 10 HCD MS/MS scans of the most intense with at least doubly charged ions (resolution 17500, AGC target $1e5$, IT 100 ms,

isolation window 4.0 m/z, normalized collision energy 25.0, intensity threshold 2e4, dynamic exclusion 20.0 s). All spectra were recorded in profile mode.

Raw data from the Q-Exactive Plus mass spectrometer were converted to Mascot generic files (MGF) format. Program MeroX (version 1.6.6.6) was used for cross-link identification (<http://www.stavrox.com>). Combined MS data in MGF format and the protein sequences in FASTA format were loaded on the program and MS spectra matching cross-linked peptides were identified. In the settings of MeroX, the precursor precision and the fragment ion precision were changed to 10.0 and 20.0 ppm, respectively. RISE mode was used and the maximum missing ions was set to 1. MeroX estimates the false discovery rate (FDR) by comparison of the distribution of the cross-link candidates found using provided protein sequences and the distribution of the candidates found from decoy search using shuffled sequences. A 2% FDR was used as the cut-off to exclude the candidates with lower MeroX scores. The results of cross-link data were exported in comma-separated values (CSV) format. Cross-link network maps were generated using the xVis web site (<https://xvis.genzentrum.lmu.de>) (Grimm *et al.*, 2015). Validation of the datasets was performed by identifying cross-linked peptides within the MBP-moeity present on our Pch2 preparation (13 intra-MBP crosslinks) and using a published crystal structure of MBP (PDB 1FQB, 34) to map C α -C α distances between identified cross-linked amino acids. The average C α -C α was 14.41 Å, which is in good agreement with the C α -C α distance (12 Å), which the cross-linked state of DSBU is able to facilitate.

3 Results

Faithful chromosome segregation in meiosis requires the controlled introduction of DNA double-strand breaks (DSBs), followed by homologous recombination and formation of physical linkages between homologous chromosomes (known as chiasmata) (Hochwagen, 2008; Marston & Amon, 2004a; V. V. Subramanian & Hochwagen, 2014; Zickler & Kleckner, 1999). Despite DSBs being a prerequisite for proper meiotic chromosome segregation, one major challenge of the programmed introduction of DSBs is the need to ensure their accurate repair, minimizing deleterious events that could compromise genome integrity. Recombination between repetitive DNA sequences can lead to such loss of integrity. Hence, DSBs located within or close to these repetitive sequences should be minimized in order to avoid genome destabilization.

Here, we aim to better understand the mechanisms by which the repetitive DNA sequences are protected from the introduction of DSBs. For that purpose, we used the ribosomal DNA (rDNA) of the budding yeast *Saccharomyces cerevisiae* as a repetitive locus model. Previous studies have shown that meiotic DSBs are almost absent from this cluster, in part due to the Sir2-dependent heterochromatin formation (Petes, 1980; Petes & Botstein, 1977). However, the edges of the rDNA array present a high risk of meiotic DSBs and genome rearrangement (Vader *et al.*, 2011). This localized DSB susceptibility requires an rDNA-boundary specific system that minimizes DSB formation, and has been shown to consist of the meiotic AAA⁺ ATPase Pch2 and the origin recognition complex subunit Orc1. Upon disruption of this ‘anti-break’ system, strong DSB formation occurs at the rDNA boundaries, leading to unequal recombination within the first ~10 rDNA repeats. Both AAA⁺ ATPases, Pch2 and Orc1, provide an ‘anti-DNA break’ mechanism to suppress DSBs, but how this system operates remains poorly understood (Vader *et al.*, 2011).

This Ph.D. study aimed to further characterize, both *in vivo* and *in vitro*, the interplay between Pch2 and Orc1. Moreover, we aimed to understand whether other subunits of ORC also play a role in Pch2 binding and functionality at the rDNA of budding yeast. In addition, we addressed whether the interaction between these two AAA⁺ complexes is direct and further characterized the molecular basis of the interaction between Pch2 and Orc1/ORC. In total, we aimed to build a comprehensive model about the association and functionality of these two AAA⁺ ATPases that collaborate to suppress rDNA-proximal DSB formation.

3.1 Pch2 interacts with the ORC complex in meiotic G2/ prophase

3.1.1 Pch2 interacts with Orc1 in a manner consistent with a stereotypical AAA⁺ client and/ or adaptor interaction

Pch2 functionally interacts with the Orc1 subunit of ORC (Vader *et al.*, 2011). However, it is not known if these proteins interact directly *in vivo*. Additionally, the biochemical basis of this interaction remains poorly understood. Pch2 and ORC are members of the AAA⁺ ATPase (ATPases associated with diverse cellular activities) superfamily, a large group of proteins involved in a wide range of cellular activities. Pch2 plays a role in several processes during meiotic G2/ Prophase, whereas the canonical function of ORC is the initial loading of the MCM helicase to drive DNA replication. Like many other AAA⁺ ATPases, Pch2 consists of two domains: a non-enzymatic NH₂-terminal domain (amino acids 1-242) and a C-terminal AAA⁺ ATPase domain (amino acids 243-564).

AAA⁺ ATPases form ring-shaped oligomeric complexes, typically hexamers, which are crucial for their ATPase activity and mechanism of action (Erzberger & Berger, 2006; Hanson & Whiteheart, 2005; Ogura *et al.*, 2004; Ogura & Wilkinson, 2001). The hallmark of this diverse group of enzymes is an ATP-binding domain, which contains the so-called ‘Walker A’ and ‘Walker B’ motifs, which are part of the ATP-binding site. A region of the Walker A motif (known as P-loop) interacts with the phosphates of the ATP, whereas the Walker B motif, besides establishing contacts with the nucleotide, harbours an amino acid sequence containing an aspartate and a glutamate residue that are crucial for ATPase activity and ATP hydrolysis (see section 1.4). As such, mutants of these two motifs are typically employed to block ATP binding and/or disrupt ATP hydrolysis. Since AAA⁺ ATPases usually involve cycles of ATP binding/hydrolysis to engage their clients or co-factors, mutants that can bind but not hydrolyse ATP can be useful to detect possible weak or transient interactions between AAA⁺ ATPases and clients/co-factors. Moreover, mutants in the Walker A or Walker B motifs are, as well, useful to understand the dependency of such interactions on ATP binding and/or hydrolysis (Babst *et al.*, 1998; Hanson & Whiteheart, 2005; Weibezahn *et al.*, 2003).

To define the interaction between Pch2 and Orc1, we first investigated whether this interaction depended on Pch2 hexamer formation and/or ATP hydrolysis activity *in vivo*. We employed an ATP hydrolysis mutant within the Walker B domain of Pch2 (Pch2-E399Q),

which we previously reported to be unable to support rDNA-associated DSB protection (Vader *et al.*, 2011) (Figure 3-1 A). In other AAA⁺ enzymes, mutating this critical residue in the Walker B motif prevents efficient ATP hydrolysis and stalls the stereotypical catalytic cycle of AAA⁺ enzymes. Mutants of the Walker B motif can therefore bind, but not release substrates, which often leads to stabilized interactions between AAA⁺ proteins and their clients and/or adaptors. Equivalent mutants in other AAA⁺ enzymes have been used to create ‘interaction traps’ and be able to detect enzyme:client and/or enzyme:adaptor interactions. We used either wild-type (WT) 3xHA-Pch2 or the Walker B mutant of Pch2 (3xHA-Pch2-E399Q) to perform *in vivo* co-immunoprecipitation (Co-IP) with Orc1-TAP tagged via α -TAP-IP during meiotic G2/prophase (5 hours into the meiotic programme).

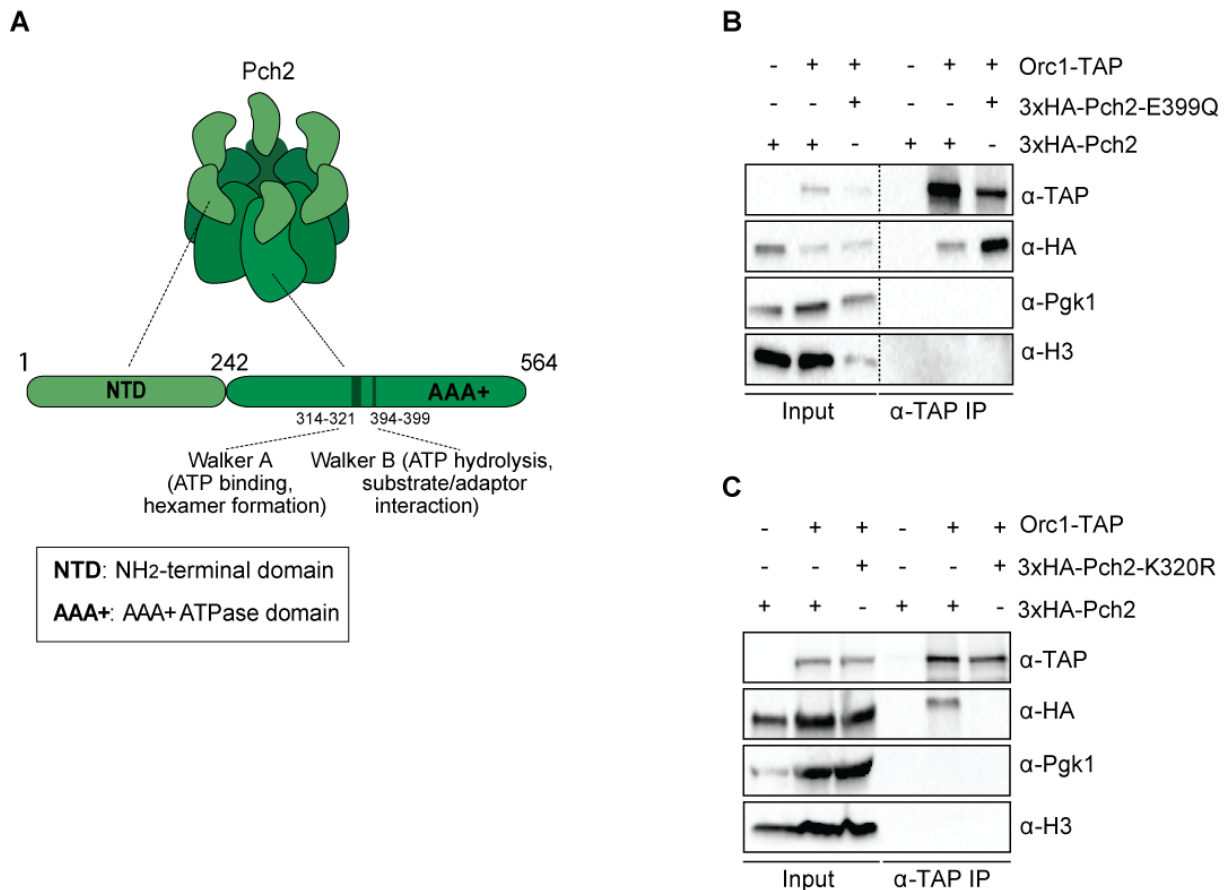


Figure 3-1 *In vivo* characterization of Pch2-Orc1

A) Schematic of hexameric Pch2 AAA⁺ assembly, with domains organization of Pch2. Pch2 harbors a non-catalytic NH₂-terminal domain (NTD; amino acids 1-242) and a COOH-terminal AAA⁺ ATPase domain (AAA⁺; amino acids 243-564). The AAA⁺ domain harbors typical motifs of the AAA⁺ ATPases (Walker A and Walker B motifs). B) Co-Immunoprecipitation (Co-IP) assay of wild-type 3xHA-Pch2 and 3xHA-Pch2-E399Q with Orc1-TAP (via α -TAP) during meiotic prophase (5 hours into meiotic programme). C) TAP-based Co-IP of wild-type 3xHA-Pch2 and 3xHA-Pch2-K320R with Orc1-TAP

Figure 3-1 (Continued)

during meiotic prophase (5 hours into meiotic programme). α -H3 and α -Pgl1 were used as loading controls.

We observed that Orc1 co-precipitated with 3xHA-Pch2 specifically, as Pch2 did not co-precipitate with untagged Orc1 (Figure 3-1 B, lanes 4 and 5). By Co-IP experiments we also showed increased interaction between 3xHA-Pch2-E399Q and Orc1-TAP, as compared to cells expressing WT 3xHA-Pch2 (Figure 3-1 B, lanes 5 and 6). We next analysed a different mutant Pch2 allele, which carried a mutation within the Walker A motif (K320R). Mutations in residues located within this motif reduce ATP binding (Hanson & Whiteheart, 2005). When we investigated the interaction between 3xHA-Pch2-K320R and Orc1-TAP via α -TAP-IP, Orc1-TAP failed to co-immunoprecipitate 3xHA-Pch2-K320R (Figure 3-1 C, lane 6). Given that mutations in the Walker A motif lead to monomerization of Pch2 *in vivo* (Herruzo *et al.*, 2016), our data suggested that the efficient interaction between Pch2 and Orc1 relies on both ATP binding and Pch2 hexamer formation. Taken together, these results indicate that Pch2 interacts with Orc1 in a manner that is consistent with a stereotypical AAA⁺:client and/or adaptor interaction, since AAA⁺ ATPases typically require the assemblage into hexamers to coordinate ATP binding/hydrolysis cycles to function with their substrates and/or induce conformational changes to their substrates.

3.1.2 Pch2 interacts with the entire ORC in meiotic G2/ prophase

Up to our knowledge, all functions ascribed to budding yeast Orc1 involve its assembly into the hetero-hexameric Origin Recognition Complex (ORC; consisting of Orc1-6) that drives DNA replication upon binding to additional factors (Bell, 2002; Bell & Labib, 2016) (Figure 3-2 A). To explore whether in addition to Orc1, other subunits of ORC also interact with Pch2, we performed co-IP assays after 5 hours into the meiotic programme. For that purpose, we generated strains containing TAP-tagged versions of different subunits of ORC (Orc1, Orc2 or Orc5), which enables comparison of interaction efficiencies of the different ORC members by probing against α -TAP. We initially tested the expression of these proteins during meiotic G2/prophase by Western blotting, which revealed similar expression levels of Orc1-TAP, Orc2-TAP and Orc5-TAP (Figure 3-2 B). We employed the *PCH2-E399Q* allele, described above, to stabilize *in vivo* interactions and to facilitate the detection of possibly weak and/or transient interactions. Our α -TAP Co-IP assays confirmed the *in vivo* interaction between Orc1-TAP and 3xHA-Pch2-E339Q (Figure 3-2 C, lane 6), and revealed an interaction between TAP-tagged

versions of Orc2/Orc5 and 3xHA-Pch2-E339Q at time point 5 hours in meiotic G2/prophase (Figure 3-2 C, lanes 7 and 8). This result was further strengthened by a Co-IP assay using α -Orc2 antibody, which also revealed an interaction between 3xFlag-Pch2-E399Q and untagged Orc2 (Figure 3-2 D, lane 3). This interaction was specific, as the Walker B mutant of Pch2 did not co-precipitate Orc2 when the IP was performed via control α -IgG antibody (Figure 3-2 D, lane 2). Although our co-IP experiments do not *per se* prove that Pch2 directly interacts with different subunits of ORC, they indicate that Pch2 is able to associate with the entire ORC during meiotic G2/prophase.

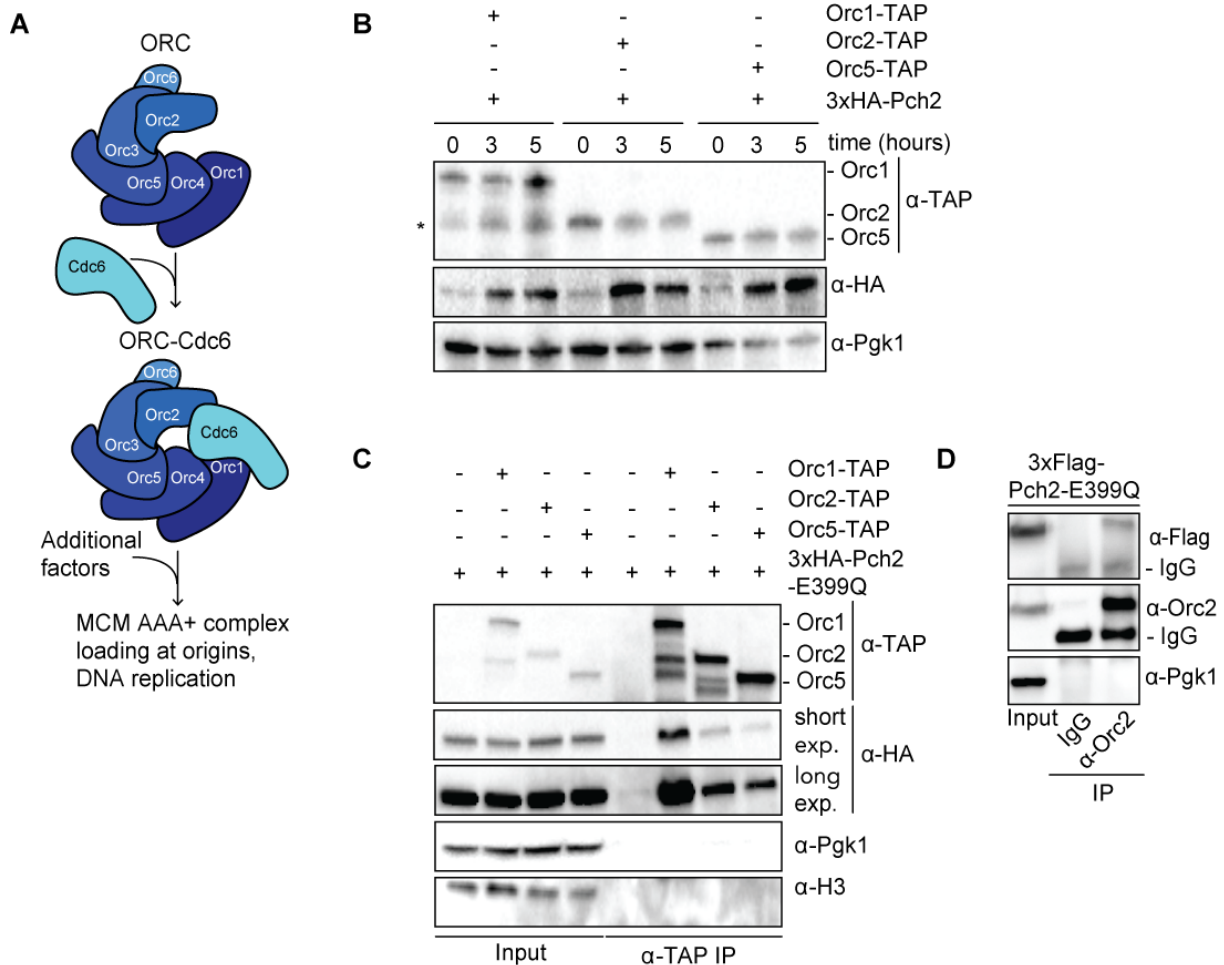


Figure 3-2 Pch2 associates with the entire ORC in meiotic G2/prophase

A) Schematic of the hetero-hexameric ORC (Orc1-6) AAA⁺ complex and its canonical role with the Cdc6 AAA⁺ protein (and additional factors) in loading the MCM replicative helicase to promote the initiation of DNA replication. B) Expression of the Orc1-TAP/Orc2-TAP/Orc5-TAP and 3xHA-Pch2 proteins, confirmed by Western blot analysis when detected with a α -TAP or α -HA antibodies, respectively. Protein extracts probed with a α -Pgk1 served as loading control. Samples for Western

Figure 3-2 (Continued)

blotting were collected 0, 3 and 5 hours after cells were induced into meiosis. Asterisk denotes Orc1-TAP degradation fragment. C) TAP-based Co-immunoprecipitation (Co-IP) assay of 3xHA-Pch2-E399Q with Orc1-TAP, Orc2-TAP and Orc5-TAP during meiotic prophase (5 hours into meiotic programme). For α -HA short and long exposures are shown. α -H3 and α -Pgk1 were used as loading controls. Strain with wild-type, untagged ORC was used as a negative control. D) Co-IP assay of 3xHA-Pch2-E399Q with untagged Orc2 (via α -Orc2 IP). Isotype IgG immunoprecipitation was used as a negative control.

3.1.3 Pch2-Orc1 function and interaction is independent of DNA replication and Cdc6

Pch2 protects ribosomal rDNA array borders (*i.e.* the \sim 1-10 outermost rDNA repeats and \sim 50 kb of single copy flanking sequences) against meiotic DSB formation (Vader *et al.*, 2011) (Figure 3-3 C). This function is also exposed when Orc1 function is impaired (via the use of the *orc1-161* temperature-sensitive allele). Since Orc1 is crucially required for DNA replication, we wanted to address whether DNA replication is involved in this rDNA-associated function of Pch2. For this, we focused our attention on Cdc6, an AAA⁺ protein that associates with ORC (*i.e.* Orc1-6) and is required for chromosomal loading of the MCM AAA⁺ replicative helicase at origins of DNA replication (Figure 3-2 A) (Bell & Labib, 2016; H. Li & Stillman, 2012).

To test whether Cdc6-dependent DNA replication plays a role in rDNA-associated DSB activity, we employed a meiosis-specific null allele of *CDC6* (*cdc6-mn*; where *CDC6* is under the control of the mitosis-specific *SSC1* promoter; *pSSC1-CDC6*) which has been shown to severely hamper pre-meiotic DNA replication (Hochwagen *et al.*, 2005), to investigate if absence of Cdc6 influenced Pch2-Orc1 function and interaction. Importantly, in the *cdc6-mn* background, despite a failure to undergo bulk DNA replication, as judged by analysis of DNA content ($2N/4N$) during meiosis (Figure 3-3 A), meiotic progression is unaffected and cells initiate DSB formation in a meiotic G2/prophase-like state (Blitzblau *et al.*, 2012; Hochwagen *et al.*, 2005). Using this allele, we observed that Cdc6 depletion did not trigger a Pch2-like phenotype at rDNA borders, as judged by Southern blotting (SB) analysis of meiotic DSB formation at the right rDNA flank (by using a probe within *YLR164W*, chromosome *XII*) (Figure 3-3 C and D). For SBs, *dmc1 Δ* background strains were used (*dmc1 Δ* is a DSB repair-deficient mutant used to detect accumulation of meiotic DSBs). We used a probe within the *YCR047C* hotspot (chromosome *III*) as a positive control for DSB formation (Figure 3-3 C and

D, lower panel). In addition, *pch2Δcdc6-mn* yeast strains efficiently formed DSBs within the right rDNA flank (Figure 3-3 D), demonstrating that bulk (Cdc6-dependent) DNA replication is not required for DSB formation in these regions in cells lacking Pch2.

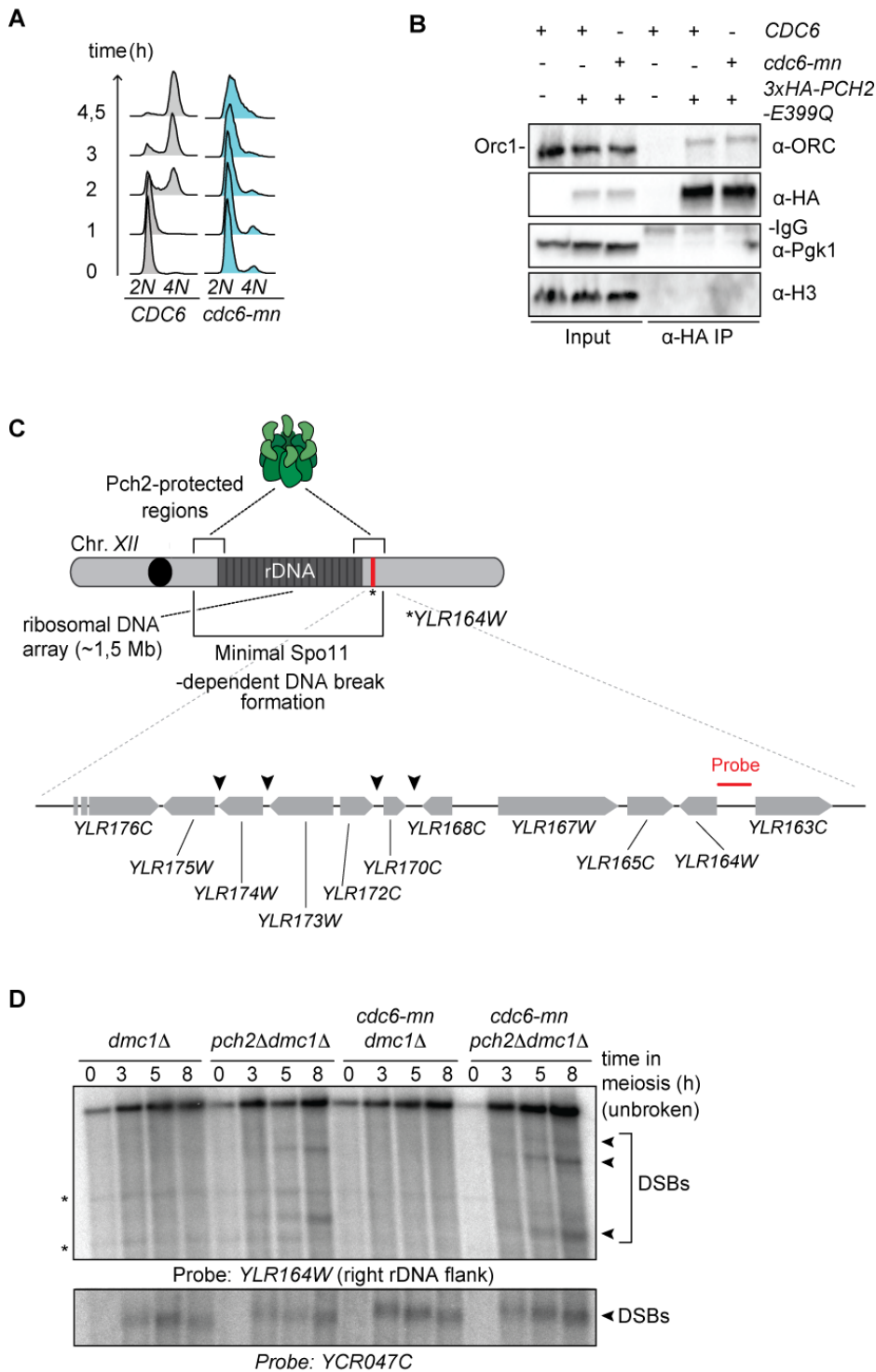


Figure 3-3 Pch2-Orc1 function and interaction is independent of DNA replication and Cdc6

A) Flow cytometry analysis of *CDC6* and *cdc6-mn* (*pSCC1::CDC6*) in meiosis. Samples were collected for DNA content analysis at the indicated time points after induction into the meiotic programme.

Figure 3-3 (Continued)

B) Co-immunoprecipitation of 3xHA-Pch2-E399Q with ORC (via α -HA-IP) during meiotic prophase (5 hours into meiotic programme) in *CDC6* and *cdc6-mn*. α -H3 and α -Pgl1 were used as loading controls. C) Schematic of the role of Pch2 in controlling Spo11-dependent DNA double-strand break (DSB) formation within the flanking regions of the budding yeast ribosomal DNA (rDNA) array located on chromosome *XII*. * indicates location of *YLR164W* locus, where DSB formation is interrogated. Lower panel: Schematic of the chromosomal organization near the rDNA right flank where meiotic DSB formation is interrogated. The radioactively labeled probe used hybridizes near *YLR164W* (Chromosome *XII*; SGD coordinates: 493,432- 493,932). Arrowheads indicate restriction sites. D) Southern blot analysis of *YLR164W* locus (right rDNA flank; Chromosome *XII*) and *YCR047C* locus (control DSB region; Chromosome *III*), in *dmc1 Δ* , *pch2 Δ dmc1 Δ* , *cdc6-mn dmc1 Δ* and *cdc6-mn pch2 Δ dmc1 Δ* background strains. *dmc1 Δ* is a DSB repair-deficient mutant used to detect accumulation of meiotic DSBs by Southern blot. Cells were induced to synchronously undergo meiosis and samples from sporulation cultures were harvested at time points 0, 3, 5 and 8 hours after meiotic induction. Asterisk indicates unspecific signal. Arrowheads indicate DSBs.

While Pch2 is expressed during the meiotic G2/prophase, Cdc6 availability is restricted to the G1 phase, both in the mitotic and meiotic programme (Drury *et al.*, 2000; Phizicky *et al.*, 2018; San-Segundo & Roeder, 1999). The constrained availability of Cdc6 during the cell cycle forms part of a tightly controlled mechanism that, in meiosis, allows for two consecutive rounds of chromosome segregation without an intervening chromosome duplication step (Hochwagen, 2008; Marston & Amon, 2004a). Particularly, Cdc6 phosphorylation by the Cyclin-Dependent Kinase (CDK) triggers the proteolytic degradation of Cdc6, therefore restricting its availability to the G1 phase of the cell cycle, where the replicative helicase loading step takes place (Drury *et al.*, 2000; Phizicky *et al.*, 2018). As such, re-replication events are prevented, ensuring genome stability. Due to the presence of Pch2 and Cdc6 in different phases of the cell cycle, we surmised that the interaction between Pch2 and Orc1 would occur independently of Cdc6 (Phizicky *et al.*, 2018). Indeed, our α -HA Co-IP assay using 3xHA-Pch2-E399Q showed that the interaction between Pch2 and Orc1 was unaffected by the impairment of *CDC6*, since we detected similar binding between Pch2 and Cdc6 in wild-type *CDC6* and *cdc6-mn* backgrounds (Figure 3-3 B, lanes 5 and 6), corroborating our idea that ORC-Pch2 assembly occurs under conditions where Cdc6 levels are functionally depleted.

In summary, the findings described in this section reveal that Pch2-Orc1 interaction and functionality at the rDNA are independent of Cdc6, and of bulk DNA replication.

3.2 *In vitro* reconstitution demonstrates a direct interaction between Pch2 and ORC

In sections 3.1.2-3.1.3, we showed that Pch2 interacts *in vivo* with ORC and that the Pch2-ORC assembly forms independently of Cdc6. However, we had still a limited understanding of how the Pch2-ORC complex forms and the biochemical properties of this complex. One question that needed to be addressed was whether the interaction between these two AAA⁺ complexes was direct. Therefore, to gain understanding of the biochemical basis underlying Pch2-ORC binding, we sought to *in vitro* reconstitute this complex. In the following sections (3.2.1-3.2.4), we focus on the approaches followed to purify both protein complexes and provide insights gained from the *in vitro* reconstitution of this assembly.

3.2.1 Optimization of Pch2 expression and purification

To purify Pch2 we initially attempted to express this protein in bacterial systems, since bacterial expression constitutes a fast approach to express recombinant proteins and presents several advantages as compared with other protein expression systems, such as typically high protein yields. Our expression tests of Pch2 using different bacteria (BL21, BL21+, C41 and Rosseta) showed that, although Pch2 was expressed, it was mostly degraded to a lower molecular weight product (See Appendix, Figure 7-1 A). Therefore we sought to test the purification of Pch2 from other sources. During our efforts to purify Pch2 a study showing the expression and purification of Pch2 from yeast was published (Chen *et al.*, 2014). Until date, this is the only study showing the purification of Pch2 from yeast. However, our attempts to purify Pch2 from yeast were not successful (not shown here).

As an alternative approach, we pursued the expression of Pch2 from insect cells. This system has become a powerful method to purify recombinant proteins, since it allows the rapid expression and optimization of different DNA constructs generally resulting in high yields of proteins. The fundamental advantage of protein expression in insect cells is that, contrary to bacterial expression, it may potentially keep the post-translational modifications of eukaryotic proteins. Since we aimed to *in vitro* reconstitute the assembly between Pch2 and ORC, and it remained unclear whether the lack of post-translational modifications (*i.e.* phosphorylation, etc.) would affect this interaction, we expressed Pch2 using this system.

It was previously shown that Pch2 carrying an NH₂-terminal GST tag was biochemically active towards its known substrate Hop1 (Chen *et al.*, 2014). Thus, we opted for expressing N-terminally-tagged GST-Pch2 using a baculovirus-based protein expression

system. Our expression tests using different ratios of virus to insect cells (*Tnao38* cells) showed that GST-Pch2 was successfully expressed after 48 h, especially when a ratio 1:10 (virus:culture) was used (See Appendix, Figure 7-1 B). We next aimed to purify this protein, using a combination of affinity chromatography (employing a GSTrap FF column; See Materials and Methods for further details) and size exclusion chromatography (SEC).

This approach allowed us to purify recombinant GST-Pch2, as shown in Figure 7-1 C (See Appendix). We noted that GST-Pch2 eluted proximal to the molecular-weight size marker peak corresponding to 670 kDa. The apparent higher molecular weight of GST-Pch2, as compared to the expected size (89 kDa, in case of a monomeric GST-Pch2; 178 kDa, in case of a GST-driven dimer formation of Pch2), could be attributed to the formation of GST-Pch2 hexamers. As already mentioned, AAA⁺ ATPases usually assemble into hexameric complexes. A GST-Pch2 hexameric complex would have a theoretical molecular weight of 534 kDa, which is a size that could correspond with the observed elution profile close to the peak of the highest molecular weight of the employed marker (670 kDa). We therefore interpreted this data to mean that the purified GST-Pch2 assembles into hexamers. Although we were able to purify this protein, an underlying issue was the lack of reproducibility in the expression of GST-Pch2 and the generally low expression of protein. We then set to scale-up the protein production but the very low yields of protein obtained precluded us from performing further *in vitro* experiments with this construction.

We further aimed to establish an alternative strategy to purify Pch2 that could be more reliable in terms of protein production. For that purpose, we employed constructs in which the sequence of budding yeast Pch2 had been codon-optimized for *Spodoptera frugiperda* (*Sf9*) insect cells. Codon optimization is a powerful tool to increase the yield of recombinant protein expression. It is based on the codon-usage bias phenomenon, by which synonymous codons are not used in equal frequencies across different species (Wang *et al.*, 2015). It has been shown that the usage of a defined subset of codons specific for an organism is related to organism-specific populations of isoaccepting tRNAs (tRNAs that carry the same amino acid but respond to different codons for that amino acid) (Ikemura, 1985; Plotkin & Kudla, 2011). Moreover, there is a positive correlation between gene expression level and the degree of its codon bias; usually, highly expressed genes have a strong codon bias, meaning that they only use a limited subset of synonymous codons, excluding others. This is correlated with the level of isoaccepting tRNAs: highly expressed genes use codons that are recognized by most isoacceptors, avoiding the usage of others (Ikemura, 1985; Plotkin & Kudla, 2011). In the

same line, several studies have demonstrated that the usage of rare codons can have a negative effect on heterologous gene expression; codons that are read by rare isoaccepting tRNAs can lead to ribosomal pausing, slow elongation and can reduce protein expression yields by impeding translation initiation. Therefore, the adaptation of codon usage (or codon optimization) can be used as a tool to increase gene expression, especially in those species where the usage and variation of tRNA concentrations is well understood (such as in bacteria and yeast) (Plotkin & Kudla, 2011; Wang *et al.*, 2015).

We therefore expected to significantly increase protein expression levels by producing Pch2 derived from its codon-optimized sequence for *Sf9* cells. Furthermore, we pursued the expression of this protein fused to two different NH₂-terminal tags: GST and His-MBP. Affinity tags might confer a relevant difference in terms of protein expression and/or solubility and can, as well, influence the folding of recombinant proteins. Our expression tests in insect cells of Pch2 and Pch2 constructs (see section 3.4 for further details on Pch2 truncated versions) (See Appendices, Figures 7-2, 7-3 and 7-4) showed that Pch2 fused with GST/His-MBP was successfully expressed. We observed that those Pch2 constructs with an NH₂-terminal MBP tag were expressed to a higher extent than those with a GST-tag (See Appendices, Figure 7-4 B, compare lanes 5-6 with 7-8, and lanes 9-10 with 11-12). Therefore, we attempted to purify His-MBP-Pch2. We designed a sequential three-step protein purification strategy based on two affinity steps (through His and MBP tag) and a size exclusion chromatography (SEC) step. More precisely, we employed an initial affinity step using a His-binding affinity column (TALON Superflow™ column). At the end of this affinity step (before protein elution), we incorporated an extra high salt wash (1 M NaCl), which successfully eliminated a higher molecular weight product that was consistently observed in our previous purification trials (not shown). After eluting with an imidazole gradient, we obtained a relatively pure protein (Figure 3-4 A). However, we observed some undesired contaminants in our preparations (Figure 3-4 A). A test with amylose beads revealed that His-MBP-Pch2 eluted from the TALON column binds successfully to these beads and that it was possible to elute the protein by using a competitive analyte (maltose) (See Appendices, Figure 7-4 C). Therefore, we incorporated an additional affinity step with amylose beads (MBP-affinity step), after the His-affinity step, in order to obtain a purer recombinant protein. Finally, our protein was separated according to its molecular weight by size exclusion chromatography (Figure 3-4 B) (for a more detailed protocol, see Materials and Methods). Mass spectrometry analysis confirmed the sequence of the purified protein as Pch2

from *S. cerevisiae* (Table 7-1, Appendices). As judged by SEC, purified Pch2 eluted at an apparent molecular weight corresponding to a hexameric assembly (predicted size ~636 kDa), confirming the prediction that this protein assembles into hexamers, a typical structure of many other AAA⁺ ATPases (Hanson & Whiteheart, 2005) (Figure 3-4 B and Figure 3-5 A).

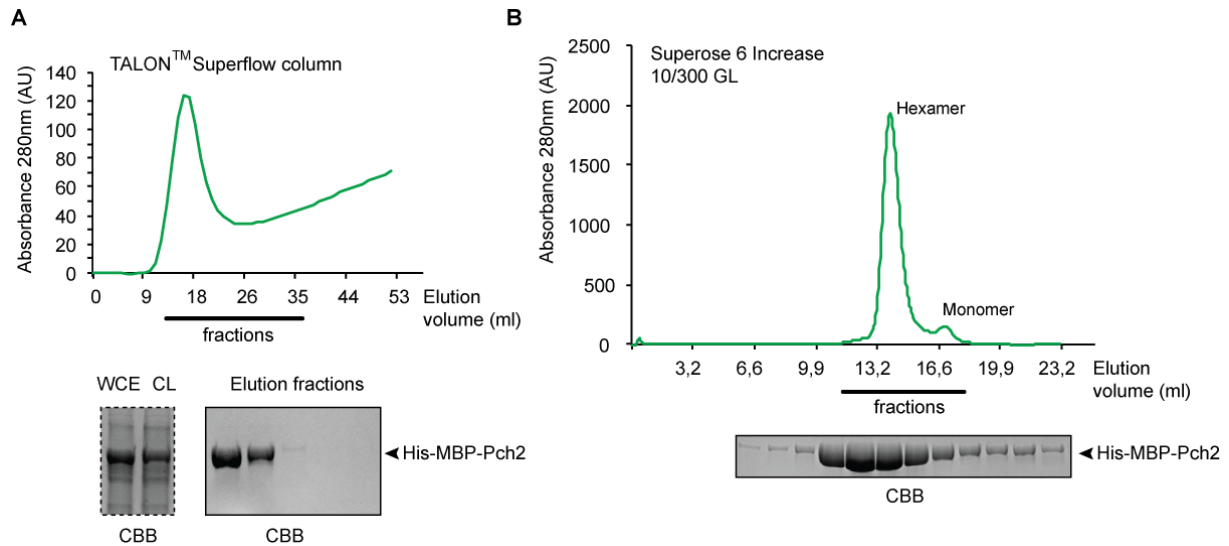


Figure 3-4 Purification strategy of His-MBP-Pch2

A) Chromatogram of His-MBP-Pch2 purified from Tnao38 insect cells via an initial affinity-step via a TALON[™] Superflow column. Whole-cell extract (WCE) and clear lysate (CL) samples are shown. Fractions of the eluted protein analysed by SDS-PAGE are marked by a black line. B) Size exclusion chromatogram (SEC) of His-MBP-Pch2 using a Superose 6 Increase 10/300 GL column. Protein fractions loaded are marked by dotted line. By SEC, two species are detected, which we interpret to correspond to hexameric and monomeric organization of His-MBP-Pch2. Proteins were visualized by Coomassie Brilliant Blue (CBB) staining. AU stands for arbitrary units.

It is worth mention that we consistently observed a minor fraction that appeared to be monomeric in the SEC profiles (size of ~106 kDa for His-MBP-Pch2) (Figure 3-4 B and Figure 3-5 A), which is consistent with the existence of monomeric and hexameric forms of Pch2 in our preparations. It was previously described that Pch2 can exist in monomeric or hexameric form depending on the nucleotide state (Chen *et al.*, 2014). However, we performed these experiments in the absence of any nucleotides, although we cannot completely exclude the possibility that some nucleotides from insect cells are associated with purified Pch2. Taken together, these data demonstrate the establishment of a purification strategy that allowed us to successfully purify His-MBP-Pch2 with protein yields suitable for downstream *in vitro* experiments.

3.2.2 Characterization and validation of Pch2 functionality

Next, we characterized and validated our recombinant His-MBP-Pch2. As mentioned above, re-analysis of hexameric fractions by SEC revealed a reappearance of the apparent monomeric peak (Figure 3-4 B and 3-5 A), suggesting that the recombinantly purified His-MBP-Pch2 exists in an equilibrium of different conformational states (*i.e.* hexameric and monomeric), with the hexameric complex being the predominant one species in our His-MBP-Pch2 preparations.

To further examine this aspect, we performed sedimentation velocity analytical ultracentrifugation (SV-AUC) experiments. To investigate concentration-dependent changes in the oligomeric state of His-MBP-Pch2, we employed SV-AUC at several different loading concentrations (ranging from 0.3 μM to 1 μM). Analytical ultracentrifugation is a powerful method for quantitative and qualitative characterization of proteins and protein complexes in solution, in terms of their hydrodynamic and thermodynamic properties (Patel *et al.*, 2015). This, in turn, allows measurements of sample properties including among others its oligomeric size, shape, molecular mass and potential concentration-dependent changes in association state, and therefore AUC is also useful to verify whether a sample is homogeneous in mass and conformation (Zhao *et al.*, 2013). Analytical ultracentrifugation characterization of proteins and protein complexes generally involves two complementary approaches: sedimentation velocity (SV) and sedimentation equilibrium (SE). Particularly, SV experiments measure the rate of sedimentation of proteins and time-dependent changes in the sedimentation boundaries. Modelling of the sedimentation boundaries in terms of sedimentation coefficient distribution, and the extraction of diffusion coefficients from the boundary shape, in turn, allows transformation of the data directly to molecular mass distribution (Balbo & Schuck, 2005; Brown *et al.*, 2009).

Analysis of the data obtained from SV runs of His-MBP-Pch2 suggested concentration-dependent changes in the oligomeric state, as evident from the shift in sedimentation coefficients under different loading concentrations (Figure 3-5 C). In order to extract molecular masses of the sedimenting species, we modelled boundaries using continuous $c(S)$ model and weight-average frictional ratios using the software Sedfit (Schuck, 2000). Molecular masses obtained in this way suggested a mixture of different oligomeric states (that could correspond to hexamer, trimer and monomer) at the lowest concentration tested (approximately 0.3 μM), though the predominant species appears to be monomeric

(sedimenting at around 5 S) (Figure 3-5 C, upper panels). This distribution changes at higher loading concentrations (approximately 1 μM), where the predominant species (sedimenting at around 12 S) corresponded to a hexameric conformation (Figure 3-5 C, lower panel). Thus, sedimentation velocity experiments point towards the fact that different species of His-MBP-Pch2 co-exist in equilibrium. Altogether, SV-AUC experiments suggest that the purified His-MBP-Pch2 exists in a mixture of several oligomeric species at low concentrations that shift to predominantly hexameric form at concentrations used for the majority of *in vitro* experiments in this Ph.D. thesis.

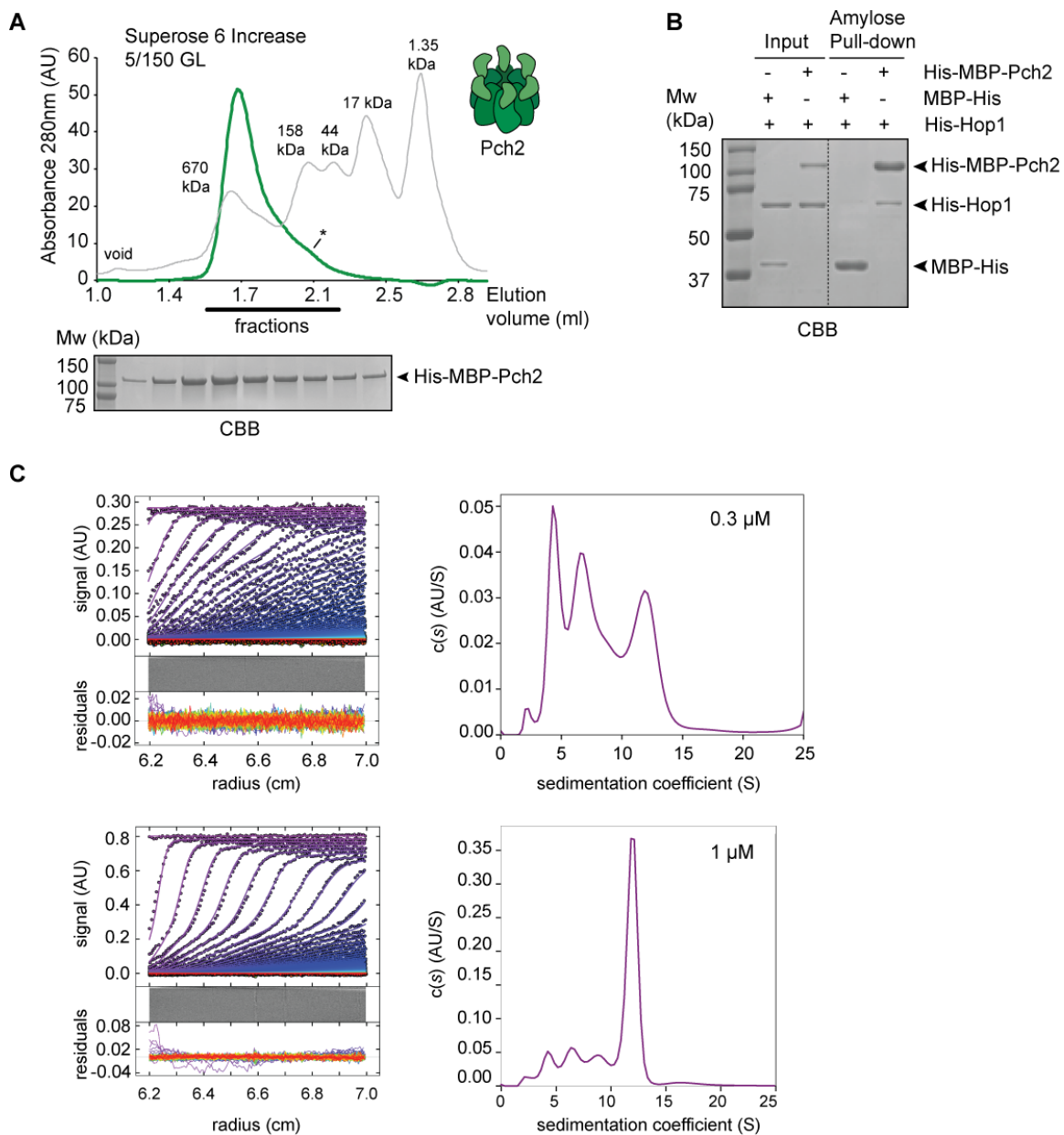


Figure 3-5 Validation of His-MBP-Pch2

A) Size exclusion chromatography (SEC) of His-MBP-Pch2 (2 μM) (green line) purified from insect cells using a Superose 6 Increase 5/150 GL column. Gray line represents a gel filtration

Figure 3-5 (Continued)

chromatography standard (Bio-Rad), for which molecular weights are indicated. Coomassie Brilliant Blue (CBB) staining of peak fractions (black line) run on SDS-PAGE gel. Asterisk indicates likely monomeric fraction of His-MBP-Pch2. AU stands for arbitrary units. B) Amylose-based pull-down of His-Hop1 and His-MBP-Pch2. 6 μM His-MBP or 1 μM His-MBP-Pch2 (assuming a hexamer of Pch2) were used. MBP-His was used as a negative control. Input and pull-down samples were analysed by SDS-PAGE followed by CBB staining. C) Analytical ultracentrifugation sedimentation velocity (AUC-SV) experiments showing concentration-dependent changes of the oligomeric conformation of His-MBP-Pch2. Left panels: Sedimentation profiles of His-MBP-Pch2 sedimenting at 42,000 rpm (circles) and best-fit continuous $c(S)$ model (solid lines) at two different concentrations: 0.3 μM (upper panel) and 1 μM (lower panel). Residuals in the form of bitmap and overlay plot are shown below. Right panel: Sedimentation coefficient distribution of the His-MBP-Pch2 at 0.3 μM (upper panel) and 1 μM (lower panel).

As a proof of the functionality of the purified His-MBP-Pch2, we next aimed to validate an *in vitro* direct interaction with a HORMA (Hop1, Rev, Mad2) domain-containing protein called Hop1, a confirmed substrate of Pch2, as previously described by Chen and co-workers (Chen *et al.*, 2014). Hop1 is an axial component of the synaptonemal complex (SC) that has been shown to interact *in vitro* with Pch2 in a nucleotide-dependent manner. For that purpose, we purified His-Hop1 from bacteria and performed pull-down assays with His-MBP-Pch2 (Figure 3-5 B). Chen *et al.* described that whereas GST-Pch2 strongly binds Hop1 in the presence of a non-hydrolysable form of ATP (ATP γs), it shows weak binding in the absence of nucleotide or in presence of ATP, probably due to the fact that the Hop1-Pch2 interactions are transient and therefore easier to detect when ATP hydrolysis cannot be completed (Chen *et al.*, 2014).

We performed pull-down assays using His-MBP-Pch2 as bait, which corroborated the interaction between Pch2 and Hop1 (Figure 3-5 B, lane 5). This interaction was specific, as we did not detect binding between Hop1 and the control used (MBP-His) (Figure 3-5 B, lane 4). However, we could not observe significant differences among the conditions tested (absence of nucleotides and presence of either ATP or ATP γs), as shown in Figure 7-6 A (Appendix). This discrepancy could be accounted for the different source of the purified proteins in the study of Chen and co-workers with respect to our work, and/or for the different protein tags (GST/His-MBP), which could affect conformation/affinity of Pch2 for its partners (see Discussion). Despite the fact that our results diverge from previous findings in terms of the dependency of nucleotides for the establishment of this interaction, it provides

clear evidence of the functionality of the purified protein His-MBP-Pch2, as it is able to interact with a known client.

3.2.3 Optimization of protein expression and purification of ORC

To pursue the *in vitro* reconstitution of the Pch2-ORC complex, we next aimed to purify ORC (*i.e.* Orc1-6). ORC has been extensively investigated in the context of DNA replication, both under *in vivo* and *in vitro* conditions (Duzdevich *et al.*, 2015; Li & Stillman, 2012; Remus & Diffley, 2009; Sclafani & Holzen, 2007; Ticaou *et al.*, 2017, 2015; Tsakraklides & Bell, 2010; Yeeles *et al.*, 2015). Most of the *in vitro* studies with purified ORC obtained this complex from budding yeast (*S. cerevisiae*). Therefore, we first aimed to purify ORC from *S. cerevisiae* following the purification protocol established by Diffley and co-workers (Frigola *et al.*, 2013) (see Materials and Methods for further details).

We purified ORC (with an NH₂-terminally CBP tag fused to Orc1) (Figure 7-6 B, Appendix), but we noted several observations that precluded us from pursuing the *in vitro* reconstitution of Pch2-ORC with ORC purified from yeast. First, in order to purify ORC from yeast, buffers should contain detergent (0.05% NP-40) presumably to avoid protein precipitation. As a consequence, ORC eluted as a broad peak of seemingly lower molecular weight than expected (~440 kDa) when loaded onto a SEC column. We attributed this to the presence of detergent in the buffer, which is known to interfere with protein topology. Moreover, the presence of detergent interfered with the absorbance at 280 nm (higher absorbance that would correspond to the amount of protein injected in SEC). Second, there is a limit in the concentration of ORC that we could achieve and when we tried to concentrate this complex to a working concentration that would allow us to perform our *in vitro* experiments (*i.e.* pull-down and analytical SEC), we observed formation of aggregates and precipitation of the complex. Taking into consideration all these observations, we decided to change the purification strategy of ORC.

Apart from the biochemical studies using ORC purified from yeast, there has been *in vitro* studies employing recombinant ORC obtained from insect cells (Bleichert *et al.*, 2013, 2015). Given that the baculovirus/insect cells protein expression system had already been established in our department and that we had already successfully purified Pch2 from that source, we next intended to purify ORC from insect cells. For that purpose, we used the biGBac method described by Weissmann *et al.* (2016) to generate two vectors containing His-

Orc1-Orc2-Orc3 and Orc4-Orc5-Orc6, respectively (Weissmann *et al.*, 2016) (See Figure 3-6 A and Materials and Methods for more details).

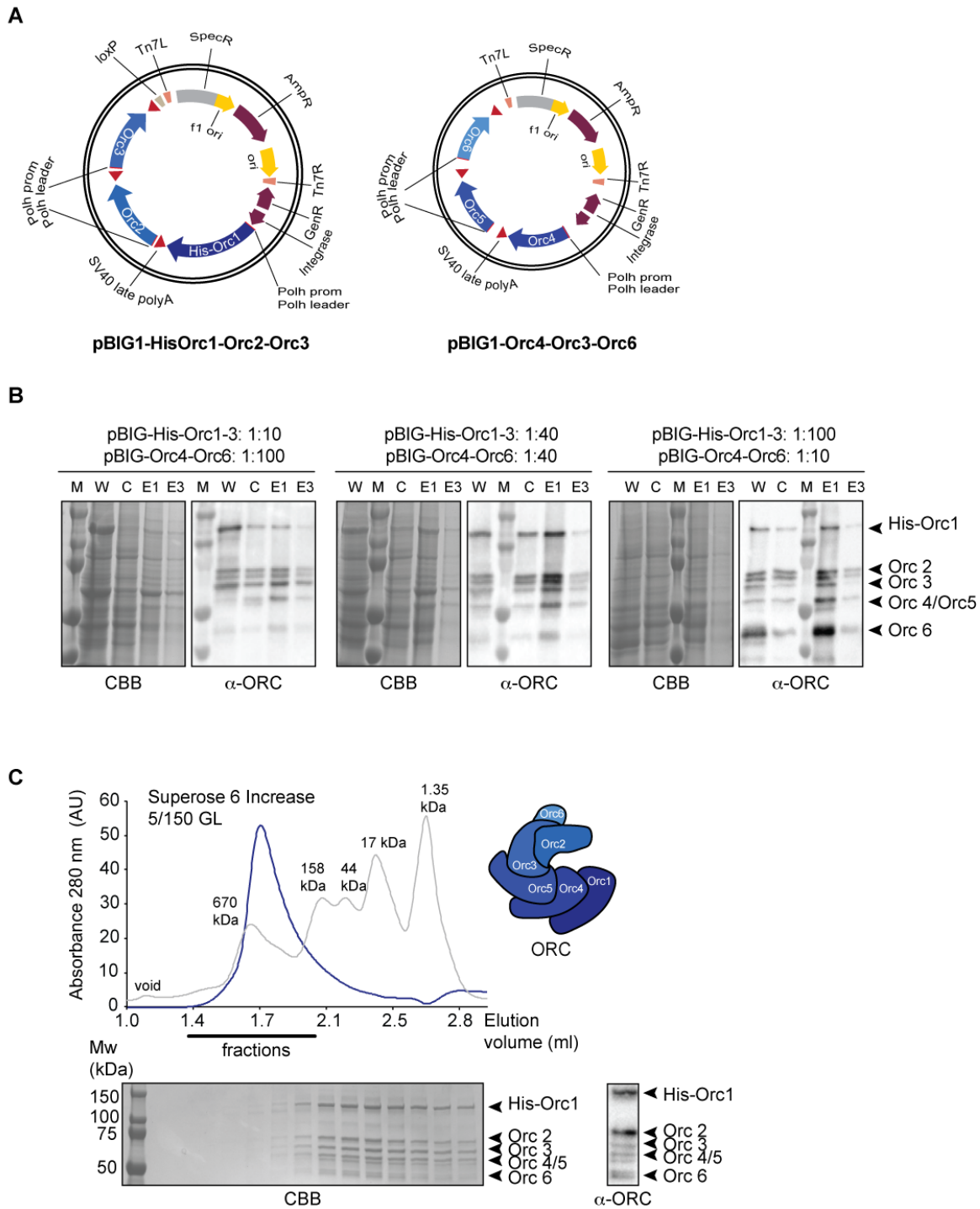


Figure 3-6 Purification strategy of His-ORC

A) Schematic representation of the plasmids used for the purification method of His-ORC (His-Orc1, Orc2-6). Sequences coding for the different subunits of ORC were cloned using the biGBac method (Weissmann *et al.*, 2016) into two different pBIG1 plasmids containing His-Orc1-Orc2-Orc3 and Orc4-Orc5-Orc6, respectively. These plasmids were used to generate baculoviruses to express and

Figure 3-6 (Continued)

purify ORC from Tnao38 insect cells. Main features of the plasmids are indicated, including antibiotic resistances. Tn7L: mini-Tn7 element (left end of the Tn7 transposon); Tn7R: mini-Tn7 element (right end of the Tn7 transposon); Polh prom/Polh leader: polyhedrin promoter/leader sequences; SpecR, AmpR, GenR: resistance to Spectinomycin, Ampicilin or Gentamycin, respectively; ori: origin of replication; loxP: Cre-mediated recombination sequence. B) Expression test of ORC in Tnao38 cells using different ratios (virus:culture) of the two baculovirus coding for His-Orc1-Orc2-Orc3 and Orc4-Orc5-Orc6, respectively. Samples were collected 48 hours after infection. Cell pellets were disrupted and a whole-cell extract (W) was collected. After centrifugation, a clear lysate (C) sample was taken. Filtered lysate was incubated with His-tag purification resin and proteins eluted with via imidazole competition. Several elution samples were taken; E1 and E3 represent elution samples. Baculovirus to culture ratios are indicated. M indicates the molecular weight marker. Protein samples were visualized by either Coomassie Brilliant Blue (CBB) staining or by probing against α -ORC (which recognizes all 6 ORC subunits). See also Figure 7-5 C, Appendices). C) Size exclusion chromatography (SEC) of His-ORC (His-Orc1, Orc2-6) purified from insect cells (2 μ M). Blue line represents SEC of purified His-ORC. Gray line represents SEC of gel filtration protein standard; molecular weight of the proteins in the gel filtration standard is indicated. CBB staining of peak fractions (black line) run on SDS-PAGE gel. AU stands for arbitrary units. Right panel: Western blot of a purified ORC (His-Orc1, Orc2-6) using α -ORC (which recognizes all 6 ORC subunits). Protein molecular weight (kDa) on SDS-PAGE gel is indicated, as compared to a protein standard ladder (M).

We performed expression tests with the two baculoviruses derived from both vectors, using different ratios of virus to culture (Figure 3-6 B and Figure 7-5; see Appendix). These expression tests revealed that ORC was successfully expressed after 48 h when we used a ratio of 1:40 (virus:culture) of both baculoviruses (Figure 3-6 B). We then pursued the purification of this protein complex by using the information gained from our expression tests. We purified ORC by affinity purification through the His-tag in Orc1, followed by a SEC step (See Materials and Methods for more details). Purified ORC eluted as a single peak (expected size ~414 kDa), providing evidence that in the purified ORC all the subunits remained assembled into a complex (Figure 3-6 C). To validate the recombinantly purified ORC, we checked its ability to interact with Cdc6, a binding protein crucial for DNA replication (see Section 3.1.3 for more details). For that purpose, we purified Cdc6 and performed an *in vitro* pull-down with ORC using ORC (His-tagged in Orc1) as bait and His beads as a control. This experiment showed that our purified ORC was able to interact *in vitro* with Cdc6 (Figure 7-6 C, see Appendix), thus, validating our ORC purification strategy.

3.2.4 Pch2 interacts directly with ORC *in vitro*

Once we purified recombinant His-MBP-Pch2 and His-ORC, we next aimed to investigate whether Pch2 directly interacted with ORC. For that purpose, we first employed solid phase pull-down experiments by immobilizing His-MBP-Pch2 on amylose beads and incubated it with His-ORC. We used 1 μM of His-ORC and 1 μM of His-MBP-Pch2 (considering a hexamer assembly for both, ORC and Pch2). 6 μM of MBP-His (considering that this tag does not oligomerize) was used as a negative control. We could pull-down ORC with His-MBP-Pch2. As shown in Figure 3-7 A and 3-7 B, ORC was not detected in pull-down experiments performed with MBP-His alone, indicating that binding between ORC and His-MBP-Pch2 was specific. Therefore, our *in vitro* pull-downs revealed that Pch2 is able to interact with the entire ORC (*i.e.* Orc1-6), demonstrating for the first time that these AAA⁺ proteins indeed interact with each other directly. Next, we aimed to reconstitute Pch2-ORC interaction in solution by performing SEC analysis (Figure 3-7 C). We mixed 1 μM His-MBP-Pch2 and 3 μM His-ORC in a total volume of 50 μL and incubated the protein mixture 2 hours on ice, before injection onto a Superose 6 5/150 GL column connected to an ÄKTAmicro FLPC system (see Materials and Methods for further details).

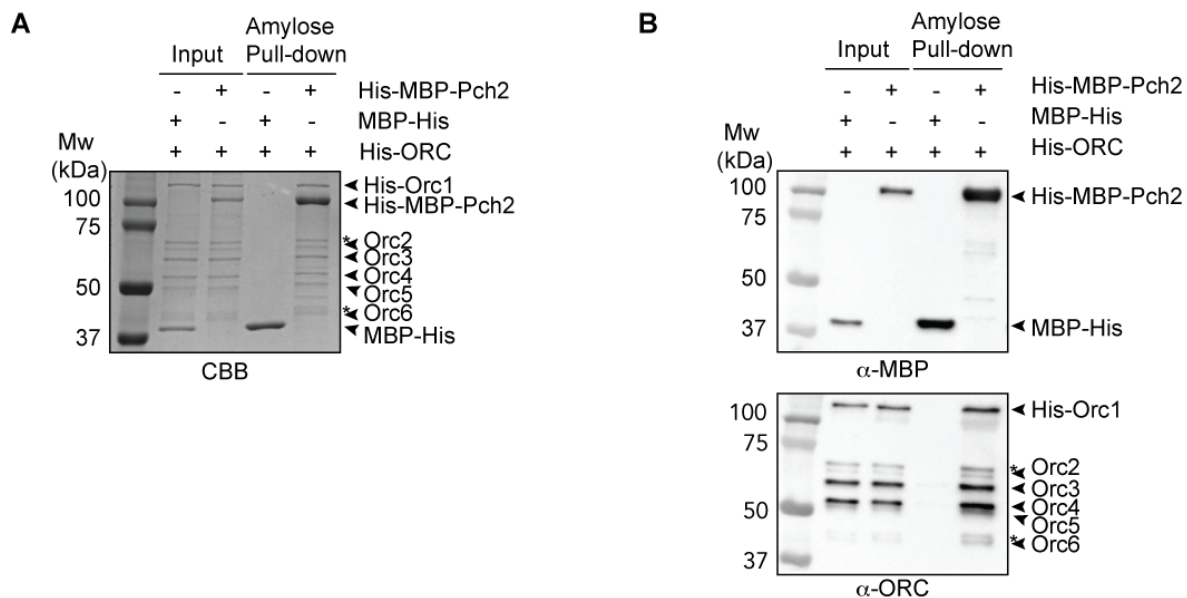


Figure 3-7 Pch2 interacts with ORC directly *in vitro*

A) Amylose based pull-down of ORC (His-Orc1, Orc2-6) and His-MBP-Pch2, both purified from insect cells (at a concentration of 1 μM , considering hexamer formation of both assemblies). 6 μM of MBP-His was used as a negative control. Inputs and pull-down samples were analysed by SDS-PAGE

Figure 3-7 (Continued)

and Coomassie Brilliant Blue (CBB) staining. Asterisk indicates plausibly degradation product of Orc2, and phosphorylated Orc6, respectively. B) Amylose based pull-down of His-ORC and His-MBP-Pch2 as in (A), analysed by SDS-PAGE and Western blot using α -MBP and α -ORC (which recognizes all 6 ORC subunits).

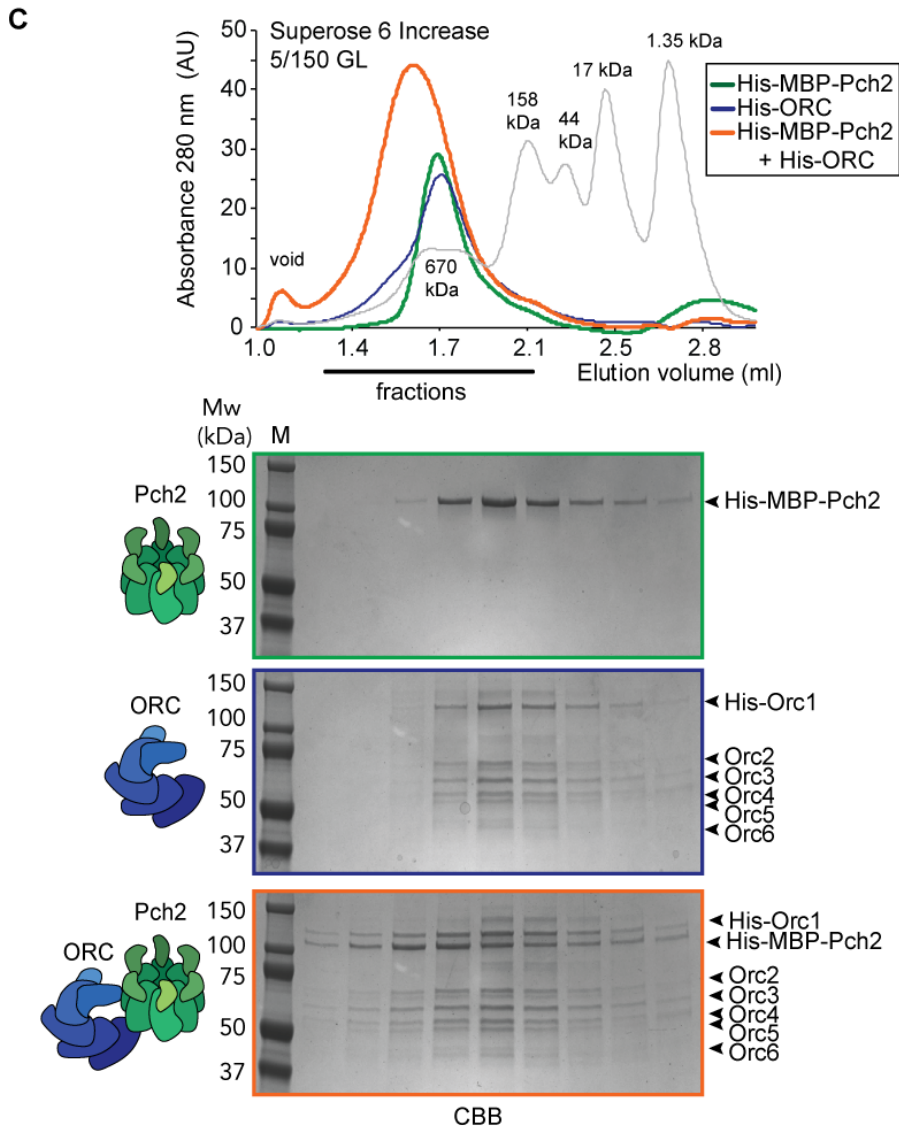


Figure 3-7 Pch2 interacts with ORC directly *in vitro* (Continued)

C) Size exclusion chromatography (SEC) of (His-MBP-Pch2)-(His-ORC) assembly. Green line represents SEC of His-MBP-Pch2. Blue line represents SEC of purified His-ORC. Orange line represents a mixed sample of His-MBP-Pch2 and His-ORC. Gray line represents SEC of gel filtration protein standard; molecular weight of the proteins in the gel filtration standard is indicated. Dotted line indicates peak fractions analysed by SDS-PAGE and CBB staining. AU stands for arbitrary units. M represents a molecular weight marker used as a reference for protein molecular weight (kDa) on SDS-PAGE gel.

Analytical SEC confirmed that ORC and Pch2 form a complex in solution, as judged by a reduced retention volume (which is indicative of a larger and/or more elongated complex) when combined, as compared to the elution profiles of Pch2 or ORC individually (Figure 3-7 C). SEC analysis suggested that ORC and Pch2 interact with each other in an ORC (Orc1-6 hexamer) to Pch2 (hexamer) fashion, yielding what would be a complex of ~1 MDa. However, analytical SEC provides only an approximate estimation on molecular weight, since the peaks of eluted proteins are always compared to a standard molecular marker, and the elution profile depends not only on molecular weight but also on the shape of the protein complex. Thus, more accurate methods (such as AUC or SEC-MALS) should be used in the future in order to more precisely determine the stoichiometry of the Pch2-ORC complex.

Taken together, the results shown here demonstrate that ORC directly interacts with Pch2 to establish a meiosis-specific AAA⁺ to AAA⁺ assembly. Since this interaction does not require Cdc6 (neither *in vivo*, nor *in vitro*), the establishment of this assembly points to a potential novel interaction of ORC with another AAA⁺ ATPase that seems distinct from the known interaction between ORC and the replicative helicase MCM.

3.3 *In vitro* cross-linking mass-spectrometry (XL-MS) characterization of Pch2-ORC

In section 3.2.4, we demonstrated a direct interaction between Pch2 and ORC. Next, we aimed to establish a more in depth high-throughput mapping of the interaction of Pch2 and ORC that could provide information regarding this assembly (for instance, to which extent Pch2 binds to different ORC subunits). To gain a better understanding about the interaction mode of these two AAA⁺ complexes, in collaboration with Dr. Dongqing Pan (Department of Mechanistic Cell Biology, Max Planck Institute of Molecular Physiology, Dortmund) we employed chemical crosslinking coupled to mass spectrometry (XL-MS) (Pan *et al.*, 2018). XL-MS is a powerful approach to identify inter- and intra-molecular protein-protein interactions and it can provide useful insights into assembly principles of protein complexes (Holding, 2015; Leitner *et al.*, 2016).

The general workflow of XL-MS involves an initial step in which protein or protein complexes are chemically cross-linked. By adding a chemical cross-link reagent to a purified protein complex, covalent bonds between reactive, surface-exposed amino acids are established (Holding, 2015; Leitner *et al.*, 2016; Tran *et al.*, 2016). Therefore, it is possible to identify those

protein residues that are in proximity with each other, based on the premise that proteins must be close enough to be cross-linked. After the cross-linking reaction, cross-linked peptides are generated by enzymatic digestion and the sequence of the cross-linked peptides is determined by tandem MS (Figure 3-8 A). There is a wide range of cross-linking reagents with different properties (*i.e.* specificity, length of the spacer between reactive groups, etc.) and the choice of one specific cross-linker influences the quality of the data set obtained. For our XL-MS experiments, we used an experimental pipeline recently developed by the Musacchio laboratory that enhances the identification of cross-linked peptides (Pan *et al.*, 2018). This XL-MS pipeline is a simplified approach that uses the cleavable cross-linker disuccinimidyl dibutyric urea (DSBU; also known as BuUrBu), followed by peptide digestion with Trypsin/LysC, enrichment of cross-linked peptides by SEC, and analysis of the obtained MS data with MeroX software (see Materials and Methods and Figure 3-8A for a schematic overview of the XL-MS workflow used in this study).

To perform XL-MS, we mixed 0.75 μM of His-MBP-Pch2 (considering an homo-hexamer) and 1.5 μM of His-ORC (His-Orc1-Orc6; hetero-hexamer) in 200 μL of buffer (30 mM HEPES pH 7.5, 150 mM NaCl, 2 mM TCEP) and incubated the proteins for 1.5 hours on ice, after which the cross-linker DSBU was added and samples were processed as described in Materials and Methods. A fraction of the protein preparation (10 μL) was collected before and after the cross-linking reaction for analyzes by SDS-PAGE and CBB (Figure 3-8 B). After processing and MS-analysis, we identified cross-linked peptides (for crosslinks see Table 7-2 and Table 7-3, Appendix). We ascertained the quality of our XL-MS dataset by identifying 13 intra-molecular MBP cross-linked peptides within the MBP-moiety present in our purified Pch2 (His-MBP-Pch2) and using a published crystal structure of MBP (PDB 1FQB, (Duan *et al.*, 2001)) we mapped C α -C α distances between identified cross-linked amino acids. The average C α -C α was 14.41 Å, which is in good agreement with the C α -C α distance (12 Å) that the cross-linked state of DSBU is able to facilitate (Table 7-2 and 7-3).

After applying a stringent cut-off analysis by setting a False-Discovery Rate (FDR) of 2% (as compared to a FDR of 5%, as reported by Pan *et al.*, 2018 we obtained a total of 313 non-redundant cross-links (Figure 3-8 C-E and Table 7-3) out of a total of 721 cross-linked peptides identified by MeroX (Table 7-3) (Pan *et al.*, 2018). We used these non-redundant cross-links to generate cross-link network maps for the Pch2-ORC assembly by using xVis web site (<https://xvis.genzentrum.lmu.de>) (Grimm *et al.*, 2015). Briefly, this online tool enables the visualization of the cross-links of a data set in different layouts, after uploading the input data in

comma-separated files. The input data comprises, among others, the coordinates of the cross-links (protein and position of the cross-link residues), protein lengths and quality scores of the mass spectrometric identification.

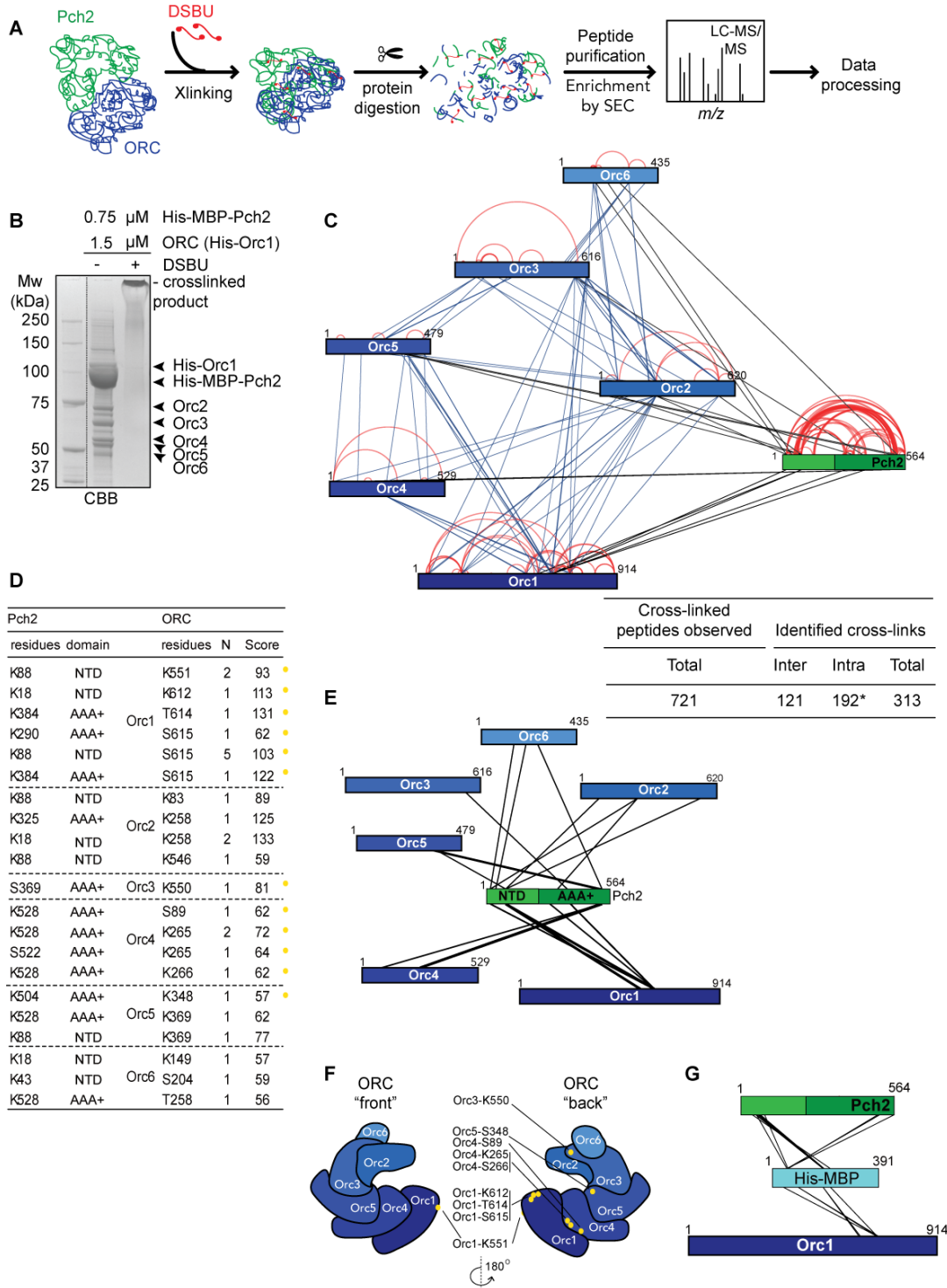


Figure 3-8 Cross-linking mass-spectrometric (XL-MS) analysis of Pch2-ORC assembly

A) Schematic of DSBU disuccinimidyl dibutyric urea (DSBU)-based cross-linking mass spectrometry (XL-MS) experimental pipeline. After cross-linking reaction with the cleavable cross-linker DSBU, cross-link peptides were digested and peptides were enriched by size exclusion chromatography (SEC)

Figure 3-8 (Continued)

using a Superdex Peptide 3.2/ 300 column. Eluted fractions were submitted to LC-MS/MS analysis and cross-links were identified by the program MeroX. B) Protein samples were taken before and after adding DSBU for analysis by SDS-PAGE and subsequent staining with Coomassie Brilliant Blue (CBB). C) Right panel: table indicating total cross-linked peptides, and derived non-redundant (inter- and intra-molecular) cross-links after applying a false discovery rate (FDR) of 2% as the cut-off to exclude the candidates with lower MeroX scores. Asterisk indicates that intra-molecular cross-link peptides include 96 Pch2-Pch2 cross-links, which can be derived from inter- or intra-molecular Pch2-Pch2 cross-links. Left panel: Schematic indicating all identified non-redundant cross-links. Blue lines: inter-ORC; red lines: intra-ORC and intra-Pch2; black: inter-Pch2-ORC. Network plots were generated using xVis (<https://xvis.genzentrum.lmu.de/login.php>). Protein lengths (amino acids) are indicated. D) Table showing inter-Pch2-ORC cross-links. Indicated are residues in Pch2, and ORC subunits, domain of Pch2 involved (NTD: 1-242, AAA⁺: 243-564). N indicates how often crosslinks were identified. MeroX score is indicated. Yellow dot indicates cross-linked ORC residues that are mapped into cartoon representation of ORC structure in (F). E) Network plot indicating identified non-redundant inter-Pch2-ORC cross-links. Protein lengths (amino acids) are indicated. F) Cartoon depiction of ORC organization, based on PDB 5v8f structure (Yuan *et al.*, 2017). Yellow dots represent ORC cross-linked residues in our XL-MS analysis. Note that, due to a lack of regions in the structure used to generate the ORC schematic representation, not all crosslinks are represented (see text for a detailed explanation of the XL-MS data set and a thorough description of the XL-MS strategy used). G) Schematic indicating inter-MBP-Pch2 and inter-MBP-Orc1 non-redundant crosslinks. Note that cross-links between MBP and Orc1 lay in the AAA⁺ ATPase domain of Orc1. These cross-links were unique (XL-MS did not reveal cross-links between peptides from MBP and any other ORC subunit), suggesting a critical role of Orc1 in Pch2 association. Protein lengths (amino acids) are indicated.

The 313 cross-links identified consist of 121 inter-molecular cross-links (*i.e.* cross-links between peptides originating from two different proteins) and 192 intra-molecular cross-links (*i.e.* cross-links between peptides originating from a single protein). We identified 96 Pch2-Pch2 cross-links (Figure 3-8 C and Figure 7-8 C, represented by red lines, and Table 7-3, Appendix). Since Pch2 forms a homo-hexamer, we cannot distinguish whether Pch2-Pch2 cross-linked peptides originate from intra- or inter-molecular cross-linked peptides. We observed 77 cross-links between ORC subunits (*i.e.* inter-ORC crosslinks) (Figure 3-8 C, represented by blue lines) and 83 intra-ORC cross-links (See also Figure 7-8 A-B and Table 7-3, Appendix).

We first compared cross-link abundance between individual ORC subunits with a published crystal structure of *S. cerevisiae* ORC to model the position of each subunit (Figure 3-8F; based on structure PBD 5v8f, ORC purified from budding yeast; (Yuan *et al.*, 2017)). This structure comprises the OCCM helicase-loading intermediate, with ORC, Cdc6, Cdt1 and MCM. We noted that neighbouring subunits often displayed the most abundant cross-links (for example Orc1/Orc2, Orc2/Orc3 and Orc3/Orc5; see Table 7-2 and 7-3). We also observed that several cross-links span considerable distance when based on the ORC structure PBD 5v8f. This could be explained by high level of flexibility within our ORC preparation, since our purified ORC is devoid of Cdc6 and also not bound to MCM-Cdt1, in contrast to the reported structure (Yuan *et al.*, 2017). This conceivably could affect complex topology. Moreover, Pch2 association with ORC could lead to structural rearrangements within the ORC assembly upon binding, which could account for the increased distance between ORC subunits as compared to PBD 5v8f.

Next, we focused on the 96 Pch2-Pch2 cross-links (Figure 3-8 C-E, see also Figure 7-8 C and Table 7-2 and 7-3). A significant fraction of these (42 out of 96; ~43.8%) consisted of cross-links between peptides from Pch2's non-catalytic NH₂-terminal domain (NTD, amino acids 1-242) with peptides from the COOH-terminal AAA⁺ domain of Pch2 (amino acids 243-564). The remaining cross-links (~56.2%) corresponded to either cross-links between peptides from Pch2's NTD (*i.e.* NTD-NTD cross-links) (19 out of 96; ~19.8%) or to cross-links between peptides from the AAA⁺ domain (*i.e.* AAA⁺-AAA⁺ cross-links) (35 out of 96; ~36.4%). These cross-linked peptides could either be a reflection of a close proximity between the NTD and AAA⁺ domains within a single Pch2 complex, or of an association between the NTD of one Pch2 monomer with the AAA⁺ domain of an adjacent (or potential more distally localized, depending on domain flexibility) AAA⁺ module, from a distinct Pch2 monomer. With regard to these observations, we note that, in biochemical purifications, mutational disruption of the NTD of Pch2 influenced the apparent formation of stable/properly assembled Pch2 hexamers (see section 3.4.3), indeed pointing towards a contribution of the NTD of Pch2 to the stable hexamerization of Pch2's AAA⁺ core.

In addition, our XL-MS approach identified 21 inter-ORC-Pch2 cross-links (Figure 3-8 C-E; represented by black lines), with the following distribution: 28.6% of cross-links with Orc1, 19% with Orc2, 4.7% with Orc3, 19% with Orc4, 14.3% with Orc5 and 14.3% with Orc6. When considering these cross-links, several observations are of note. First, we identified cross-links that contain Pch2 peptides from both its enzymatic AAA⁺ core (12 out of 21; 57%) and its

non-catalytic NTD (9 out of 21; 43%) (see also Figure 7-8). This data showed that Pch2 establishes extensive contacts with the ORC complex, whereby both its enzymatic core and its NTD are involved. This is in line with the fact that many AAA⁺ ATPases (including TRIP13, the mammalian homolog of Pch2 (Alfieri *et al.*, 2018; Ye *et al.*, 2017a)) engage clients/adaptors via an initial engagement using their NTDs, and subsequently show interactions mediated through AAA⁺ core:client binding (Hanson & Whiteheart, 2005). The observation that both Pch2's AAA⁺ core and NTD are involved in ORC binding, is consistent with a scenario in which Pch2 binds to ORC in a AAA⁺: client and/or adaptor-type engagement. It is conceivable that Pch2 uses its NTD for the initial recognition of ORC, whereas subsequent AAA⁺ mediated interactions stabilize the Pch2-ORC complex formation.

In addition, a large fraction of the total Pch2-ORC cross-links is established between Pch2 and Orc1/Orc2 (10 out of 21; 48%). Although these two subunits are the largest polypeptides of the ORC complex (which might affect the distribution of the observed cross-links), we noted that Orc1/Orc2 are neighbouring the position that is occupied by Cdc6 when it interacts with ORC (Figure 3-8 F). Since in our preparations, Cdc6 is not present, this space remains unoccupied, and presumably, Pch2 could utilize this “vacated” Cdc6-binding position to interact with ORC. In line with this, as mentioned earlier, Cdc6 and Pch2 have mutually exclusive expression patterns and in section 3.1.3, we demonstrated that 3xHA-Pch2-E399Q is able to co-precipitate ORC in a background with impaired *CDC6* (*cdc6-mn*) (Figure 3-3 C), demonstrating that *in vivo* binding of Pch2 to ORC occurs independently of Cdc6 (Figure 3-3 C) (Ayad, 2005; Elsasser *et al.*, 1999; Nguyen *et al.*, 2001; Phizicky *et al.*, 2018).

To further investigate the position of our identified Pch2-ORC cross-links, we mapped the identified 21 inter-ORC-Pch2 cross-links onto the same ORC structure, PBD 5v8f, see above (Yuan *et al.*, 2017), Figure 3-8 F; cross-linked residues are marked by a yellow dot). Given the absence of regions of ORC within the used crystal structure, we were unable to map several of the ORC-Pch2 cross-links (*i.e.* cross-links with the Orc2, Orc5 and Orc6 subunits). Nonetheless, mapping of observed cross-links confirmed that there is a distribution of cross-linked residues across a large region of ORC, reinforcing the idea that Pch2 establishes extensive contacts with the ORC complex. Interestingly, when we analysed the position of these residues in the abovementioned structure, we noted that three cross-linked residues within Orc1 (K612, T614 and S615) were located in a position that is shielded by Cdc6, according to the ORC-Cdc6-Cdt1-MCM complex structure (PBD 5v8f (Yuan *et al.*, 2017)). This observation

indicates that Pch2 potentially uses binding interfaces within ORC that are implicated in Cdc6 engagement. Future experiments will be performed to test this hypothesis (see Discussion).

Although our XL-MS dataset reveals extensive contacts between Pch2 and individual ORC subunits, our findings concur well with the idea that within ORC, Orc1 functions as a central interacting partner of Pch2. More precisely, we analysed our XL-MS dataset for inter-molecular cross-links containing peptides from the MBP-moiety that is NH₂-terminally fused to Pch2 in our purified His-MBP-Pch2. Interestingly, this analysis revealed, in addition to 17 inter-molecular cross-links between MBP and Pch2 (which are expected since these two polypeptides are covalently linked), 6 MBP-Orc1 inter-molecular cross-links (situated in peptides of the AAA⁺ core of Orc1) (Figure 3-8 G, and Table 7-3). Specifically, we detected the following inter-molecular cross-links containing peptides from Orc1 and the His-MBP-moiety (His-MBP-Orc1 inter-molecular cross-links): His-MBP_K187-Orc1_T628, His-MBP-K41-Orc1_K695, His-MBP_K214-Orc1_K695, His-MBP_K95-Orc1_K695, His-MBP_K187-Orc1_K623, His-MBP-K_75-Orc1_S700. In contrast, we observed no cross-links between MBP and other ORC subunits. Since efficient crosslinking depends on proximity of ~ 12Å between Cα's of cross-linked amino acids (Pan *et al.*, 2018), these data argue that Orc1 is in close vicinity of MBP and, by extension, Pch2. It is worth mentioning that the cross-links between Orc1 and Pch2 are within amino acids from the AAA⁺ domain of Orc1 and that all ORC subunits, except from Orc6, contain AAA⁺ or AAA⁺-like domains (see section 3.3) (Figure 1-9).

Based on the data described in this section, we conclude that Pch2 establishes extensive contacts with different ORC subunits and that it employs both its NTD and AAA⁺ ATPase domains to bind to ORC. Moreover, mapping of the Pch2-ORC cross-links yielded by our XL-MS dataset points towards Pch2 binding to ORC in a similar fashion as Cdc6 when engaging ORC during replication; in other words, our data suggests that Pch2 employs, at least partially, common binding interfaces to Cdc6 in order to engage ORC. Finally, our XL-MS data suggested that within ORC, the Orc1 subunit plays a crucial role in mediating the interaction between Pch2 and ORC. This hypothesis will be further addressed in section 3.5.3.

3.4 Biochemical delineation of the Pch2-ORC complex formation

In the previous sections, we identified a direct interaction between Pch2 and ORC. In addition, we demonstrated that Pch2 establishes contacts with different subunits of ORC with Orc1 possibly being the central Pch2 binding partner.

The main characteristic of the diverse AAA⁺ ATPase family is that they share a similar architecture, consisting of an NH₂-terminal domain (NTD) and one or two AAA⁺ ATPase modules that typically assemble into hexameric rings (reviewed in Hanson & Whiteheart, 2005). As a member of this family, Pch2 contains a non-catalytic NTD, beside a single COOH-terminal AAA⁺ ATPase domain (Figure 1A) (Figure 3-9 A). The non-catalytic NTD of AAA⁺ ATPases is involved in engaging clients/adaptors. On the other hand, many of the associations between two AAA⁺ proteins rely on inter-domain AAA⁺ interactions. For instance, inter-domain AAA⁺ contacts between individual ORC subunits are crucial for the establishment of ORC complex formation (Bell & Kaguni, 2013; Bell & Labib, 2016). Our XL-MS data set identified cross-links between both the NTD and AAA⁺ domain of Pch2 with different ORC subunits (Figure 3-8 and 7-8), suggesting that both domains of Pch2 might play a function in establishing this interaction. Our next aim, described in the following sections (3.4.1-3.4.3), was to thus investigate whether indeed the NTD is involved in Pch2-ORC assembly and to define the minimal region of Pch2 necessary for ORC binding.

3.4.1 The NH₂-terminal domain (NTD) of Pch2 is necessary for ORC-binding

In an attempt to better comprehend the molecular basis of Pch2-ORC function and the implication of the two architectural modules of Pch2 (NTD and AAA⁺ ATPase), we first performed mutational analyses to systematically assess the influence of Pch2 N-terminus in binding of this complex. Initially, by yeast two-hybrid (Y2H) experiments we confirmed the interaction between full-length Pch2 and Orc1, consistent with previous findings that identified a fragment of Orc1 AAA⁺ domain as a Pch2 interactor by Y2H screening (Vader *et al.*, 2011) (Figure 3-9 B, rows 1 and 2). Our Y2H assay revealed that Pch2 lacking its NTD (NTD: amino acids 2-242) was unable to interact with Orc1 (Figure 3-9 B, row 3). This was an interesting observation, as it is known that in AAA⁺ ATPases, the assembly into oligomers is mediated via the AAA⁺ modules, which are held in an intimate physical connection forming typically hexameric structures. As Orc1 also harbors an AAA⁺ ATPase domain and forms part of the bigger hexameric ORC (whose association is partially mediated by the AAA⁺ contacts of neighboring subunits), and Pch2 also harbors such a domain, we initially hypothesized that the interaction between Pch2 and Orc1 would be mediated through the ATPase domain of Pch2.

We further investigated the interaction between Pch2 and Orc1 in meiotic

G2/prophase, by expressing an identical truncated version of Pch2 (3xFlag-Pch2-243-564).

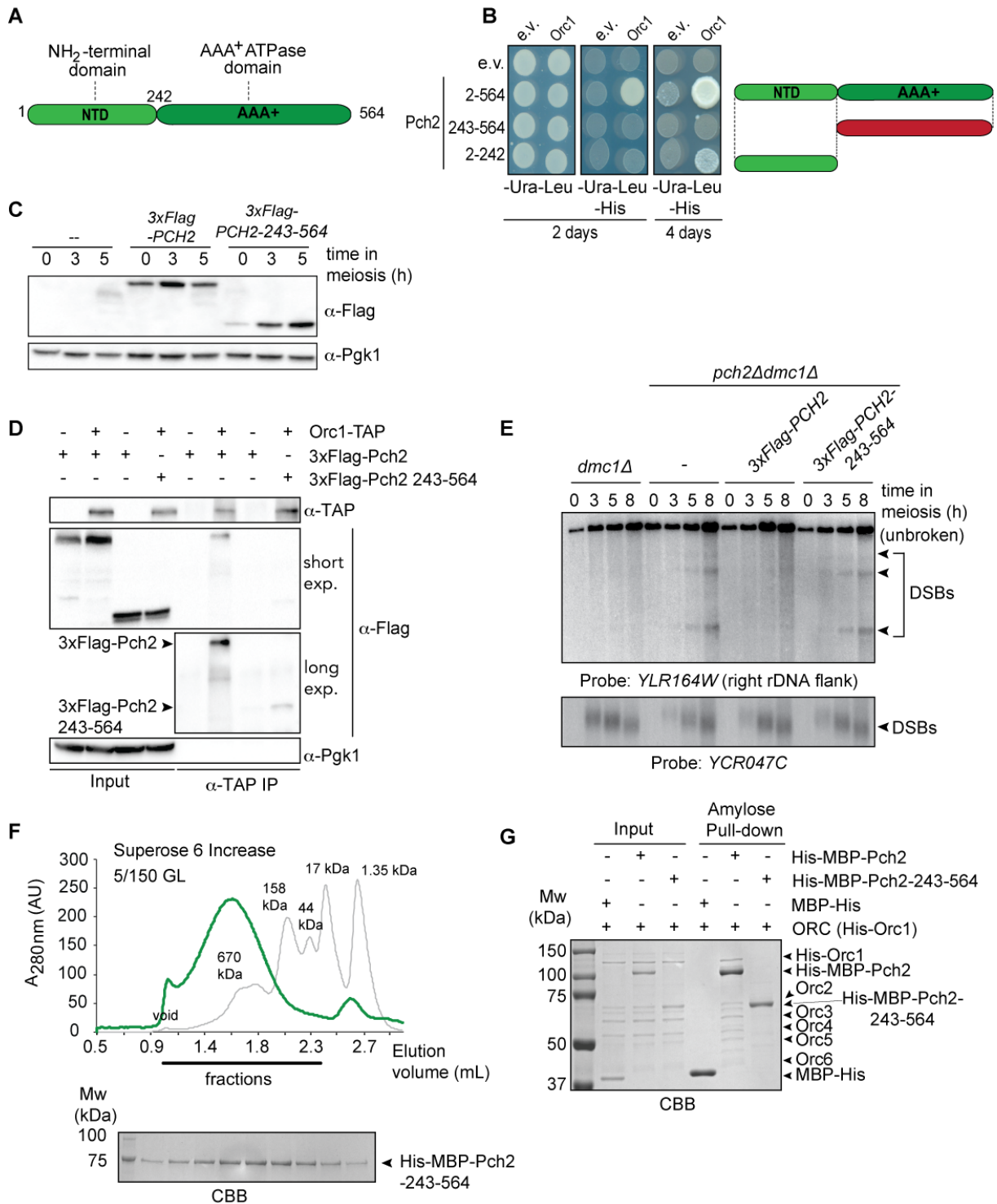


Figure 3-9 The NH₂-terminal domain (NTD) of Pch2 is required for ORC-binding and Pch2 rDNA-associated function

A) Schematic of Pch2 domain organization, with an NH₂-terminal domain (NTD; amino acids 2-242) and an AAA⁺ ATPase domain (AAA⁺; 243-564). B) Yeast two-hybrid (Y2H) analysis between Orc1 and

Figure 3-9 (Continued)

full-length Pch2 (amino acids 2-564), Pch2-AAA⁺ domain or Pch2-NTD. e.v. indicates empty vector. Y2H strains were grown 2-4 days in either –Ura–Leu control plate or specific growth plate (–Ura–Leu–His). Right: Schematic of Pch2 domain organization; Green indicates interaction with Orc1 via Y2H. Red indicates a lack of interaction with Orc1, as judged by Y2H. C) Western blot analysis of yeast strains carrying wild-type *3xFlag-PCH2* or *3xFlag-PCH2-243-564* in a *pch2Δdmc1Δ* background, as used in (D). Samples from sporulation cultures were collected at indicated time points after meiotic induction. α -Pgl1 was used as a loading control. An untagged strain was used as a control. D) Co-immunoprecipitation of 3xFLAG-Pch2 and 3xFLAG-Pch2-243-564 with Orc1-TAP (via α -TAP) during meiotic prophase. Samples were harvested after 4 hours into meiotic programme. For α -Flag short and long exposures are shown. α -Pgl1 was used as a loading control. An untagged ORC strain was used as a negative control. E) Southern blot analysis of *YLR164W* locus (right rDNA flank; Chromosome XII) and *YCR047C* locus (control DSB hotspot; Chromosome III), in *dmc1Δ*, *pch2Δdmc1Δ*, *3xFLAG-PCH2 pch2Δdmc1Δ* and *3xFLAG-PCH2-243-564 pch2Δdmc1Δ* background. *dmc1Δ* is a mutation that allows the detection of accumulated meiotic DSBs by Southern blot. F) Size exclusion chromatogram (SEC) of His-MBP-Pch2-243-564 (represented in green) loaded onto a Superose 6 Increase 5/150 GL column. Protein standard with molecular weights is depicted in gray. Black line represents the fractions analyzed by SDS-PAGE and Coomassie Brilliant Blue (CBB) staining. G) Amylose based pull-down of ORC (His-Orc1, Orc2-6) purified from insect cells, with His-MBP-Pch2 or His-MBP-Pch2-243-564. 1 μ M of each (ORC, His-MBP-Pch2 and His-MBP-Pch2-243-564) considering hexamer formation was used. 6 μ M of MBP-His was used as a negative control. Input and pull-down samples were loaded onto SDS-PAGE gels and stained by CBB.

Western blot of samples collected from strains undergoing meiosis showed that 3x-Flag-Pch2-243-564 harboured similar expression kinetics relative to full length Pch2, with expression peaking at ~4-5 hours after meiotic induction (Figure 3-9 C). We subsequently performed Co-IP experiments with this Pch2 truncation lacking the NTD in strains harbouring TAP-tagged Orc1. Our α -TAP co-IP showed that 3x-Flag-Pch2-243-564 was impaired in its ability to interact with Orc1 (Figure 3-9 D, lane 8). Nevertheless, we noted a residual interaction of Pch2-243-564 with Orc1 that might indicate a certain degree of affinity of this truncated protein towards Orc1 (Figure 3-9 D).

To further confirm the involvement of the NTD of Pch2 in the establishment of the interaction between Pch2 and Orc1, we next purified Pch2 lacking its NTD (His-MBP-Pch2-243-564) from insect cells. By SEC, we observed that this truncated version of Pch2 eluted at an apparent size that indicated a more extended shape or less organized assembly as compared

to full length Pch2 (Figure 3-9 F). We observed a similar behaviour when purifying Pch2 proteins that harbour specific amino acid mutations within the NTD (see section 3.4.3). These findings imply a role for the NTD in stabilizing and/or maintaining Pch2 into a stable, well-ordered hexamer. As anticipated, pull-down assays using purified His-MBP-Pch2-243-564 showed that the interaction between Pch2 with ORC was abolished (Figure 3-9 G, lane 6). This result is in line with an important contribution of the NTD of Pch2 in establishing the interaction with ORC. However, given that we observed a different elution pattern by SEC when purifying His-MBP-Pch2-243-564 than expected (see above), the *in vitro* results with this purified construct should be interpreted with caution. A possibility exists that we were not able to detect a biochemical interaction between His-MBP-Pch2-243-564 and ORC because this construct is not properly folded into a hexameric complex (as it would be predicted); or additionally this truncated form of Pch2 aggregates. Although *in vivo* we consistently observed a residual interaction between the AAA⁺ ATPase domain of Pch2 and ORC, we did not observe such an interaction *in vitro*. This could be accounted for the possible oligomerization/aggregation issues in this truncated Pch2, as suggested by the elongated shape of purified His-MBP-Pch2-243-564 observed by SEC. Another possibility could be that the affinity of the purified AAA⁺ ATPase domain of Pch2 for ORC is not sufficient to be able to detect it with our *in vitro* pull-downs. If so, we would expect that increasing the local concentration of His-MBP-Pch2-243-564 in our pull-down experiments would allow us to detect the residual binding with ORC observed *in vivo*.

We next assessed whether the NTD of Pch2 played a role in mediating Pch2 function during meiotic G2/prophase. For that purpose, we performed Southern Blot (SB) assays of meiotic synchronized cultures to study DSB formation at the rDNA. In case of a role of the NTD of Pch2 in binding Orc1/ORC, Pch2 lacking its NTD would not associate with Orc1/ORC and we would then expect to detect DSB formation at the rDNA proximal region in such Pch2 mutant. We had previously pursued these SB experiments with a TAP affinity-tag version of Pch2; although the proteins were expressed during meiosis in a similar fashion as wild type Pch2, our SBs revealed that the TAP tag interfered with Pch2 function, as TAP-tagged Pch2 was not able to rescue Pch2 function in suppressing rDNA-DSBs in a *pch2Δ* background (Figure 7-7, Appendix). Therefore, we used Flag-tagged constructs of Pch2 to perform SBs. Importantly, our SB also demonstrated that the wild-type 3xFlag-Pch2 construct was functional (*i.e.* rDNA-associated function of Pch2 is not affected by its fusion to the Flag tag), since it could restore Pch2 function in a *pch2Δ* strain in terms of suppression of DSB formation at the

rDNA (*i.e.* *3xFlag-PCH2 pch2Δ* did not show breaks in the tested locus). In agreement with the idea of Pch2-NTD playing a role in Pch2/ORC binding, we found that cells expressing 3xFlag-Pch2-243-564 exhibited rDNA border-associated DSB formation in *pch2Δ* cells, as judged by Southern blotting using a probe within the right flank of the rDNA (*YLR164W* locus, chromosome *XII*) (Figure 3-9 E). Similarly as before, we used a probe within the *YCR047C* locus (chromosome *III*) as a positive control for DSB formation. Altogether, the data described in this section demonstrate that Pch2 lacking its AAA⁺ ATPase domain is not sufficient for either ORC binding or DSB suppression at the rDNA borders.

3.4.2 Functional dissection of Pch2 interaction with ORC

We next asked whether the NTD of Pch2 alone was sufficient for Orc1/ORC binding. To assess this, we performed Y2H analysis using a series of COOH-truncated fragments of Pch2. These truncations were all guided by Pch2 sequence conservation and secondary structure predictions (based on PSIPRED protein sequence analysis) among multiple alignments of Pch2 homologs in different organisms (Figure 7-2 and Figure 7-3, Appendix). Our Y2H analysis revealed that the NTD of Pch2 (consisting of amino acids 2-242) was sufficient to establish the interaction with Orc1/ORC (Figure 3-9 B, row 4 and Figure 3-10A). Together with data described in section 3.4.1, this result suggested that the interaction between these two AAA⁺ ATPases is mediated via the NTD of Pch2, which is sufficient to bind to Orc1, or at least, that the NTD plays a crucial role in the interaction between these proteins. Moreover, these data were in good agreement with our XL-MS analysis, which pointed out towards a contribution of the NTD in mediating the binding of Pch2 to ORC (see section 3.3). The involvement of the NTD of Pch2 in ORC binding was in line with the fact that many AAA⁺ ATPases mediate interaction with their binding partners mostly via the NTD. Such is the case of p97/Cdc48/NSF, which interacts with the vast majority of its partners through its NTD (reviewed in Hanson & Whiteheart, 2005). Therefore, Pch2 could follow a similar mechanism of interaction with Orc1/ORC, in which the NTD mediates the binding between both proteins.

We next aimed to further map the specific region within the NTD of Pch2 required for binding with Orc1. Similarly as described above, we performed Y2H assays with truncated constructs of Pch2. These further truncations of the NTD allowed us to narrow down the minimal region of Pch2 (containing amino acids 2-144) able to interact with Orc1 (Figure 3-10A). In agreement with these observations, our XL-MS analysis identified several crosslinks

between Pch2 and ORC-subunits that consisted of Pch2-peptides that are located within this region of the NTD (K88, K18, K43; Figure 3-8 C-E), underscoring the importance of this domain in mediating the interaction between Pch2 and ORC. We attempted to express corresponding Pch2-NTD fragments in meiosis but observed that these fragments were poorly expressed (data not shown), which precluded us from performing *in vivo* interaction studies. Instead, we opted to perform *in vitro* experiments to further confirm the role of the NTD of Pch2 in mediating interaction with ORC. For this, we attempted to express and purify recombinant NTD fragments. We noted that, similarly to our *in vivo* observations, many of these recombinant fragments were poorly expressed or aggregated under purifying conditions (data not shown). However, we managed to purify the minimal NH₂-terminal fragment of Pch2 (His-MBP-Pch2-2-144) that was sufficient for Orc1 interaction, as shown in our Y2H analysis (Figure 3-10 A). It is worth mentioning that the SEC profile of this truncated version of Pch2 consisted of two elution peaks (Figure 7-6 C, Appendix); the main peak seemed to correspond to a bigger assembly of this protein, possibly due to aggregation of this construct due to the lack of the AAA⁺ ATPase module and, presumably, of proper protein folding. The second elution peak observed by SEC analysis, suggested that this fragment exists as a monomer (expected size ~59 kDa), which is in agreement with the crucial role AAA⁺ domains play in mediating hexamerization of AAA⁺ complexes. For our *in vitro* experiments, we therefore employed only the protein that seemingly eluted as a monomer. In order to corroborate that this purified protein behaved as a stable monomer and did not further aggregate, we re-analysed our purified His-MBP-Pch2-2-144 into a SEC column connected to an ÄktaMicro system. The SEC profile confirmed indeed that this protein was a stable monomer and did not further form aggregates (Figure 3-10 B). Therefore, we used this purified truncated version of Pch2 for *in vitro* studies.

Pull-down experiments showed that this fragment was capable of interacting with ORC, albeit to a significantly less extent than full length Pch2 (Figure 3-10 C and D) (of note, by Western blotting of these pull-down reactions, we detected background binding of the control protein MBP-His to some of the ORC subunits (mostly Orc3 and Orc4/5) but not to Orc1). However, the binding of those ORC subunits with His-MBP-Pch2-2-144 was higher than with MBP-His, demonstrating that binding between this truncated NTD version of Pch2 and His-ORC is specific. The lower interaction could be accounted for several reasons. First, it could indicate the existence of additional binding interfaces between Pch2 and ORC that lie outside of this minimal region of Pch2 (amino acids 2-144). In agreement with that is the

observation of additional cross-links containing peptides from regions outside of the NTD of Pch2, as shown in our XL-MS data (Figure 3-8 C-E), and the residual *in vivo* interaction we detected between Pch2- Δ NTD and Orc1 (see section 3.4.1). Second, hexamer formation of Pch2 (driven by AAA⁺ to AAA⁺ interactions) could increase the local effective concentration of the NTD, contributing to the efficient binding between Pch2 and ORC. Therefore, it would be expected that, as His-MBP-Pch2-2-144 does not contain the AAA⁺ ATPase domain of Pch2 (and thus cannot hexamerize), the interaction between this fragment and ORC would be reduced as compared with full-length Pch2. This latter interpretation concurs well with our observation that the *in vivo* interaction between Pch2 and Orc1 is severely diminished in cells expressing a Pch2 Walker A domain mutant (Figure 3-1 C), which has been described to disrupt ATP binding and hexamerization (Herruzo *et al.*, 2016).

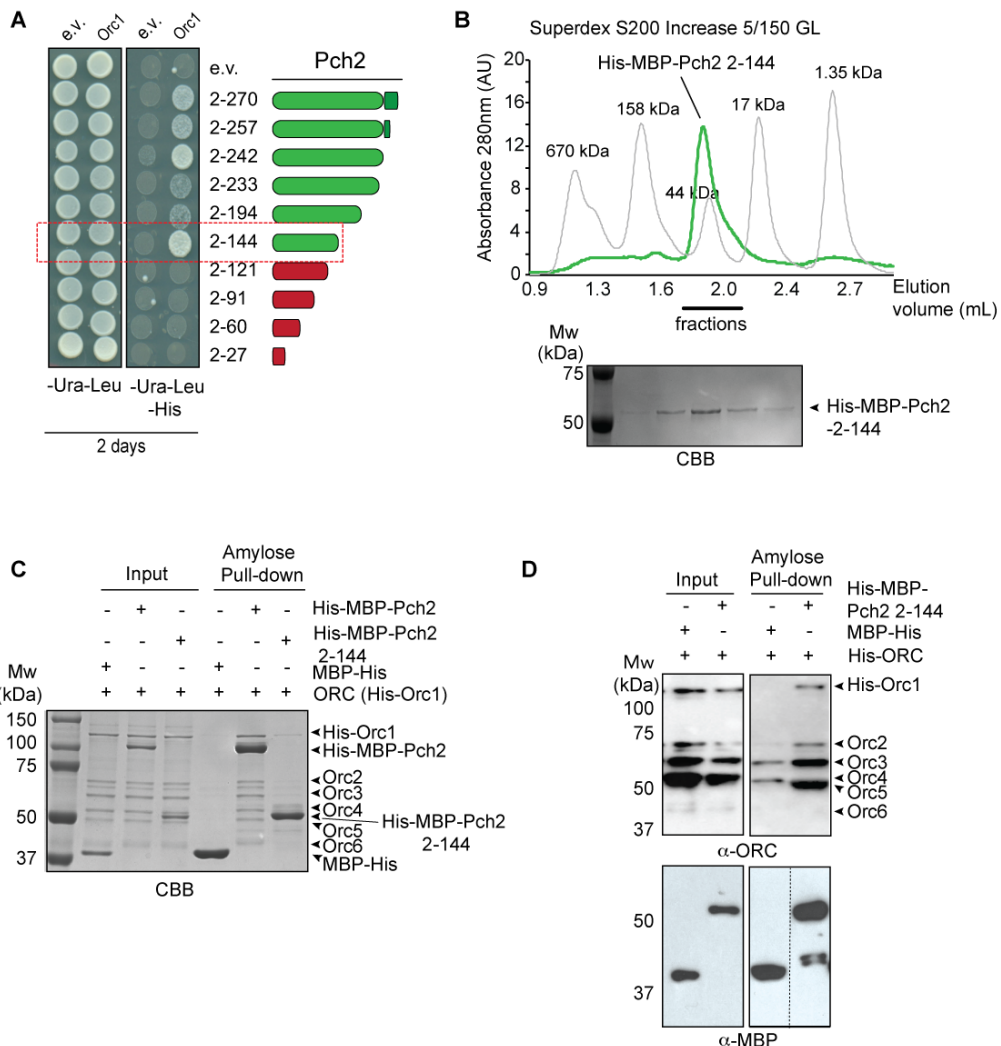


Figure 3-10 Dissection of the role of the NTD of Pch2 in ORC association

A) Yeast two-hybrid (Y2H) analysis between Orc1 and NH₂-terminal fragments of Pch2 (amino acids 2-270, 2-257, 2-242, 2-233, 2-194, 2-144, 2-121, 2-91, 2-60, 2-27). Y2H strains were grown 2 days in -Ura-Leu solid medium (control plate) or -Ura-Leu-His solid medium (specific growth plate). Green

Figure 3-10 (Continued)

represents interaction. Red represents no interaction. e.v. stands for empty vector. Red-dotted box indicates the minimal fragment of Pch2 that showed interaction with Orc1. B) Size exclusion chromatography (SEC) of His-MBP-Pch2-2-144 (6 μ M) loaded into a Superdex S200 Increase 5/150 GL column. Green line represents His-MBP-Pch2-2-144 purified from insect cells. Gray line represents protein standard (molecular weights of each peak are indicated). Coomassie Brilliant Blue (CBB) staining of the peak fractions (black line). AU stands for arbitrary units. C) Amylose based pull-down of ORC (His-Orc1, Orc2-6) (1 μ M, considering hexameric formation) purified from insect cells, with His-MBP-Pch2 (1 μ M, considering hexamer formation) or His-MBP-Pch2-2-144 (6 μ M). MBP- His (6 μ M) was used as a negative control. Input and pull-down samples were analysed by SDS-PAGE and CBB staining. D) Amylose based pull-down of ORC (His-Orc1, Orc2-6) with His-MBP-Pch2 or His-MBP-Pch2-2-144. A 2-fold excess of His-MBP-Pch2-2-144 fragment as compared with the pull-down assay in (C) was used. Input and pull-down samples were analysed by Western blot using α -MBP and α -ORC (which recognises the 6 ORC subunits).

In summary, the findings presented in this section demonstrate that the NTD of Pch2 is sufficient for binding with ORC and provides a crucial contribution to Pch2-ORC complex formation. In addition, we identified a minimal region within the NTD of Pch2 able to recapitulate the interaction with ORC *in vitro* and data presented here indicated that, although Pch2-NTD is sufficient for ORC binding, the AAA⁺ ATPase domain of Pch2 also contributes to the association of these protein assemblies.

3.4.3 Point mutations in the NTD of Pch2 disrupt ORC-binding

In section 3.4.2, we delineated the domains of Pch2 necessary for ORC binding and identified a minimal region of Pch2 (comprising from amino acid 2-144) able to interact with ORC. Strikingly, we noted that in our Y2H the interaction between Pch2 and Orc1 was undetectable in a fragment in which the first 12 amino acids of Pch2 were not present (Figure 3-11 A, rows 2-3). Consistently with this result, we observed a lack of interaction in a truncated version of Pch2 in which amino acids 1-12 were removed from the shortest fragment we had previously identified to be able to bind to Orc1 (Figure 3-11 A, rows 4-5). These findings provided evidence that these first twelve amino acids were involved in the interaction between Pch2 and Orc1, even though these residues are not *per se* sufficient for Pch2 interaction with Orc1 (Figure 3-10 A, rows 8-11).

To further investigate the nature of this fragment of Pch2 and understand its implication in Orc1 binding, we analysed sequence conservation in the NTD domain of Pch2,

with a special focus on the most N-terminal amino acid residues. We found a strong conservation (within the budding yeast *Saccharomyces* class only) of the first stretch of amino acids in the NTD (Figure 7-2). Secondary structure predictions (based on PSIPRED) suggested that this region might be folded into a β -strand. We identified several conserved residues within the first 12 amino acids (V5, D6, V9, R10) as being likely to provide essential contributions to the structural organization of this region. To determine the relevance of these amino acids of Pch2 in Orc1 binding, we replaced the above-mentioned amino acids for alanine residues. Y2H assays with these point mutants revealed that the interaction between Pch2 and Orc1 was abolished with any of the substitutions (V5AD6A and V9AR10A), as shown in Figure 3-11 B.

Based on the biochemical reconstitution of the Pch2-ORC assembly, we next wanted to investigate whether the *in vitro* interaction of these Pch2 mutants with ORC was disrupted. Similarly as before, we produced GST-tagged Pch2 containing the aforementioned alanine-substitutions within amino acids 1-12 and an expression test showed that these mutants were produced in insect cells (Figure 7-4 A, see Appendix). Nonetheless, due to the technical drawbacks of the GST-tagged constructs explained in section 3.2.1, we switched to *S. frugiperda* codon-optimized baculoviruses for these Pch2 point mutants (His-MBP-tagged). Although these mutated versions of Pch2 were expressed, by SEC these proteins seemed to aggregate or form higher molecular weight assemblies (data not shown), similarly to what we observed when purifying the AAA⁺ ATPase domain of Pch2 (His-MBP-Pch2-243-564) (see section 3.4.1). These SEC profiles again pointed towards an important contribution of the NTD to the proper complex assembly of Pch2, at least in our *in vitro* constructs. Thus, these observations precluded us from performing *in vitro* interaction studies with ORC.

We then aimed to probe the interaction between ORC and the Pch2 mutants *in vivo*. Since the SEC profiles obtained while purifying these Pch2 mutants pointed towards a possible effect of these amino acid substitutions in the stability of Pch2 and its proper folding and, given that our Y2H findings were based on a lack of interaction between Pch2 and Orc1, we evaluated the possibility that the absence of such interaction could be due to the fact that the protein harbouring the above-mentioned point mutations was unstable and/or degraded. However, protein expression of these mutants of Pch2 in the Y2H yeast strains employed argued against this possibility (not shown here). In line with this, expression of Flag-tagged versions of the Pch2 mutants revealed that these proteins were expressed in meiosis to similar levels as wild type 3xFlag-Pch2 (Figure 3-11 C).

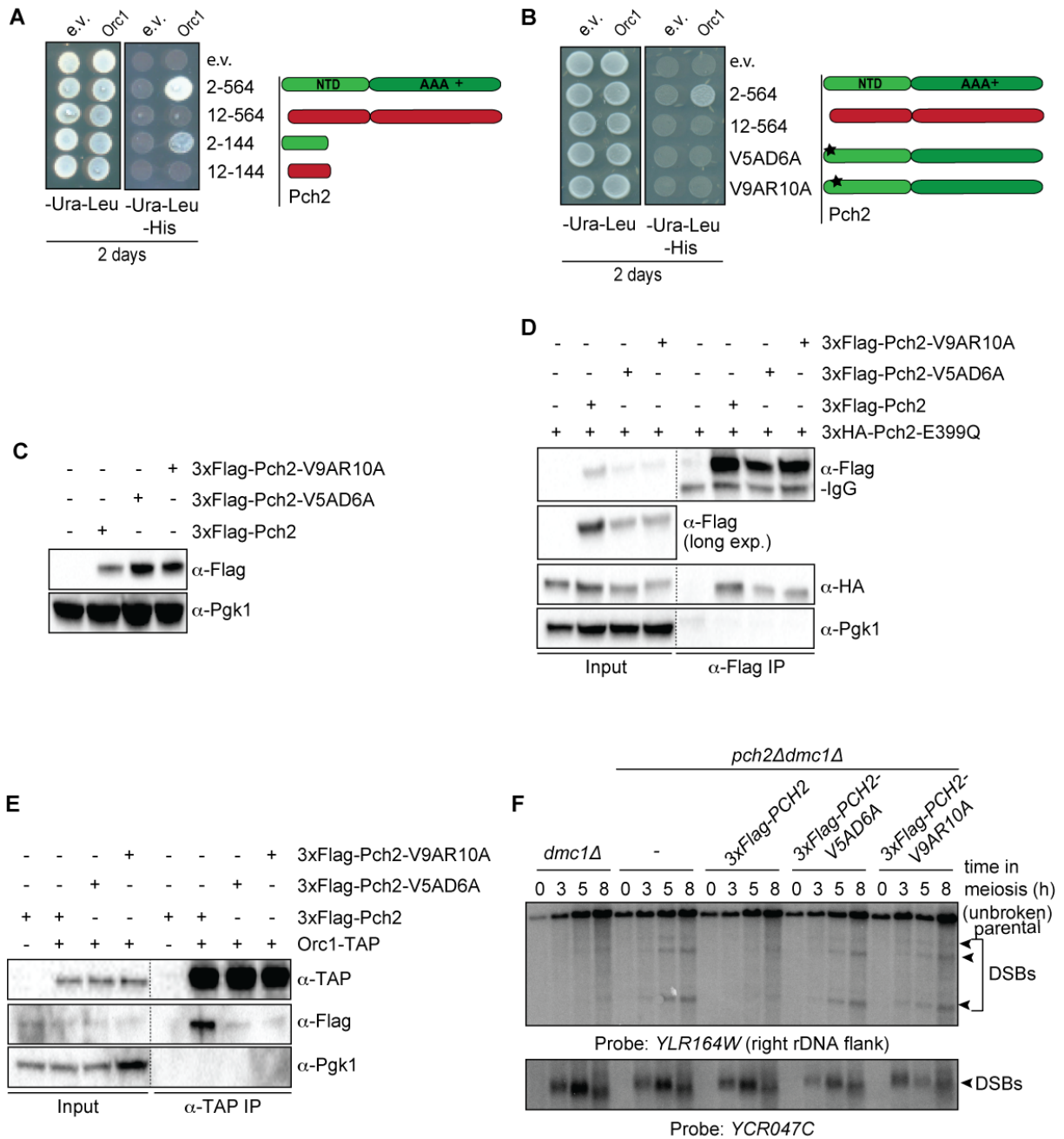


Figure 3-11 Point mutations in the NTD of Pch2 disrupt ORC-binding

A) Yeast two-hybrid (Y2H) assay between Orc1 and full-length Pch2 (amino acids 2-564), Δ12-Pch2 (12-564), minimal Pch2 fragment identified able to interact with Orc1 (2-144) and 12-144 Pch2. Y2H strains were grown 2 days in -Ura-Leu solid medium (control plate) or -Ura-Leu-His solid medium (specific growth plate). Green represents interaction. Red represents no interaction. e.v. stands for empty vector. B) Y2H assay performed similarly as in (A), but with the following Pch2 constructs: 2-564, 12-564 and point mutants within the NTD of Pch2 (V5AD6A and V9AR10A). Point mutations are depicted in a star-shape. C) Western blot analysis confirming expression of Flag-tagged proteins in

Figure 3-11 (Continued)

yeast strains carrying *3xFlag-PCH2-V9R10*, *3xFlag-PCH2-V5D6* or *3xFlag-PCH2*. Protein extracts were prepared from yeast lysates of sporulation samples harvested after 5 hours into meiosis. α -Pgk1 was used as a loading control. D) Flag-based co-immunoprecipitation (Co-IP) in strains carrying *3xHA-PCH2-E399Q* and either *3xFlag-PCH2-V9R10*, *3xFlag-PCH2-V5D6* or *3xFlag-PCH2*. Samples of sporulation cultures were taken after 4.5 hours into the meiotic programme. For α -Flag, short and long exposures are shown. α -Pgk1 was used as loading control. A strain carrying only *3xHA-PCH2-E399Q* was used as a negative control. E) TAP-based Co-IP in strains carrying *ORC1-TAP* and either *3xFlag-PCH2-V9R10*, *3xFlag-PCH2-V5D6* or *3xFlag-PCH2*. Samples of sporulation cultures were taken after 4.5 hours into the meiotic programme. Input and IP samples were analysed by SDS-PAGE and Western blot probing against α -TAP, α -Flag or α -Pgk1 (loading control). A strain carrying *3xFlag-PCH2* and untagged *ORC1* was used as a negative control. F) Southern blot analysis of *YLR164W* locus (right rDNA flank; Chromosome XII) in *dmc1 Δ* , *pch2 Δ dmc1 Δ* , *cdc6-mn dmc1 Δ* and *cdc6-mn pch2 Δ dmc1 Δ* background strains. *YCR047C* locus (Chromosome III) was used as a control DSB region. *dmc1 Δ* is a DSB repair-deficient mutant used to detect accumulation of meiotic DSBs by Southern blot. Cells were induced to synchronously undergo meiosis and samples from sporulation cultures were collected at indicated time points after meiotic induction. Arrowheads indicate DSBs.

In order to further address the integrity of these mutants of Pch2, we tested their *in vivo* interaction with Pch2. For this, we examined the ability of these mutants to bind to other Pch2 molecules (*i.e.* Pch2 is expected to establish contacts with itself mostly through AAA⁺ ATPase to AAA⁺ ATPase interactions). If the point mutants would completely disrupt Pch2 structure, it would be predicted that the proteins harbouring these mutations would not be able to interact with Pch2. We performed co-IP experiments (via α -Flag) with yeast strains carrying *3xHA-PCH2-E399Q* and different versions of Pch2 Flag-tagged (*3xFlag-PCH2*, *3xFlag-PCH2-V5AD6A* and *3xFlag-PCH2-V9AR10A*). These experiments demonstrated that the Pch2 proteins with the above-mentioned amino acid substitutions retained the ability to interact with Pch2 (and likely oligomerizing), providing further evidence of the stability of these mutants (Figure 3-11 D).

Next, we focused on the interaction of the different mutants of Pch2 with Orc1 *in vivo*. With that purpose, we created yeast strains carrying a TAP-tag version of Orc1 and a 3xFlag-tagged Pch2. Pch2 expression of these mutated versions was comparable to wild-type Pch2 in meiosis, as shown by Western Blot (Figure 3-11 C). Reassuringly, our results revealed that while the full length Pch2 was able to bind to Orc1 *in vivo* during the meiotic program, the interaction of the Pch2 mutants with Orc1 was severely impaired (Figure 3-11 E, lanes 6, 7

and 8), as judged by α -TAP Co-IP and subsequent Western blotting. It is worth noting that even if the interaction of both Pch2 point mutants (V5D6 and V9R10) with Orc1 was not completely abolished, these mutants showed a dramatic decrease in terms of Orc1 binding (Figure 3-11 E).

Together, these data suggested that these residues perform a crucial role in terms of interaction between Pch2 and Orc1. This raised the question of whether these conserved amino acids of Pch2 were also important in terms of functionality with Orc1/ORC. We hypothesized that point mutations on the V5D6 or V9R10 residues would show a *pch2* Δ phenotype, due to the impaired binding to Orc1. To test this, we assessed DSB formation by performing SB in yeast strains harbouring Flag-tagged versions of these mutations. SB analysis showed formation of DSBs at the rDNA right flank (*YLR164W*) in these Pch2 mutants, pointing towards the fact that these amino acids are necessary for Pch2 functionality in suppressing DSB formation at the rDNA locus (Figure 3-11 F).

Taken together, the results presented here support the idea that the NTD domain of Pch2, and more precisely, specific residues within it (V5D6 and V9R10) are crucial in the establishment of a binding interface with Orc1 and for Pch2 function at the budding yeast rDNA.

3.5 *In vivo* analysis of the functional connection between Pch2/ ORC

As already mentioned, a previous study demonstrated that Pch2 is required to prevent rDNA-associated meiotic DSB formation (Vader *et al.*, 2011). The same study reported that inactivating Orc1 (via a temperature-sensitive allele of Orc1, *orc1-161*) triggered a similar rDNA-associated phenotype as observed in *pch2* Δ cells. Moreover, Vader and co-workers proved that the *orc1-161* conditional mutant failed to localize Pch2 in the nucleolus (where the rDNA assembles), suggesting a role of Orc1 as a “landing platform” that facilitates Pch2 recruitment at the rDNA. Thus, with these data, the authors concluded that Orc1 and Pch2 collaborate to protect the rDNA against DSB formation and instability in meiosis.

Our biochemical analysis demonstrated that Pch2 binds to ORC, but yet we observed several aspects indicating that Orc1 played a central role in mediating this interaction. Firstly, we consistently found that Pch2 harboured the strongest interaction with Orc1, relative to other ORC subunits (Orc2 and Orc5), as deduced from Co-IP assays (see section 3.1.2 and Figure 3-2C). Secondly, our XL-MS dataset revealed cross-links between the MBP-moiety NH₂-

terminally fused to Pch2 and Orc1 (and not any other ORC subunit), suggesting that Orc1 is in close proximity of MBP and therefore to Pch2 (see section 3.3 and Figure 3-8 G). Therefore, the question remained whether other ORC subunits (*i.e.* Orc2, Orc3, Orc4, Orc5 and Orc6) played a role in the previously described functionality of Orc1 together with Pch2, regarding both the involvement of other ORC subunits in preventing rDNA proximal DSB formation and their role in Pch2 localization.

So far, there is a vast amount of literature reporting that all functions ascribed to ORC in mediating chromosome-associated processes in yeast depend on ORC integrity and association with origins of replication (Foss *et al.*, 1993; Fox *et al.*, 1997; Loo *et al.*, 1995; Shimada & Gasser, 2007; Suter *et al.*, 2004). In the next sections (3.5.1-3.5.4), we sought to address whether the entire ORC and its association to origins of replication is required for Pch2 function at rDNA borders.

3.5.1 Functional depletion of Orc2 and Orc5

Since ORC subunits are essential for cell viability, we first attempted to inactivate different ORC components by using strains containing temperature-sensitive (*ts*) alleles of Orc2 and Orc5 (*orc2-1* and *orc5-1*, respectively) (Bell *et al.*, 1995; Foss *et al.*, 1993; Loo *et al.*, 1995; Shimada & Gasser, 2007). Although we were able to observe that Orc2 and Orc5 could be inactivated using these conditional alleles (not shown here), we often encountered issues with these strains (*i.e.* poor growth) that hampered the reliable execution of meiotic experiments. This, together with the fact that meiosis itself is sensitive to high temperatures (necessary to completely inactivate these alleles) led us to search for other methods that could allow us to inactivate ORC subunits in a more controlled manner.

As an alternative approach, we employed the “anchor-away” method to inactivate selected ORC subunits (Haruki *et al.*, 2008). This method allows the functional depletion of a protein of interest localized in the nucleus by tethering it to a cytoplasmic protein (anchor) upon the addition of a small molecule known as rapamycin. The anchor protein (large ribosomal subunit) is fused to the 12 kDa FK506 binding protein (2xFKBP12), whereas the target protein is fused to the FKBP12-rapamycin-binding (FRB) domain of mTOR. The addition of rapamycin, which binds to FKBP12, creates a surface for the binding of the FRB-tagged target protein. Therefore, by using the extensive ribosomal flux through the nucleus during the maturation process, it is possible to re-direct proteins from the nucleus to the

cytoplasm. The anchor-away technique has been proven to efficiently deplete chromosomal factors in budding yeast meiosis (Ballew & Lacefield, 2019; Cardoso da Silva *et al.*, 2019; Vincenten *et al.*, 2015).

Thus, in an attempt to deplete other ORC subunits from the nucleus, we generated *ORC2* and *ORC5* alleles that carried an FRB-tag (for technical reasons we were not able to generate an *orc1-FRB* allele) (Figure 3-12 A). Yeast strains carrying these alleles are modified to achieve depletion upon rapamycin; they harbour an *RPL13A-2xFBKP12* that acts as the anchor protein; since rapamycin is toxic to wild type yeast, anchor-away strains also carry a mutated version of *TOR1* (*tor1-1*) and deletion of *FPR1* (*fpr1Δ*) (Haruki *et al.*, 2008). Next, we aimed to verify the efficacy of these alleles, similarly as shown in the ORC temperature-sensitive alleles. In an effort to do so, we initially performed yeast cell growth spotting assays in either YPD solid medium (as control) or YPD solid medium supplemented with 1 µg/mL of rapamycin. We used such concentration of rapamycin as previously established by Haruki *et al.* and which other studies in meiosis have proved to cause efficient nuclear depletion of various proteins (Cardoso da Silva *et al.*, 2019; Haruki *et al.*, 2008; Subramanian *et al.*, 2016).

It is known that cells defective in ORC subunits fail in DNA replication and thus, trigger mitotic cell arrest and loose viability (Foss *et al.*, 1993; Fox *et al.*, 1997; Loo *et al.*, 1995; Shimada & Gasser, 2007). As expected, we observed that mitotically proliferating cells with FRB-tagged versions of *ORC2* or *ORC5* (*orc2-FRB* and *orc5-FRB*) exhibited a strong growth defect when spotted on solid YPD medium supplemented with rapamycin (Figure 3-12 B), whereas the cells were viable when grown on the control medium, which demonstrated efficient nuclear (functional) depletion. To further investigate the efficacy and timing of this functional depletion by the anchor-away technique, we used flow cytometry to query DNA replication in logarithmically growing cultures after treatment with 1 µg/mL of rapamycin. This analysis revealed that addition of rapamycin (t=0) in the *orc2-FRB*, *RPL13A-2xFBKP12*, *tor1-1*, *fpr1Δ*, *dmc1Δ* and *orc5-FRB*, *RPL13A-2xFBKP12*, *tor1-1*, *fpr1Δ*, *dmc1Δ* backgrounds caused DNA replication to cease, as judged by an accumulation of yeast cells with unreplicated DNA (2N) in the FRB-tagged *ORC2/ORC5* strains, as compared to the control strain (Figure 3-12 C). This effect on DNA replication was clearly detectable after 180 min from the addition of rapamycin, although the first effects were observed after 90 minutes. Together, these experiments indicate a rapid functional depletion of Orc2 and Orc5 upon the addition of rapamycin in vegetative growing cells.

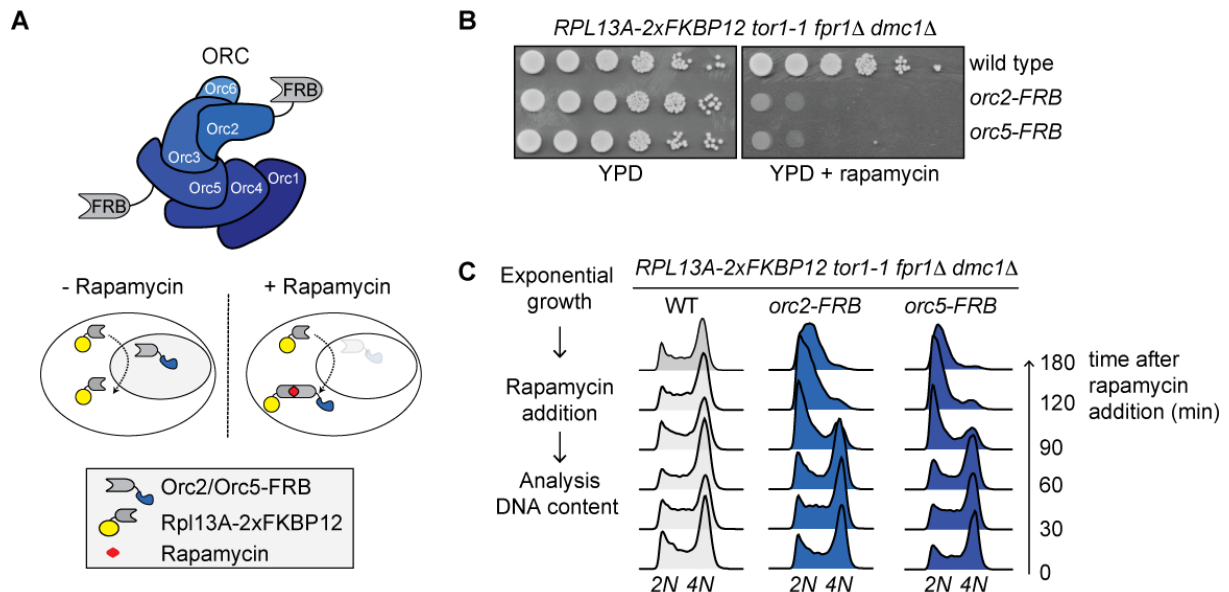


Figure 3-12 Functional depletion of Orc2 and Orc5

A) Schematic of ORC assembly and anchor-away method (Haruki *et al.*, 2008). *ORC2* and *ORC5* are tagged with FRB. Upon addition of rapamycin, Orc2-FRB and Orc5-FRB are functionally depleted from the nucleus by tethering to a receptor localized in the cytoplasm (Rpl13A-2xFKBP12), which binds FRB. B) Yeast cell growth assay for anchor-away strains: untagged, *orc5-FRB* (*orc5-FRB*, *RPL13A-2xFKBP12*, *tor1-1*, *fpr1Δ*, *dmc1Δ*) and *orc2-FRB* (*orc2-FRB*, *RPL13A-2xFKBP12*, *tor1-1*, *fpr1Δ*, *dmc1Δ*) with 10-fold serial dilutions. Yeast strains were grown on YP-Dextrose (YPD) or YPD+rapamycin (1 μg/mL). C) Flow cytometry analysis of vegetative growing control strain or yeast strains carrying *orc2-FRB* (*orc2-FRB*, *RPL13A-2xFKBP12*, *tor1-1*, *fpr1Δ*, *dmc1Δ*), *orc5-FRB* (*orc5-FRB*, *RPL13A-2xFKBP12*, *tor1-1*, *fpr1Δ*, *dmc1Δ*). Cells were treated with rapamycin (1 μg/mL) at the start of the time course (t=0), and efficiency of the anchor-away technique was inferred from defects in DNA replication upon addition of rapamycin (*i.e.* accumulation of 2N-containing cells).

3.5.2 rDNA-associated function of Pch2 is likely independent of Orc2/Orc5 function

We next investigated the role of other ORC subunits and the dependency on ORC integrity for rDNA-associated meiotic DSB suppression. As mentioned at the beginning of this section, previous work had shown that inactivating Orc1 via a ts-mutant (*orc1-161*) caused an rDNA-associated phenotype similar to *pch2Δ* (*i.e.* increased DSB formation at rDNA flanks) (Vader *et al.*, 2011). In an effort to address this question, we used the anchor-away system with the ORC alleles described in section 3.5.1. We performed time-courses using yeast strains carrying these alleles (*orc2-FRB*, *orc5-FRB*) and assessed DSB formation by SB analyses (Figure 3-13). We noted that, contrary to what we observed in mitotic cultures (Figure 3-12 C),

pre-meiotic DNA replication timing appeared mostly unaffected under rapamycin treatment (*i.e.* slight delay in meiotic progression, as compared to the control strain) (Figure 3-13 B). MCM association to origins of replication, which is the crucial ORC-dependent step for DNA replication, occurs prior to induction of the meiotic program (Blitzblau *et al.*, 2012; Phizicky *et al.*, 2018). In our experiments, rapamycin was added to the cultures simultaneously to the induction of meiosis and therefore after MCM association with origins had occurred (via ORC recruitment) (Figure 3-13 A). Thus, nuclear depletion of ORC in our experimental setup was not expected to significantly interfere with efficient pre-meiotic DNA replication.

We next induced strains carrying the *orc2-FRB* or *orc5-FRB* alleles and wild type cells to synchronously undergo meiosis when either rapamycin or a control (DMSO) was added to the cultures at time point zero hours (t=0 h) and analysed DSB formation at the rDNA, similarly as performed earlier. Southern blotting revealed that rapamycin-induced depletion of Orc2 and Orc5 did not trigger an increase in rDNA-associated DSB formation (*i.e.* we did not detect DSBs at the *YLR164W* locus (Chromosome XII) in *orc2-FRB*, *RPL13A-2xFBKP12*, *tor1-1*, *fpr1Δ*, *dmc1Δ* or *orc5-FRB*, *RPL13A-2xFBKP12*, *tor1-1*, *fpr1Δ*, *dmc1Δ* cells upon addition of rapamycin), in contrast to what has been reported for *pch2Δ* and *orc1-161* cells (Figure 3-13 C) (Vader *et al.*, 2011). Importantly, meiotic formation at a control locus (*YCR047C*, Chromosome III) occurred normally, in agreement with our flow cytometry analysis and reassuring that meiotic progression in the *ORC2/ORC5* anchor-away system was comparable to the control strain. We have shown that Orc2/Orc5 are depleted in cycling cells using the yeast cell growth assay and progression through the cell cycle as a proxy. However, we cannot rule out that the effect on DSBs (*i.e.* increased DSB formation) would exclusively be achieved upon an acute reduction in the levels of ORC, which we cannot guarantee with our experiments in meiosis. Altogether, the data provided here seems to suggest that the rDNA-associated function of Pch2 can occur under conditions where Orc2/Orc5 are depleted from the nucleus.

It is known that ORC function is closely linked to its association with origins of replication, and this, in turn, relies on ORC integrity (Bell *et al.*, 1995; Foss *et al.*, 1993; Loo *et al.*, 1995; Shimada & Gasser, 2007). We next asked whether the *pch2Δ*-like phenotype at the rDNA boundaries was dependent on ORC association to origins of replication. For this, we performed chromatin-immunoprecipitation coupled to quantitative PCR (ChIP-qPCR) in yeast strains harboring *Orc1-TAP* and *orc2-FRB* in order to test the association of ORC to origins of replication under conditions of nuclear depletion of Orc2 (by addition of rapamycin). For this,

we analyzed the enrichment of Orc1-TAP at a selected origin (*ARS1116*, chromosome *XI*) and, as a negative control, at a chromosomal arm region (*PPR1*, chromosome *XII*) and compared this enrichment in cultures treated with either rapamycin (1 $\mu\text{g}/\text{mL}$) or DMSO (control) added at time point zero in the meiotic cultures.

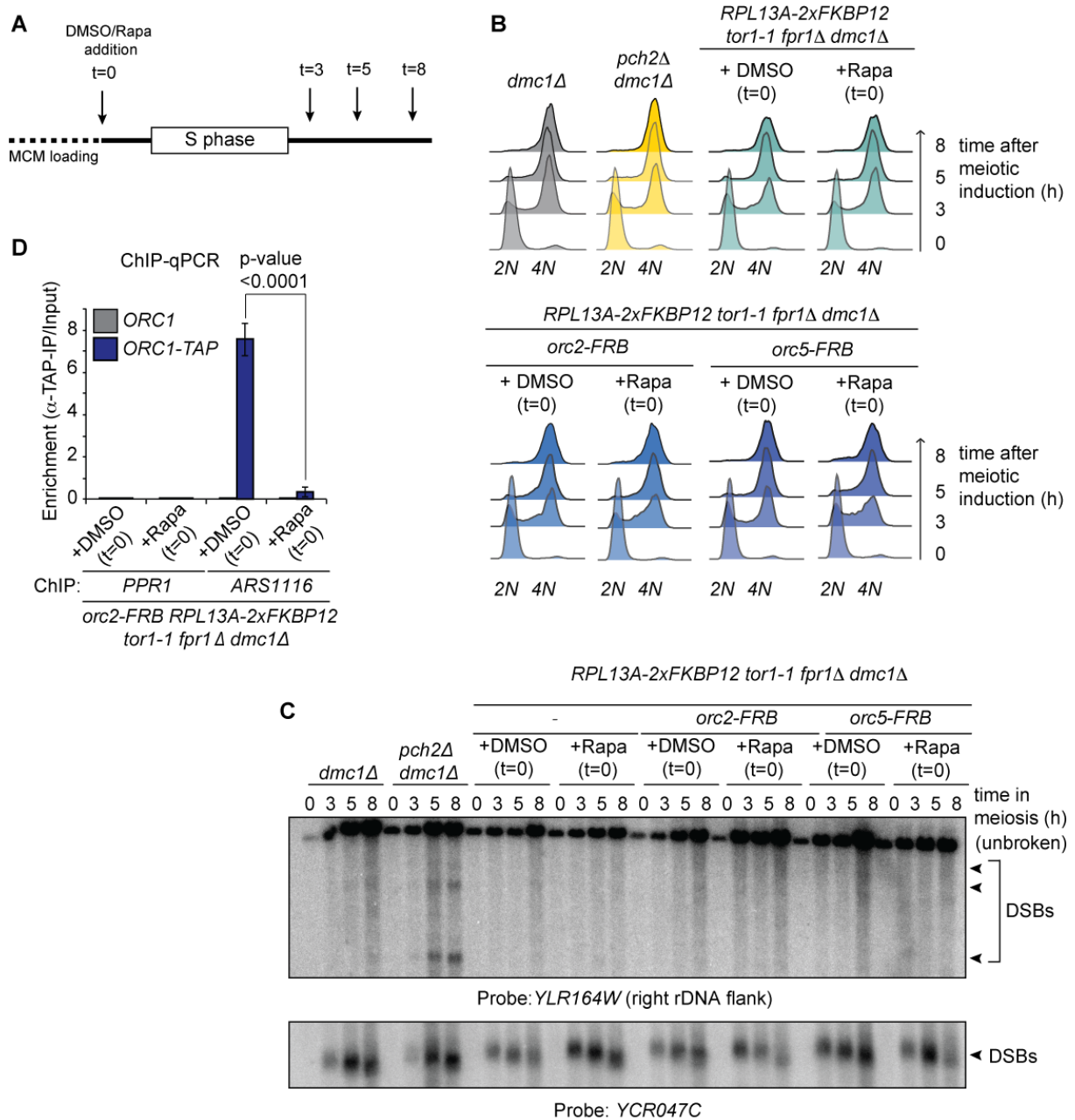


Figure 3-13 rDNA-associated function of Pch2 is likely independent of Orc2/Orc5 function

A) Schematic representation of the strategy used for Southern blot analysis of meiotic yeast cultures, as shown in (C). Cells were induced to synchronously undergo meiosis. Rapamycin (1 $\mu\text{g}/\text{mL}$) or DMSO (control) were added at time point 0 hours. S phase indicates the Synthesis phase (DNA replication). Samples from sporulation cultures were taken at time points 0, 3, 5 and 8 hours after

Figure 3-13 (Continued)

induction of meiosis and processed for flow cytometry analysis (B) and Southern blot (C). B) Flow cytometry analysis of strains used for Southern blot in (C). Rapamycin (1 $\mu\text{g}/\text{mL}$) or DMSO were added in the control strain (*RPL13A-2xFBKP12, tor1-1, fpr1 Δ , dmc1 Δ*), *orc2-FRB* strain (*orc2-FRB, RPL13A-2xFBKP12, tor1-1, fpr1 Δ , dmc1 Δ*) and *orc5-FRB* strain (*orc5-FRB, RPL13A-2xFBKP12, tor1-1, fpr1 Δ , dmc1 Δ*). Neither rapamycin, nor DMSO were added to the *dmc1* or *pch2 Δ dmc1 Δ* strains. C) Southern blot analysis at the *YLR164W* locus (right rDNA flank; Chromosome *XII*) and *YCR047C* locus (control DSB region; Chromosome *III*) in the strains used in (B). Rapamycin (1 $\mu\text{g}/\text{mL}$) or DMSO was added at indicated time point 0 hours in all strains except from *dmc1 Δ* and *pch2 Δ dmc1 Δ* strains (used as a positive control for DSB formation at the rDNA). *dmc1 Δ* is a DSB repair-deficient mutant that is employed to detect accumulation of meiotic DSBs. D) TAP-based ChIP-qPCR in *ORC1* and *ORC1-TAP* anchor-away strains for *ORC2* (*orc2-FRB, RPL13A-2xFBKP12, tor1-1, fpr1 Δ , dmc1 Δ*). Rapamycin (1 $\mu\text{g}/\text{mL}$) or DMSO was added at the start of the time course, and yeast cells were harvested 4 hours after meiotic induction. Primers that amplify *PPR1* (Chromosome *XII*; control locus at a chromosomal arm region) and a selected origin of replication (*ARS1116* (Chromosome *XI*)) were used. Experimental data is the average of five biological replicates. Standard error (s.e.m.) is indicated. Significance was calculated using an unpaired t-test, p-value < 0,0001.

Since ORC binding to origins of replication is dependent on ORC integrity, we expected that removing one of the subunits of this complex would compromise the association of ORC to origins. Indeed, upon the addition of rapamycin, we observed a near-complete loss of Orc1 from the origin of replication tested (*ARS1116*) in *ORC1-TAP, orc2-FRB, RPL13A-2xFBKP12, tor1-1, fpr1 Δ , dmc1 Δ* strains (Figure 3-13 D and E). In order to further prove functional depletion of Orc2, it would be important to compare the localization of Orc1 in *ORC1-TAP, orc2-FRB, RPL13A-2xFBKP12, tor1-1, fpr1 Δ* yeast cultures treated with either DMSO or rapamycin. However, our attempts to perform immunofluorescence (IF) analysis of Orc1 localization in the nucleolus failed due to technical reasons. Nonetheless, our ChIP-qPCR analyses further corroborated that by using our anchor-away setup, Orc2 is efficiently depleted from the nucleus. Importantly, since under identical rapamycin treatment we failed to observe rDNA-associated DSB formation (Figure 3-13 C), these data suggest that ORC association to origins of replication in the non-nucleolar DNA is perhaps not strictly required for the function of Orc1/Pch2 in locally suppressing DSBs during meiotic G2/prophase.

Therefore, the findings presented here offer evidence for an origin-independent role of Orc1 (together with Pch2) that is molecularly distinct from the role of Orc1/ORC in DNA

replication. Association of ORC outside origins has been previously reported by other groups, although the function of ORC at those sites is still not fully clear (Chang *et al.*, 2011; Shor *et al.*, 2009). Thus, we propose that during meiotic G2/prophase, ORC is repurposed and interacts with Pch2 in a biochemical and functional manner that is uniquely distinct from its well-documented role at origins of replication. This possibility is further explored in the Discussion.

3.5.3 Orc1 is a central mediator of the interaction between ORC-Pch2

In the previous section, we showed that Orc2/Orc5 functional depletion did not lead to a detectable phenotype similar to that observed when Orc1 is impaired via a ts-mutant allele of *ORC1* (*orc1-161*) (Vader *et al.*, 2011). Although this could be due to differences in levels of depletion between the anchor-away technique and the use of the *orc1-161* allele, this data reinforced the idea that Orc1 could be a central mediator in the Pch2-ORC interaction. In this line, our XL-MS data revealed the presence of cross-links between the MBP moiety fused to our purified Pch2 and Orc1, and not any other ORC subunit, indicating that Pch2 and Orc1 are in close proximity (section 3.3 and Figure 3-8 G). In addition, besides Orc1 being identified as an interactor of Pch2 via a Y2H screen (Vader *et al.*, 2011), here we showed that, when comparing Pch2 Co-IP efficiencies of Orc1, Orc2 and Orc5, Pch2 interaction with Orc1 was consistently more evident as compared to the other ORC members tested (Figure 3-2 C). Taken together, these results strengthened our hypothesis that, even if Pch2 is able to interact with the entire ORC, the Orc1 subunit plays a crucial role in establishing the Pch2-ORC assembly. We then aimed to further investigate the interaction between Pch2-Orc1/ORC. In an effort to do so, we analysed the interaction between Pch2 and individual ORC subunits (Orc1-4, and Orc6; Orc5 was not queried for technical reasons) by using Y2H analysis. Our Y2H assay confirmed the interaction between Orc1 and Pch2, as reported earlier (Vader *et al.*, 2011), but did not observe an interaction between Pch2 and Orc2, Orc3, Orc4 or Orc6 (Figure 3-14 A), likely indicative of Orc1 being central for Pch2 association.

Additionally, based on the idea that Orc1 is important for mediating binding between Pch2 and ORC, we predicted that the absence of Orc1 should lead to a decreased association between Pch2 and other ORC components. In order to test this premise, we performed Co-IP experiments to examine the interaction between Pch2 and TAP-tagged Orc2/Orc5 in the presence of a ts-mutant of Orc1 (*orc1-161*). Co-IP assays were performed with cell lysates grown at 23°C and harvested after 4 hours in the meiotic programme. α -TAP Co-IP with cells harbouring *ORC2-TAP*, *3xHA-PCH2* in an *orc1-161* background revealed that indeed Orc2-

TAP interaction with 3xHA-Pch2 was impaired, as compared with the control strain (*ORC2-TAP*, *3xHA-PCH2*, *ORC1*), in which Orc2-TAP was able to co-precipitate 3xHA-Pch2 (Figure 3-14 B, lanes 7 and 8). This interaction was specific, as an Orc2-untagged strain failed to co-precipitate 3xHA-Pch2 (Figure 3-14 B, lane 5 and 6). Similarly, we performed α -TAP Co-IP with cell lysates of strains carrying *ORC5-TAP*, *3xHA-PCH2-E399Q* in either an *ORC1* or *orc1-161* background, grown at 23°C and harvested after 4 hours into the meiotic programme. This experiment showed that Orc5-TAP was able to specifically co-precipitate 3xHA-Pch2-E399Q (Figure 3-14 C). In contrast, impairing Orc1 protein levels via the *orc1-161* mutant allele impaired the binding between Orc5-TAP and 3xHA-Pch2-E399Q (Figure 3-14 C).

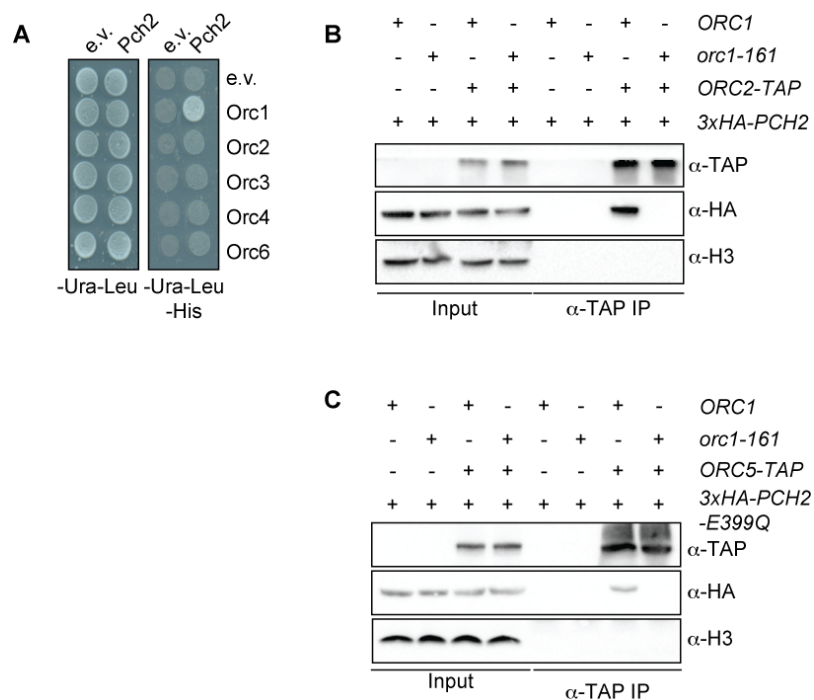


Figure 3-14 Orc1 is a central mediator of the interaction between Pch2 and ORC

A) Yeast two-hybrid assay between Pch2 and Orc1, Orc2, Orc3, Orc4 and Orc6, grown 2 days in – Ura–Leu solid medium (control plate) or –Ura–Leu–His solid medium (specific growth plate). e.v. indicates empty vector. B) Co-immunoprecipitation assay of 3xHA-Pch2 with Orc2-TAP in wild-type *ORC1* or *orc1-161* backgrounds (via α -TAP) during meiotic prophase (4 hours into meiotic programme). α -H3 is used as a loading control. Experiments were performed at 23°C. C) Co-immunoprecipitation of 3xHA-Pch2-E399Q with Orc5-TAP in wild-type *ORC1* or *orc1-161* backgrounds (via α -TAP) during meiotic prophase (4 hours into meiotic programme). Experiments were performed at 23°C. Histone H3 (α -H3) is used as a loading control.

Thus, the results presented here emphasize the hypothesis that Orc1 might be central in mediating Pch2 binding to ORC and therefore, depletion of this ORC member likely precludes

Pch2 association to Orc2 or Orc5. Alternatively, absence of Orc1 would lead to the disruption of the ORC assembly, which in turn potentially prevents binding of Orc2 or Orc5 to Pch2, arguing that impairment of the interaction between Pch2 and Orc2/Orc5 is rather a consequence of the disassembly of the ORC complex and not necessarily a consequence of Orc1 being the central interactor. These interpretations are further explained in the Discussion (see section 4.4).

3.5.4 Implication of the BAH domain of Orc1 in Pch2/ORC interaction

As described in section 3.3, our XL-MS data suggested a central role of Orc1 in establishing the binding between Pch2 and ORC. Our findings described in section 3.5.3 further supported this idea. However, these results raised the question of how Orc1 might be playing this primary role in the interaction between Pch2 and ORC. In an attempt to elucidate the basis that lay behind this particular Orc1 role, we first focused on the differences in the domain architecture among ORC components, with a special emphasis on Orc1. It is known that among the six budding yeast ORC subunits, Orc1 through Orc5 contain AAA⁺ or AAA⁺-like domains, being the Orc1 member the main source of AAA⁺ ATPase activity of this complex. In contrast, Orc6 does not harbour such a domain (Duncker *et al.*, 2009; Li & Stillman, 2012). Besides the AAA⁺ domain, Orc1-5 subunits contain one or two putative winged-helix (WHD) DNA-binding motif in the C-terminal region that appears to mediate DNA binding.

One particularity of Orc1, the largest subunit of ORC, is that it contains an additional bromo-adjacent homology (BAH) domain in its N-terminus (H. Li & Stillman, 2012). BAH domains are discrete (~ 200 amino acids) protein domains that are present in a diverse range of nuclear proteins and play a fundamental role in chromatin structure by interacting with nucleosomes (Yang & Xu, 2013). Given structural studies showing similar structure between the BAH domain of the Orc1-related protein Sir3 bound to nucleosomes, it is likely that yeast Orc1's BAH domain might bind nucleosomes in a direct fashion (Arnaudo *et al.*, 2013). Indeed, a recent investigation elucidated the structure of the Orc1 BAH-nucleosome complex and revealed that interaction between this domain of Orc1 and nucleosomes is essential to maintain the integrity of the rDNA boundaries during meiosis (see below) (De Ioannes *et al.*, 2019). Several yeast studies have shown that the BAH domain of Orc1 is not strictly required for DNA replication (Bell *et al.*, 1995; Müller *et al.*, 2010a). However, recent work has revealed the importance of this domain for the association of ORC with chromatin and regulation of origin activity. In this line, it has been reported that Orc1's BAH domain

contributes to the association of ORC with most yeast origins of replication, being required for the normal activity of a subset of origins throughout the budding yeast genome (Li & Stillman, 2012; Müller *et al.*, 2010b). In addition to its role in the initiation of DNA replication, Orc1 is also involved in transcriptional silencing at the mating-type loci and telomeres. Several studies in this field have reported that the BAH domain of Orc1 is necessary to perform its silencing function at these loci, since Orc1's BAH motif recruits the silent information regulator 1 (Sir1), which in several protein recruitment steps leads to the assembly of the SIR complex, necessary for silencing (Hickman & Rusche, 2010; N. Yang & Xu, 2013) (see section 1.3). Moreover, Orc1 is involved in preventing DSB formation and NAHR at the rDNA and a study demonstrated that a deletion of the BAH domain of Orc1 (*Abah-ORC1*) leads to an increase in DSBs, similarly to what is observed in *pch2Δ* cells (Vader *et al.*, 2011). This observation pointed towards the idea that Pch2 needs the BAH domain of Orc1 either for being properly localized to those sites of the rDNA where its function is required or for interaction between Pch2 and Orc1/ORC.

Thus, we next aimed to study the implication of the BAH domain in the interaction between Pch2 and ORC. To assess how Orc1's BAH motif affected Pch2 binding to Orc1, we performed Y2H analysis with truncated versions of Orc1 (Figure 3-15 A and B). These results revealed that Pch2 was not able to bind to the BAH domain of Orc1 alone (amino acids 2-235). By contrast, we detected an interaction between Pch2 and Orc1 in an Orc1 construct where the BAH domain had been deleted (Δ bah-Orc1: amino acids 235-914). We observed increased growth of cells expressing this truncated version of Orc1 when compared to the full-length Orc1. However, at this stage we cannot exclude that this might be due to differences in the expression level of these proteins.

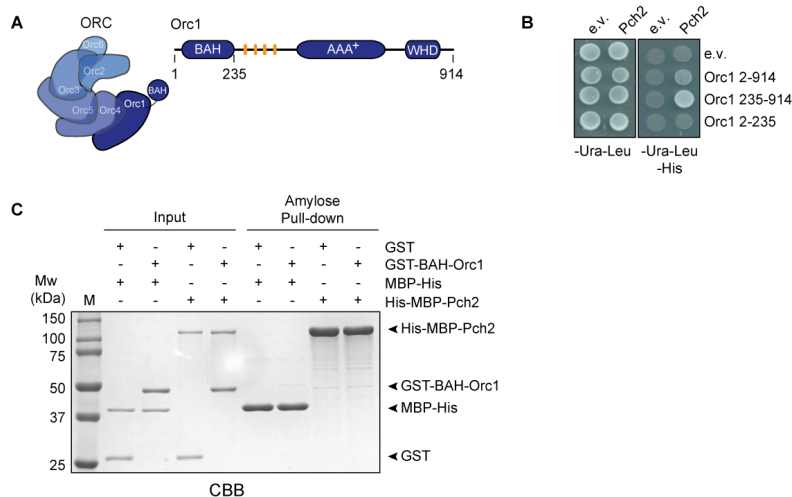


Figure 3-15 The BAH domain of Orc1 is not sufficient for Pch2 association

Figure 3-15 (Continued)

A) Schematic of ORC and the Bromo-adjacent homology (BAH) domain of Orc1. Orc1 (amino acids 1-914) harbors a chromatin-binding module (BAH domain; amino acids 1-235), an AAA⁺ ATPase domain and a Winged-helix domain (WHD). Basic patch (BP) of Orc1 is depicted in orange between the BAH domain and the AAA⁺ module. The BAH domain is depicted as an “extension” of Orc1 for clarity. B) Yeast two-hybrid (Y2H) analysis between Pch2 and full-length Orc1 (amino acids 2-914), Dbah-Orc1 (amino acids 235-914) or BAH-Orc1 (amino acids 2-235). Y2H strains were grown in either –Ura–Leu control plate or specific growth plate (–Ura–Leu–His). e.v. indicates empty vector. C) Amylose-based pull-down of GST-BAH-Orc1 (3 μM), purified from bacteria, and His-MBP-Pch2 (1 μM, considering hexameric formation), purified from insect cells. GST (3 μM) and MBP-His (6 μM) were used as controls. Input and pull-down samples were analysed by SDS-PAGE and Coomassie Brilliant Blue (CBB) staining.

We further examined the role of the BAH domain in the interaction between Pch2-ORC using an *in vitro* approach. For this purpose, we purified the BAH domain of Orc1 (GST-BAH-Orc1) from bacteria and analysed its binding to Pch2 *in vitro*. In agreement with the Y2H spotting assay, pull-down assays using His-MBP-Pch2 as bait showed that BAH-Orc1 and Pch2 were also not able to interact directly (Figure 3-15 C). MBP-His and GST were used as controls. Similarly, we purified Δbah-ORC (*i.e.* Δbah-Orc1-Orc2-Orc3-Orc4-Orc5-Orc6) (Figure 3-16A) and tested the ability of this mutated ORC to interact with Pch2. In agreement with the Y2H assay, our pull-down showed a direct interaction between Δbah-ORC and Pch2 (Figure 3-16 B). This binding was specific, as Δbah-ORC did not interact with the MBP-His control (Figure 3-16 B, lanes 8 and 9). Full-length ORC was used as a positive control for the interaction with His-MBP-Pch2 under the conditions tested (Figure 3-16 B, lanes 6 and 7). Binding between His-MBP-Pch2 and Δbah-ORC was further confirmed by SEC analysis. We observed a reduction in the retention volume when these two protein complexes were mixed, as compared to their individual retention volumes (Figure 3-16 C). Both the Y2H and the *in vitro* experiments presented here provided evidence that the Pch2 can bind to ORC when Orc1 lacks its BAH domain, pointing to an “indirect” or allosteric function of this domain in mediating Pch2 function. Corroborating these findings, no cross-links were detected between the BAH domain of Orc1 and Pch2, as judged by XL-MS (Figure 3-8, Table 7-2 and 7-3).

Additionally, we evaluated the effect of Orc1’s BAH motif in the Pch2-ORC association *in vivo*. It is worth mentioning that deletion of this domain of Orc1 does not

prevent cell cycle progression, neither in cycling cells nor in meiosis (Bell *et al.*, 1995; Vader *et al.*, 2011). To analyse this, we performed co-IP experiments in yeast strains containing *3xHA-PCH2* and TAP-tagged versions of either a wild-type allele of *ORC1* or a Δ *bah-Orc1* allele. Interestingly, we observed that the interaction between Δ *bah-Orc1*-TAP and *3xHA-Pch2* was severely impaired, as compared to wild-type *Orc1*-TAP, as judged via α -TAP Co-IP with cell lysates harvested after 4 hours in meiosis (Figure 3-16 D). As negative controls *pch2* Δ , *ORC1*-TAP or *pch2* Δ , Δ *bah-ORC1*-TAP strains were used.

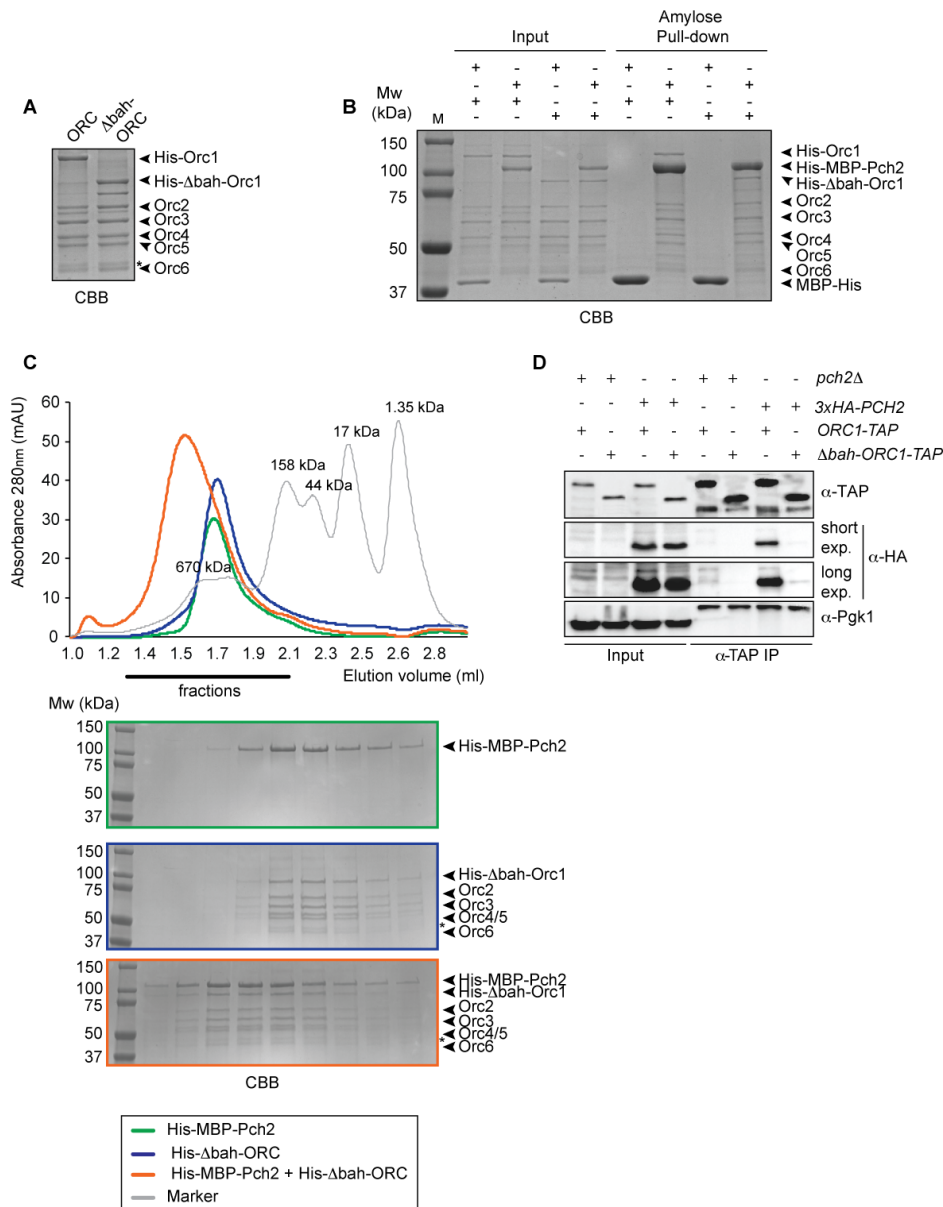


Figure 3-16 Implications of the BAH domain of Orc1 in Pch2/ORC interaction

A) Purified ORC (His-Orc1, Orc2-6) and Δ *bah*-ORC (Δ *bah*-His-Orc1, Orc2-6) from insect cells visualized via Coomassie Brilliant Blue (CBB) staining. B) Amylose pull-down of His-MBP-Pch2(1 μ M, considering hexamer) and either ORC or Δ *bah*-ORC (1 μ M, considering hexamer). Input

Figure 3-16 (Continued)

and pull-down samples were analysed by SDS-PAGE and CBB staining. MBP-His was used as a negative control. C) Size exclusion chromatography (SEC) of (His-MBP-Pch2)-(Δ*Abah*-ORC) assembly. Green line represents SEC of His-MBP-Pch2. Blue line represents SEC of purified Δ*Abah*-ORC. Orange line represents a mixed sample of His-MBP-Pch2 and His-ORC. Gray line represents SEC of gel filtration standard; molecular weights of the proteins present in the standard are indicated. Black line indicates peak fractions analysed by SDS-PAGE and CBB staining. AU stands for arbitrary units. Asterisk indicates the Orc6-phosphorylated band. D) Co-immunoprecipitation assay of meiotic lysates of yeast strains harboring *ORC1-TAP* or *Δbah-ORC1-TAP* and *3xHA-PCH2* (via α-TAP IP). Cells were induced to undergo synchronous meiosis and harvested 4 hours after meiotic induction. Input and IP samples were analysed by SDS-PAGE and Western blot probing against α-HA, α-TAP and α-Pgk1 (loading control). For α-HA, short and long exposures are shown. Strains carrying *ORC1-TAP* or *Δbah-ORC1-TAP* and *pch2Δ* were used as negative controls.

These findings contrast with our *in vitro* experiments, in which we could not observe an effect of the deletion of Orc1's BAH domain with regard to Pch2 binding. In this respect, it is worth mentioning that a recent investigation showed that mutations that lower the affinity of the Orc1's BAH domain for nucleosomes result in accumulation of DSBs at the rDNA (De Ioannes *et al.*, 2019). Thus, Orc1 interaction with nucleosomes (via its BAH domain) is likely to play a role in maintaining the integrity of the rDNA borders during meiosis. Since DSB induction at the rDNA boundaries is dependent on the catalytic activity of the histone deacetylase Sir2 (Gottlieb & Esposito, 1989; Imai *et al.*, 2000; Mieczkowski *et al.*, 2007; Vader *et al.*, 2011), one explanation to our seemingly contradictory *in vivo* and *in vitro* results could be that the BAH domain of Orc1 is not strictly necessary for Pch2/ORC binding, but that by deleting Orc1's BAH domain could affect the association of ORC to distinct DNA regions, which would potentially influence Pch2 binding to ORC *in vivo*. Other possible explanations that could account for the discrepancies between the *in vivo* and *in vitro* results are further explained in the Discussion section.

Taken together, the results described in this section demonstrate that whereas Orc1's BAH domain is not *per se* necessary for direct binding between Pch2 and Orc1/ORC *in vitro*, it is essential for *in vivo* interaction between these two ATPases complexes. We hypothesize that the discrepancy between our *in vivo* and *in vitro* results could be due to the role of the BAH domain of Orc1 in recruiting ORC to specific (yet to be determined) locations. In sum, our results suggest an interesting connection between Orc1's BAH domain, chromatin structure and Pch2 association to ORC.

4 Discussion

A key event of meiosis is the programmed introduction of DNA double-strand breaks (DSBs), which initiates reciprocal DNA exchange between homologous chromosomes, known as inter-homolog crossover (CO) recombination. Inter-homolog CO recombination ultimately leads to the formation of physical linkages between homologs, called chiasmata, that are crucial for faithful chromosome segregation in meiosis I. Despite DSBs being critical for the proper execution of meiosis, DSB introduction in certain genomic zones, such as the repetitive ribosomal DNA (rDNA), can be deleterious. DSBs within repetitive regions endanger genome integrity since they are prone to non-allelic homologous repair (NAHR), a major cause of chromosomal re-arrangements and several diseases in humans (Marston & Amon, 2004a; Sasaki *et al.*, 2010; Subramanian & Hochwagen, 2014). As such, meiotic DSB formation is an intrinsically hazardous event for the organism and thus, mechanisms exist to protect these particularly vulnerable regions.

In budding yeast, DSB formation within the rDNA is suppressed by a mechanism that involves the silencing protein Sir2, which establishes a special repressed chromatin state. Although Sir2 prevents DSB introduction within the rDNA, the Sir2-dependent heterochromatin formation at the rDNA is responsible for meiotic DSB formation at the rDNA boundaries (Gottlieb & Esposito, 1989; Vader *et al.*, 2011). DSBs situated at the edges of repetitive regions are also at high-risk of meiotic NAHR. Prior data on the budding yeast rDNA showed that DSB prevention at the rDNA flanks is accomplished by two AAA⁺ ATPases, named Pch2 (Pachytene checkpoint 2) and Orc1 (the largest subunit of the Origin Recognition Complex, ORC). Upon disruption of this border-specific Pch2-Orc1 anti-DSB system, there is increased DSB formation and recombination specifically in the outermost rDNA repeats, leading to NAHR and rDNA instability (Vader *et al.*, 2011). However, the mechanism and features defining this protective anti-DSB system operating in the rDNA borders remain unexplored. Particularly, it was still not known whether Pch2 and Orc1 interact directly, and whether other subunits of the hetero-hexameric ORC are involved in this binding and in DSB protection at the rDNA-borders. In addition, the molecular basis of the assembly of the Pch2-Orc1/ORC complex remained unexplored. Here, we show that *in vivo* Pch2 associates with other ORC subunits besides Orc1, and likely with the entire ORC. In addition, we demonstrate that Pch2 interaction with ORC occurs in a direct manner and provide insights about the interaction mode of these two AAA⁺ ATPases macromolecular

complexes. Moreover, our data reinforce the role of Orc1, among all the ORC components, as the main determinant in the association with Pch2 during meiotic G2/prophase. Finally, we provide evidence that supports the notion that the DSB protective function of Pch2-ORC at the rDNA does not necessitate ORC binding to origins of replication, which is required for the canonical role of ORC in driving the initiation of DNA replication.

4.1 Pch2 interaction with Orc1 is analogous to stereotypical AAA⁺ ATPases association

The meiosis-specific budding yeast AAA⁺ ATPase Pch2 is considered a master regulator of meiotic G2/prophase (see section 1.4.1). The first observation indicating that Pch2 played a role at the budding yeast rDNA was made by San-Segundo and Roeder (San-Segundo & Roeder, 1999), who showed increased rates of meiotic rDNA recombination upon deletion of Pch2 and also demonstrated that Pch2 was enriched in the nucleolar region, where the rDNA assembles. Subsequent studies by the Hochwagen group demonstrated that the Sir2-dependent heterochromatin present at the rDNA has a DSB-promoting effect at the rDNA boundaries (Vader *et al.*, 2011), and revealed that DSB formation at the rDNA edges is protected by Pch2. This study identified via a yeast two-hybrid (Y2H) screening a fragment of Orc1 comprising the AAA⁺ module of this protein as a Pch2 interactor. This interaction was also confirmed *in vivo* and the authors demonstrated that Orc1 collaborates with Pch2 in its rDNA-proximal DSB prevention role.

Here, we showed that Pch2 interacts with Orc1 in meiotic G2/prophase in a manner consistent with a typical AAA⁺ ATPase-like interaction. As mentioned in the Introduction, AAA⁺ ATPases form oligomeric assemblies, typically hexamers, in which common surfaces of the adjacent subunits constitute the bipartite nucleotide-binding site, and this conformation is critical for the function of these protein assemblies (Erzberger & Berger, 2006; Hanson & Whiteheart, 2005; Ogura *et al.*, 2004; Ogura & Wilkinson, 2001). This nucleotide-binding domain harbors typical motifs, Walker A and Walker B motifs, that contribute to ATP binding and/or hydrolysis. We found that binding of ATP to Pch2 is necessary for interaction with Orc1 *in vivo* by performing Co-IP assays with a mutant allele of Pch2 that carries a lysine to arginine mutation in the Walker A motif (*PCH2-K320R*). It was previously described that mutations in the Walker A motif disrupt Pch2 ATPase binding *in vitro* and such mutations lead to the dissociation of hexameric AAA⁺ ATPases into monomers, as it is the case with the bacterial heat-shock protein HslU and the SV40 LTag helicase (Chen *et al.*, 2014; Wendler *et al.*, 2012a). In line with this role of the Walker A motif in the

oligomerization of AAA⁺ ATPases, Pch2-K320A (a mutation that harbours functional similarities with the Pch2-K320R) fails to immunoprecipitate Pch2-K320A, suggesting that ATP binding is required for the stable formation of Pch2 hexamers *in vivo* (Herruzo *et al.*, 2016). Since we observed that Pch2-K320R disrupts the interaction with Orc1, we hypothesize that Pch2 binding to Orc1 relies on both ATP binding and Pch2 hexameric conformation. However, work by the San-Segundo laboratory revealed that the Walker A-deficient Pch2-K320A protein is evenly dispersed throughout the cell, rather than being enriched in the nucleolar region, as it occurs for the wild-type protein, indicating that ATP binding and stability of the Pch2 hexamer are important for proper localization of Pch2 (Herruzo *et al.*, 2016). Given the behavior of Pch2-K320A, we cannot rule out the possibility that the lack of interaction between Pch2 Walker A mutant that we used in this study (Pch2-K320R) and Orc1 is due to mislocalization of Pch2-K320R (*i.e.* this mutant might fail as well to localize at the nucleolus, where presumably Pch2 interacts with Orc1). Immunofluorescence analysis and cell fractionation assays would be critical to confirm the proper cellular localization of this mutant in SK1 yeast strains (of note, the study of Herruzo *et al.*, was performed using BR yeast strains). Alternatively, the fact that binding between Pch2-K320R and Orc1 is impaired could account for the lack of recruitment of this Pch2 mutant to the nucleolar region (*i.e.* the inability of Pch2-K320 to associate with Orc1 could prevent the Orc1-mediated recruitment of this Walker A mutant of Pch2 to the nucleolus). Our *in vitro* reconstitution has the potential to overcome the effects of the possible mislocalization of this Pch2 Walker A mutant. We have already generated His-MBP-Pch2-K320R and His-MBP-Pch2-K320A constructs and future experiments should focus on addressing the interaction of these mutants with recombinant ORC *in vitro*.

Since binding of AAA⁺ ATPases with their substrates/co-factors depends on reactions of nucleotide hydrolysis and release, substitutions of a critical glutamic acid residue in the Walker B motif have been employed as substrate/co-factor trapping mutants (as such mutations impair ATP hydrolysis without affecting ATP binding) (Babst *et al.*, 1998; Hanson & Whiteheart, 2005; Wendler *et al.*, 2012b). In this study, we showed that the interaction of Pch2 with Orc1 is more robust in a Walker B mutant motif of Pch2 in which the glutamic acid at the residue 399 is substituted by a glutamine (Pch2-E399Q), with respect to wild-type Pch2 (Figure 3-1). This result is in agreement with studies of other AAA⁺ ATPases mutated in this conserved motif. For instance, the bacterial ClpB chaperone interacts with its protein substrates in a more stable manner as compared to the wild-type when the Walker B motifs of

both its AAA⁺ domains are mutated (E279A/E678A) (Weibezahn *et al.*, 2003). Similarly, a substrate/co-factor trap mutant has been used in the AAA⁺ ATPase NSF (N-ethyl maleimide sensitive factor), involved in fusion of cellular membranes, to show interaction with its binding partner α -SNAP (soluble NSF attachment protein); α -SNAP co-precipitates with the NSF *in vivo* only when NSF harbors a mutation in its Walker B motif (E329Q) (Dalal *et al.*, 2004). Thus, the finding that the Walker B mutant of Pch2 (Pch2-E399Q) shows an increased binding with Orc1 relative to wild-type Pch2 demonstrates that the *in vivo* interaction between Pch2 and Orc1 depends on Pch2 ATP hydrolysis. It would also be interesting to identify the ATPase requirements for Orc1/ORC. Importantly, Pch2 ATPase activity is critical for its function in rDNA-proximal DSB protection, as cells carrying the *pch2-E399Q* mutant allele show the same rDNA-associated phenotype than *pch2* Δ cells (Vader *et al.*, 2011). Altogether, the present findings provide evidence that Pch2 interaction with Orc1 depends on Pch2 ATP hydrolysis activity and likely relies on ATP binding and proper Pch2 hexamerization.

4.2 Interaction between Orc1 (ORC) and Pch2

4.2.1 The entire ORC is involved in the interaction with Pch2 *in vivo*

As already mentioned, Orc1 is a member of the hetero-hexameric ORC, a complex composed of 6 subunits (Orc1-Orc6) that is critical for DNA replication. Although distinct ORC subunits play other roles besides replication (*e.g.* Orc2 in sister-chromatid cohesion, Orc1 in transcriptional silencing), these functions seem in most studied cases to be executed in the context of the entire ORC complex. While several studies in metazoans cells showed that Orc1 appears to be lacking from ORC at defined points in the cell cycle (such as in human HeLa cells, where Orc1 dissociates from chromatin during S phase and re-associates at the end of mitosis), budding yeast ORC remains associated to chromatin throughout the *S. cerevisiae* cell cycle, also in meiosis (Blitzblau *et al.*, 2012; DePamphilis, 2005; Diffley *et al.*, 1995; Liang & Stillman, 1997).

So far, it remained unclear whether other ORC components (besides Orc1) also interact with Pch2. In line with the aforementioned knowledge about budding yeast ORC, we hypothesized that other subunits of ORC would also interact with Pch2. Indeed, our co-immunoprecipitation (Co-IP) experiments (Figures 3-2 C) revealed the binding of Pch2 to Orc2 and Orc5 during meiotic G2/prophase, suggesting that the entire ORC associates with Pch2. Of note, we used the substrate trap mutant of Pch2 (Pch2-E399Q) in these experiments,

based on our previous Co-IP assays (Figure 3-1), to facilitate the detection of possible weak or transient interactions. Importantly, we recursively observed a higher intensity band in the Orc1 subunit in comparison with Orc2 or Orc5. Given that all these components are fused to the same tag (TAP tag) in their respective Co-IPs, this difference cannot be attributed to preferential recognition of the Orc1 subunit by the TAP antibody. Instead, we interpret this to mean that within ORC, Orc1 is the critical interactor of Pch2 (further discussed in section 3.5.3). Alternatively, given that *S. cerevisiae* ORC remains as a complex throughout the cell cycle, it is conceivable that only Orc1 binds to Pch2 and the other ORC components tested (Orc2 and Orc5) are observed in our Co-IP assays simply because they are intrinsically associated to Orc1 in the ORC (Orc1-Orc6) assembly. Our results thus demonstrate that Pch2 associates with Orc1 when Orc1 is assembled with other ORC subunits (*i.e.* Orc2/Orc5), and imply that Pch2 associates with Orc1 in the context of the entire ORC during meiotic G2/prophase.

4.2.2 Interaction of Pch2 with ORC is independent of Cdc6

During DNA replication ORC associates with another AAA⁺ ATPase protein called Cdc6, promoting the loading of the MCM replicative helicase at origin DNA. We next investigated whether the interaction between Pch2 and ORC depends on Cdc6, by employing a meiosis-specific null allele of *CDC6* (*cdc6-mn*). Pch2 expression is induced during meiotic S-phase and peaks in G2/prophase, whilst Cdc6 availability is restricted to the G1 phase of the cell cycle, also in pre-meiotic G1 phase (see Introduction) (DePamphilis, 2005; Nguyen *et al.*, 2001; San-Segundo & Roeder, 1999).

As anticipated, due to the mutually exclusive expression pattern of Pch2 and Cdc6 in meiosis, our experiments indicated that the interaction between Pch2 and ORC is independent of Cdc6 (Figure 3-3 B) (as judged by the similar interaction observed in wild type and *cdc6-mn* yeast cells). We studied if Cdc6 is necessary for the Pch2-Orc1 role in suppressing DSB formation at the rDNA borders. While the *pch2Δ* and *orc1-161* mutants show an increased DSB formation at the rDNA borders (*i.e.* the ~1-10 outermost rDNA repeats and ~50 kb of single copy flanking sequences) (Vader *et al.*, 2011), the *cdc6-mn* mutant did not trigger an increase in DSB formation at the right rDNA flank tested (Figure 3-3 C and D). In spite of observing defects in DNA replication in the *cdc6-mn* mutant background, we also observed formation of DSBs at the right DNA flank in the *pch2Δcdc6-mn* strains. These results are in line with data from others, who showed that despite exhibiting defects in meiotic DNA

replication, the *cdc6-mn* mutants progress normally through meiosis and undergo DSB formation in meiotic G2/prophase (Hochwagen *et al.*, 2005).

Thus, we demonstrated that Cdc6 is not required for Pch2-ORC interaction and that Cdc6 is dispensable for the Pch2-Orc1 role in DSB suppression at the rDNA borders. Moreover, our data point towards a potential novel interaction of ORC with another member of the AAA⁺ ATPase family (Pch2) that is distinct from the known interaction between ORC and MCM, since ORC-MCM association requires Cdc6.

4.2.3 The interaction between Pch2 and ORC is direct

In this study, we provided evidence that Pch2 interacts with ORC *in vivo*. However, whether this interaction was direct remained unclear. In order to test if Pch2 binds to ORC directly, we designed strategies to purify both macromolecular complexes. Even if there have been several biochemical and structural studies with the mammalian homolog of Pch2 (TRIP13), little is known about the biochemical properties of Pch2 from *S. cerevisiae* (Alfieri *et al.*, 2018; Ye *et al.*, 2017a, 2015). Budding yeast Pch2 has been mainly studied genetically and cytologically, and only one study reported the use of purified Pch2 from *S. cerevisiae* (Chen *et al.*, 2014). Up to date the structure of budding yeast Pch2 remains unsolved. It is worth mentioning that so far all the biochemical research with Pch2/TRIP13 has focused on the relation of this AAA⁺ ATPase with HORMA-domain containing proteins, such as Mad2. Here we addressed for the first time the interaction between Pch2 with another AAA⁺ ATPase (ORC) *in vitro*.

In order to reconstitute the Pch2-ORC interaction, we extensively attempted different approaches to purify budding yeast Pch2 and finally established a purification strategy that allowed us to obtain recombinant His-MBP-Pch2. We observed by size exclusion chromatography (SEC) that His-MBP-Pch2 eluted as the expected molecular size of a hexameric complex (Figure 3-4 and 3-5 A). This is in good agreement with several AAA⁺ ATPase family members (such as Cdc48/p97/NSF) that have been shown to form oligomeric complexes, typically hexamers. However, our results diverge slightly from the other study of purified budding yeast Pch2, in which Pch2 was monomeric and its hexameric assembly was only observed in the presence of a non-hydrolysable analog of ATP (ATP γ S) (Chen *et al.*, 2014) (see below).

As already mentioned, assembly into oligomers is a hallmark of AAA⁺ ATPases and in many cases, their assembly into higher-order oligomeric states depends on the presence of nucleotides. Such behavior has been described for the budding yeast AAA⁺ ATPase Vps4, a protein involved in cargo transport from an endosome to the lysosome-like vacuole (Babst *et al.*, 1998). Vps4 exists as a dimer when it is nucleotide-free or ADP-bound, whilst it assembles into a decameric complex in an ATP-locked state. Similar behaviors have been observed with the mammalian homolog of Pch2 (TRIP13); SEC-MALS showed that *Mus musculus* TRIP13 adopts a range of oligomeric states ranging from monomer to hexamer, consistent with findings from *S. cerevisiae* (Ye *et al.*, 2015). Moreover, the higher-molecular weight TRIP13 oligomers increase upon the addition of either ATP or ATP γ S. However, our finding that recombinant His-MBP-Pch2 assembles into a hexamer even without nucleotides, is consistent with the *C. elegans* PCH-2, which forms a stable hexamer both with and without nucleotides (Ye *et al.*, 2015). The differences of nucleotide-dependent oligomeric formation observed in the recombinant His-MBP-Pch2 of this study and Pch2 purified from budding yeast, could be due to the different affinity tag used (His-MBP and GST, respectively), as affinity tags may affect the oligomeric state of AAA⁺ proteins. The GST tag is known to form dimers in solution and Alani *et al.* demonstrated that this tag affects the oligomeric state of GST-Pch2; whereas untagged Pch2 assembles into monomers and only forms hexameric rings upon the presence of nucleotides, the presence of a GST tag eliminates the dependency of the nucleotide for oligomer formation (Chen *et al.*, 2014). Although dimerization of GST has been proposed to facilitate the arrangement of Pch2 into hexameric rings, such behavior is not expected from the MBP-tag, which is not known to dimerize. However, it is possible that the affinity tag used here might favor the formation of a stable conformer without the need for nucleotides.

Our SEC experiments showed recurrently a minor peak that we initially attributed to a monomeric His-MBP-Pch2. We employed sedimentation velocity analytical ultracentrifugation (SV-AUC) to elucidate whether our purified Pch2 was present in distinct oligomeric states. SV-AUC corroborated that the oligomeric assemblage of His-MBP-Pch2 depended on the concentration of the protein present: at higher concentrations the predominant species was hexameric, whilst at lower concentrations we could detect different conformational species, with the monomeric being the most abundant (Figure 3-5 C). These results indicate that in the purified His-MBP-Pch2, different species likely co-exist in equilibrium.

In addition, we demonstrated that His-MBP-Pch2 is functional since it is able to interact with its known client Hop1 (a HORMA-domain-containing protein) (Figure 3-5 B and 7-6). Contrary to Alani *et al.*, who described weak binding of GST-Pch2 and Hop1 unless ATP γ s was present, we did not observe differences in the interaction with respect to the presence of oligonucleotides, at least under the conditions tested (Figure 7-6 A). Once again, this could be due to a different behaviour of GST-Pch2 and His-MBP-Pch2 due to their respective tags (of note, we used equivalent concentrations of Hop1 and Pch2 as reported by Alani *et al.*). Another possibility that could account for the discrepancy regarding the influence of nucleotides in Pch2-Hop1 binding is that the purified His-MBP-Pch2 is not active. Since we purified Pch2 from another source (insect cells as compared to the Pch2 protein from the aforementioned study, obtained from budding yeast) the recombinant Pch2 used here could lack some post-translational modifications that might be needed for its activity, and that might be present in the Pch2 protein purified from a more native environment (*i.e.* budding yeast). If the purified His-MBP-Pch2 is not active (*i.e.* unable to hydrolyse ATP), adding nucleotides would not be expected to influence binding between Pch2 and Hop1.

Hence, although we cannot conclude at this stage the reason underlying the discrepancies observed in the Pch2-Hop1 binding with respect to the presence of nucleotides, our results offer evidence that the purified His-MBP-Pch2 assembles predominantly into an hexamer (with other oligomeric states), as observed in other Pch2 homologs and we demonstrated that the purification strategy used provides a functional His-MBP-Pch2 (in terms of interaction with a known partner). Similarly, we designed a strategy to purify ORC (His-tagged in the Orc1 subunit) from insect cells (Figure 3-6) and validated by mass spectrometry the presence of all ORC subunits in our recombinant preparation (Table 7-1, Appendix). Binding between Cdc6 and ORC (purified from other sources) has been previously shown *in vitro* and here we confirmed this interaction by pull-down assays as a proxy to validate the functionality of ORC purified by our established methodology (Figure 7-6 A) (Frigola *et al.*, 2013; Remus *et al.*, 2009; Speck *et al.*, 2005).

Here, we demonstrated for the first time that Pch2 and ORC bind directly *in vitro* by two different approaches. First, by solid-phase pull-down using recombinant His-MBP-Pch2 and His-ORC we revealed that binding between both AAA⁺ ATPases is direct. Of note, we worked with a concentration of His-MBP-Pch2 (1 μ M, considering hexamer formation) in which the SV-AUC performed suggested a predominant hexameric conformation of His-

MBP-Pch2. We showed that interaction between His-MBP-Pch2 and His-ORC is direct and also specific under the conditions tested. Second, we demonstrated a direct interaction between His-MBP-Pch2 and His-ORC by analytical SEC (Figure 3-7 C). Upon combination of these two proteins, we detected a shift towards the left in the elution profile, as compared to the individual proteins, indicating formation of a higher molecular weight complex (and thus direct interaction between both proteins in solution). We interpreted that the shift observed by SEC when His-MBP-Pch2 and ORC are mixed together reflects an interaction between both proteins in a hexamer:hexamer fashion, which would yield a Pch2-ORC complex of approximately 1 MDa. However, we are aware of the limitations of analytical SEC to determine stoichiometry of complex assemblies, as the elution profiles not only depend on molecular weight, but also on the shape of the protein, and it is thus, only possible to get a rough estimation of the protein molecular weight. Moreover, it is likely that different oligomeric species of His-MBP-Pch2 exist (besides the predominant hexameric assembly) and that we failed to detect them due to the poor resolution of this technique. Thus, in order to determine the stoichiometry of the Pch2-ORC assembly, more accurate methods should be performed, such as AUC or SEC-MALS (SEC coupled to multiangle light scattering). SEC-MALS has been used by others to gain insight into the oligomeric assemblage and molecular weight measurements of PCH-2 from *C. elegans* and *M. Musculus* TRIP13 (Ye *et al.*, 2015). Technical issues pertaining the purification of ORC precluded us to further address this question in a more thorough manner.

Analytical SEC experiments revealed a small peak at around the expected size of a monomer of His-MBP-Pch2 that did not change its elution profile upon combination with His-ORC. We interpret this to indicate that monomeric His-MBP-Pch2 does not bind to His-ORC in solution or alternatively, that His-MBP-Pch2 in its monomeric state has lower affinity than higher oligomeric assemblies (such as hexamers). Previous studies have shown that Pch2K320A monomerizes *in vivo* (Herruzo *et al.*, 2016). In order to assess whether a monomer of Pch2 can bind to ORC, we generated His-MBP-Pch2-K320R constructs and the most conventional amino acid substitution K→A (His-MBP-Pch2-K320A) and aim to further test the *in vitro* interaction between these mutants of Pch2 and ORC in the future.

One question that future research should address is the dependency of nucleotides in the interaction between Pch2 and ORC. Pull-down assays and analytical SEC experiments should be performed in the presence of either ATP or non-hydrolysable ATP (ATP γ s). Similar approaches should be done with the substrate-trapping mutant of Pch2 (E399Q) to

determine if ATP hydrolysis influences the establishment of the Pch2-ORC assembly. Based on our *in vivo* results, we would expect His-MBP-Pch2-E399Q to also show a stronger binding to His-ORC *in vitro*. Likewise, we would expect that binding of a non-hydrolysable analog of ATP (ATP γ s) would stabilize the interaction between His-MBP-Pch2 and His-ORC. Moreover, it would be interesting to test whether the ATPase activity of Pch2 depends on or is influenced by ORC binding, and in similar lines, to test if ORC ATPase activity is also influenced upon Pch2 association.

In summary, we demonstrated for the first time a direct interaction between the meiosis-specific protein Pch2 and the initiator of DNA replication, ORC. Although the exact stoichiometry of the Pch2-ORC assembly remained to be addressed in the frame of this study, based on the experiments presented here we suggest that this meiotic macromolecular complex interacts in a hexamer-to-hexamer fashion. Moreover, these findings identified a novel interacting partner of ORC and add a cellular function distinct from the known roles of ORC in DNA replication, silencing and sister-chromatid cohesion to this protein complex.

4.2.4 Insights gained through XL-MS suggest a role of Pch2-NTD in the interaction with ORC

Although in this study we provided the first evidence that Pch2 and ORC interact directly *in vitro* (Figure 3-7 and 3-8), the exact molecular details of the interaction between these two complexes remained elusive. In the last years, work by the Corbett and Barford laboratories have provided significant insights into the structure of the mammalian Pch2 homolog (TRIP13) and its biochemical activities towards HORMA-domain containing proteins (Alfieri *et al.*, 2018; Ye *et al.*, 2017a, 2015). However, biochemical work with budding yeast Pch2 is scarce and up to now no published structure is available for this protein. On the contrary, biochemical work with ORC has been extensive, and several recent studies have unveiled the structure of ORC (or trimmed portions of ORC) in *Drosophila*, human and *S. cerevisiae* with different degrees of resolution. ORC is primarily known for its function in DNA replication and thus, most of the published structures of this complex include not only ORC but also additional factors necessary to form the ORC-Cdc6-Cdt1-Mcm2-7 (OCCM) helicase-loading intermediate. The most recent structure of budding yeast ORC also included an origin DNA sequence and hence, has elucidated critical insights about how ORC interacts with ARS consensus sequences (ACS) and the B1 element present in the

origin DNA (Bleichert *et al.*, 2015; Li *et al.*, 2018; Sun *et al.*, 2014, 2012; Tocilj *et al.*, 2017; Yuan *et al.*, 2017).

The molecular characteristics of the meiosis-specific interaction between ORC and Pch2 remained unexplored. In addition, up to date, the level of interaction among the different ORC subunits in meiosis is unknown and the extent to which Pch2 associates with different ORC subunits remained an open question. To tackle that, we used a chemical cross-linking coupled to mass spectrometry (XL-MS) strategy developed in the Mussachio laboratory (Max Planck Institute of Molecular Physiology, Dortmund) with our recombinant His-MBP-Pch2 and His-ORC (Pan *et al.*, 2018). XL-MS is employed to gain insights into inter- and intra-molecular protein-protein interactions and it is a suitable approach to characterize protein assemblies (Holding, 2015; Leitner *et al.*, 2016). Particularly, we employed a methodology that uses a cleavable cross-linker (DSBU or BuUrBu) that enables the identification of pairs of lysine, serine or threonine side chains that are within 12 Å in a native complex; the mapped cross-links obtained are considered distance restraints that serve to generate a rough physical model of the complex. This simplified XL-MS pipeline has been successful in providing reliable cross-link data sets of interactions among kinetochore subcomplexes ranging from 4 to 10 subunits (so-called KMN network) (Pan *et al.*, 2018).

We initially ascertained the quality of the cross-links obtained by this methodology by mapping the intra-molecular MBP cross-links peptides identified within the MBP-moiety present on His-MBP-Pch2 on a published crystal structure (PDB 1FQB) (Duan *et al.*, 2001). The average C α -C α distance between cross-linked amino acids was 14.41 Å, which is in good agreement with the C α -C α distance (12 Å) that the cross-linked state of DSBU is able to facilitate (Table 7-2 and 7-3, Appendix). This experimental XL-MS set-up allowed us to obtain a total of 313 non-redundant cross-links (after applying a stringent cut-off analysis by setting an FDR of 2%), of which 121 cross-links are inter-molecular and 192 intra-molecular (Figure 3-8). Our strategy identified extensive intra- and inter-ORC cross-links (Figure 3-8 and Table 7-2 and 7-3). The network maps generated showed a similar distribution of intra-molecular cross-links within several ORC subunits (Orc1-Orc6) as reported by Yuan *et al.* In addition, we attested the inter-ORC cross-links by network maps and by using a crystal structure of ORC (PDB 5v8f) to model the position of each subunit (Grimm *et al.*, 2015; Yuan *et al.*, 2017). Even though we observed that neighbouring subunits have the most abundant cross-links, several cross-links differed from the study of Yuan *et al.*, as they span considerable distance when compared with the ORC structure. This discrepancy could be

explained by the fact that, in the reported structure, ORC is in combination with additional proteins (Orc-Cdc6-Cdt1-Mcm2-7) forming the complex referred to as OCCM. Studies comparing ORC-Cdc6 structure in the absence or presence of Cdt1-Mcm2-7 have shown that, although they both have a ring-shaped conformation, ORC-Cdc6 undergoes a profound conformational change upon interaction with Cdt1-Mcm2-7 (not only in the Orc1 subunit) (Sun *et al.*, 2014). Thus, it is plausible that the topology of ORC or the position of the different ORC subunits is more constrained in the PDB 5v8f structure than in our Pch2-ORC assembly, in which ORC could have a higher level of flexibility that could account for the more distant inter-ORC cross-links observed in our preparations. Indeed, Cdc6 binding to ORC induces conformational changes to ORC, particularly re-orientating the N-terminal BAH domain of the Orc1 subunit, and these Cdc6-induced conformational changes in ORC are thought to increase DNA specificity of ORC and are probably the basis that ORC transforms from a recognizer of origins of replication to the machinery responsible of loading the MCM replicative helicase (Sun *et al.*, 2012). Of note, the BAH region is not resolved in the model of the published crystal structure and we did not observe cross-links between Pch2 and the Orc1's BAH domain (Table 7-2 and 7-3, Appendix). Alternatively, another source of the dissimilar results observed in some of the inter-ORC cross-links of our data set as compared to those reported by Yuan *et al.* could be the presence of ATP γ S in the above-mentioned structure, since it is well-known that many AAA⁺ ATPases undergo conformational changes in the presence of nucleotides.

Another interesting possibility is that binding of Pch2 to ORC leads to structural rearrangements within the ORC assembly. Finally, for the study that yielded the aforementioned crystal structure of ORC (PDB 5v8f), a different pipeline was used, involving the non-cleavable cross-linker bis-sulfosuccinimidyl suberate (BS³), which has a shorter spacer arm of 8 carbon atoms (as compared to the 11 carbon atoms of DSBU, used here); shorter cross-linkers can react with residues of a narrower range, but the cross-linking efficiency is lower. Both studies (Yuan *et al.* and this study) identified subsets of interactions and we cannot consider as contradictory that different cross-linkers cross-link different set of residues, particularly when the length of cross-linkers is different. Importantly, we identified identical cross-links in both datasets. Hence, we cannot exclude that the differences observed could be, at least partially, a reflection of the different cross-linker and set-up used. In short, the XL-MS approach used in this study yielded similar inter-ORC cross-link distribution that previously reported, but our findings differ to some extent from those of Yuan *et al.* We

interpret that this discordance could be due to differences either in the complexes bound to ORC in our study (Pch2) with respect to the work of Yuan *et al.* or in the experimental approach used to generate the cross-links data sets.

The XL-MS also identified Pch2-Pch2 cross-links (Figure 3-8 C and E, Figure 7-8, Table 7-3; see Appendix), out of which 44% consisted of cross-links between peptides from the NH₂-terminal domain (NTD, amino acids 1-242) with peptides from the COOH-terminal AAA⁺ domain of Pch2 (amino acids 243-564). Additional cross-links consisted of cross-links between peptides from two AAA⁺ domains. We cannot determine whether the Pch2-Pch2 cross-links are inter- or intra-molecular cross-links, since Pch2 assembles into oligomers (*i.e.* hexamers) and these cross-links could be a reflection of the close proximity between the domains within a single Pch2 complex or, alternatively, of an interaction of a domain of one Pch2 monomer with another domain of an adjacent (or potentially more distant) monomer of Pch2. On one hand, the Pch2-Pch2 cross-links between AAA⁺ domains probably indicate the presence of extensive contacts among the AAA⁺ domains of a hexameric Pch2, which is expected from AAA⁺ ATPases, as these proteins oligomerize through their ATPase domains (Erzberger & Berger, 2006; Hanson & Whiteheart, 2005; Ogura *et al.*, 2004; Ogura & Wilkinson, 2001) (see Introduction). On the other hand, cross-links between NTD and ATPase domains of Pch2 might imply that the NTD of Pch2 has a certain degree of flexibility. This is in agreement with data from the Corbett laboratory in which cross-linking data sets of TRIP13 revealed intra-molecular cross-links between residues of the NTD and AAA⁺ domain (beside cross-links between AAA⁺ domains) (Ye *et al.*, 2017a). In the same line, the NTDs of related ATPases, such as NSF, are highly mobile and, upon substrate binding, can “swing upward” to enable engagement of the substrate by the AAA⁺ domain pore loops (Zhao *et al.*, 2015). Such a mechanism has been proposed for TRIP13 NTD, whose binding to its client p31(comet) seems to drive NTD rotation to allow the interaction of p31(comet)-bound Mad2 with the pore loops of AAA⁺ domain (see section 1.4.1.2) (Ye *et al.*, 2017a). Hence, we showed that the obtained Pch2-Pch2 cross-links mirror interactions of the typical organization from AAA⁺ ATPases, including TRIP13.

By this XL-MS strategy, we identified inter-molecular cross-links between Pch2 and ORC (Figure 3-8). We showed that Pch2 establishes extensive cross-links with all the ORC subunits and most of these cross-links lied in the AAA⁺ ATPase domain of the ORC components. Nonetheless, delineation of the domains present in most ORC members is not clearly defined in the literature and therefore, the possibility that some cross-links are present

within the WHD or other regions cannot be ruled out. Our data unveiled that these cross-links contain both, peptides of Pch2 from its enzymatic AAA⁺ core (~57%) and its non-catalytic NTD (~43%) (Figure 3-8 and Figure 7-8). The Orc1-Pch2 interaction was initially identified via a yeast two-hybrid screen in which Pch2 was able to bind to a fragment containing the AAA⁺ ATPase core of Orc1 (Vader *et al.*, 2011). Since AAA⁺ ATPases assemble into oligomers through interactions via their AAA⁺ domains and both, Pch2 and ORC are members of this family, we initially speculated that association of Pch2 with Orc1 (and the other ORC proteins) would be through the AAA⁺ domain of Pch2 (Hanson & Whiteheart, 2005; Ogura & Wilkinson, 2001). However, our XL-MS data argued against this initial hypothesis, since it revealed cross-links not only from Pch2 ATPase core but also from its NTD. These findings are consistent with many AAA⁺ ATPases, including TRIP13, which use their NTD for the initial engagement of substrates/co-factors, followed by interactions through the AAA⁺ core (Alfieri *et al.*, 2018; Ye *et al.*, 2017a). Thus, based on the findings state above, we concluded that Pch2 establishes contacts with ORC using both, Pch2's NTD and ATPase domains.

As stated above, Orc1, Orc2, and Orc4 are the ORC subunits that yielded more abundant cross-links with Pch2. Particularly, Orc1 and Orc2 cross-links represent 48% of the intra-molecular cross-links between ORC and Pch2. Given that Orc1 and Orc2 are the largest proteins of ORC, there is a possibility that this might affect the relative distribution of the cross-links. Biochemical and structural work with ORC has elucidated that ORC consists of a hexameric ring partially open and that during DNA replication the space present between the Orc1 and Orc2 subunits is transiently occupied by the AAA⁺ ATPase Cdc6 (Bleichert *et al.*, 2015; Duncker *et al.*, 2009; Sun *et al.*, 2014). We then speculated that, since Cdc6 is not present in the purified His-ORC in this study, Pch2 could be utilizing, at least partially, the binding-surface that Cdc6 uses during replication, which could explain the high distributions of cross-links in the Orc1 and Orc2 subunits, as judged by our XL-MS data set. This hypothesis is consistent with our earlier data that showed that *in vivo* binding between Pch2 and ORC is independent of Cdc6 (see section 3.1.3 and Figure 3-3).

Mapping of the inter-molecular Pch2-ORC cross-links onto the ORC structure mentioned above (PBD 5v8f) allowed us to get an insight about the position of these cross-links within the ORC assembly. This crystal structure failed to cover some regions of ORC, so we were unable to map several Pch2-ORC cross-links within some ORC subunits (particularly, the Orc2, Orc5, and Orc6 subunits). By using the PyMOL software we

visualized that several Pch2-Orc1 cross-links were located in a region that is shielded by Cdc6 in the OCCM complex (PBD 5v8f) (Yuan *et al.*, 2017). This again reiterated that Pch2 could occupy, at least to some extent, common binding regions used by Cdc6 to engage ORC. As mentioned earlier, so far, there is only one putative model of the budding yeast Pch2 structure generated by SWISS-MODEL based on the structure from *C.elegans* PCH-2 (4xgu.1) (Ye *et al.*, 2015). Since Cdc6 is also an AAA⁺ ATPase, one possibility is that the ATPase domain of Pch2 occupies the region that Cdc6 employs to associate to ORC. Even if the theoretical model of Pch2 structure “fits” in the PBD 5v8f (after manually removing Cdc6 from the structure using PyMOL), this could be merely due to the fact that both, Pch2 and Cdc6 have to some extent similar protein sequences (75% sequence identity, as calculated by Blast2seq). Thus, this approach to evaluate whether Pch2 utilizes similar binding mode to Cdc6 to associate with ORC might have some constraints taking into consideration that most of the cross-links in the Orc1/Orc2 subunits correspond to cross-links from the NTD of Pch2. In addition, the idea that Pch2 might engage to ORC using common regions occupied by Cdc6 on ORC needs to be interpreted with caution, due to the differences in the ORC preparation as outlined above. However, it might hint to an interesting possibility that Pch2 and Cdc6 might engage ORC in a similar manner.

One interesting possibility that our work could not address is whether Pch2 might utilize binding surfaces similar to Cdc6 in order to bind to ORC, as our data suggest. To test this, we are currently generating yeast mutants in the Orc1 region (normally shielded by Cdc6) where we observed cross-links. We plan to use such alleles to address whether mutations in this region disrupt or affect Pch2 binding to ORC *in vivo* (by performing Co-IP assays). If this is the case, we would expect that mutations in this patch of ORC would show a similar phenotype to the *orc1-161* mutant (*i.e.* increased DSB formation at the rDNA boundaries). Our preliminary experiments ruled out the possibility that these amino acid substitutions in ORC could interfere with Cdc6 binding and thus, would affect cell viability. Another possibility is that this region of Orc1 is contributing to Pch2 binding, but mutations on it would not completely disrupt the association between ORC and Pch2 *in vivo*, since we have provided evidence that other ORC subunits are also involved in Pch2 interaction. Nevertheless, if that patch of Orc1 is important for Pch2 interaction, we would expect reduced binding between Orc1 and Pch2 in our co-IP experiments, at least to some extent. Similarly, if the contribution of this Orc1 region is only partial, we would expect a limited effect in DSB formation at the rDNA and we could assess this by Southern blot-associated quantification of

the DSB levels. Alternatively, we intend to do *in vitro* competition assays with purified components (His-MBP-Pch2, His-ORC and GST-Cdc6) to test whether Pch2 can compete for ORC binding when ORC is complexed with Cdc6. This should provide insights into whether Pch2 binding to ORC is compatible with Cdc6-ORC binding or if binding to ORC with Pch2 and Cdc6 is mutually exclusive also *in vitro*. Since our data suggested that Pch2 and Cdc6 might share common regions of interaction with ORC, another possibility to test whether Pch2 and Cdc6 compete for ORC binding is to address if the presence of Pch2 can interfere with the role of Cdc6 in MCM loading. MCM complexes loaded *in vivo* and in extracts remain bound to DNA even after a high-salt treatment (Bowers *et al.*, 2004; Donovan *et al.*, 1997). Work from others has used an *in vitro* set-up to detect recruitment and loading of MCM into origin DNA by combining the proteins needed for MCM loading (OCCM complex) in presence or absence of ATP/ATP γ S and performing low/high-salt washes (Remus *et al.*, 2009). All the experiments mentioned (co-IP assays, SB analysis, *in vitro* competition and MCM loading assays) have the potential of providing information of whether Pch2 shares binding properties with Cdc6 regarding ORC binding. Thus, we suggest that Pch2 and Cdc6 might utilize common binding sites to engage to ORC. This possibility remains to be addressed in future studies.

Despite all the aforementioned limitations, the XL-MS strategy employed here demonstrated that Pch2 establishes contacts with all the ORC subunits, reinforcing our previous data (co-IP experiments and *in vitro* assays) and the notion that Pch2 not only binds Orc1, but the entire ORC. Importantly, the XL-MS presented here suggested that Pch2 uses, not only its AAA⁺ ATPase core, but also its non-catalytical NTD to associate to ORC, in line with the role of the NTD in engaging partner proteins in other members of the AAA⁺ ATPase family. The role of the different domains of Pch2 is discussed in the following section. Additionally, our cross-link data further strengthened the central role of Orc1 in establishing the binding with Pch2. This possibility is further discussed in section 4.4.

4.3 Delineation of Pch2 reveals a minimum region sufficient for ORC binding

4.3.1 The NH₂-terminal domain (NTD) of Pch2 is necessary for ORC-binding

The investigations discussed in section 4.2 revealed a role of the NTD of Pch2 in the binding to ORC and it is well established that members of the AAA⁺ ATPase family use their non-catalytically NTD to engage clients/adaptors (Erzberger & Berger, 2006; Hanson &

Whiteheart, 2005; Meyer & Weihl, 2014; Tucker & Sallai, 2007). To systematically investigate the influence of Pch2-NTD in binding ORC, we initially performed Y2H assays with full-length (FL) Pch2 or with truncated versions of Pch2 containing either the NTD or the AAA⁺ ATPase domain and assessed the interaction with the Orc1 subunit. We showed that Pch2-FL interacted with Orc1, corroborating previous findings (Vader *et al.*, 2011) and our Co-IP results (Figure 3-9 B). Our Y2H assays identified the NTD of Pch2 as sufficient to binding to Orc1. By contrast, the AAA⁺ domain of Pch2 did not show interaction with Orc1, confirming the role of the Pch2 NTD in Orc1 binding and corroborating our XL-MS data (Figure 3-8). Hence, these results offer further proof for the role of the ATPase domain in the interaction with Orc1, lending support to our XL-MS data set, which identified several cross-links between different ORC subunits and the AAA⁺ core of Pch2. Here, the AAA⁺ ATPase domain of Pch2 could be either providing additional contacts for Orc1 binding or increasing local concentration of the NTD of Pch2 by a “crowding” effect due to hexamerization of Pch2, or a combination of both. Our investigations on the interaction between Orc1 (ORC) and either full-length Pch2 (3xFlag-Pch2-2-564) or a trimmed version containing Pch2-ATPase domain (3xFlag-Pch2-243-564) in meiotic G2/prophase, showed that both proteins were expressed at comparable levels and in a similar fashion during meiotic G2/prophase (Figure 3-9 C). By Co-IP we observed that the interaction between Pch2-ATPase domain and Orc1 was severely impaired, in agreement with the Y2H assay (Figure 3-9 D).

We considered the possibility that the impairment of the interaction between the Pch2-ATPase domain and Orc1 *in vivo* could be accounted for the mislocalization of this truncated version of Pch2 within the cell. In wild-type budding yeast meiosis, Pch2-FL accumulates mostly at the rDNA region of chromosome *XIII* (nucleolus), with a fraction associating to the synaptonemal complex (SC) along synapsed chromosomes (Börner *et al.*, 2008; Herruzo *et al.*, 2016; San-Segundo & Roeder, 1999; Subramanian *et al.*, 2016; Vader *et al.*, 2011). The nucleolar localization of Pch2 seems to be restricted to budding yeast, as in Pch2 orthologs in plants and worms, Pch2 is only localized to the SC (Deshong *et al.*, 2014; Lambing *et al.*, 2015; Miao *et al.*, 2013). We wondered if the severely reduced interaction between the ATPase domain of Pch2 and Orc1 could be due to the inability of Pch2-ATPase to be properly localized into the nucleolus, where the interaction with Orc1/ORC presumably occurs. Work from the San-Segundo laboratory recently reported the existence of a basic patch of 17-residues comprising from amino acid 42 to 58 that resembled a nuclear or nucleolar localization signal (NLS/NoLS) (Herruzo *et al.*, 2019). The deletion of this amino

acid stretch prevented localization of Pch2 to the nucleolus and its association with SC proteins. Since this potential NLS/NoLS is situated at the NTD, it is conceivable that the impaired interaction between the ATPase domain of Pch2 and Orc1 *in vivo* reflects a defect in the localization of this truncated Pch2 version. It is important to note that in the Y2H system interaction between the proteins occurs in the nucleus (since proteins are fused to the GAL4 activation/binding domain, which usually contains an NLS); however, our Y2H did not reveal interaction between Pch2-ATPase domain and Orc1, which at least partially, argues against the lack of this interaction being a consequence of the mislocalization of this protein. We aimed to test the possibility of the mislocalization of Pch2-ATPase domain, but our cell fractionation assays failed to provide a clear answer to the localization of this truncated protein.

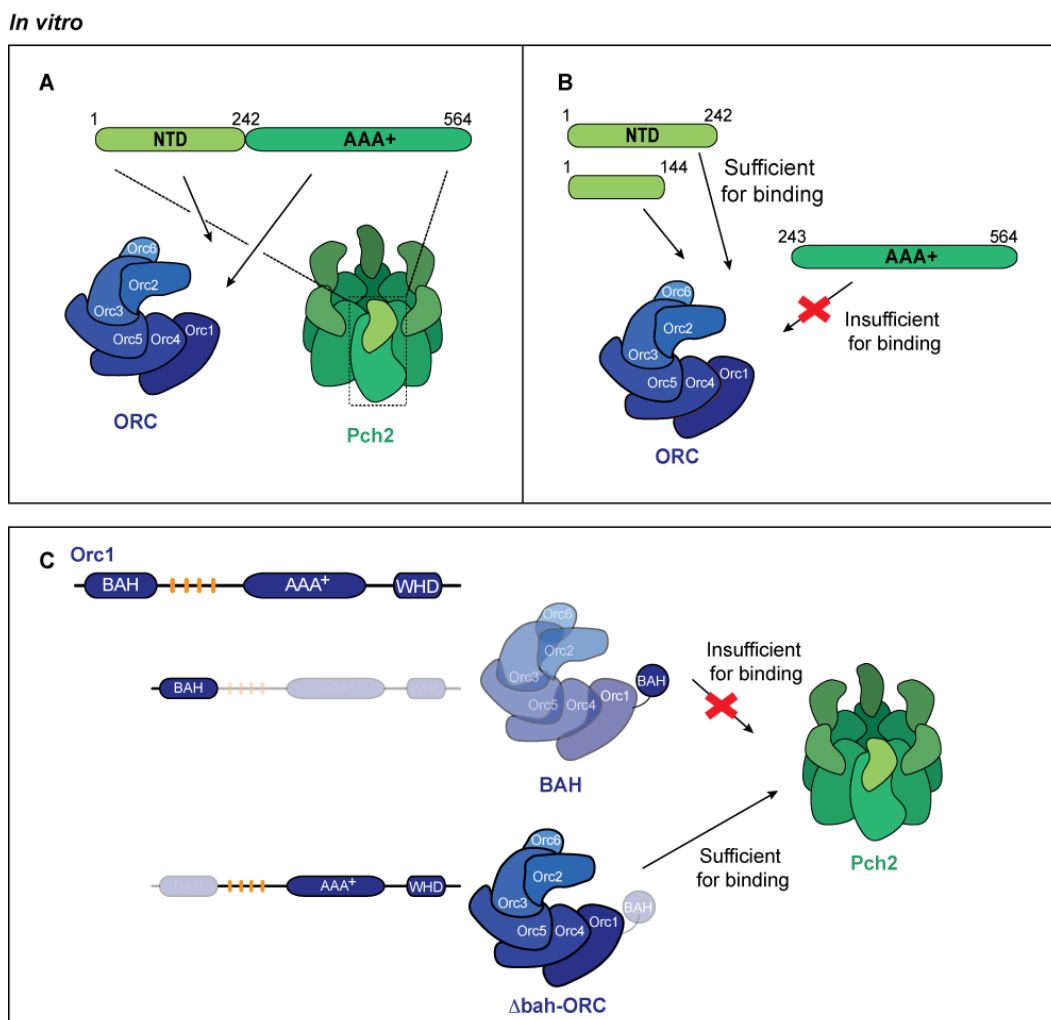


Figure 4-1 *In vitro* characterization of the interaction between Pch2 and ORC

A) Our *in vitro* data demonstrate that the homo-hexameric Pch2 (green) and the entire hetero-hexameric ORC (Orc1-6) (blue) interact directly, and suggest that Pch2 and ORC interact in an hexamer:hexamer manner. This interaction is mediated by binding between ORC and both domains of

Figure 4-1 (Continued)

Pch2, the non-catalytical NH₂-terminal domain (NTD, amino acids 1-242; light green) and the AAA⁺ ATPase domain (AAA⁺, amino acids 243-564; dark green). B) Disruption of the NTD of Pch2 abolishes the interaction with ORC *in vitro*. On the contrary, the NTD of Pch2 is sufficient for ORC binding and we delineated a minimal fragment of Pch2 (amino acids 1-144) that retains the ability to associate with ORC. C) The Bromo-adjacent homology (BAH) domain does not affect Pch2 engagement *in vitro*; Orc1's BAH domain is not sufficient to interact with ORC, and Δbah-ORC is able to interact with Pch2. The BAH domain of ORC is represented as an “extension” of ORC for clarity. Red cross indicates impairment of the interaction. Orange lines represent the basic patch of Orc1 (Orc1-BP), involved in origin recognition. These representations are based on *in vitro* experiments presented here, including analytical size exclusion chromatography (SEC), pull-down assays and cross-linking mass spectrometry (XL-MS).

To circumvent the possible effects of the mislocalization of the Pch2-ATPase domain on its association with Orc1/ORC, we tested this interaction *in vitro*. Importantly, we were unable to detect an interaction using purified His-MBP-Pch2-243-564 and His-ORC, which is in agreement with our *in vivo* data. These findings suggest that even if the ATPase core of Pch2 contributes to ORC binding (as judged by several cross-links revealed by XL-MS between the ATPase core of Pch2 and several ORC subunits, and by the stronger binding of Pch2-FL as compared to the Pch2-NTD, as shown by Y2H), it is not *per se* sufficient to engage ORC. It is worth mentioning that the SEC profile of His-MBP-Pch2-243-564 indicated that this truncated protein eluted at an apparent size indicating either a more extended shape or a less organized assembly, as compared to Pch2-FL (Figure 3-9 F). These data, together with *in vitro* findings using specific mutations of Pch2 NTD discussed below (see section 4.3.3), suggested a role for the NTD in stabilizing and/or maintaining Pch2 into a well-order hexameric assembly. Hence, we cannot rule out at this point that the lack of interaction between His-MBP-Pch2-243-564 and His-ORC could be accounted for an alteration in the conformation in the former protein.

We next investigated whether the NTD of Pch2 played a role in suppressing meiotic DSB formation at the rDNA in G2/prophase and showed, by Southern blotting, that yeast strains harboring 3xFlag-Pch2-243-564 exhibited DSB formation at the right flank of the rDNA, as observed in a *pch2Δ* background (Figure 3-9 E) (Figure 4-2). This is in agreement with our *in vivo* and *in vitro* interaction studies since we expected that the impaired interaction with Orc1/ORC seen in this construct would phenocopy *pch2Δ* with regard to DSB formation at the rDNA-proximal regions. Thus, the results discussed here provided

further evidence for a role of the NTD domain of Pch2 in engaging Orc1/ORC, both *in vivo* and *in vitro*. Even if a study suggested the presence of an NLS-like stretch in the NTD of Pch2 of BR strains, a substitution of the proposed NLS of Pch2 by a canonical SV40 NLS brought back Pch2 to the nucleus but did not completely restore the normal distribution of Pch2 in the nucleolus, as it would be expected (Herruzo *et al.*, 2019). To completely exclude the effects of truncating the Pch2 NTD in cellular localization, future work should focus on immunofluorescence assays to show the localization of Pch2 and its ATPase domain in yeast cells of the SK1 background used here. Moreover, we find likely that the truncation of the NTD of Pch2 leads to changes in the structural organization of Pch2 that could account for the effects of the interaction with Orc1, at least partially. This is in line with our *in vitro* data, which pointed towards the disruption of the NTD altering the conformation of the Pch2 assembly. Research with multiple members of the AAA⁺ ATPase family has provided a firm understanding about the role of the NTD in recognizing and binding clients or adaptors (see section 1.4) (Erzberger & Berger, 2006; Hanson & Whiteheart, 2005; Meyer & Wehl, 2014). However, to our knowledge, only a few studies have addressed the possibility of a function of the NTD of AAA⁺ ATPases in the proper oligomerization of these proteins.

As mentioned earlier, research with these enzymes has shown that oligomerization and, particularly, hexamerization occurs via interactions among their AAA⁺ core, but previous work might have disregarded possible collaborative effects of the NTDs in the appropriate formation of oligomers. Such a role of the NTD has been shown for the *Escherichia coli* AAA⁺ ATPase FtsH, a metalloprotease involved in the degradation of integral membrane proteins (Akiyama & Ito, 2000). This protein consists of an N-terminus with a membrane-targeting domain, which is involved in engaging membrane-embedded proteins, and an AAA⁺ module that is followed by a C-terminal protease domain, and its main function is to maintain the integrity of the cellular envelope by removing misfolded membrane proteins. Like other AAA⁺ enzymes, FtsH has a homo-oligomeric structure and it has been shown that the N-terminal region mediates the interaction between the FtsH subunits and thus, is required for oligomerization (Akiyama & Ito, 2000; Akiyama *et al.*, 1995). Hence, the NTD of Pch2 might have collaborative effects and contribute to oligomer formation and thus, disruption of this domain could lead to the observed impairment of the interaction between Pch2-AAA⁺ ATPase domain and Orc1.

4.3.2 Functional dissection of the NTD of Pch2

So far, we provided evidence that the Pch2-NTD is necessary for the interaction between Pch2 and ORC and to prevent DSBs at the rDNA border. Our Y2H assays suggested that the NTD of Pch2 is sufficient for Orc1 binding (Figure 3-9 B), and our XL-MS analysis also revealed several cross-links between distinct ORC subunits and peptides from the NTD of Pch2 (Figure 3-8 and 7-8). Alignment of the protein sequences of Pch2 and Pch2 orthologs of different species revealed the existence of an extended region of the NTD of Pch2, which is present only within yeasts, but not in the mammalian orthologs of Pch2 (TRIP13) in *Mus musculus* or *Homo sapiens* (Figure 7-2, Appendix). We performed truncations of the N-terminus of Pch2, based on sequence conservation and secondary structure predictions guided by the aforementioned alignments, to identify the minimal region of Pch2-NTD that is able to recapitulate this interaction (Figure 3-10 A). This approach allowed us to delineate a minimal region that shows interaction with Orc1, comprising amino acid 2 to 144 of Pch2-NTD (Figure 3-10).

To test whether this fragment can recapitulate binding to ORC, we reconstituted the interaction between His-MBP-Pch2-2-144 and ORC *in vitro*. Purification of recombinant His-MBP-Pch2-2-144 displayed two elution peaks (Figure 7-6 D). We attributed this peak (with a higher molecular weight close to the void) to the formation of a bigger assembly due to aggregation of this construct, possibly due to the lack of the ATPase module and misfolding of the protein. The elution profile of the second peak suggested monomeric formation of His-MBP-Pch2-2-144. This observation corroborated the effects seen in the elution profile of other fragments of the NTD (His-MBP-Pch2-2-233 and His-MBP-2-257; not shown here) and is in line with a role of the ATPase core in promoting and maintaining a proper oligomeric formation. We were able to show by SEC that the second elution peak stayed in a seemingly monomeric conformation, as expected since this construct lack the hexamerization (ATPase) domain. By pull-down assays, we demonstrated that the apparent monomeric His-MBP-Pch2-2-144 retained its ability to interact with ORC *in vitro* (Figure 3-10 C and D), which is in good agreement with the XL-MS data in which we detected several cross-links between ORC and peptides of Pch2 within the 2-144 region. However, we observed a substantial decrease in the interaction as compared to the binding detected in the pull-down experiments using Pch2-FL. This finding further supported the idea that the AAA⁺ ATPase domain of Pch2 contributes to Pch2-ORC binding (although it is not sufficient for binding to ORC), as our XL-MS data suggested. In addition, the decreased *in vitro* binding with respect to Pch2-FL

concur well with the fact that Pch2 AAA⁺ ATPase domain seems to retain certain degree of ability to interact with Orc1-TAP, and that interaction between the Walker A mutant of Pch2 (Pch2-K320R), which affects ATP binding and hexamerization *in vivo*, and Orc1-TAP was severely impaired *in vivo* (see section 3-1 C) (Herruzo *et al.*, 2016). We showed by pull down that the interaction between His-MBP-Pch2-2-144 and His-ORC was weaker compared to FL-Pch2. We speculate that the lower interaction seen with His-MBP-Pch2-2-144 accounted for the lack of hexamerization of this protein. In this case, we would expect a stronger binding to His-ORC by increasing the local effective concentration of His-MBP-Pch2-2-144 in solid-phase pull-down assays, which we indeed were able to show (Figure 3-10 D).

Thus, the results discussed in this section provided further evidence for a role of Pch2-AAA⁺ ATPase domain in providing additional contributions to the binding to ORC. More importantly, the findings presented here demonstrated that the N-terminus of Pch2 is sufficient for ORC binding and we further delineated a minimal region of Pch2 that is able to sustain association with ORC. In addition, a large stretch of the Pch2 NTD is only conserved within yeasts (Figure 7-2) and it is possible to speculate that the extended NTD of Pch2 in *S. cerevisiae* arose to mediate a specific role of Pch2 in rDNA protection in meiotic G2/prophase (potentially by mediating its binding to ORC). With respect to this, it is worth mentioning that Pch2 is only localized in the nucleolus in yeast (where the rDNA, which has a special heterochromatin structure defined by Sir2-deacetylation, assembles), whereas Pch2 performs other non-nucleolar-associated roles in higher organisms. Though, it is worth mentioning that even if the NTDs of Pch2/TRIP13 are different, both regions maintain the potential to interact with HORMA-domain-containing proteins (Hop1/meiotic HORMADS and p31 (comet)) (Chen *et al.*, 2014; West *et al.*, 2018; Ye *et al.*, 2015).

4.3.3 Point mutations in the NTD of Pch2 disrupt ORC-binding

Our Y2H assays (Figure 3-11 A and B) unveiled that upon deletion of the first 12 amino acids of the minimal region of Pch2 sufficient for ORC binding *in vitro* (Pch2-2-144), Pch2 was unable to interact with Orc1. This result was recapitulated by a construct of Pch2 in which only these 12 aa were truncated (Pch2-13-564) (Figure 3-11). Nevertheless, we also showed that these amino acids are not sufficient for binding to Orc1 since several truncated Pch2 fragments (Pch2-2-121, Pch2-2-91, Pch2-2-60, Pch2-2-27) harbouring these residues were also not able to interact with Orc1, by Y2H assays. Although these residues located in the outermost region of Pch2 NTD are not sufficient for Orc1 binding, our findings hinted

towards a contribution of this small patch of residues in the interaction between Pch2 and Orc1.

As stated above, by sequence alignments, we showed that there is a strong conservation of the first stretch of amino acids of Pch2 NTD, only within the budding yeast *Saccharomyces* class, and that this region might be folded into a β -strand, in base of PSIPRED secondary structure predictions (Figure 7-2). We identified several conserved residues within the amino acid stretch comprising residues 1-12 (V5, D6, V9, R10) and our Y2H assays with pair-wise mutations of these amino acids (V5AD6A and V9AR10A) showed that substitution of these residues abolishes interaction with Orc1, confirming a role of these amino acids in associating with Orc1. Our Western blotting analysis of these Pch2 mutated versions argued against the possibility that the lack of interaction seen by Y2H could be due to issues with protein expression of these constructs (*i.e.* the protein is unstable or degraded).

We next approached the *in vitro* reconstitution of the interaction between these mutants (His-MBP-Pch2-V5D6 or His-MBP-Pch2-V9R10) and purified His-ORC. By SEC, we observed that His-MBP-Pch2-V5D6 and His-MBP-Pch2-V9R10 seem to form higher molecular weight assemblies or more elongated conformers, as compared to the His-MBP-Pch2. We noticed that the elution profile of these mutants bore a high resemblance with the elution profile of the ATPase domain of Pch2 (His-MBP-Pch2-243-564) (Figure 3-9), which reinforces the idea that the NTD of Pch2 plays a critical role in oligomerization or in maintaining the proper organization of the Pch2 assembly, as seen in other AAA⁺ ATPases (Akiyama & Ito, 2000; Akiyama *et al.*, 1995). Together with these observations in the SEC elution profiles, our attempts to purify these Pch2 mutants yielded low amounts of protein, which precluded us from pursuing *in vitro* experiments with these Pch2 mutants.

Since we had previously shown by Co-IPs experiments that Orc1-TAP interacts with 3xFlag-Pch2 (Figure 3-9 D), we opted for testing the *in vivo* interaction between either 3xFlag-Pch2-V5AD6A or 3xFlag-Pch2-V9AR10A and Orc1-TAP by Co-IP assays, as an alternative to the *in vitro* approach. As we suspected that such mutations in the NTD of Pch2 could cause protein misfolding or aggregation, based on the elution profiles by SEC (see above), we designed an experimental set-up to determine whether this was the case as well *in vivo*. We were able to demonstrate that Pch2 harboring the abovementioned point mutations retained the ability to interact with 3xHA-Pch2-E399Q *in vivo* (Figure 3-11 D), indicating that these Pch2 mutants are able to interact with other Pch2 subunits and likely, that

oligomerization of these mutants is not compromised. Although we cannot completely exclude that there are partial or subtle effects of these mutations in the overall Pch2 organization, these results argued against the fact of these mutants being completely misfolded and provided further evidence that these mutants are stable in meiosis. In agreement with this, we showed that these mutants are expressed during meiosis at similar levels and timing as the wild-type Pch2. Co-IP experiments performed in this study substantiated our previous Y2H findings, which already suggested that the abovementioned mutations within Pch2-NTD disrupt the interaction with Orc1 (Figure 3-11 E). Thus, we provided evidence that the interaction between 3xFlag-Pch2-mutants and Orc1 during meiotic G2/prophase is severely impaired (Figure 3-11). Further experiments should intend to optimize the protein purification yield of His-MBP-Pch2-V5AD6A and His-MBP-Pch2-V9AR10A, and test their ability to *in vitro* interact with purified His-ORC. These experiments should recapitulate a decrease in the interaction between ORC and Pch2 carrying the point mutations.

We then hypothesized that 3xFlag-Pch2-V5AD6A and 3xFlag-Pch2-V9R10A would phenocopy the rDNA-associated effects seen in a *pch2Δ* background since mutations of these Pch2-NTD residues impaired binding to Orc1 *in vivo*. As hypothesized, we detected increased levels of DSBs at the right flank of the rDNA by Southern blotting in these Pch2 mutants (Figure 3-11 F), reinforcing the notion that these amino acids are required for the functionality of Pch2 with Orc1 in budding yeast meiosis. Further experiments should be performed in order to assess the localization of these proteins (*i.e.* immunofluorescence studies showing localization of these mutated proteins in the nucleolus, as previously reported for wild-type Pch2) and exclude that the rDNA-associated phenotype of these mutants is a consequence of their mislocalization (San-Segundo & Roeder, 1999; Subramanian *et al.*, 2016; Vader *et al.*, 2011) (Figure 4-2). As mentioned earlier, a previous study proposed the existence of a nuclear localization signal (NLS)-like patch within the NTD of Pch2, whose deletion impairs Pch2 localization in the nucleolus (Herruzo *et al.*, 2019). However, this region comprises a stretch of amino acids (amino acids 42 to 58 of Pch2) that is present in our point mutants. Altogether, we believe that the observed effects in terms of interaction with Orc1 and rDNA-associated phenotype in these mutants indicate a contribution of these amino acids to the function of Pch2 at the rDNA.

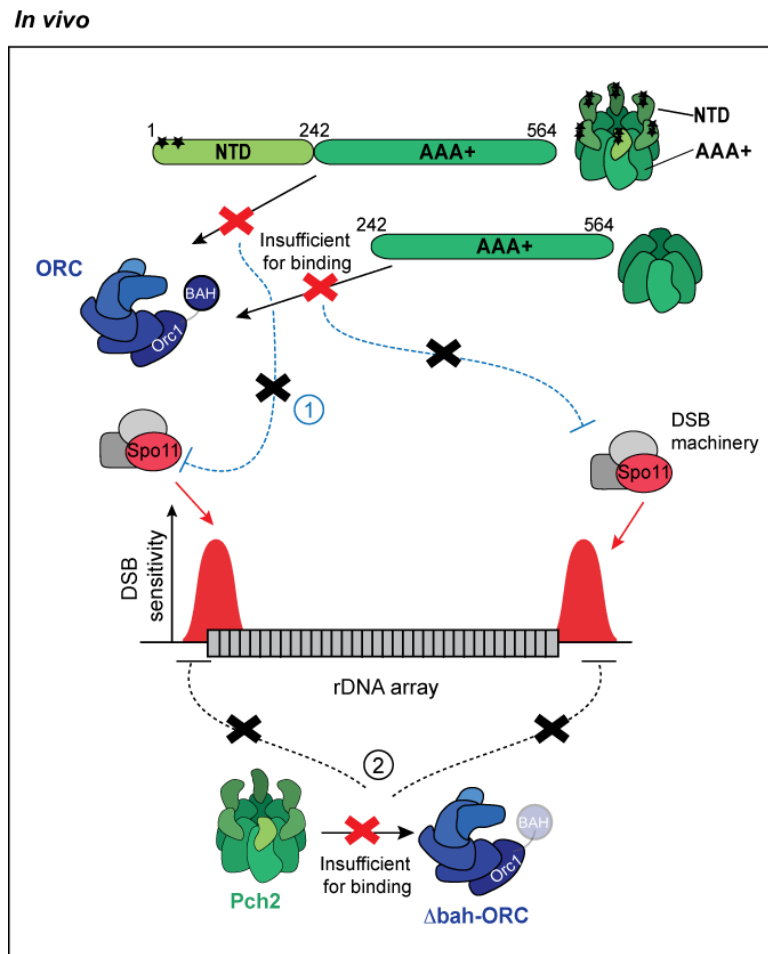


Figure 4-2 Delineation of the Pch2-ORC interaction in terms of rDNA-associated DSB formation

Point mutations in the NH₂-terminal domain (NTD) of Pch2, as well as deletion of Pch2's NTD, disrupt association with ORC *in vivo*, leading to the increased DNA double-strand break (DSB) formation at the rDNA boundaries (1). Deleting the Bromo-adjacent homology (BAH) domain of Orc1 abolishes interaction with Pch2, equally leading to increased DSBs at the rDNA borders (2). Note that deletion of the BAH domain does not affect the association between ORC and Pch2 *in vitro*. We hypothesize that the effects of deleting Orc1's BAH domain in the Pch2-ORC rDNA associated function observed *in vivo* indicate a crucial role of Orc1 in enabling localization of Orc1/ORC to specific (yet to be known) non-ARS sites, derived from the ability of the BAH domain to "sense" the chromatin status and the specialized repressed chromatin present within the rDNA. Red cross indicates impairment of the interaction between Pch2 (and Pch2 mutants) and ORC/Δbah-ORC. Black cross represents the disruption of the protective function of Pch2 and ORC at the rDNA boundaries, which leads to the increased meiotic DSB formation at the rDNA edges (depicted in red) by the DSB machinery (of which Spo11 is the catalytic core).

An interesting avenue for future research would be to test whether these amino acids of Pch2 are not only important for Pch2 function with Orc1 to promote rDNA-boundary protection against DSBs, but also for other Pch2 functions. Pch2 interacts with the SC axis

protein Hop1 *in vitro* and it uses its ATPase activity to displace Hop1 from DNA upon chromosome synapsis (Chen *et al.*, 2014). Mutants of the central SC protein Zip1 fail to synapse and undergo a pachytene-checkpoint meiotic arrest. Hop1 is also involved in this checkpoint since its phosphorylation at Thr318 by the Mec1/Tel1 kinases is necessary for Mek1 activation (see Introduction) (Börner *et al.*, 2008; Herruzo *et al.*, 2016; Subramanian *et al.*, 2016). Pch2 functions to remove Thr318-phosphorylated Hop1 from synapsed chromosomes and thus, defects in synapsis can be read out in terms of Hop1-pThr318 accumulation. Further research should focus on testing whether Pch2 carrying the point mutations discussed here can perform the Pch2-Hop1 meiotic role. If these amino acids are not important for Pch2-associated removal of Hop1-pThr318, these mutants should rescue Pch2 function in an *ndt80Δpch2Δ* background (*i.e.* Thr318-phosphorylated Hop1 should be removed; *ndt80Δ* is a pachytene-arrest background). We have already generated strains carrying these Pch2 mutants in an *ndt80Δ* background.

In addition, Pch2 promotes inter-homolog (IH) bias, with partial redundancy with another protein called Rad17 (Ho & Burgess, 2011; Wu & Burgess, 2006). A hallmark of mutants defective in IH bias is the formation of unviable spores. Whereas *rad17Δ* and *pch2Δ* single mutants give 37.1% and 92.2% of viable spores, respectively, *rad17Δpch2Δ* double mutant yields <0.1% of viable spores, indicating that these proteins have partially redundant roles to achieve the recombination bias. Our preliminary experiments to investigate if the V5D6 and/or V9R10 residues have a role in this process (by assessing spore viability in strains carrying these mutants in a *rad17Δpch2Δ* background) seemed to indicate that these residues also play a function in the IH role of Pch2 since these mutated versions of Pch2 are not able to restore *pch2Δ*, as judged by spore viability). Previous work has proposed that Pch2 acts in IH bias by direct interaction with the N-terminal region of Xrs2 (a component of the MRX complex) and it is conceivable to imagine that disruption of residues V5D6 or V9R10 of Pch2 could affect this interaction and thus, Pch2-mediated IH role. These preliminary results suggest that these Pch2 amino acids might be critical for Pch2 functions beyond rDNA protection.

In conclusion, the findings discussed here imply that amino acids (V5D6/V9R10) situated within a limited stretch of Pch2 that is conserved only among budding yeasts are crucial in the establishment of a binding interface with Orc1 and thus, for Pch2-Orc1 functionality at the rDNA boundaries. Moreover, our preliminary findings suggest that these

residues might be important to perform other Pch2-associated processes during meiotic G2/prophase, presumably by mediating the interaction of Pch2 with other factors.

4.4 Orc1 has a prominent role in mediating interaction with Pch2

Although several ORC subunits have been involved in functions beside DNA replication in budding yeast (such as the role of the Orc1 subunit in establishing transcriptional silencing at the mating-type loci and Orc2 function in mediating sister-chromatid cohesion), all these roles seem to be executed in concert with the other ORC subunits (*i.e.* the ORC proteins described to perform these roles, Orc1 and Orc2, are assembled with the other subunits to constitute ORC) and, up to our knowledge, there is not a cellular function performed by a distinct ORC subunit alone in budding yeast (Hemerly *et al.*, 2009; Nguyen *et al.*, 2015; Popova *et al.*, 2018; Suter *et al.*, 2004; Triolo & Sternglanz, 1996).

Here, we provided the first evidence that Pch2 interacts with multiple ORC subunits, both *in vivo* and *in vitro*. *In vivo*, Orc1/Orc2/Orc5 immunoprecipitate Pch2-FL (Figure 3-2), suggesting that the entire ORC is involved in associating with Pch2 during the meiotic G2/prophase. *In vitro*, we have reconstituted the Pch2-ORC macromolecular assembly, demonstrating that interaction between these two AAA⁺ ATPases is direct, and our XL-MS data confirmed that Pch2 establishes contacts with several ORC subunits (Figure 3-8). Nonetheless, along with the investigations presented here we noted several cues, suggesting that within ORC, Orc1 might be the critical subunit for Pch2-ORC association or might have a distinctive contribution towards this binding. First, as already discussed in section 4.2.1, we have shown that Pch2-E399Q consistently co-immunoprecipitated Orc1-TAP more efficiently than Orc2-TAP or Orc5-TAP during meiosis (Figure 3-2 C). Second, we observed a similar behavior in the *in vitro* pull-downs using His-MBP-Pch2-2-144 and His-ORC, in which binding of this trimmed Pch2 protein seemed to be more evident and specific with Orc1 than with the other subunits (Figure 3-10 D). Third, our XL-MS revealed inter-molecular cross-links containing peptides from Orc1 and the His-MBP-moiety that is NH₂-terminally fused to Pch2 in the purified His-MBP-Pch2. By contrast, the XL-MS approach did not reveal cross-links between MBP and other ORC subunits. Since efficient cross-linking in the strategy employed depends on the proximity of Cα's of cross-linked amino acids, these data implied that Orc1 is positioned close to MBP and, by extension, Pch2 (Pan *et al.*, 2018). Forth, by Y2H assays we were able to reproduce the interaction between Orc1 and Pch2 previously

reported by Vader *et al.*, but we did not observe an interaction between any of the other individual ORC subunits tested (Orc2, Orc3, Orc4, and Orc6) and Pch2, reinforcing the idea that Orc1 is crucial to establish Pch2-ORC binding (Vader *et al.*, 2011).

To further test whether Orc1 plays a central role in the Pch2-ORC association, we performed Co-IP assays to examine the interaction between Pch2 and TAP-tagged Orc2/Orc5 in a strain in which Orc1 protein levels are impaired by using the *orc1-161* mutant. Strains harboring the *orc1-161* allele grow normally at the permissive temperature (23 °C), but shift to 37 °C results in DNA replication defects, cell cycle delay and rapid loss of viability (Gibson *et al.*, 2006). This allele causes increased DSB formation at the rDNA boundaries, the same phenotype as *pch2Δ* (Vader *et al.*, 2011) (Figure 4-3).

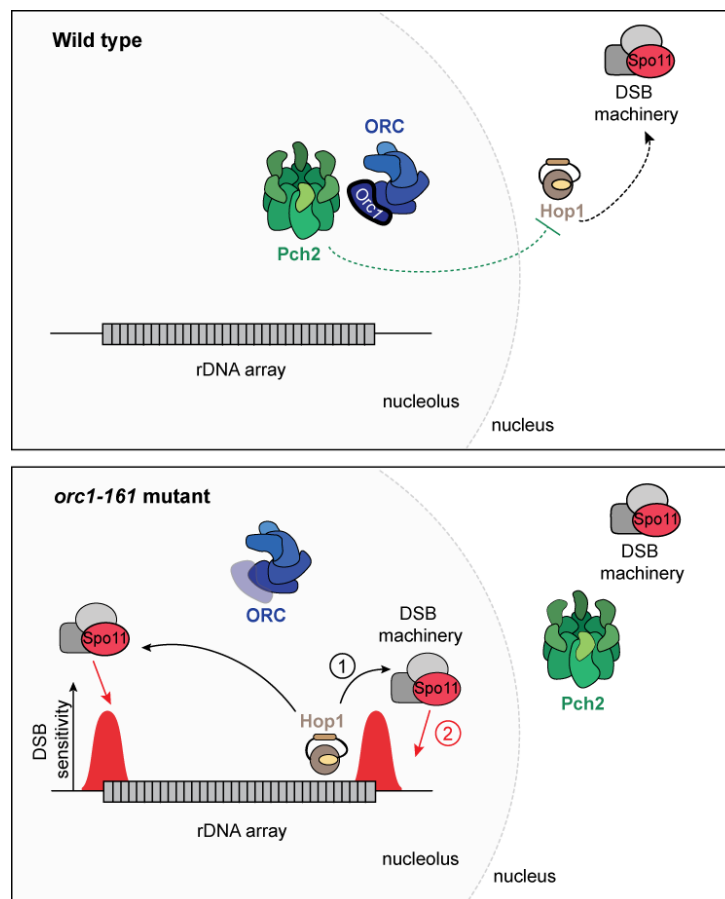


Figure 4-3 Simplified model of Pch2 and ORC function at the budding yeast ribosomal DNA (rDNA)

In a wild type strain, Pch2 localization to the nucleolus is driven by ORC-mediated recruitment. Pch2 associates with the entire ORC, although among the ORC members, the Orc1 subunit seems to play a critical role in Pch2-ORC functionality at the rDNA. Pch2 likely prevents formation of DNA double-

Figure 4-3 (Continued)

strand breaks (DSBs) by excluding from the nucleolus the HORMA-domain containing protein Hop1, which is necessary for DSB formation by the DSB machinery (of which Spo11 is the catalytic core). In the *orc1-161* mutant, Pch2 fails to localize in the nucleolus due to the impairment of Orc1 protein levels in this mutant. The lack of Pch2 recruitment to the nucleolus would enable Hop1 (depicted in brown) localization in this nuclear structure (1), which would in turn lead to formation of DSB at the rDNA boundaries (indicated in red) by the DSB machinery (2). Note that the nucleolus is a membraneless “organelle” and the gray dotted line represents the hypothetical boundary between nucleolus and nucleus for simplicity. These schematics are based in work published by others (San-Segundo and Roeder, 1999; Vader *et al.*, 2011; Herruzo *et al.*, 2016) and our findings presented here.

We thus reasoned that impairing Orc1 protein levels by using the *orc1-161* allele would lead to a decrease association between Pch2 and other ORC subunits. Indeed, we demonstrated that Orc2-TAP and Orc5-TAP cannot immunoprecipitate 3xHA-Pch2 or 3xHA-Pch2-E399Q, respectively, in this mutant. These findings strengthened the idea that Orc1 is the main binder of Pch2. However, another possibility is that the ORC assembly is dismantled when Orc1 is absent and therefore prevent binding of Pch2 with Orc2/Orc5. In addition, it was previously reported that in the *orc1-161* background, Pch2 fails to localize to the nucleolus and it is thus, plausible that the absence of interaction between Orc2/Orc5 and Pch2 is due to the loss of Pch2 location (Vader *et al.*, 2011). Alternatively, regardless of Pch2 location, Orc1 could be its main binder within ORC and/or presence of Orc1 could be strictly required for Pch2 to bind and therefore, impairment of Orc1 would not favor Pch2 association with Orc2/Orc5.

Taken together, the data discussed here provide evidence that even if Pch2 is able to bind to ORC, the largest subunit of this complex (Orc1) seems to be the core binder of Pch2. These findings point towards a situation in which Orc1 potentially provides the main surfaces to bind Pch2 and the other ORC subunits contribute or help in Pch2 association. Although we have demonstrated that Orc1 is required for Pch2-ORC binding, whether Orc1 alone is sufficient to bind Pch2 remains to be addressed. Testing this possibility *in vivo* is intrinsically challenging, as we would have to impair all ORC subunits but Orc1, which would result in defects in DNA replication and unviability (since all the ORC components are essential for cell growth) (Dillin & Rine, 1995; Foss *et al.*, 1993; Fox *et al.*, 1995; Gibson *et al.*, 2006). As another approach to tackle this question, we aim to test the *in vitro* interaction between purified His-Orc1 and His-MBP-Pch2. Up to our knowledge, biochemical and structural

studies have solely focused on the entire ORC, and the purification of individual ORC subunits has not been yet reported, probably due to their instability once not bound or relying on other ORC components for their stability. However, our preliminary expression tests using insect cells showed efficient expression of His-Orc1 alone and we aim to further purify this protein and probe the interaction with Pch2 *in vitro*. If Orc1 is the core binder and the other ORC subunits are merely providing additional binding surfaces, we expect binding between His-Orc1 and His-MBP-Pch2, probably to a reduced extent, as would be presumed due to the absence of the other binding regions within other ORC subunits. By contrast, if we are not able to recapitulate binding *in vitro* between His-MBP-Pch2 and His-Orc1, this would indicate that Pch2 indeed needs other ORC subunits to bind to Orc1, being either because Orc1 necessitates the other ORC subunits to be properly assembled or because, even if Orc1 is the central binder of Pch2, it is not sufficient for Pch2 association.

In short, we have provided several pieces of evidence that appear to indicate that Orc1 is the main binder of Pch2 within the ORC complex. So far, it remained unexplored whether other ORC subunits are implicated, not only in binding to Pch2 but also in ORC-Pch2 functionality at the rDNA, discussed in the next section.

4.5 Orc2/Orc5 subunits are dispensable for Pch2-ORC mediated DSB protection at the rDNA

A number of studies have provided evidence that the chromosome-associated processes attributed to yeast ORC rely on ORC integrity and association of this complex to specific sites (origins of replication or autonomously replicating sequence, ARSs) (Foss *et al.*, 1993; Shimada & Gasser, 2007; Suter *et al.*, 2004). Moreover, in vegetatively growing *S. cerevisiae* ORC seems to associate with replication origins throughout the cell cycle (DePamphilis, 2005; Diffley *et al.*, 1995; Liang & Stillman, 1997). So far, it was known that the Orc1 subunit is needed for Pch2 functionality at the rDNA, but whether other subunits of ORC are also necessary to prevent rDNA-proximal meiotic DSB formation remained unclear. Based on our interaction studies between Pch2 and ORC and the current literature on ORC, we hypothesized that the entire ORC would play a role in protecting the rDNA-boundaries against DSB formation during meiosis.

4.5.1 Efficient depletion of distinct ORC subunits

Since all ORC subunits are necessary for cell growth and mutations in ORC genes cause defects in DNA replication, we sought to employ conditional mutants of specific ORC subunits to assess DSB formation at the rDNA. We pursued different strategies that allowed us to deplete distinct ORC members. Initially, we generated strains carrying the *ts*-mutants of Orc2 (*orc2-1*) and Orc5 (*orc5-1*). Such *ts*-mutants have been extensively used to explore ORC function in yeast during mitosis (Bell, 2002; Dillin & Rine, 1995; Foss *et al.*, 1993; Fox *et al.*, 1995; Shimada *et al.*, 2002). For instance, the *orc2-1* mutant causes cell cycle arrest at the restrictive temperature, indicative of defects in DNA replication. This mutant also disrupts silencing at the mating-type loci even at the permissive temperature (Foss *et al.*, 1993). Expression of the *orc2-1* mutant is decreased at the permissive temperature, accounting for approximately 10% of protein levels relative to wild-type Orc2 (Shimada *et al.*, 2002). We initially tested that *orc2-1* and *orc5-1* alleles impaired these subunits in mitosis, as judged by cell growth spotting assays at the permissive (23°C) and restrictive temperatures (34°C). We noted that the *ts*-strains showed poor growth in the pre-sporulation media that often impeded the execution of our meiotic time-courses. In addition, we observed differences among these mutants, as judged by flow cytometry analysis, in which the *orc1-161* strains showed more acute defects in DNA replication than the *orc2-1* and *orc5-1* strains (not shown here). Thus, we reasoned that these differences would hinder the interpretation of the Southern blotting experiments used to detect meiotic DSBs. Moreover, by using these mutants it is not possible to exclude side effects caused by the temperature shift, especially considering that meiosis itself is sensitive to the high temperature necessary to completely inactivate the *ts*-alleles.

Therefore, we established another approach that enabled us to deplete distinct ORC subunits in a reliable and reproducible manner. Besides the use of ORC *ts*-mutants, only an additional system has been used to deplete a selected ORC subunit (Orc2) during budding yeast mitosis (Shimada & Gasser, 2007; Shimada *et al.*, 2002). This approach used an *orc2-1* copy placed under the control of the GAL UAS promoter (*pGAL::orc2-1*), which allows high expression of *orc2-1* in medium containing galactose (even when cells are grown at 37 °C), but the gene is tightly repressed in the presence of glucose-containing medium. This approach would not be feasible for meiosis since the “on/off switch” depends on the presence of carbon sources in the medium, which is not compatible with meiotic induction that requires carbon source limitation to commit to the meiotic programme.

As an alternative approach to the *ts*-mutants and the glucose repression system, we employed the anchor-away method to deplete distinct ORC subunits (Orc2 and Orc5) (Haruki *et al.*, 2008). This method relies on the inducible dimerization of FKBP12 (FK506 binding protein) and FRB (FKBP12-Rapamycin Binding-FRB domain of human mTOR)-tagged proteins that enables rapid functional depletion of nuclear proteins based on the extensive ribosomal flux. By using FKBP12 as anchor protein and adding rapamycin, a drug that simultaneously binds to FRB and FKBP12, a ternary complex forms with the protein of interest, which is tagged with FRB (Figure 3-12). Thus, the anchor-away method allows the re-direction of proteins from the nucleus to the cytoplasm. Several groups have proven the ability of this technique to deplete chromosomal factors in budding yeast, including a nucleolar protein, Rpa135, a subunit of the RNA polymerase I, and several proteins also in meiosis (Albert *et al.*, 2016; Cardoso da Silva *et al.*, 2019; Subramanian *et al.*, 2016; Vincenten *et al.*, 2015). However, no studies employing the anchor-away technique to deplete selected ORC subunits, neither in mitosis nor in meiosis have been described so far.

By viability assays, we showed that strains carrying FRB-tagged *ORC2* or *ORC5* alleles exhibit growth defects in mitotically proliferating cells in the presence of rapamycin, indicating DNA replication defects and thus, efficient nuclear depletion. In addition, by querying DNA replication in logarithmically growing cultures, we demonstrated that rapamycin treatment in the *orc2-FRB* and *orc5-FRB* backgrounds caused the accumulation of $2N$ -containing cells (*i.e.* cells with unreplicated DNA) after 90-180 minutes from the addition of rapamycin, indicating that DNA replication was defective (Figure 3-12), and thus, that Orc2 and Orc5 are functionally depleted upon the addition of rapamycin in vegetatively growing cells. Contrary to the *ts*-mutants (in which we observed growth disparities among the *orc1-161*, *orc2-1* and *orc5-1* *ts*-yeast strains), cells containing the *orc2-FRB* or *orc5-FRB* alleles appear to progress similarly through both, mitosis and meiosis (as judged by analysis of DNA content by flow cytometry) (Figure 3-12 C and 3-13 B, and see below), emphasizing the validity of the anchor-away technique. Another reason why we favored the use of this technique as a system to functionally deplete distinct ORC subunits, rather than the *ts*-mutants, is that the former system enables a more tight regulation since it is possible to control the timing of the depletion by the addition of rapamycin. Taken together, we established an efficient and reliable system that allows the depletion of selected ORC subunits (Figure 4-3 and 4-4).

4.5.2 ORC might not need to associate with ARS sequences for its rDNA protective function

We next tested whether impairment of Orc2 or Orc5 by the anchor-away technique caused a similar phenotype during meiotic G2/prophase than impairment of Orc1. In contrast to the experiments with mitotically dividing cells, our meiotic time courses showed that pre-meiotic DNA replication timing in the *orc2-FRB* or *orc5-FRB* strains was only slightly delayed upon rapamycin treatment as compared to control cells (Figure 3-13 B). Previous ChIP-qPCR studies during meiosis have demonstrated that, whereas ORC is associated with replication origins through both meiotic divisions, the MCM helicase is already present at origins during the pre-meiotic G1 phase, which implies that MCM association to origins of replication (via ORC-dependent recruitment) occurs prior to the induction of the meiotic programme (Phizicky *et al.*, 2018). Since the addition of rapamycin in our experimental set-up occurred simultaneously to meiotic induction (and presumably MCMs are loaded prior to meiotic entry), we expected that nuclear depletion of ORC by rapamycin treatment would not significantly interfere with efficient pre-meiotic DNA replication. The minor replication delay seen in the *orc2-FRB* and *orc5-FRB* strains could either be due to synchronization differences within the cell population or a consequence of rapamycin exposure during the cell washes prior to meiotic induction. It is worth mentioning that cells exhibit a G1-population peak until 1-1.5 hours after meiotic induction (before DNA replication in S phase) that could indicate that MCM loading still takes place during this time; thus, the slight replication delay of the *orc2-FRB* and *orc5-FRB* strains could also be, to some extent, a reflection of MCMs being not completely “loaded” at the start of the meiotic induction.

Contrary to the phenotype reported in the *orc1-161* background strains, nuclear-depletion of either Orc2 or Orc5 did not trigger rDNA-associated DSB formation (Figure 3-13 C). Based on the viability effects seen during vegetative growth, we believe that Orc2/Orc5 are depleted from the nucleus since rapamycin exposure in this set-up extends to up to 8 hours. However, although we provided evidence that both Orc2 and Orc5, are depleted from the nucleus in cycling cells (by using spotting growth assays and progression through cell cycle as a proxy, Figure 3-12 and 3-13), we cannot exclude that effects in DSB formation could be observed only upon complete reduction in the levels of ORC, which we cannot guarantee based on our current meiotic experiments (see below). Taken together, these findings indicate that Pch2 function at the rDNA-boundary region can be executed in situations where Orc2 or Orc5 are depleted from the nucleus (Figure 4-4).

While in budding yeast, DNA sequences have a determinant role for ORC binding (*i.e.* this protein complex binds to consensus DNA sequences (ARS consensus sequences, ACSs) that are necessary, but not sufficient for ORC binding), in higher eukaryotes and fission yeast, ORC does not seem to have such specificity for DNA sequences and its association to DNA is rather dependent on the chromatin structure (Li & Stillman, 2012; Méchali *et al.*, 2013). Although *S. cerevisiae* ORC recognizes the ACSs, ORC association to DNA in this organism is also influenced by the local chromatin environment (Eaton *et al.*, 2010). As mentioned earlier, budding yeast ORC associates to ARS sequences to serve as a loading platform for other factors implicated in DNA replication. Moreover, ORC sites also function as silencers to recruit SIR proteins and initiate the formation of silent chromatin at the mating-type loci and telomeres (see Introduction).

Our ChIP-qPCR data suggested that Pch2 function at the rDNA periphery can be performed in conditions where ORC is not associated to ARSs (Figure 3-13). By TAP-ChIP-qPCR in an *ORC1-TAP* and *orc2-FRB* strain we were able to demonstrate that, upon addition of rapamycin, Orc1 was almost completely lost (21.6 fold difference, DMSO relative to rapamycin) from the selected origin of replication tested (*ARS1116*). This is in agreement with the notion that ORC binding to origins of replication depends on ORC integrity and therefore, removing one of the ORC subunits (Orc2) via rapamycin addition, compromises association of ORC to origins of replication (Foss *et al.*, 1993; Fox *et al.*, 1995; Loo *et al.*, 1995; Shimada & Gasser, 2007; Suter *et al.*, 2004). Importantly, in addition to our findings that demonstrated the efficacy of the anchor-away technique during vegetative growth (Figure 3-12), our ChIP-qPCR analysis corroborated that this approach enables Orc2 nuclear depletion also in meiosis (Figure 3-13). Thus, we provided the first evidence that the anchor-away technique is suitable to deplete specific ORC members during meiosis. Since our Southern blotting experiments unveiled that depletion of Orc2 or Orc5 via the anchor-away method does not lead to DSB formation at the rDNA-borders (Figure 3-13 C), our data indicate that ORC association to origins of replication might not be strictly required for Pch2/Orc1 function to locally suppress DSBs at the rDNA-edges during meiotic G2/prophase.

Based on previous work (Vader *et al.*, 2011) and the data presented here, impairment of only the Orc1 subunit, but not Orc2 or Orc5, leads to DSB formation at the rDNA boundaries in meiotic G2/prophase. As mentioned earlier, functions of ORC (beyond DNA replication) in which individual ORC subunits have been involved (*i.e.* Orc1 in transcriptional silencing, Orc2 in sister chromatid cohesion) seem to be executed in the context of the entire

complex. This is mostly attributed to the fact that in budding yeast (and also the fission yeast *S. pombe*) ORC (Orc1-6) remains bound to chromatin throughout the cell cycle, which differs from observations in multicellular eukaryotes, in which one or more ORC subunits disengage from ORC/chromatin after assembly of the pre-RC is complete. For instance, in *Drosophila* embryos and mammalian cells, Orc1 dissociates from the chromatin during M or S phase, respectively, while the remaining ORC subunits stay chromatin-bound. However, this does not seem to be associated with an Orc1-independent function, but rather to regulation and ubiquitination-mediated degradation of this subunit to prevent re-replication (DePamphilis, 2005; Nguyen *et al.*, 2001). Another study provided evidence that in mouse zygotes, Orc4 is capable of existing in the cytoplasm and functioning separately from the other ORC components and that this subunit might be involved in the extrusion of the polar body in female mice meiosis (Nguyen *et al.*, 2015).

Based on the findings discussed in this section, we envision several possibilities that could reconcile the data from our Southern blotting experiments (in which nuclear depletion of Orc2 or Orc5 did not lead to DSB formation at the rDNA) and the ChIP-qPCR data (which showed that nuclear depletion of Orc2 also leads to near-complete loss of Orc1 from a selected ARS). As already mentioned, it was previously reported that impairment of *ORC1* via the *orc1-161* allele increases DSB formation at the rDNA boundaries, phenocopying effects seen in *pch2Δ* cells (Vader *et al.*, 2011). Here, we have employed another system (the anchor-away technique) that allows nuclear depletion of Orc2 and Orc5, both in mitosis and meiosis (Figure 3-12 and 3-13). Thus, the underlying principle by which distinct ORC subunits are “depleted” in both studies is fundamentally different and consequently, the strength of the impairment of ORC components might also differ between these methodologies. For technical reasons we could not create an *orc1-FRB* allele, so we are aware that the ability to compare phenotypes derived from the two depletion systems may be limited. Moreover, this study unveiled that Orc1 association to ARSs is disrupted (at least in the tested ARS) upon nuclear depletion of Orc2 via rapamycin treatment. However, we could envision a situation in which the nuclear Orc2 levels are reduced upon rapamycin addition, but Orc2 is not completely depleted by the anchor-away technique. Residual levels of Orc2 could be sufficient to prevent DSB formation at the rDNA-borders (in conjunction with Pch2), but reduction of Orc2 at the nucleus could prevent association of Orc1 to ARSs, since after MCM is loaded onto the DNA, Orc1/ORC would not be strictly required at the ARSs. This is in line with the principle of the “ORC cycle” described in fly embryos or mammalian

cells, in which Orc1 is selectively ubiquitinated and target for degradation after licensing for DNA replication. Nevertheless, such a mechanism has not been described in yeast. Though, it would be interesting to test DSB formation upon co-depletion of Orc2 and Orc5; if the lack of DSB formation at the rDNA in the *orc2-FRB* or *orc5-FRB* strains is due to insufficient nuclear depletion of these ORC subunits, we predict that simultaneously impairing both ORC members would cause a stronger nuclear depletion and subsequently result in increased DSB levels at the rDNA boundaries. Our preliminary experiments showed that yeast strains carrying a combination of the *orc2-FRB* and *orc5-FRB* alleles manifest more apparent defects in pre-meiotic replication than strains carrying single alleles of both ORC subunits, indicating that the nuclear depletion of Orc2 and Orc5 in the double-FRB strains is more acute. Supporting the Southern blot data with single depleted ORC subunits, preliminary experiments upon simultaneous depletion of both ORC subunits did not reveal DSB formation in the double-FRB strain, strengthening the notion that Orc1 is probably the main ORC subunit functioning with Pch2.

Although in this study we showed that the anchor-away system is functional also in meiosis, as we detected a near-complete loss of Orc1 from the selected ARS tested (*ARS1116*; Chrm. *XI*) (Figure 3-13 D), our investigations so far demonstrated reduction in the Orc1-association only in a single ARS. Hence, we cannot exclude that nuclear depletion is not equally efficient in different ARSs spread throughout the genome. In this regard, it would be interesting to map the genome-wide binding of ORC with the aid of high throughput DNA sequencing. Particularly, it would be important to show that nuclear depletion of Orc2 or Orc5 in the *orc2-FRB* or *orc5-FRB* strains, respectively, also leads to reduction of Orc1 association at the ARSs present within the rDNA locus. To our knowledge, ChIP experiments at the rDNA locus have exclusively been performed during mitosis (J. Huang & Moazed, 2003). Our preliminary ChIP-qPCR experiments at the ARS present at the rDNA in anchor-away yeast strains carrying *ORC1-TAP* and *orc2-FRB* seem to indicate that indeed, Orc1 is also depleted from the nucleus upon rapamycin addition. It is important to note that due to the repetitive nature of the rDNA and the presence of an ARS per rDNA repeat, it is not technically possible to discern the exact location of ORC binding within the distinct repeats of the rDNA. Also, there is a possibility that ORC associated with Pch2 is only present at ARSs in repeats nearby the rDNA borders. Up to date, ORC association to DNA during meiosis has not been the focus of much attention. However, it is clear that in budding yeast, ORC binding to ARSs is intrinsically determined by DNA consensus sequences, although chromatin

organization also influences ORC-origin DNA association in budding yeast (Eaton *et al.*, 2010; Lipford & Bell, 2001; Méchali *et al.*, 2013; Yoshida *et al.*, 2013). Moreover, mapping of the MCM subunit Mcm2 has revealed a major overlap between Mcm2 binding sites in both cell division programmes (mitosis and meiosis), though a subset of pre-meiotic origins showed differential Mcm2 loading and many pre-meiotic origins show a delay as compared to mitosis (Blitzblau *et al.*, 2012). Since MCM is recruited via ORC, mapping of Mcm2 could potentially serve as a proxy for ORC binding sites in meiosis. Such mapping suggests that ORC would potentially be found in association to virtually the same ARSs sites in meiosis and mitosis, but a conclusive study proving this is needed. In this line, further research should be focused to perform a genome-wide analysis of ORC in meiosis, as it would be useful to be able to correlate these sites with Pch2 binding sites.

Based on the data discussed here and the fact that the anchor-away technique has been proven to efficiently remove both from the nucleus and the nucleolus specific proteins, our findings suggest that association of ORC to origins of replication is not strictly required for Pch2/Orc1 function in suppressing DSBs at the rDNA boundaries (Albert *et al.*, 2016; Ballew & Lacefield, 2019; Cardoso da Silva *et al.*, 2019; Subramanian *et al.*, 2016; Vincenten *et al.*, 2015). An important implication of the findings presented here is that they point towards a “repurposing” of the ORC assembly involved in DNA replication to perform a meiosis-specific role in combination with Pch2. Our results support the idea that the ORC assembly involved in preventing DSB formation at the rDNA is not bound to ARSs, in contrast to what occurs in other ORC-associated functions (DNA replication and transcriptional silencing; see above). In agreement with this, ORC has been found to perform functions non-dependent of its association with ARSs in vegetatively growing cells. Specifically, the Fox laboratory identified a class of ORC binding sites, which are distinct from origins of replication and silencers, and consist mostly of protein-coding genes that are highly expressed and function in several metabolic pathways (Shor *et al.*, 2009). These ORC-associated sites (named ORC-interacting genes or ORF-ORC genes) differ from replication sites in various aspects. First, besides binding ORC and MCM, these sites do not function as origins of replication. Second, these sites do not contain canonical ORC binding motifs and are frequently located downstream of replication origins. And third, they are localized in protein-coding regions transcribed by RNA Polymerase II (RNA-PolII). As many of these ORF-ORC genes are involved in metabolic processes, it has been proposed that these novel ORC-sites play a role in the coordination of the nutrient status with DNA replication.

Remarkably, a recent study from our group demonstrated that, within the non-rDNA chromatin, Pch2 associates with a subset of actively RNA-PolIII transcribed genes during meiosis and that active transcription is required for the recruitment of Pch2. However, Pch2 association is not uniquely determined by transcriptional strength (*i.e.* if the gene is more or less transcribed by RNA-PolIII) or DNA sequence. Interestingly, the Orc1 subunit has also been shown to be necessary for Pch2 association with these actively transcribed genes. Thus, the current literature proposes a link between ORC, Pch2, transcription, and metabolism (Cardoso da Silva *et al.*, 2019; Shor *et al.*, 2009). The data discussed in this section suggest that Pch2/Orc1(ORC) function at the budding yeast rDNA does not require ORC binding to origins of replication and thus, underscores a non-canonical role for ORC during meiotic G2/prophase. This non-canonical role for ORC is in agreement with the connection between Pch2 and Orc1 at genomic regions that are distinct from origins of replication (Cardoso da Silva *et al.*, 2019).

Based on the findings discussed in this section and the current literature from our group and others, we speculate that different ORC assemblies might exist and that ORC could be bound to non-ARS sites during meiosis, also within the rDNA (and/or the rDNA boundaries). We envision the possibility that the ORC assembly involved in preventing DSBs at the rDNA boundaries does not need to be associated to ARSs. In relation to this hypothesis, unpublished observations from our group revealed that Pch2 does not associate to the ARS present within the rDNA. How could then two ORC “populations” be recruited to different sites? And is Orc1 performing a function in isolation (*i.e.* without being associated with other ORC subunits) together with Pch2? Although it cannot be ruled out that Orc1 could be performing the Pch2-associated function at the rDNA on its own (*i.e.* without the other ORC components), based on the current literature this possibility seems unlikely (see above).

We hypothesize that the association of ORC to distinct regions (ARSs and non-ARSs) is driven either by post-translational modifications of this complex (that might be different in mitosis versus meiosis) or by intrinsic properties of some of the ORC subunits. In relation to this last point, it is worth noting that Orc1 is the only ORC component that harbors a Bromo-adjacent homology (BAH) domain, a domain present in several chromatin-associated proteins and that is typically considered as a “reader” of the chromatin status. Since the rDNA is a heterochromatic region, a possibility could be that the BAH domain of Orc1 is specifically recognizing the chromatin status in this loci and drives ORC to positions distinct from ARSs, where Pch2 would, in turn, be recruited. We speculate that this BAH-mediated recruitment

could be due to the special protection that the rDNA locus needs during meiosis because of the programmed DSB formation. Hence, differential recruitment of Orc1 (and in turn, ORC) could, at least partially, explain our findings that seem to indicate that, within ORC, Orc1 might perform a critical role in Pch2-ORC association and function at the rDNA.

As stated above, Pch2 recruitment to the rDNA is dependent on Orc1. Future work should explore if Pch2 localization in the rDNA is as well affected upon the impairment of other members of the ORC assembly. In this regard, we have generated yeast strains carrying HA-tagged Pch2 and either *orc2-FRB* or *orc5-FRB*. Our preliminary immunofluorescence (IF) experiments seem to indicate that Pch2 localizes to the nucleolus in these strains upon addition of rapamycin, in line with our Southern blotting experiments in the *orc2-FRB* or *orc5-FRB* strains, which did not reveal DSB formation at the rDNA upon rapamycin treatment. Presumably, if Orc1 is the central element in the ORC assembly required to prevent DSBs at the rDNA during meiotic G2/prophase, we would predict that nuclear depletion of Orc2 or Orc5 would lead to a reduction of Orc2/5 in the nucleus and nucleolus, but that it would not affect the recruitment of HA-Pch2 to the nucleolus. Our preliminary experiments seem to indicate that, indeed, HA-Pch2 localization does not vary upon depletion of either Orc2 or Orc5. Further work will focus on performing IF of meiotic chromosome spreads in a strain carrying *ORC1-TAP* and *orc2-FRB*, to address the localization of Orc1 upon nuclear depletion of Orc2. As the Southern blot experiments in strains harboring *orc2-FRB* did not reveal DSBs at the rDNA right flank (Figure 3-13 C), we expect that Orc1 localization is not changed upon the addition of rapamycin. In principle, this would seem contradictory to the ChIP-qPCR data discussed earlier, which suggested a reduction of Orc1 in an *orc2-FRB* strain after rapamycin treatment. However, the expected result of Orc1 localization at the rDNA (*i.e.* Orc1 localization does not vary upon rapamycin addition in an *orc2-FRB* strain) concurs well with the notion that Orc1 might be a central component of ORC in driving Pch2-ORC association, and that the other ORC subunits might just be required for the stability of the complex and thus, Orc1 could be still able to operate with Pch2. Our ChIP-qPCR data could then be a reflection of a different population of ORC that is not bound to ARS and that is responsible for the rDNA protective function (see above).

In sum, the evidence discussed in this section support the idea that Pch2/Orc1(ORC) anti-DSB function at the rDNA is executed away from ARS-sites and that Orc1 might play a critical role in driving proper association of the ORC-Pch2 complex to specific genomic locations that need of special protection during meiotic G2/prophase. Future experiments

should be addressed to better comprehend this proposed non-canonical role of ORC during meiosis, with a special focus on providing a comprehensive analysis of ORC sites during meiosis and on understanding the exact features that influence ORC binding to different sites during the meiotic programme (Figure 4-5).

4.5.3 The BAH domain of Orc1 is not necessary for Pch2-ORC binding despite being required for Pch2-ORC functionality at the rDNA

Orc1, the largest subunit of ORC, presents the particularity that its domain organization contains, besides the AAA⁺-like module and the winged-helix domain (WHD) present in other ORC components (Orc1-5), an NH₂-terminal Bromo-adjacent homology (BAH) domain. BAH domains are present in chromatin-associated proteins and their main feature is that they can recognize distinct chromatin modifications and interact specifically with nucleosomes. The BAH domain of Orc1 can directly bind to nucleosomes (De Ioannes *et al.*, 2019). Although this domain is not required for replication, it contributes to the association of ORC with most of the origins of replication in budding yeast and it is necessary for normal activity in a subset of origins (Li & Stillman, 2012; Müller *et al.*, 2010a). Moreover, recent structural work has suggested that ORC-binding sites in eukaryotes are determined by Orc1-BAH domain and Orc1 basic patches (BPs), which are located between the BAH and the AAA⁺ domains (Li *et al.*, 2018). Contrary to DNA replication, the BAH domain of Orc1 is essential for transcriptional silencing (see Introduction).

The findings presented here suggested that the Orc1 subunit performs a critical role in the association and function with Pch2 at the budding yeast rDNA (Figure 4-2). In addition, a previous study showed that deleting the BAH domain of Orc1 (*Abah-Orc1*) leads to an increase in DSBs at the rDNA right flank, the same phenotype observed in *pch2Δ* cells (Vader *et al.*, 2011). These data led us to hypothesize that the BAH domain of Orc1 could perform a role in the interaction with Pch2. However, several pieces of evidence gained from our work argue against a direct involvement of this domain of Orc1 in Pch2 engagement. First, our Y2H analysis showed that the BAH domain of Orc1 alone is not able to bind Pch2, whereas deleting this domain (*Abah-Orc1*) did not seem to affect the interaction with Pch2 (Figure 3-16 B and C). Second, the bacterially purified BAH domain of Orc1 (GST-BAH-Orc1) was not able to interact with purified His-MBP-Pch2 (Figure 3-15 C), underscoring that the Orc1-BAH domain is not sufficient to establish binding with Pch2. Third, we demonstrated that *Abah*-His-ORC is capable of interacting with His-MBP-Pch2 *in vitro* (both

in solid-phase pull-down experiments and analytical SEC) and we did not observe any appreciable difference with respect to the binding between full His-ORC and His-MBP-Pch2, at least under the conditions tested (Figures 3-7 C and 3-16 C). Fourth, we did not detect any cross-links between Orc1-BAH domain and Pch2, as judged by XL-MS (Figure 3-8 and Table 7-3). Thus, our findings offered compelling evidence that the BAH domain of Orc1 is not sufficient and is not directly involved in Pch2 binding to ORC.

In contrast to the data discussed above, our co-IP experiments demonstrated that the interaction between Orc1 and Pch2 was severely impaired in strains carrying a deletion of the BAH domain of Orc1 (*Abah-Orc1* allele) (Figure 3-16 D). This reduced interaction between Orc1 and Pch2 in the *Abah-Orc1* mutant cannot be due to defects in DNA replication since meiotic progression is only slightly affected upon deletion of this domain, in agreement with previous studies of this mutant allele in meiosis (Vader *et al.*, 2011). It is plausible that the discrepancies between our *in vivo* and *in vitro* results regarding the role of Orc1-BAH domain in association with Pch2 are a consequence derived from the fact that in the *in vitro* experiments protein concentration could be favoring this interaction, whereas such concentrations required for a direct interaction might not occur *in vivo*. Nonetheless, we were able to detect *in vivo* interaction between Pch2 and full-length Orc1 and, although we cannot fully discard that *Abah-Orc1* could have a lower affinity for Pch2, we speculate that this could not account for such a dramatic difference in the interaction between these complexes *in vitro* and *in vivo*. We also cannot exclude that potential post-translational modifications of ORC could account for such differences and thus, that context-dependent modifications of ORC could regulate its ability to bind to Pch2.

The BAH domain of Orc1 interacts with nucleosomes juxtaposed to origins of replication in yeast, flies, plants, and humans (Kuo *et al.*, 2012; Li *et al.*, 2016; Müller *et al.*, 2010a). Based on the current literature and our findings discussed here, we propose that the BAH domain of ORC is not *per se* involved in providing a binding interface for Pch2 engagement, but rather influences Pch2 binding to ORC *in vivo* due to intrinsic differences in the locations of ORC determined by the BAH domain of the Orc1 subunit, which specifically recognizes nucleosome modifications. It is worth mentioning that in metazoans Orc1 specifically recognizes dimethylation at lysine 20 of histone H4 (H4K20me2), a histone modification enriched at origins. In the same lines, mutations on the BAH domain of Orc1 have been linked to a form of primordial dwarfism, known as Meier-Gorlin syndrome.

Disruption of Orc1-BAH-H4K20me2 also leads to dwarfism in zebrafish, which proposes a link between this epigenetic mark (H4K20me2) and metazoan DNA replication, and thus reinforces the pivotal role of the Orc1-BAH domain in recognizing specific nucleosome modifications (Bleichert *et al.*, 2013; Kuo *et al.*, 2012).

The hypothesis that the BAH domain of the Orc1 subunit specifically binds and recognizes nucleosome modifications is further strengthened by recent findings, which offered evidence that mutations in the BAH domain of Orc1 that lower its affinity for nucleosomes lead to increased DSB formation at the rDNA (De Ioannes *et al.*, 2019). Hence, Orc1 interaction with nucleosomes via its BAH domain is needed to maintain integrity in the rDNA borders during meiosis, which concurs well with previous investigations in which deletion of the BAH domain of Orc1 resulted in DSB formation at the rDNA edges (Vader *et al.*, 2011). To test whether interaction of ORC with nucleosomes (via the BAH domain of Orc1) plays a role in binding to Pch2, it would be useful to perform *in vitro* assays (*i.e.* pull-downs) to examine whether binding between His-ORC and His-MBP-Pch2 is influenced by addition of nucleosomes (and in turn, by ORC association to nucleosomes) *in vitro*.

In addition, recent work from our group has demonstrated that the BAH domain of Orc1 contributes to the targeting of Pch2 to non-nucleolar regions (Cardoso da Silva *et al.*, 2019). The association to nucleosomes with the BAH domain of the Orc1-homolog Sir3 is sensitive to methylation of lysine 79 on histone H3 (H3K79me) and the activity of the methyltransferase Dot1 (and thus, methylation state on H3K79) has been shown to be determinant for Pch2 localization along chromosomes (Cavero *et al.*, 2016; De Ioannes *et al.*, 2019). Remarkably, Dot1 activity is associated with active transcription by RNA-PolII, which suggests a link between recent findings from our group (that showed that Pch2 association along the non-rDNA region is dependent on active RNA-PolII transcription) and Orc1-BAH domain capacity to sense RNA-PolII transcription-associated Dot1 activity on neighboring nucleosomes (Wood *et al.*, 2018). Hence, current literature by our group and others indicate that the epigenetic state (*i.e.* specific chromatin modifications) might contribute to Pch2 recruitment.

Thus, based on the data presented here and recent research on the field, we speculate that localization of Pch2 to the nucleolus could also be driven by Orc1-mediated recruitment to specific sites within the rDNA (or at the rDNA periphery), and that the crucial role that the Orc1 subunit performs within the ORC assembly is a reflection of the ability of Orc1-BAH

domain to “sense” specific chromatin modifications or the specialized chromatin established at the rDNA locus. A recent study reported that contrary to its homolog Sir3, which has a preference for binding to unmodified nucleosomes, the BAH domain of Orc1 has a similar affinity for unacetylated and acetylated nucleosomes in lysine 16 on histone H4 (De Ioannes *et al.*, 2019). The histone H4 tail plays well-established roles in chromatin condensation and interacts with the BAH domain of Orc1 in a similar manner that the Sir3 BAH domain, helping to anchor the tail to the BAH domain surface.

Comparative ChIP-seq data analysis has underlined that most of the confirmed Orc1 binding sites are nucleosome-depleted. Origins in silent chromatin (HM loci and telomeres) show low levels of H4K16 acetylation, probably as a consequence of the Sir2 deacetylase activity in those regions (because of the establishment of silenced chromatin), whilst the majority of euchromatic origins show peaks of acetylated H4K16 at the nucleosomes surrounding Orc1 binding sites. It is important to note that although the Sir2 histone deacetylase prevents DSB formation within the rDNA, it has a DSB promoting activity at the rDNA boundaries (Gottlieb & Esposito, 1989; Imai *et al.*, 2000; Mieczkowski *et al.*, 2007; Vader *et al.*, 2011). It is possible that Orc1 (and in turn, ORC) is “sensing” the chromatin local status at the rDNA and surroundings; binding to acetylated nucleosomes nearby the rDNA would protect neighboring nucleosomes from the Sir2 deacetylase activity and in turn, safeguard these regions from DSB formation.

The Orc1 BAH domain differs from Sir3 BAH domain in that in Orc1 the N-terminal tail projects out of the core BAH domain and interacts with neighboring molecules (Connelly *et al.*, 2006; Yang *et al.*, 2013). Binding of Orc1 to adjacent nucleosomes could lead to conformational changes in the BAH domain of Orc1, which could, in turn, allow Pch2 binding. Association of Orc1-BAH domain to distinct histone modifications could lead to differential conformational changes within Orc1 (and ORC) and this could, at least, partially explain the enrichment of the recruitment of Pch2 to the nucleolus. Understanding the exact position of ORC (*i.e.* if ORC is bound exclusively to the ARSs in the rDNA or to other locations, and whether ORC is recruited to rDNA boundaries) would provide useful insights about ORC role in protecting rDNA edges against DSB formation and thus, future work should focus on assessing the exact location of ORC during meiotic G2/prophase.

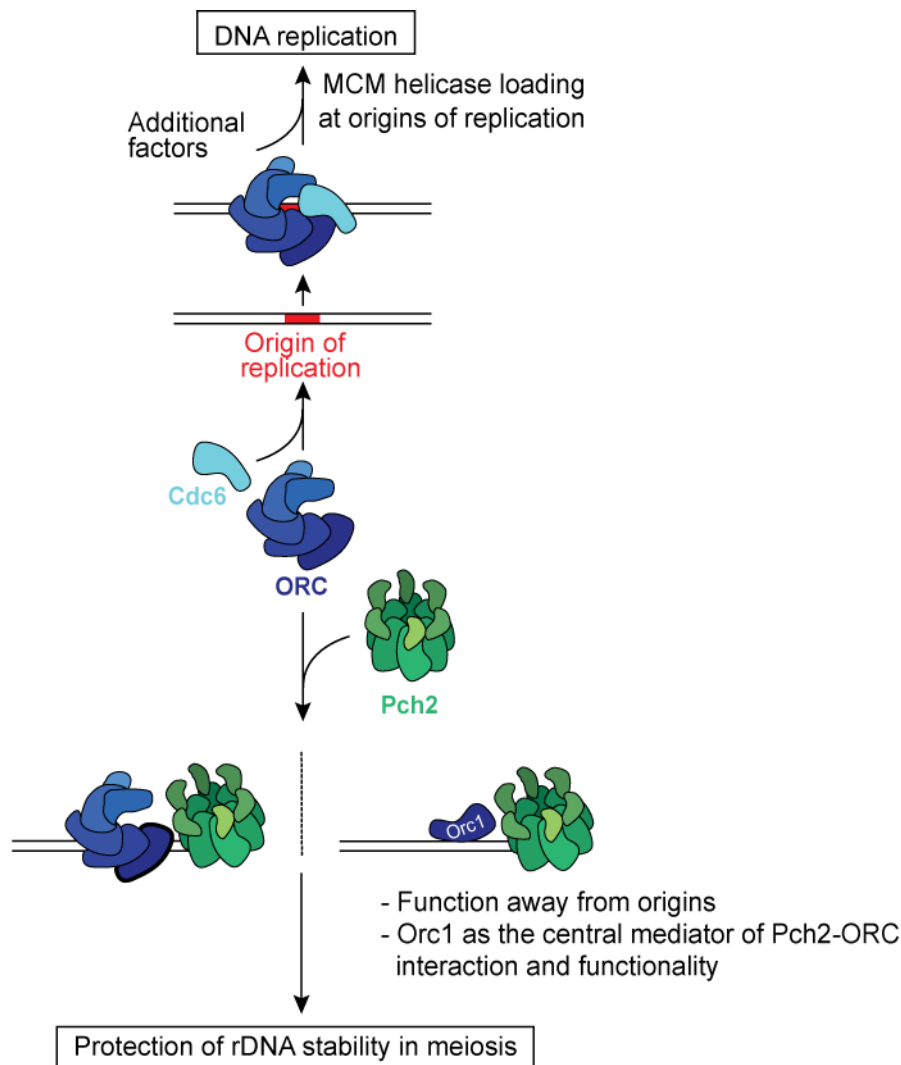


Figure 4-5 Model depicting the origin-independent function of Pch2-Orc1/ORC in local meiotic DSB control

The hetero-hexameric ORC (Orc1-6) (represented in dark blue) associates with origins of replication or autonomously replicating sequences (ARSS) (depicted in red). ORC interacts with the AAA⁺ ATPase Cdc6 (light blue) (and additional factors) in order to drive the recruitment of the MCM replicative helicase and initiate DNA replication. We hypothesize that Pch2 and ORC function away from origins of replication (in contrast with the role of ORC in DNA replication) in order to protect the budding yeast ribosomal DNA (rDNA) from meiotic DNA double-strand break (DSB) formation. There is a possibility that Pch2 could also interact with Orc1 alone (not-associated with the other ORC members). Interaction of ORC with Pch2 is independent of Cdc6, which together with the fact that ORC association to its canonical sites (*i.e.* ARSS) is not needed for Pch2-ORC rDNA-associated function, indicates a novel role of ORC, and possibly repurposing of ORC/Orc1 during budding yeast meiosis.

Therefore, prevention of DSB formation at rDNA boundaries could be a reflection of a dual mechanism; on one hand, the BAH domain of Orc1 could be acting as a sensor to anchor Orc1 (and the other subunits of ORC) to specific sites (non-ARS sites, based on our findings) and such Orc1/ORC recruitment would be facilitated by the specialized chromatin established by Sir2. Binding of ORC to those sites would subsequently protect nucleosomes from Sir2-mediated deacetylation. On the other hand, ORC positioning in those sites would recruit Pch2, which presumably would exclude the HORMA-domain protein Hop1 (which is necessary for DSB formation). We envision that BAH-mediated recruitment of ORC would be upstream and ORC likely acts as a landing platform to drive Pch2 to specific sites, where ORC and Pch2 would collaborate in order to suppress DSB at the rDNA boundaries. We propose that the central role of Orc1 could be a consequence of *i*) its BAH domain recognition of the chromatin state in the rDNA and/or adjacent regions, which directs Pch2 to those sites and *ii*) Pch2 engagement to binding surfaces present within Orc1 (probably due to the gap existing between the Orc1 and Orc2 subunits and to the fact that Pch2 could be using common binding interfaces to the AAA⁺ ATPase Cdc6) (see section 4.2.4).

Collectively, the *in vivo* and *in vitro* analyses presented here reveal insights about the establishment of a meiosis-specific AAA⁺ assembly between Pch2 and ORC. These findings broaden the list of known ORC-interactors by revealing a novel direct binding partner of ORC (*i.e.* Pch2). In addition, we also uncover a hitherto unknown direct association partner of Pch2, besides the already described HORMA-domain-containing proteins. Furthermore, we *in vitro* reconstituted the Pch2-ORC assembly, which combined with *in vivo* analysis, has extended the understanding of the interaction between Pch2 and another AAA⁺ protein complex. We provide evidence that the role of Pch2/ORC in DSB suppression at the rDNA is executed away from origins of replication (in contrast with the canonical role of ORC in DNA replication initiation), and strongly relies on Orc1. Finally, this doctoral work reveals characteristics of the Pch2-ORC AAA⁺ assembly and highlights certain plasticity in the ability of ORC to interact with distinct AAA⁺ proteins. Understanding the biochemical, structural and functional connections between these two ATPases in more detail will be an avenue for future research.

5 Summary

Programmed DNA double-strand break (DSB) formation followed by homologous crossover recombination is crucial to establish physical linkages between homologous chromosomes and to ensure faithful chromosome segregation during meiosis. However, the introduction of DSBs within repetitive DNA elements is a major source of genomic instability, due to the possibility of DSBs repairing by non-allelic homologous recombination (NAHR). Indeed, DSBs in such repetitive regions can cause genome rearrangements and chromosome missegregation, which is linked to several genetic disorders and birth defects in humans.

In this study, we investigated how the repetitive ribosomal DNA (rDNA)-boundaries of the budding yeast *Saccharomyces cerevisiae*, which are also at high risk of NAHR, are protected against the introduction of DSBs. Particularly, we focused on the interplay of two AAA⁺ ATPases, the meiosis-specific Pch2 and the Orc1 subunit of the hetero-hexameric Origin Recognition Complex (ORC; Orc1-Orc6), which are involved in the protection of the rDNA edges against DSBs. We demonstrated that *in vivo* Pch2 associates not only with the Orc1 subunit but also with Orc2 and Orc5, suggesting that Pch2 is able to associate with the entire ORC during meiotic G2/prophase. In addition, we reconstituted this macromolecular Pch2-ORC assembly and showed, by cross-link mass-spectrometry (XL-MS), that both the NH₂-terminal domain (NTD) and the AAA⁺ domain of Pch2 are involved in the interaction with ORC. Moreover, we showed that deletion of the NTD of Pch2 severely impairs the interaction with ORC *in vivo* and *in vitro* and that the Pch2-AAA⁺ domain alone is not able to prevent rDNA-associated DSB formation. In addition, we delineated the minimal region within the NTD of Pch2 (amino acids 2-144) that is sufficient to recapitulate binding with ORC *in vitro*. We also identified residues within this region that are critical for establishing an association with ORC and for Pch2-Orc1 functionality at the rDNA.

To understand the role of other ORC subunits in the rDNA protection against meiotic DSB formation, we developed experimental approaches to functionally deplete selected ORC members (Orc2 and Orc5). Using this system, we revealed that Pch2-Orc1 functionality at the rDNA can occur in conditions of nuclear depletion of these subunits. By performing chromatin immunoprecipitation coupled to quantitative PCR (ChIP-qPCR) we showed that the function of Pch2-Orc1 at the rDNA does not require binding of ORC to its canonical sites (*i.e.* origins of replication). Furthermore, we have provided evidence that a chromatin-binding

module of Orc1 (the bromo-adjacent homology (BAH) domain) is necessary for Pch2-ORC binding *in vivo*, besides not been directly involved in the *in vitro* binding of these complexes. These data suggests that *in vivo* interaction between both AAA⁺ ATPases is influenced by the local chromatin environment, which might be a reflect of the ability of Orc1-BAH domain to associate with regions with specific nucleosome features and in turn, to direct Orc1/ORC to sites distinct from origins of replication, enabling recruitment of Pch2 to these sites.

Altogether, the data presented in this study demonstrate a direct interaction between Pch2 and ORC and reveals that, within ORC, Orc1 might have a critical contribution to both binding and functionality of this meiotic anti-DSB system. The fact that the function of Pch2-Orc1 in locally suppressing DSBs during meiotic G2/prophase presumably does not depend on the association of ORC to origins of replication likely represents an origin-independent role of Orc1/ORC. This role is distinct from its canonical one in DNA replication and seems to indicate that during meiotic G2/prophase, Orc1/ORC is repurposed to perform a function with the meiosis-specific AAA⁺ ATPase Pch2.

6 Zusammenfassung

Während des Zellteilungsprozesses Meiose ist die beabsichtigte Entstehung von DNA Doppelstrangbrüchen (DSB) und die darauffolgende homologe Crossover Rekombination essentiell, um homologe Chromosomen physisch miteinander zu verbinden und eine akkurate Verteilung der Chromosomen zu gewährleisten. Die Entstehung von DSB in repetitiven DNA Elementen ist dabei eine Hauptursache für genomische Instabilität, da die DSB durch nicht-allelische homologe Rekombination (NAHR) repariert werden könnten. Innerhalb solcher repetitiven DNA Elemente können DSB zu genomischer Umordnung und Fehlverteilung der Chromosomen führen. In Bezug zum menschlichen Körper ist dies ein möglicher Auslöser für verschiedene genetische Erkrankungen oder Geburtsfehler.

In dieser Studie untersuchten wir, wie die durch NAHR gefährdeten Grenzen der repetitiven ribosomalen DNA (rDNA) der Bäckerhefe *Saccharomyces cerevisiae* vor der Entstehung von DSB geschützt sind. Dabei lag der Fokus insbesondere auf dem Zusammenspiel der beiden AAA⁺ ATPasen Pch2, ein Meiose-spezifisches Protein, und Orc1, eine Untereinheit des hetero-hexamerschen Origin Recognition Komplexes (ORC; Orc1-Orc6). Diese beiden AAA⁺ ATPasen sind an dem Schutz der rDNA-Grenzen vor DSB beteiligt. *In vivo* konnten wir nachweisen, dass Pch2 sowohl mit der Orc1-Untereinheit, als auch mit den Untereinheiten Orc2 und Orc5 verbunden ist, was darauf hindeutet, dass Pch2 mit dem gesamten OR-Komplex während der meiotischen G2/Prophase assoziiert ist. Des Weiteren rekonstruierten wir die makromolekulare Zusammenlagerung von Pch2-ORC und zeigten mittels Cross-Link Massenspektrometrie (XL-MS), dass die NH₂-terminale Domäne (NTD) und die AAA⁺ Domäne von Pch2 an der Interaktion mit ORC beteiligt sind. Außerdem veranschaulichten wir *in vivo* und *in vitro*, dass durch die Entfernung der NTD von Pch2 die Interaktion mit ORC gravierend vermindert wird und dass die AAA⁺ Domäne von Pch2 alleine nicht fähig ist, die rDNA-assoziierten DSB zu verhindern. Darüber hinaus beschrieben wir *in vitro* die minimalste Region innerhalb der NTD von Pch2 (Aminosäuren 2-144), die ausreichend ist, um die Verbindung mit ORC herzustellen. Abschließend identifizierten wir die Aminosäurereste innerhalb dieser Region, die für die Assoziation mit ORC und die Funktionsfähigkeit von Pch2-Orc1 an der rDNA essentiell sind.

Um die Rolle anderer Untereinheiten des ORC bei der Beschützung der rDNA vor meiotischen DSB zu verstehen, entwickelten wir experimentelle Ansätze, die es uns ermöglichten, selektierte ORC-Untereinheiten (Orc2 und Orc5) aus dem Nucleus funktionell

zu entfernen. Mit diesen Ansätzen konnten wir zeigen, dass die Funktionsfähigkeit von Pch2-Orc1 an der rDNA nicht beeinträchtigt ist, wenn die selektierten Untereinheiten entfernt wurden. Mittels Chromatin-Immunpräzipitation gekoppelt an quantitativer PCR (ChIP-qPCR) wiesen wir nach, dass für die Funktionsfähigkeit von Pch2-Orc1 an der rDNA die Bindung des ORC an seinen kanonischen Bindestellen (d.h. Replikationsursprünge) nicht benötigt wird. Im Zuge dessen ergeben sich Hinweise dafür, dass eine Chromatin-Bindestelle von Orc1 (bromo-adjacent homology (BAH) Domäne) für die *in vivo* Bindung von Pch2-ORC notwendig ist, obwohl diese nicht direkt bei der *in vitro* Bindung dieser Komplexe involviert ist. Die Daten deuten darauf hin, dass *in vivo* die Interaktion zwischen beiden AAA⁺ ATPasen durch die lokale Umgebung des Chromatins beeinflusst wird. Dies könnte bedeuten, dass die Orc1-BAH-Domäne die Fähigkeit besitzt, sich mit Regionen, die spezifische Nukleosom-Eigenschaften haben, zu assoziieren. Durch diese Fähigkeit wiederum könnte Orc1/ORC zu Regionen gelenkt werden, die von den Replikationsursprüngen zu unterscheiden sind, und somit die Rekrutierung von Pch2 zu diesen Regionen ermöglicht.

Zusammenfassend kann festgehalten werden, dass eine direkte Interaktion zwischen Pch2 und ORC vorliegt und dass die Orc1-Untereinheit einen vermeintlich wichtigen Beitrag zu der Bindung und Funktionsfähigkeit bei diesem Anti-DSB System in der Meiose leistet. Aufgrund der Tatsache, dass die Funktionstüchtigkeit von Pch2-Orc1 bei der lokalen Unterdrückung der DSB während der meiotischen G2/Prophase vermutlich nicht von der Assoziation des ORC mit den Replikationsursprüngen abhängig ist, handelt es sich hierbei um eine Replikationsursprung-unabhängige Rolle von Orc1/ ORC. Diese Rolle ist von der kanonischen bei der DNA Replikation zu unterscheiden und scheint darauf hinzudeuten, dass Orc1/ORC während der meiotischen G2/Prophase umfunktioniert wird, um eine Funktion mit der Meiose-spezifischen AAA⁺ ATPase Pch2 auszuführen.

7 Appendices

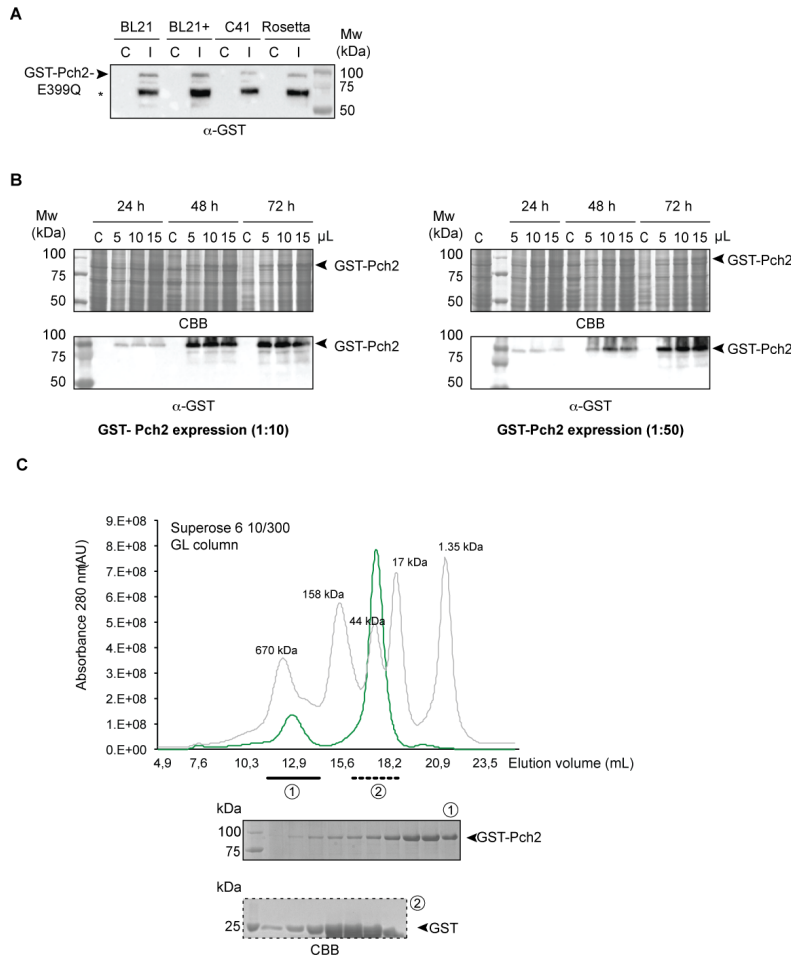


Figure 7-1 Expression and purification of GST-tagged Pch2

A) Protein expression test of GST-Pch2-E399Q in different bacteria strains: BL21(DE), BL21-CodonPlus (DE3)-RIPL, C41 (D43) and Rosetta™ (D43) competent cells. Arrowheads indicate GST-Pch2-E399Q. Asterisk indicates degradation band. C stands for control (not induced) and I stands for induced (protein induction by addition of IPTG). B) and C) Protein expression tests of GST-Pch2 in insect cells using a different ratio of baculovirus to culture (right panel, 1:10; left panel, 1:50). Different amounts of protein samples were loaded (5, 10 and 15 μL). C stands for control (insect cells not infected with baculovirus). Insect cells samples were collected at indicated time points (24 h, 48 h and 72 h) after baculovirus infection. Samples were analysed via SDS-PAGE followed by either Coomassie Brilliant Blue (CBB) staining or Western blot (α-GST). C) Size exclusion chromatogram (SEC) of GST-Pch2 purified from insect cells. Green indicates SEC profile of GST-Pch2. Gray indicates SEC of gel filtration standard and molecular weight of the proteins are shown. AU stands for arbitrary units. The first peak (continuous line) indicates GST-Pch2 (likely in an hexameric conformation). The second peak (dotted line) indicates GST-tag (likely dimers). Eluted protein samples were analysed by SDS-PAGE and CBB staining.

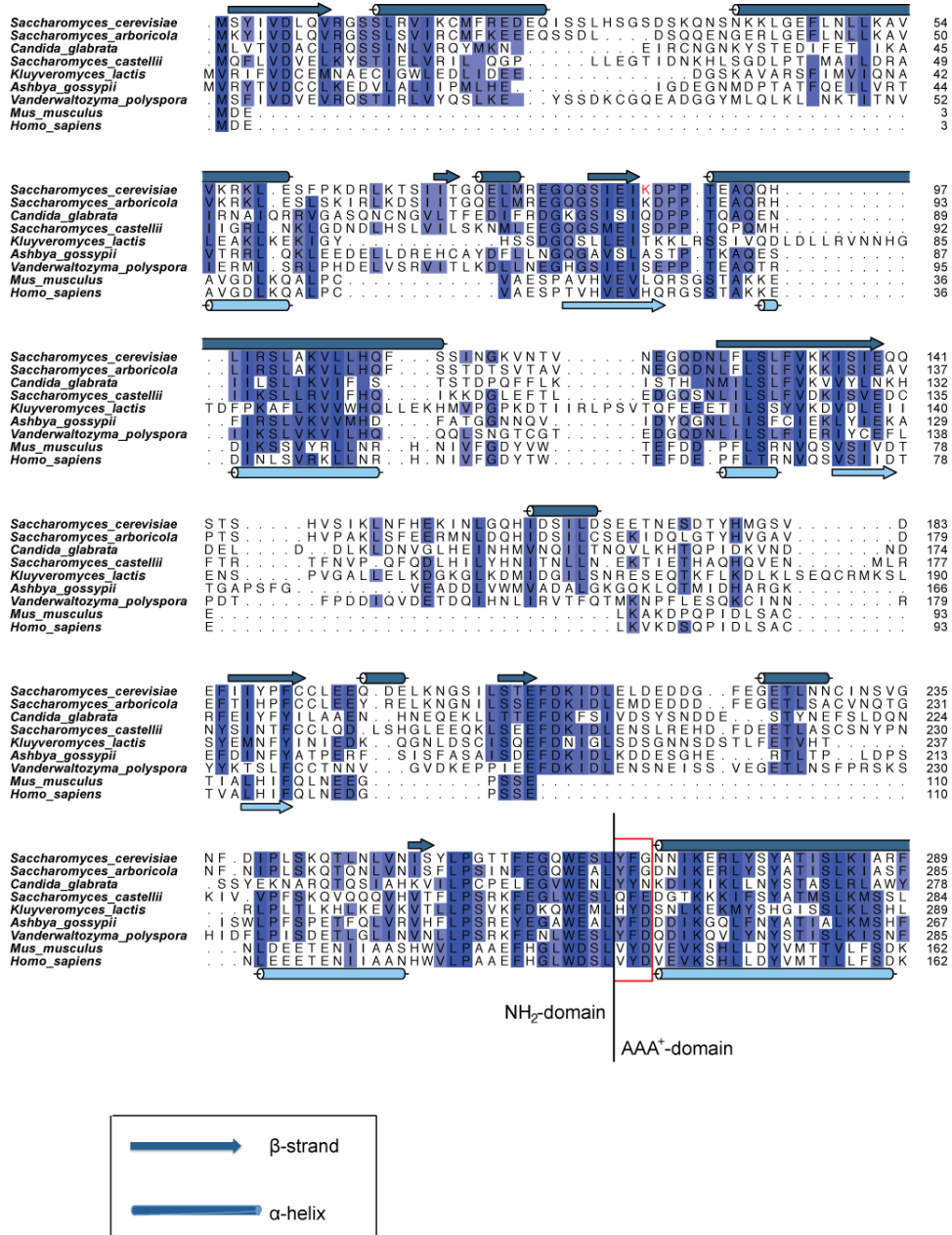


Figure 7-2 Pch2 alignment of the NH₂-terminal domain

Sequence conservation of the NH₂-terminal domain of Pch2 among different organisms. To determine a set of Pch2 orthologs, a total of 90 genomes, spread over the eukaryotic tree of life, was used. For clarity, only alignments of the *Saccharomyces* class, *Mus musculus* and *Homo sapiens* are shown. The alignment was made with MAFFT (Katoh *et al.*, 2002) with the L-INS-I iterative method. Secondary structure predictions based on PSIPRED protein sequence analysis tool (<http://bioinf.cs.ucl.ac.uk/psipred/>) are shown. Dark blue arrows indicate β-strand secondary structure in *S. cerevisiae*; dark blue cylinders indicate α-helix structure in the same. Light blue shows predicted β-strand secondary structure in humans, whereas light blue cylinders indicate predicted α-helix structure the same. Red square indicates the N-linker sequence.

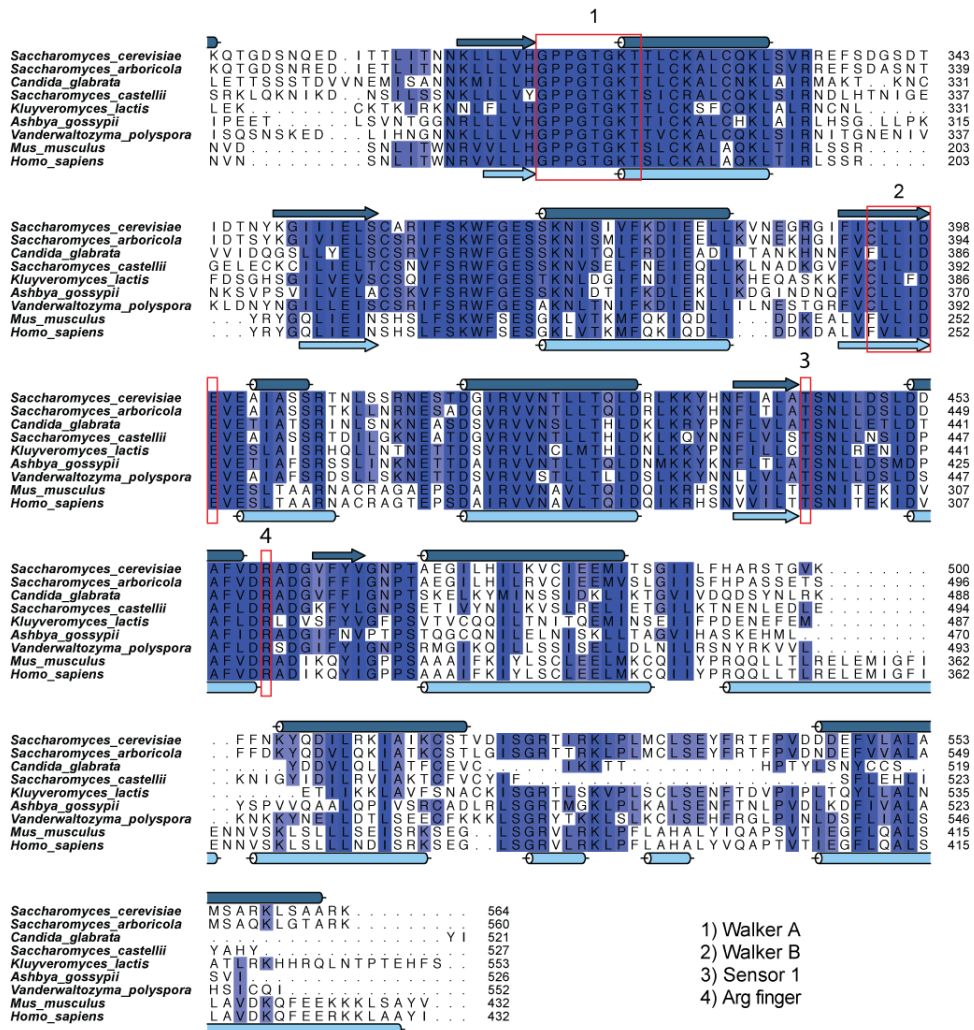


Figure 7-3 Pch2 alignment of the AAA⁺ ATPase domain of Pch2

Sequence conservation of the AAA⁺ ATPase domain of Pch2 among different organisms. The alignment was made with MAFFT (Kato *et al.*, 2002) and secondary structure predictions are based on PSIPRED protein sequence analysis tool (<http://bioinf.cs.ucl.ac.uk/psipred/>), as indicated in Supplementary Figure 7. Dark blue arrows indicate β -strand secondary structure in *S. cerevisiae*; dark blue cylinders indicate α -helix structure in the same. Light blue shows predicted β -strand secondary structure in humans, whereas light blue cylinders indicate predicted α -helix structure the same. Red squares indicate the Walker A (1) and Walker B (2) motifs, the sensor 1 region (3) and the arginine (Arg) finger (4).

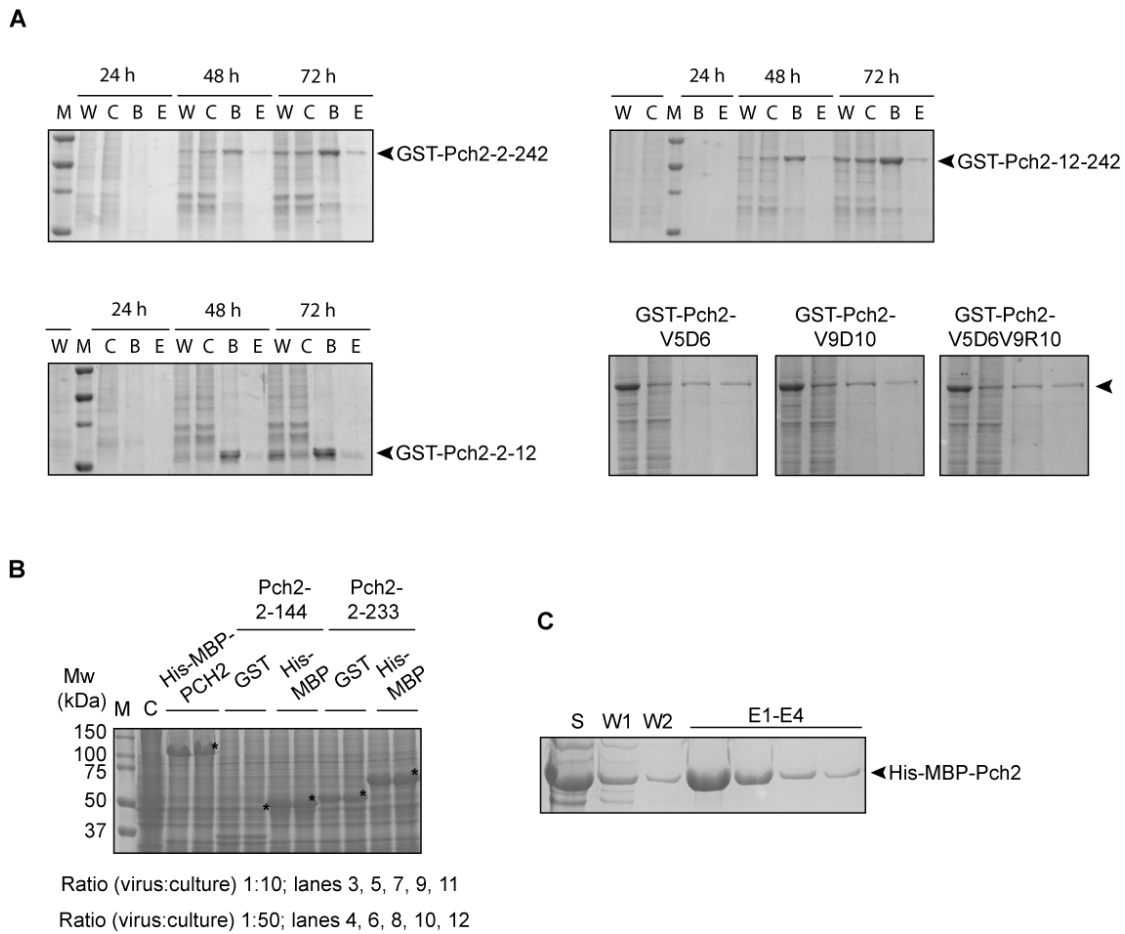


Figure 7-4 Expression tests of GST- and MBP-tagged Pch2 constructs

A) Expression test in insect cells of GST-tagged NH₂-terminal domain (NTD) of Pch2 (amino acids 2-242) (left, upper panel), GST-Pch2-12-242 (left, lower panel), GST-Pch2-2-12 (right, upper panel) or GST-Pch2 point mutants in which the following residues V5D6, V9R10 or V5D6V9R10 were substituted by alanine residues (right, lower panel). Samples were collected 24, 48 or 72 hours after baculovirus infection and processed to give whole-cell extract (W) and clear lysate (C) samples. C samples were incubated with GSH-beads (B) and finally eluted via competition with glutathione (eluted fraction, E). M indicates molecular weight marker. Arrowheads indicate the protein of interest.

B) Expression test in insect cells of *Spodoptera frugiperda* codon-optimized constructs of Pch2 carrying either a His-MBP or GST tag. C stands for control cells (insect cells not infected with baculovirus). Asterisks denote the band corresponding to the protein of interest. The following ratios virus to culture were used: for lanes 3, 5, 7, 9 and 11, a ratio virus:culture of 1:10 was used. For lanes 4, 6, 8, 10 and 12, a ratio 1:50 was used.

C) Amylose resin binding test of His-MBP-Pch2. S indicates supernatant; W1 and W2 stand for the buffer washes of His-MBP-Pch2-bound to amylose resin; E1-E4 stand for eluted fractions of His-MBP-Pch2, after eluting with buffer containing 10 mM of maltose.

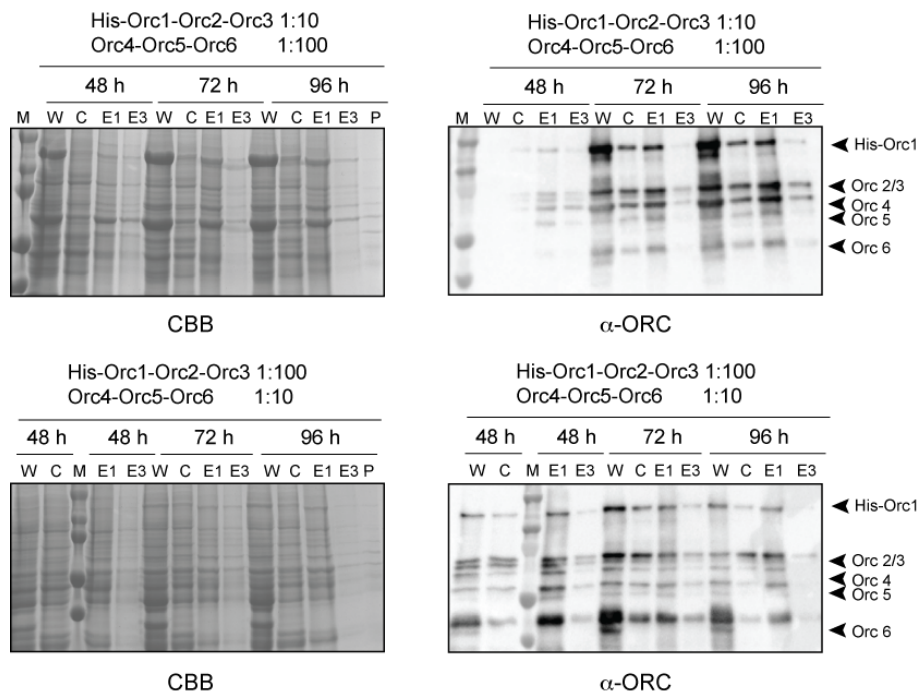


Figure 7-5 Expression test of ORC in insect cells

Baculovirus encoding His-Orc1-Orc2-3 and Orc4-Orc5-Orc6 were used at different ratios (baculovirus:culture) and collected 72 (upper panel) or 96 hours (lower panel) after infection. Three different combinations of baculovirus:culture ratios were used (1:10/1:100, 1:40/1:40, 1:100/1:10; see figure for clarity). W: whole-cell extract; C: clear lysate; E1, E3: elution fractions. Samples were analysed by SDS-PAGE, followed by either Coomassie Brilliant Blue (CBB) staining (left panels) or Western blot using α -ORC (right panels).

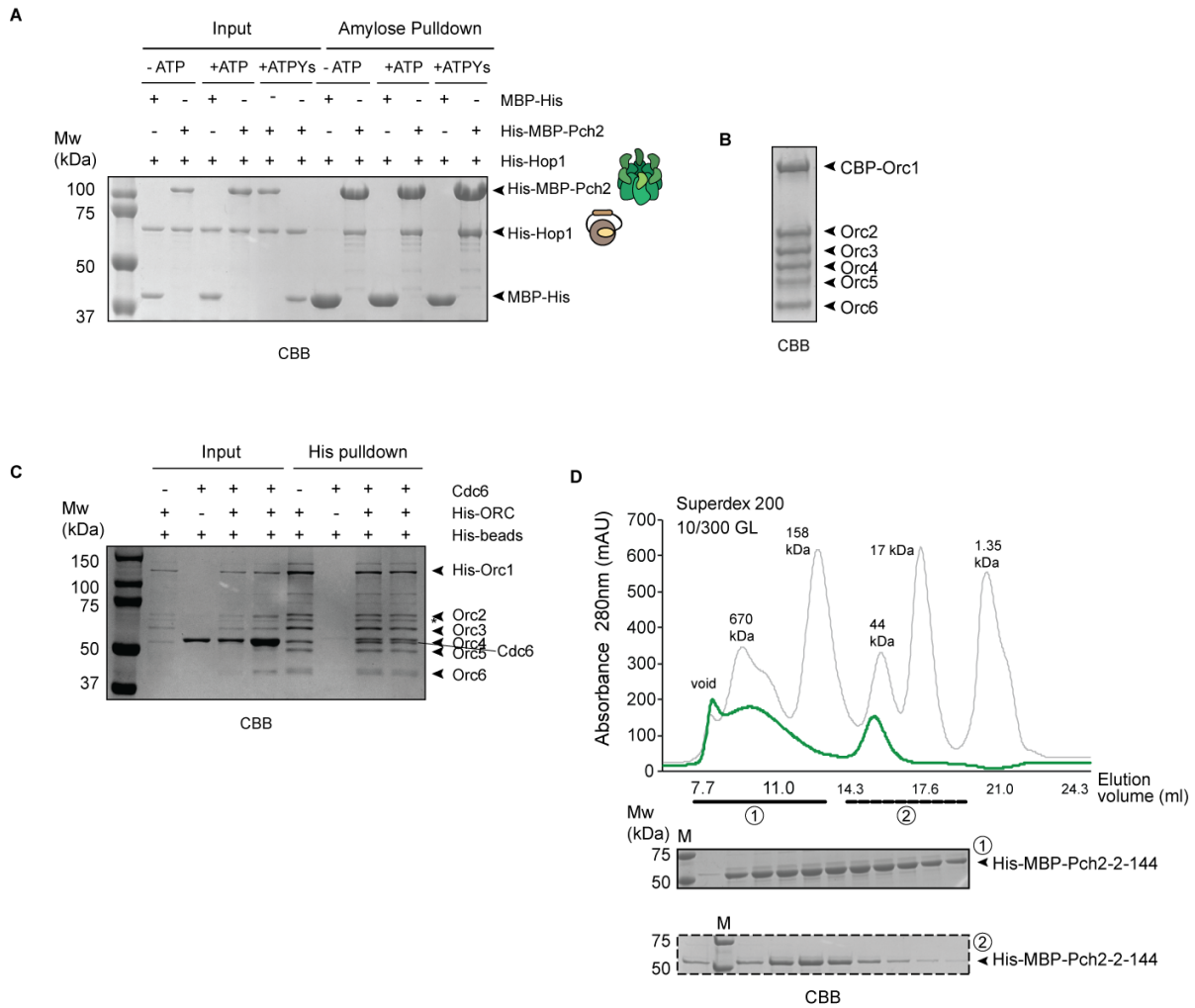


Figure 7-6 Biochemical characterization of recombinant Pch2 and ORC

A) Amylose pull-down of His-Hop1 (6 μ M) purified from bacteria and His-MBP-Pch2 (1 μ M, considering hexameric formation) purified from insect cells, in the absence or presence of ATP or a non-hydrolysable analog of ATP (ATPYs). MBP-His (6 μ M) was used as negative control. Input and pull-down samples were analysed by SDS-PAGE followed by Coomassie Brilliant Blue (CBB) staining. B) Sieve exclusion chromatography (SEC) fraction of purified CBP-ORC (CBP-Orc1, Orc2-6) from budding yeast, visualized via CBB staining. C) His-based pull-down of His-ORC (His-Orc1, Orc2-6) purified from insect cells and Cdc6 purified from bacteria. His-beads were used as a negative control. 1 μ M of ORC (considering hexamer) and 6 μ M of Cdc6 were used in pull-down reactions in lanes 3 and 7, whereas 1 μ M of ORC and 18 μ M of Cdc6 were used in lanes 4 and 8. Input and pull-down samples were analysed by SDS-PAGE and CBB staining. D) SEC of His-MBP-Pch2-2-144 (green line) using a Superdex 200 10/300 GL column and purified from insect cells. Gray line represents protein standard and molecular weights are indicated. AU stands for arbitrary units. The first peak (black line) indicates the aggregate of His-MBP-Pch2-2-144. The second peak (dotted line) indicates monomeric His-MBP-Pch2-2-144, used for further interaction assays.

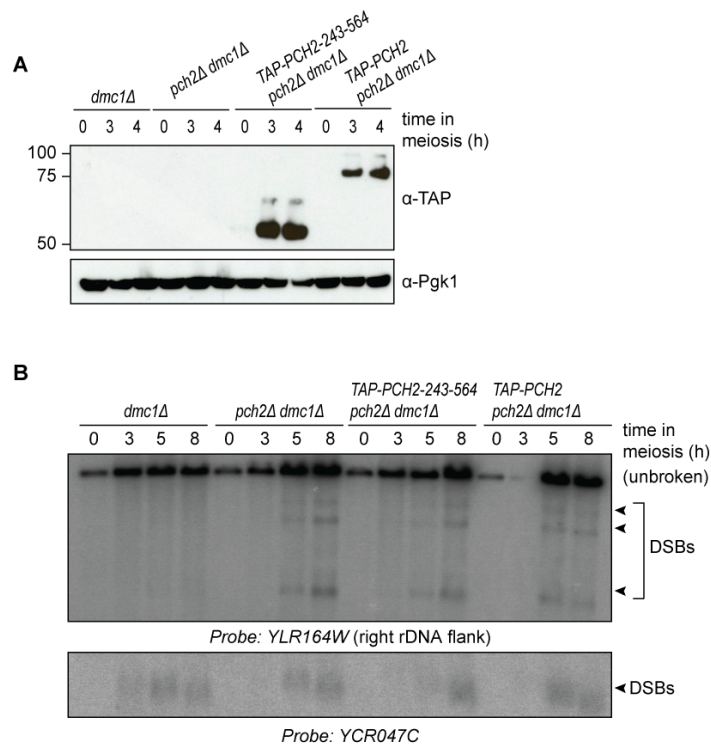


Figure 7-7 Tagging of Pch2 with TAP-tag leads to impairment of Pch2 function

A) Western blot showing expression of TAP-Pch2-243-564 and TAP-Pch2 at indicated time points in meiosis. α -Pgk1 was used as loading control. B) Southern blot analysis of *YLR164W* locus (right rDNA flank; Chromosome *XII*) and *YCR047C* locus (control DSB region; Chromosome *III*), in *dmc1Δ*, *pch2Δdmc1Δ*, *TAP-PCH2-243-564 pch2Δdmc1Δ* and *TAP-PCH2 pch2Δdmc1Δ* background strains. Cells were induced to synchronously undergo meiosis and samples from sporulation cultures were harvested at time points 0, 3, 5 and 8 hours after meiotic induction. *dmc1Δ* is used to detect accumulation of meiotic DSBs. Arrowheads indicate the position of the DSBs.

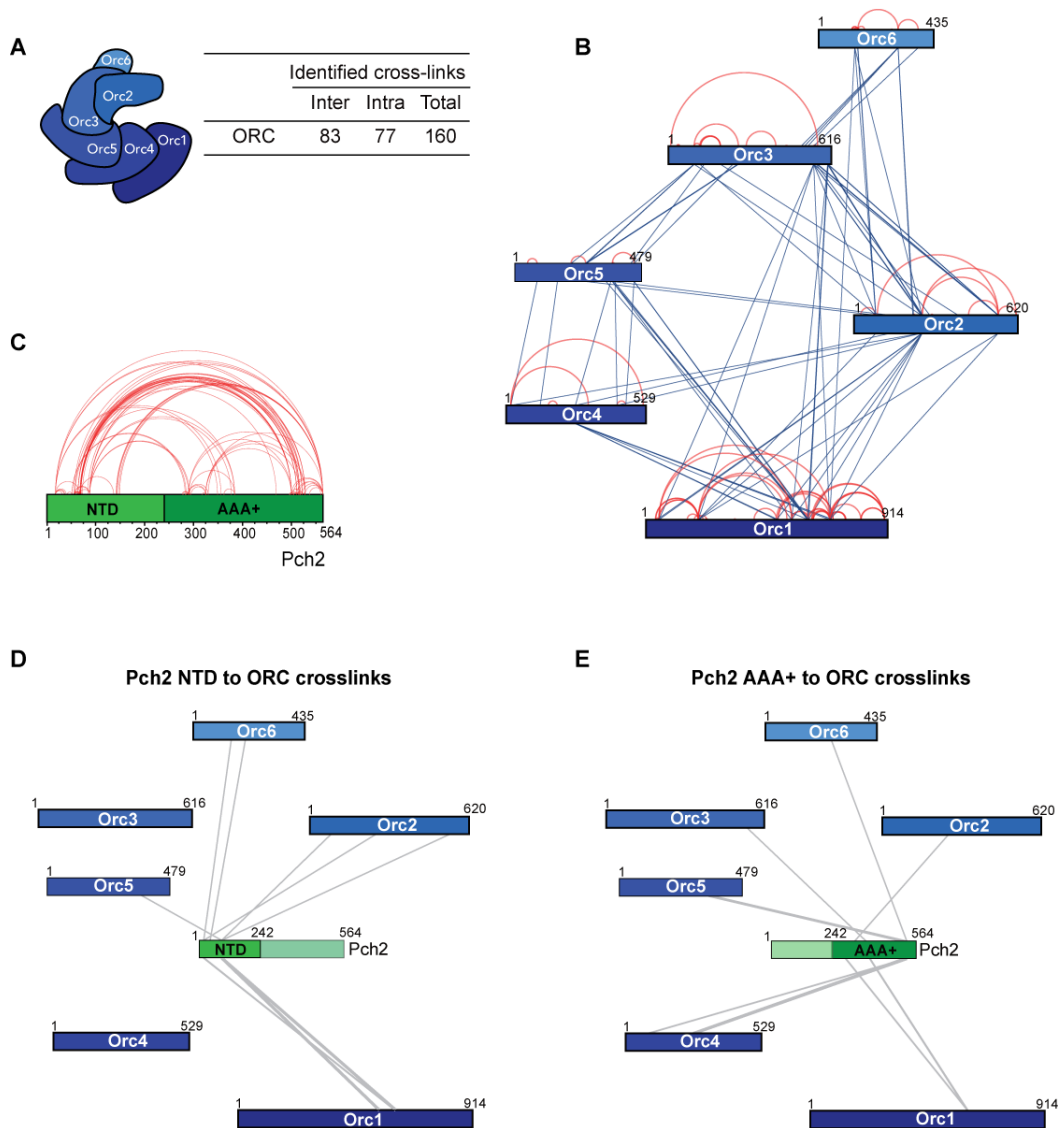


Figure 7-8 Cross-links identified by XL-MS

A) Table indicating inter-ORC and intra-ORC cross-linked peptides (non-redundant (inter- and intramolecular) crosslinks after applying a false discovery rate (FDR) of 2%). B) Schematic indicating identified inter-/intra-ORC non-redundant cross-links. Blue represents inter-ORC cross-links; red indicates intra-ORC cross-links. C) Schematic of Pch2 structure (NTD: NH₂-terminal domain; AAA⁺: AAA⁺ ATPase domain) indicating Pch2-Pch2 crosslinks (in red). Note that we classified the Pch2-Pch2 crosslinks as intra-molecular (see section 3.3 for further details). D) Schematic indicating identified non-redundant inter-molecular cross-links between the NTD of Pch2 and ORC. E) Schematic of non-redundant inter-molecular cross-links between the AAA⁺ ATPase domain of Pch2 with ORC. Protein lengths (amino acids) of the ORC subunits and Pch2 are indicated. Network plots were generated using xVis web site (<https://xvis.genzentrum.lmu.de>).

Table 7-1 Mass spectrometry analysis of purified Pch2 and ORC

Protein IDs	Protein names	Gene names	Unique peptides	Sequence coverage (%)	(kDa)	(aa)	Intensity	MS/MS count
P54784	Origin recognition complex subunit 1	<i>ORC1</i>	67	71,9	104,4	914	2,4541E+11	450
P54791	Origin recognition complex subunit 4	<i>ORC4</i>	39	83,4	60.705	529	1,4592E+11	279
P50874	Origin recognition complex subunit 5	<i>ORC5</i>	36	78,3	55.289	479	1,3894E+11	269
P54790	Origin recognition complex subunit 3	<i>ORC3</i>	39	73,4	72.076	616	1,3801E+11	258
P32833	Origin recognition complex subunit 2	<i>ORC2</i>	42	64	71.237	620	1,1003E+11	201
P38826	Origin recognition complex subunit 6	<i>ORC6</i>	35	69,2	50.295	435	83714000000	130
P38126	Pachytene checkpoint 2	<i>PCH2</i>	51	78,2	63,46	564	6,9364E+11	533

Table 7-2 Cross-links identified by XL-MS of Pch2-ORC

List of all intra- and inter-molecular cross-links in the Pch2-ORC assembly identified by XL-MS. Available in the electronic version of this PhD thesis.

Table 7-3 Cross-links identified by XL-MS analysed by MeroX

List of cross-links in the Pch2-ORC assembly analysed by MeroX (www.StavroX.com) after applying an FDR (false discovery rate) of 2%. Cross-links are grouped as follows: all cross-links after applying a 2% FDR; Pch2-ORC inter-molecular cross-links; His-MBP-Pch2 inter-molecular; Pch2-ORC; Pch2-Pch2 intra-molecular; His-MBP-His-MBP intra-molecular. Pch2-ORC overview represents the total cross-links between Pch2 for each ORC subunit. Available in the electronic version of this PhD thesis.

Table 7-4 Comparative analysis of the intra- and inter-ORC cross-links

Comparison of the cross-links found in our XL-MS data set and by Yuan *et al.*, 2017. Available in the electronic version of this PhD thesis.

Table 7- 5 Oligonucleotides used for cloning

Oligonucleotides used for cloning (by restriction cloning and Gibson assembly). Available in the electronic version of this PhD thesis.

Table 7-6 Oligonucleotides used for the ORC assembly into pLIB vectors (biGBac system)

Oligonucleotides used for cloning ORC into pLIB vectors for ORC expression in insect cells Available in the electronic version of this PhD thesis.

Table 7-7 Oligonucleotides used for ChIP-qPCR

Oligonucleotide	Sequence
<i>PPR1</i> -forward	5'-AGAACGTCATCTCCGGAATCT-3'
<i>PPR1</i> -reverse	5'-TGGGCACGATGAGAGAAAGT-3'
<i>ARS1116</i> -forward	5'-AAGCTTTTCATCCCAGCAGA-3'
<i>ARS1116</i> -reverse	5'-TTTTTGTCGTTGTTTCGATTCA-3'

Primer efficiencies (calculated using standard procedures) were as follows: (*PPR1*=1.998, *ARS1116*=1.991)

Table 7-8 Plasmids used for yeast transformation and protein expression

Plasmids used for yeast transformation and protein expression. Available in the electronic version of this PhD thesis.

Table 7-9 Yeast strains used in this PhD thesis

Strain	Genotype	Figure
GV48	<i>MATa</i> , <i>ho::LYS2, lys2, leu2::hisG, his4X::LEU2-URA3, ura3, arg4-nsp, dmc1Δ::ARG4</i> <i>MATalpha</i> , <i>ho::LYS2, lys2, leu2::hisG, his4B::LEU2, ura3, arg4-Bgl2, dmc1Δ::ARG4</i>	3-3 D 3-9 E 3-11 F 3-13 B 3-13 C
GV49	<i>MATa</i> , <i>ho::LYS2, lys2, ura3, leu2::hisG, his4B::LEU2, arg4-Bgl II</i> <i>MATalpha</i> , <i>ho::LYS2, lys2, ura3, leu2::hisG, his4X::LEU2 (Bam)-URA3, arg4-Nsp</i>	3-16 D
GV933	<i>MATa</i> , <i>ho::LYS2, lys2, ura3, leu2::hisG, trp1::hisG, his3::hisG, his4B::LEU2, arg4-Bgl II, pch2::URA3:pPCH2(300bp):3HA-PCH2</i> <i>MATalpha</i> , <i>ho::LYS2, lys2, ura3, leu2::hisG, trp1::hisG, his3::hisG, his4B::LEU2, arg4-Bgl II, pch2::URA3:pPCH2(300bp):3HA-PCH2</i>	3-1 B 3-1 C 3-14 B
GV1185	<i>MATa</i> , <i>ho::LYS2, lys2, ura3, leu2::hisG, TRP1, HIS3, arg4-Bgl II, pch2::URA3:pPCH2(300bp):3HA-PCH2, orc1::orc1-161 (ts-allele)</i> <i>MATalpha</i> , <i>ho::LYS2, lys2, ura3, leu2::hisG, TRP1, ARG, HIS3, his4B::LEU2, pch2::URA3:pPCH2(300bp):3HA-PCH2, orc1::orc1-161</i>	3-14 B
GV1192	<i>MATalpha</i> , <i>ho::LYS2, lys2, ura3, leu2::hisG, TRP, his3::hisG, his4B::LEU2, arg4-Bgl II/nspI, dmc1Δ::ARG4, pch2Δ::KanMX, Cdc6::KanMX6::Psccl: CDC6</i> <i>MATa</i> , <i>ho::LYS2, lys2, ura3, leu2::hisG, TRP, arg4-Bgl II/Nsp, his4X::LEU2-(Bam)-URA3, arg4-Nsp, pch2Δ::KanMX4, dmc1Δ::ARG4, Cdc6::KanMX6::Psccl: CDC6</i>	3-3 D
GV1269	<i>MATa</i> , <i>ho::LYS2, lys2, ura3, leu2::hisG, TRP, his4B::LEU2, arg4-Bgl II, dmc1Δ::ARG4, pch2Δ::KanMX4</i> <i>MATalpha</i> , <i>ho::LYS2, lys2, ura3, leu2::hisG, TRP, his4B::LEU2, arg4-BglII, dmc1Δ::ARG4, pch2Δ::KanMX4</i>	3-3 D
GV1506	<i>MATa</i> , <i>ho::LYS2, lys2, ura3, leu2::hisG, HIS3, pch2::URA3:pPCH2(300bp): 3HA-PCH2, orc1::ORC1- TAP::HIS3</i> <i>MATalpha</i> , <i>ho::LYS2, lys2, ura3, leu2::hisG, TRP1, HIS3, his4B::LEU2, pch2::URA3:pPCH2(300bp):3HA-PCH2, orc1::ORC1-TAP::HIS3</i>	3-1 B 3-1 C 3-2 B 3-16 D
GV1508	<i>MATa</i> , <i>ho::LYS2, lys2, ura3, leu2::hisG, HIS3, trp1::hisG, his4B::LEU2, orc2::ORC2-TAP::HIS3, pch2::URA3:pPCH2(300bp):3HA-PCH2</i> <i>MATalpha</i> , <i>ho::LYS2, lys2, ura3, leu2::hisG, HIS3, trp1::hisG, orc2::ORC2-TAP::HIS3, pch2::URA3:pPCH2(300bp):3HA-PCH2</i>	3-2 B 3-14 B

Strain	Genotype	Figure
GV1537	<i>MATa</i> , <i>ho::LYS2, lys2, ura3, leu2::hisG, TRP1, HIS3, ARG4, ORC5-TAP::HIS3, pch2::URA3:pPCH2(300bp):3HA-PCH2</i> <i>MATalpha</i> , <i>ho::LYS2, lys2, ura3, leu2::hisG, trp1::hisG, his3::hisG, ARG4, his4B::LEU2, ORC5-TAP::HIS3, pch2::URA3:pPCH2(300bp):3HA-PCH2</i>	3-2 B
GV1945	<i>MATa</i> , <i>ho::LYS2, lys2, ura3, leu2::hisG, HIS3, trp1::hisG, his4B::LEU2, orc2::ORC2-TAP::HIS3, pch2::URA3:pPCH2(300bp):3HA-PCH2, orc1::orc1-161</i> <i>MATalpha</i> , <i>ho::LYS2, lys2, ura3, leu2::hisG, HIS3, trp1::hisG, his4B::LEU2, orc2::ORC2-TAP::HIS3, pch2::URA3:pPCH2(300bp):3HA-PCH2, orc1::orc1-161</i>	3-14 B
GV1966	<i>MATa</i> , <i>ho::LYS2, lys2, ura3, leu2::hisG, ARG4, TRP1, HIS3, orc1::ORC1-TAP::HIS3, pch2::URA3:pPCH2(300bp):3HA-pch2-K320R</i> <i>MATalpha</i> , <i>ho::LYS2, lys2, ura3, leu2::hisG, arg4-bglII, TRP1, HIS3, his4B::LEU2, orc1::ORC1-TAP::HIS3, pch2::URA3:pPCH2(300bp):3HA-pch2-K320R</i>	3-1 C
GV2030	<i>yGV864, [pGAD], [pGBD]</i>	3-14 A 3-9 B 3-11 B
GV2036	<i>yGV864, [pGAD], [pGBD-PCH2]</i>	3-9 B 3-11 B
GV2060	<i>yGV864, [pGAD], [pGBD-PCH2 2-242]</i>	3-9 B
GV2061	<i>yGV864, [pGAD], [pGBD-PCH2-242-565]</i>	3-9 B
GV2085	<i>MATa</i> , <i>ho::LYS2, lys2, ura3, leu2::hisG, TRP1, HIS3, arg4-Bgl II, pch2::URA3:pPCH2(300bp):3HA-PCH2-E399Q, orc1::ORC1-TAP::HIS3</i> <i>MATalpha</i> , <i>ho::LYS2, lys2, ura3, leu2::hisG, TRP1, HIS3, his4B::LEU2, arg4-Bgl II, pch2::URA3:pPCH2(300bp):3HA-PCH2-E399Q, orc1::ORC1-TAP::HIS3</i>	3-1 B 3-2 C
GV2086	<i>MATalpha</i> , <i>ho::LYS2, lys2, ura3, leu2::hisG, TRP1, HIS3, his4B::LEU2, arg4-Bgl II, pch2::URA3:pPCH2(300bp):3HA-PCH2-E399Q</i> <i>MATa</i> , <i>ho::LYS2, lys2, ura3, leu2::hisG, TRP1, his4B::LEU2, arg4-Bgl II, pch2::URA3:pPCH2(300bp):3HA-PCH2-E399Q</i>	3-2 C 3-3 A 3-3 B 3-14 C
GV2098	<i>MATalpha</i> , <i>ho::LYS2, lys2, ura3, leu2::hisG, his3::hisG, trp1::hisG, orc1::TRP1, ura3::orc1ΔNTD(1-235)-TAP::HIS3::URA3, pch2::URA3:pPCH2(300bp):3HA-PCH2</i> <i>MATa</i> , <i>ho::LYS2, lys2, ura3, leu2::hisG, his3::hisG, trp1::hisG, his4B::LEU2, orc1::TRP1, ura3::orc1ΔNTD(1-235)-TAP::HIS3::URA3, pch2::URA3:pPCH2(300bp):3HA-PCH2</i>	3-16 D

Strain	Genotype	Figure
GV2099	<i>MATa</i> , <i>ho::LYS2</i> , <i>lys2</i> , <i>ura3</i> , <i>leu2::hisG</i> , <i>TRP</i> , <i>his3::hisG</i> , <i>ARG4</i> , <i>pch2Δ::KanMX</i> , <i>orc1::ORC1-TAP::HIS3</i> <i>MATalpha</i> , <i>ho::LYS2</i> , <i>lys2</i> , <i>ura3</i> , <i>leu2::hisG</i> , <i>trp1::hisG</i> , <i>his3::hisG</i> , <i>arg4-Nsp/arg4</i> , <i>his4X::LEU2-(Bam)-URA3</i> , <i>pch2Δ::KanMX</i> , <i>orc1::ORC1-TAP::HIS3</i>	3-16 D
GV2114	<i>yGV864</i> , [<i>pGAD-ORC1</i>], [<i>pGBD</i>]	3-14 A 3-9 B 3-11 B
GV2115	<i>yGV864</i> , [<i>pGAD-ORC1</i>], [<i>pGBD-PCH2-1-242</i>]	3-9 B
GV2116	<i>yGV864</i> , [<i>pGAD-ORC1</i>], [<i>pGBD-PCH2-242-565</i>]	3-9 B
GV2117	<i>yGV864</i> , [<i>pGAD-ORC1</i>], [<i>pGBD-PCH2</i>]	3-9 B 3-11 B
GV2155	<i>MATa</i> , <i>ho::LYS2</i> , <i>lys2</i> , <i>ura3</i> , <i>leu2::hisG</i> , <i>TRP1</i> , <i>HIS3</i> , <i>ARG4</i> , <i>pch2::URA3:pPCH2(300bp):3HA-PCH2-E399Q</i> , <i>orc2::ORC2-TAP::HIS3</i> <i>MATalpha</i> , <i>ho::LYS2</i> , <i>lys2</i> , <i>ura3</i> , <i>leu2::hisG</i> , <i>TRP1</i> , <i>HIS3</i> , <i>ARG4</i> , <i>his4B::LEU2</i> , <i>pch2::URA3:pPCH2(300bp):3HA-PCH2-E399Q</i> , <i>orc2::ORC2-TAP::HIS3</i>	3-2 C
GV2156	<i>MATa</i> , <i>ho::LYS2</i> , <i>lys2</i> , <i>ura3</i> , <i>leu2::hisG</i> , <i>TRP1</i> , <i>HIS3</i> , <i>arg4-Bgl II</i> , <i>pch2::URA3:pPCH2(300bp):3HA-PCH2-E399Q</i> , <i>ORC5-TAP::HIS3</i> <i>MATalpha</i> , <i>ho::LYS2</i> , <i>lys2</i> , <i>ura3</i> , <i>leu2::hisG</i> , <i>TRP1</i> , <i>HIS3</i> , <i>arg4-Bgl II</i> , <i>pch2::URA3:pPCH2(300bp):3HA-PCH2-E399Q</i> , <i>ORC5-TAP::HIS3</i>	3-2 C 3-14 C
GV2203	<i>MATa</i> , <i>ho::LYS2</i> , <i>lys2</i> , <i>ura3</i> , <i>leu2::hisG</i> , <i>his3::hisG</i> , <i>trp1::hisG</i> , <i>RPL13A-2XFKBP12::TRP1</i> , <i>fpr1Δ::KanMX4</i> , <i>tor1-1::HIS3</i> , <i>ORC2-FRB::KanMX6</i> <i>MATalpha</i> , <i>ho::LYS2</i> , <i>lys2</i> , <i>ura3</i> , <i>leu2::hisG</i> , <i>his3::hisG</i> , <i>trp1::hisG</i> , <i>RPL13A-2XFKBP12::TRP1</i> , <i>fpr1Δ::KanMX4</i> , <i>tor1-1::HIS3</i> , <i>ORC2-FRB::KanMX6</i>	3-13 B 3-13 C
GV2207	<i>MATa</i> , <i>ho::LYS2</i> , <i>lys2</i> , <i>ura3</i> , <i>leu2::hisG</i> , <i>his3::hisG</i> , <i>trp1::hisG</i> , <i>his4X::LEU2-URA3</i> , <i>trp1::pPch2::TRP1</i> , <i>dmc1Δ::ARG4</i> , <i>pch2Δ::KanMX</i> <i>MATalpha</i> , <i>ho::LYS2</i> , <i>lys2</i> , <i>ura3</i> , <i>leu2::hisG</i> , <i>his3::hisG</i> , <i>trp1::hisG</i> , <i>his4X::LEU2-URA3</i> , <i>trp1::pPch2::TRP1</i> , <i>dmc1Δ::ARG4</i> , <i>pch2Δ::KanMX</i>	3-9 D 3-11 F
GV2315	<i>yGV864</i> , [<i>pGAD-ORC1</i>], [<i>pGBD-PCH2-2-194</i>]	3-11 A
GV2316	<i>yGV864</i> , [<i>pGAD-Orc1</i>], [<i>pGBD-PCH2-2-144</i>]	3-11 A
GV2321	<i>yGV864</i> , [<i>pGAD</i>], [<i>pGBD-PCH2-2-194</i>]	3-11 A
GV2322	<i>yGV864</i> , [<i>pGAD</i>], [<i>pGBD-PCH2-2-144</i>]	3-11 A
GV2345	<i>MATa</i> , <i>ho::LYS2</i> , <i>lys2</i> , <i>leu2::hisG</i> , <i>his4X::LEU2-URA3</i> , <i>ura3</i> , <i>arg4(-nsp)</i> , <i>TRP1</i> , <i>dmc1Δ::ARG4</i> , <i>ctf19Δ::KanMX6</i> , <i>cdc6::KanMX6::pSCC1:CDC6</i> <i>MATalpha</i> , <i>ho::LYS2</i> , <i>lys2</i> , <i>leu2::hisG</i> , <i>ura3</i> , <i>arg4(-nsp)</i> , <i>dmc1Δ::ARG4</i> , <i>cdc6::KanMX6::pSCC1:CDC6</i>	3-3 D

Strain	Genotype	Figure
GV2366	<i>MATa, ho::LYS2, lys2, ura3, leu2::hisG, his3::hisG, arg4, trp1::hisG, RPL13A-2XFKBP12::TRP1, fpr1::KanMX4, tor1-1::HIS3, ORC2-FRB::KanMX6, dmc1Δ::ARG4</i> <i>MATalpha, ho::LYS2, lys2, ura3, leu2::hisG, his3::hisG, arg4, trp1::hisG, RPL13A-2XFKBP12::TRP1, fpr1::KanMX4, tor1-1::HIS3, ORC2-FRB::KanMX6, dmc1Δ::ARG4</i>	3-12 B 3-12 C 3-13 B 3-13 C
GV2367	<i>MATa, ho::LYS2, lys2, leu2::hisG, ura3, arg4-Bgl2, his3::hisG, trp1::hisG, RPL13A-2XFKBP12::TRP1, fpr1::KanMX4, tor1-1::HIS3, dmc1Δ::ARG4</i> <i>MATalpha, ho::LYS2, lys2, leu2::hisG, ura3, arg4-Bgl2, his3::hisG, trp1::hisG, RPL13A-2XFKBP12::TRP1, fpr1::KanMX4, tor1-1::HIS3, dmc1Δ::ARG4</i>	3-12 B 3-12 C 3-13 B 3-13 C
GV2380	<i>yGV864, [pGAD-C1], [pGBDU-C1 -Pch2 12-564]</i>	3-11 A 3-11 B
GV2381	<i>yGV864, [pGADC1-Orc1], [pGBDU-C1 -Pch2 12-564]</i>	3-11 A 3-11 B
GV2383	<i>yGV864, [pGAD-C1], [pGBDU-C1 -Pch2 12-144]</i>	3-11 A
GV2384	<i>yGV864, [pGADC1-Orc1], [pGBDU-C1 -Pch2 12-144]</i>	3-11 A
GV2393	<i>MATa, ho::LYS2, lys2, leu2::hisG, ura3, arg4-Bgl2, his3::hisG, trp1::hisG, RPL13A-2XFKBP12::TRP1, fpr1::KanMX4, tor1-1::HIS3, ORC5-FRB::KanMX6, dmc1Δ::ARG4</i> <i>MATalpha, ho::LYS2, lys2, leu2::hisG, ura3, arg4-Bgl2, his3::hisG, trp1::hisG, RPL13A-2XFKBP12::TRP1, fpr1::KanMX4, tor1-1::HIS3, ORC5-FRB::KanMX6, dmc1Δ::ARG4</i>	3-12 B 3-12 C 3-13 B 3-13 C
GV2397	<i>yGV864, [pGAD], [pGBD-PCH2-2-60]</i>	3-11 B
GV2401	<i>yGV864, [pGAD], [pGBDU-PCH2-2-27]</i>	3-11 B
GV2402	<i>yGV864, [pGAD-ORC1], [pGBDU-PCH2-2-27]</i>	3-11 B
GV2428	<i>yGV864, [pGAD-C1], [pGBDU-C1-PCH2-V5AD6A]</i>	3-11 B
GV2429	<i>yGV864, [pGAD-C1-ORC1], [pGBDU-C1-PCH2-V5AD6A]</i>	3-11 B
GV2430	<i>yGV864, [pGAD-C1], [pGBDU-C1-PCH2-V9AR10A]</i>	3-11 B
GV2431	<i>yGV864, [pGAD-C1-ORC1], [pGBDU-C1-PCH2-V9AR10A]</i>	3-11 B
GV2724	<i>MATalpha, ho::LYS2, lys2, leu2::hisG, his4X::LEU2-URA3, his3::hisG, ura3, trp1::hisG, dmc1Δ::ARG4, pch2Δ::KanMX, trp1:pPCH2-3xFLAG-6XGLY-V9R10 FL Pch2::TRP1</i> <i>MATa, ho::LYS2, lys2, leu2::hisG, his4X::LEU2-URA3, his3::hisG, ura3, trp1::hisG, dmc1Δ::ARG4, pch2Δ::KanMX, trp1:pPCH2-3xFLAG-6XGLY-V9R10 FL Pch2::TRP1</i>	3-11 F
GV2731	<i>MATa, ho::LYS2, lys2, leu2::hisG, his4X::LEU2-URA3, his3::hisG, ura3, ARG4, trp1:pPCH2-3xFLAG-6XGLY-V5D6 Pch2::TRP1, dmc1Δ::ARG4, pch2Δ::KanMX</i> <i>MATalpha, ho::LYS2, lys2, leu2::hisG, his4X::LEU2-URA3, his3::hisG, ura3, ARG4, trp1:pPCH2-3xFLAG-6XGLY-V5D6 Pch2::TRP1, dmc1Δ::ARG4, pch2Δ::KanMX</i>	3-11 F

Strain	Genotype	Figure
GV2741	<i>MATa</i> , <i>ho::LYS2, lys2, leu2::hisG, his4X::LEU2-URA3, his3::hisG, ura3, trp1: 3xFLAG-6XGLY-Pch2::TRP1, pch2Δ::KanMX, ARG4</i> <i>MATalpha</i> , <i>ho::LYS2, lys2, leu2::hisG, his4X::LEU2-URA3, his3::hisG, ura3, trp1: 3xFLAG-6XGLY-Pch2::TRP1, pch2Δ::KanMX, ARG4</i>	3-9 D
GV2760	<i>MATalpha</i> , <i>ho::LYS2, lys2, leu2::hisG, his4X::LEU2-URA3, his3::hisG, ura3, dmc1Δ::ARG4, trp1:pPCH2-3xFLAG-6XGLY-deltaNTD-Pch2::TRP1, pch2Δ::KanMX, ARG4</i> <i>MATa</i> , <i>ho::LYS2, lys2, leu2::hisG, his4X::LEU2-URA3, his3::hisG, ura3, dmc1Δ::ARG4, trp1:pPCH2-3xFLAG-6XGLY-deltaNTD-Pch2::TRP1, pch2Δ::KanMX, ARG4</i>	3-9 C 3-9 D
GV2799	<i>MATa</i> , <i>ho::LYS2, lys2, leu2::hisG, his3::hisG, trp1:pPCH2-3xFLAG-6XGLY-FL Pch2::TRP1, pch2Δ::KanMX, ARG4, his4X::LEU2-URA3</i> <i>MATalpha</i> , <i>ho::LYS2, lys2, leu2::hisG, his3::hisG, trp1:pPCH2-3xFLAG-6XGLY-FL Pch2::TRP1, pch2Δ::KanMX, ARG4, his4X::LEU2-URA3</i>	3-11 E
GV2813	<i>MATa</i> , <i>ho::LYS2, lys2, leu2::hisG, his4XΔ::LEU2-URA3, his3::hisG, ura3, trp1: 3xFLAG-6XGLY-Pch2-243-564::TRP1, pch2Δ::KanMX, ARG4, orc1::ORC1-TAP::HIS3</i> <i>MATalpha</i> , <i>ho::LYS2, lys2, leu2::hisG, his4X::LEU2-URA3, his3::hisG, ura3, trp1: 3xFLAG-6XGLY-Pch2-243-564::TRP1, pch2Δ::KanMX, ARG4, orc1::ORC1-TAP::HIS3</i>	3-9 D
GV2814	<i>MATalpha</i> , <i>ho::LYS2, lys2, ura3, leu2::hisG, his3::hisG, trp1::hisG, his4X::LEU2-URA3, trp1:pPch2::TRP1, pch2Δ::KanMX, orc1::ORC1-TAP::HIS3</i> <i>MATa</i> , <i>ho::LYS2, lys2, ura3, leu2::hisG, his3::hisG, trp1::hisG, his4X::LEU2-URA3, trp1:pPch2::TRP1, pch2Δ::KanMX, orc1::ORC1-TAP::HIS3</i>	3-16 D
GV2815	<i>MATalpha</i> , <i>ho::LYS2, lys2, leu2::hisG, his3::hisG, his4X::LEU2-URA3, ura3, ARG4, trp1:pPCH2-3xFLAG-6XGLY-V5D6 Pch2-Pch2::TRP1, pch2Δ::KanMX, orc1::ORC1-TAP::HIS3</i> <i>MATa</i> , <i>ho::LYS2, lys2, leu2::hisG, his3::hisG, ura3, ARG4, trp1:pPCH2-3xFLAG-6XGLY-V5D6 Pch2-Pch2::TRP1, pch2Δ::KanMX, orc1::ORC1-TAP::HIS3</i>	3-11 E
GV2816	<i>MATa</i> , <i>ho::LYS2, lys2, leu2::hisG, his4X::LEU2-URA3, his3::hisG, ura3, trp1: 3xFLAG-6XGLY-Pch2::TRP1, pch2Δ::KanMX, ARG4, orc1::ORC1-TAP::HIS3</i> <i>MATalpha</i> , <i>ho::LYS2, lys2, leu2::hisG, his4X::LEU2-URA3, his3::hisG, ura3, trp1: 3xFLAG-6XGLY-Pch2::TRP1, pch2Δ::KanMX, ARG4, orc1::ORC1-TAP::HIS3</i>	3-9 D 3-11 E

Strain	Genotype	Figure
GV2817	<i>MAT</i> α , <i>ho::LYS2, lys2, his4X::LEU2-URA3, his3::hisG, ura3, trp1::hisG, ARG4, pch2Δ::KanMX, trp1:pPCH2-3xFLAG-6XGLY-V9R10 FL Pch2-Pch2::TRP1, orc1::ORC1-TAP::HIS3</i> <i>MAT</i> α , <i>ho::LYS2, lys2, his4X::LEU2-URA3, his3::hisG, ura3, trp1::hisG, ARG4, pch2Δ::KanMX, trp1:pPCH2-3xFLAG-6XGLY-V9R10 FL Pch2-Pch2::TRP1, orc1::ORC1-TAP::HIS3</i>	3-11 E
GV2878	<i>MAT</i> α , <i>ho::LYS2, lys2, leu2::hisG, his4X::LEU2-URA3, his3::hisG, ura3, trp1::hisG, pch2Δ::KanMX, ARG4, trp1:pPch2-3xFLAG-6XGLY-Pch2E399Q::TRP1</i> <i>MAT</i> α , <i>ho::LYS2, lys2, leu2::hisG, his4X::LEU2-URA3, his3::hisG, ura3, trp1::hisG, pch2Δ::KanMX, ARG4, trp1:pPch2-3xFLAG-6XGLY-Pch2E399Q::TRP1</i>	3-2 D
GV2973	<i>MAT</i> α , <i>ho::LYS2, lys2, leu2::hisG, his3::hisG, ura3, trp1::hisG, pch2Δ::KanMX, trp1:pPCH2-3xFLAG-6XGLY-FL Pch2::TRP1, his4X::LEU2-URA3, ura3, arg4-nsp, dmc1Δ::ARG4</i> <i>MAT</i> α , <i>ho::LYS2, lys2, leu2::hisG, his3::hisG, ura3, trp1::hisG, his4B::LEU2, pch2Δ::KanMX, trp1:pPCH2-3xFLAG-6XGLY-FL Pch2::TRP1, dmc1Δ::ARG4</i>	3-9 C 3-9 D 3-11 F
GV3324	<i>MAT</i> α , <i>ho::LYS2, lys2, ura3, leu2::hisG, his3::hisG, ARG4, trp1::hisG, RPL13A-2XFKBP12::TRP1, fpr1::KanMX4, tor1-1::HIS3, ORC2-FRB::KanMX6, pch2::URA3:pPCH2(300bp):3HA-PCH2</i> <i>MAT</i> α , <i>ho::LYS2, lys2, ura3, leu2::hisG, his3::hisG, ARG4, trp1::hisG, RPL13A-2XFKBP12::TRP1, fpr1::KanMX4, tor1-1::HIS3, ORC2-FRB::KanMX6, pch2::URA3:pPCH2(300bp):3HA-PCH2</i>	3-12 B
GV3338	<i>MAT</i> α , <i>ho::LYS2, lys2, ura3, leu2::hisG, TRP, HIS3, ARG4, pch2::URA3:pPCH2(300bp):3HA-pch2-E399Q, cdc6::KanMX6::pSCC1:CDC6</i> <i>MAT</i> α , <i>ho::LYS2, lys2, ura3, leu2::hisG, TRP, HIS3/his3::hisG, his4B::LEU2, ARG4, pch2::URA3:pPCH2(300bp):3HA-pch2-E399Q, cdc6::KanMX6::pSCC1:CDC6</i>	3-3 A 3-3 B
GV3415	<i>MAT</i> α , <i>ho::LYS2, lys2, ura3, leu2::hisG, TRP, HIS3, arg4-Bgl II, pch2::URA3:pPCH2(300bp):3HA-pch2-E399Q, ORC5-TAP::HIS3, orc1::orc1-161</i> <i>MAT</i> α , <i>ho::LYS2, lys2, ura3, leu2::hisG, TRP, HIS3, ARG4, pch2::URA3:pPCH2(300bp):3HA-PCH2-E399Q, ORC5-TAP::HIS3, orc1::orc1-161</i>	3-14 C
GV3417	<i>MAT</i> α , <i>ho::LYS2, lys2, ura3, leu2::hisG, TRP, HIS3 his4B::LEU2, arg4-Bgl II, pch2::URA3:pPCH2(300bp):3HA-PCH2-E399Q</i> <i>MAT</i> α , <i>ho::LYS2, lys2, leu2::hisG, his3::hisG, ura3, trp1::hisG, ARG4, pch2Δ::KanMX, trp1:pPCH2-FLAG tag V9R10 FL Pch2-Pch2::TRP1</i>	3-11 C 3-11 D

Strain	Genotype	Figure
GV3418	<i>MATalpha, ho::LYS2, lys2, ura3, leu2::hisG, TRP, HIS3</i> <i>his4B::LEU2, arg4-Bgl II</i> <i>pch2::URA3:pPCH2(300bp):3HA-PCH2-E399Q</i> <i>MATa, ho::LYS2, lys2, leu2::hisG, his4X::LEU2-URA3,</i> <i>his3::hisG, ura3, ARG4, trp1:pPCH2-FLAG tag V5D6 Pch2-</i> <i>Pch2::TRP1,dmc1Δ::ARG4, pch2Δ::KanMX</i>	3-11 D 3-11 D
GV3419	<i>MATalpha, ho::LYS2, lys2, ura3, leu2::hisG, TRP, HIS3</i> <i>his4B::LEU2, arg4-Bgl II</i> <i>pch2::URA3:pPCH2(300bp):3HA-PCH2-E399Q</i> <i>MATa, ho::LYS2, lys2, leu2::hisG, his4X::LEU2-URA3,</i> <i>his3::hisG, ura3, trp1:pPCH2-FLAG tag FL Pch2::TRP1,</i> <i>pch2Δ::KanMX, ARG4</i>	3-11 D 3-11 D
GV3778	<i>yGV864, [pGAD], [pGBD-PCH2-2-91]</i>	3-10 A
GV3779	<i>yGV864, [pGAD], [pGBD-PCH2-2-121]</i>	3-10 A
GV3780	<i>yGV864, [pGAD], [pGBD-PCH2-2-233]</i>	3-10 A
GV3781	<i>yGV864, [pGAD], [pGBD-PCH2-2-257]</i>	3-10 A
GV3782	<i>yGV864, [pGAD], [pGBD-PCH2-2-270]</i>	3-10 A
GV3791	<i>yGV864, [pGAD-ORC1], [pGBD-PCH2-2-233]</i>	3-10 A
GV3793	<i>yGV864, [pGAD-ORC1], [pGBD-PCH2-2-121]</i>	3-10 A
GV3802	<i>yGV864, [pGAD-ORC], [pGBD-PCH2-2-91]</i>	3-10 A
GV3803	<i>yGV864, [pGAD-ORC], [pGBD-PCH2-2-60]</i>	3-10 A
GV3823	<i>yGV864, [pGAD-ORC1], [pGBD-PCH2-2-270]</i>	3-10 A
GV3824	<i>yGV864, [pGAD-ORC1], [pGBD-PCH2-2-257]</i>	3-10 A
GV3968	<i>yGV864, [pGAD-ORC2], [pGBD]</i>	3-14 A
GV3974	<i>yGV864, [pGAD-ORC2], [pGBD-PCH2]</i>	3-14 A
GV3976	<i>yGV864, [pGAD-ORC3], [pGBD-PCH2]</i>	3-14 A
GV3977	<i>yGV864, [pGAD-ORC3], [pGBD]</i>	3-14 A
GV3978	<i>yGV864, [pGAD-ORC4], [pGBD-PCH2]</i>	3-14 A
GV3979	<i>yGV864, [pGAD-ORC4], [pGBD]</i>	3-14 A
GV3980	<i>yGV864, [pGAD-ORC6], [pGBD-PCH2]</i>	3-14 A
GV3981	<i>yGV864, [pGAD-ORC6], [pGBD]</i>	3-14 A
GV4033	<i>MATa, ho::LYS2, lys2, leu2::hisG, his4X::LEU2-URA3,</i> <i>his3::hisG, ura3, trp1:pPCH2-3xFLAG-6XGLY-Pch2 243-</i> <i>564::TRP1, pch2::KanMX, ARG4</i> <i>MATalpha, ho::LYS2, lys2, leu2::hisG, his3::hisG, URA3,</i> <i>trp1:pPCH2-3xFLAG-6XGLY-Pch2 243-564::TRP1,</i> <i>pch2Δ::KanMX, ARG4, ndt80Δ::LEU2</i>	3-9 D
GV4411	<i>MATalpha, ho::LYS2, lys2, ura3, leu2::hisG, his3::hisG,</i> <i>trp1::hisG, RPL13A-2XFKBP12::TRP1, fpr1::KanMX4, tor1-</i> <i>1::HIS3, ORC2-FRB::KanMX6, orc1::ORC1-TAP::HIS3</i> <i>MATa, ho::LYS2, lys2, ura3, leu2::hisG, his3::hisG,</i> <i>trp1::hisG, RPL13A-2XFKBP12::TRP1, fpr1::KanMX4, tor1-</i> <i>1::HIS3, ORC2-FRB::KanMX6, orc1::ORC1-TAP::HIS3</i>	3-13 D

8 Bibliography

- Acquaviva, L., Székvölgyi, L., Dichtl, B., Solange Dichtl, B., de La Roche Saint André, C., Nicolas, A., & Géli, V. (2013). The COMPASS subunit Spp1 links histone methylation to initiation of meiotic recombination. *Science*, 339(6116), 215-218.
- Akiyama, Y., & Ito, K. (2000). Roles of multimerization and membrane association in the proteolytic functions of FtsH (HflB). *The EMBO Journal*, 19(15), 3888–3895.
- Akiyama, Y., Yoshihisa, T., & Ito, K. (1995). FtsH, a Membrane-bound ATPase, Forms a Complex in the Cytoplasmic Membrane of *Escherichia coli*. *The Journal of Biological Chemistry*, 270(40), 23485–23490.
- Albert, B., Knight, B., Merwin, J., Martin, V., Ottoz, D., Gloor, Y., Bruzzone, M.J., Rudner, A., Shore, D. (2016). A Molecular Titration System Coordinates Ribosomal Protein Gene Transcription with Ribosomal RNA Synthesis. *Molecular Cell*, 64(4), 720–733.
- Alfieri, C., Chang, L., & Barford, D. (2018). Mechanism for remodelling of the cell cycle checkpoint protein Mad2 by the ATPase TRIP13. *Nature*, 559(7713), 274–278.
- Aparicio, O. M., Weinstein, D., & Bell, S. P. (1997). Components and dynamics of DNA replication complexes in *S. cerevisiae*: redistribution of MCM proteins and Cdc45p during S phase. *Cell*, 91(1), 59–69.
- Aravind, L., & Koonin, E. V. (1998). The HORMA domain: a common structural denominator in mitotic checkpoints, chromosome synapsis and DNA repair. *Trends in Biochemical Sciences*, 23(8), 284–286.
- Arias, E. E., & Walter, J. C. (2007). Strength in numbers: Preventing rereplication via multiple mechanisms in eukaryotic cells. *Genes and Development*, 21(5), 497–518.
- Arnaudo, N., Fernández, I. S., McLaughlin, S. H., Peak-Chew, S. Y., Rhodes, D., & Martino, F. (2013). The N-terminal acetylation of Sir3 stabilizes its binding to the nucleosome core particle. *Nature Structural and Molecular Biology*, 20(9), 1119–1122.
- Augustin, S., Gerdes, F., Lee, S., Tsai, F. T. F., Langer, T., & Tatsuta, T. (2009). An Intersubunit Signaling Network Coordinates ATP Hydrolysis by m-AAA Proteases. *Molecular Cell*, 35(5), 574–585.
- Ayad, N. G. (2005). CDKs give Cdc6 a license to drive into S phase. *Cell*, 122(6), 825–827.
- Babst, M., Wendland, B., Estepa, E. J., & Emr, S. D. (1998). The Vps4p AAA ATPase regulates membrane association of a Vps protein complex required for normal endosome function. *The EMBO Journal*, 17(11), 2982–2993.
- Balbo, A., & Schuck, P. (2005). Analytical ultracentrifugation in the study of protein self-

- association and heterogeneous protein-protein interactions. *Protein-Protein Interactions: A Molecular Cloning Manual*, (301), 253–277.
- Ballew, O., & Lacefield, S. (2019). The DNA damage checkpoint and the spindle position checkpoint: guardians of meiotic commitment. *Current Genetics*, 65(5), 1135–1140.
- Baudat, F., Buard, J., Grey, C., Fledel-Alon, A., Ober, C., Przeworski, M., Coop, G., De Massy, B. (2010). PRDM9 is a major determinant of meiotic recombination hotspots in humans and mice. *Science*, 327(5967), 836–840.
- Bell, S. P. (2002). The origin recognition complex: From simple origins to complex functions. *Genes and Development*, 16(6), 659–672.
- Bell, S. P. (2017). Rethinking origin licensing. *eLife*, 6, e24052.
- Bell, S. P., & Kaguni, J. M. (2013). Helicase loading at chromosomal origins of replication. *Cold Spring Harbor Perspectives in Biology*, 5(6), a010124.
- Bell, S. P., & Labib, K. (2016). Chromosome duplication in *Saccharomyces cerevisiae*. *Genetics*, 203(3), 1027–1067.
- Bell, S. P., Mitchell, J., Leber, J., Kobayashi, R., & Stillman, B. (1995). The multidomain structure of Orc1 p reveals similarity to regulators of DNA replication and transcriptional silencing. *Cell*, 83, 563–568.
- Bell, S. P., & Stillman, B. (1992). ATP-dependent recognition of eukaryotic origins of DNA replication by a multiprotein complex. *Nature*, 357(6374), 128–134.
- Berchowitz, L., & Copenhaver, G. (2010). Genetic Interference: Dont Stand So Close to Me. *Current Genomics*, 11(2), 91–102.
- Bhalla, N., & Dernburg, A. F. (2005). Cell biology: A conserved checkpoint monitors meiotic chromosome synapsis in *Caenorhabditis elegans*. *Science*, 310(5754), 1683–1686.
- Bishop, D. K., Park, D., Xu, L., & Kleckner, N. (1992). DMC1: A meiosis-specific yeast homolog of *E. coli* recA required for recombination, synaptonemal complex formation, and cell cycle progression. *Cell*, 69, 439–456.
- Bishop, D. K., & Zickler, D. (2004). Early decision: Meiotic crossover interference prior to stable strand exchange and synapsis. *Cell*, 117(1), 9–15.
- Biswas, M., Maqani, N., Rai, R., Kumaran, S. P., Iyer, K. R., Sendinc, E., Smith, J.S., Laloraya, S. (2009). Limiting the Extent of the RDN1 Heterochromatin Domain by a Silencing Barrier and Sir2 Protein Levels in *Saccharomyces cerevisiae*. *Molecular and Cellular Biology*, 29(10), 2889–2898.
- Blat, Y., Protacio, R. U., Hunter, N., & Kleckner, N. (2002). Physical and functional interactions among basic chromosome organizational features govern early steps of

- meiotic chiasma formation. *Cell*, *111*(6), 791–802.
- Bleichert, F. (2019). Mechanisms of replication origin licensing: a structural perspective. *Current Opinion in Structural Biology*, *59*, 195–204.
- Bleichert, F., Balasov, M., Chesnokov, I., Nogales, E., Botchan, M. R., & Berger, J. M. (2013). A Meier-Gorlin syndrome mutation in a conserved C-terminal helix of Orc6 impedes origin recognition complex formation. *eLife*, *2*, e00882.
- Bleichert, F., Botchan, M. R., & Berger, J. M. (2015). Crystal structure of the eukaryotic origin recognition complex. *Nature*, *519*(7543), 321–326.
- Blitzblau, H. G., Bell, G. W., Rodriguez, J., Bell, S. P., & Hochwagen, A. (2007). Mapping of Meiotic Single-Stranded DNA Reveals Double-Strand-Break Hotspots near Centromeres and Telomeres. *Current Biology*, *17*(23), 2003–2012.
- Blitzblau, H. G., Chan, C. S., Hochwagen, A., & Bell, S. P. (2012). Separation of DNA replication from the assembly of break-competent meiotic chromosomes. *PLoS Genetics*, *8*(5).
- Bodnar, N. O., & Rapoport, T. A. (2017). Molecular Mechanism of Substrate Processing by the Cdc48 ATPase Complex. *Cell*, *169*(4), 722–735.
- Boos, D., Frigola, J., & Diffley, J. F. X. (2012). Activation of the replicative DNA helicase: breaking up is hard to do. *Current Opinion in Cell Biology*, *24*(3), 423–430.
- Borde, V., & de Massy, B. (2013). Programmed induction of DNA double strand breaks during meiosis: setting up communication between DNA and the chromosome structure. *Current Opinion in Genetics & Development*, *23*(2), 147–155.
- Borde, V., Goldman, A. S. H., & Lichten, M. (2000). Direct coupling between meiotic DNA replication and recombination initiation. *Science*, *290*(5492), 806–809.
- Börner, G. V., Barot, A., & Kleckner, N. (2008). Yeast Pch2 promotes domainal axis organization, timely recombination progression, and arrest of defective recombinosomes during meiosis. *Proceedings of the National Academy of Sciences of the United States of America*, *105*(9), 3327–3332.
- Bowers, J. L., Randell, J. C. W., Chen, S., & Bell, S. P. (2004). ATP hydrolysis by ORC catalyzes reiterative Mcm2-7 assembly at a defined origin of replication. *Molecular Cell*, *16*(6), 967–978.
- Brar, G. A., Kiburz, B. M., Zhang, Y., Kim, J. E., White, F., & Amon, A. (2006). Rec8 phosphorylation and recombination promote the step-wise loss of cohesins in meiosis. *Nature*, *441*(7092), 532–536.
- Brautigam, C. A. (2015). Calculations and Publication-Quality Illustrations for Analytical

- Ultracentrifugation Data. In *Methods in Enzymology* (1st ed., Vol. 562).
- Brewer, B. J., & Fangman, W. L. (1987). The localization of replication origins on ARS plasmids in *S. cerevisiae*. *Cell*, *51*(3), 463–471.
- Brown, P. H., Balbo, A., & Schuck, P. (2009). On the analysis of sedimentation velocity in the study of protein complexes. *European Biophysics Journal*, *38*(8), 1079–1099.
- Buck, S. W., Maqani, N., Matecic, M., Hontz, R. D., Fine, R. D., Li, M., & Smith, J. S. (2016). RNA Polymerase i and Fob1 contributions to transcriptional silencing at the yeast rDNA locus. *Nucleic Acids Research*, *44*(13), 6173–6184.
- Buck, S. W., Sandmeier, J. J., & Smith, J. S. (2002). RNA Polymerase I Propagates Unidirectional Spreading of rDNA Silent Chromatin. *Cell*, *111*(7), 1003–1014.
- Buonomo, S. B. C., Clyne, R. K., Fuchs, J., Loidl, J., Uhlmann, F., & Nasmyth, K. (2000). Disjunction of homologous chromosomes in meiosis I depends on proteolytic cleavage of the meiotic cohesin Rec8 by separin. *Cell*, *103*(3), 387–398.
- Carballo, J. A., Johnson, A. L., Sedgwick, S. G., & Cha, R. S. (2008). Phosphorylation of the Axial Element Protein Hop1 by Mec1/Tel1 Ensures Meiotic Interhomolog Recombination. *Cell*, *132*(5), 758–770.
- Carballo, J. A., Panizza, S., Serrentino, M. E., Johnson, A. L., Geymonat, M., Borde, V., Klein, F., Cha, R. S. (2013). Budding yeast ATM/ATR control meiotic double-strand break (DSB) levels by down-regulating Rec114, an essential component of the DSB-machinery. *PLoS Genetics*, *9*(6), 39–40.
- Cardoso da Silva, R., Villar-Fernandez, M. A., & Vader, G. (2019). Active transcription and Orc1 drive chromatin association of the AAA+ ATPase Pch2 during meiotic G2/prophase. *bioRxiv*, doi: <https://doi.org/10.1101/777003>
- Carpenter, A. T. C. (1987). Gene conversion, recombination nodules, and the initiation of meiotic synapsis. *BioEssays*, *6*(5), 232–236.
- Cavero, S., Herruzo, E., Ontoso, D., & San-Sengundo, P. A. (2016). Impact of histone H4K16 acetylation on the meiotic recombination checkpoint in *Saccharomyces cerevisiae*. *Microbial Cell*, *3*(12), 606–620.
- Chang, F. J., May, C. D., Hoggard, T., Miller, J., Fox, C. A., & Weinreich, M. (2011). High-resolution analysis of four efficient yeast replication origins reveals new insights into the ORC and putative MCM binding elements. *Nucleic Acids Research*, *39*(15), 6523–6535.
- Chen, C., Jomaa, A., Ortega, J., & Alani, E. E. (2014). Pch2 is a hexameric ring ATPase that remodels the chromosome axis protein Hop1. *Proceedings of the National Academy of Sciences*, *111*(1), E44–E53.

- Chu, S., DeRisi, J., Eisen, M., Mulholland, J., Botstein, D., Brown, P. O., & Herskowitz, I. (1998). The transcriptional program of sporulation in budding yeast. *Science*, *282*(5389), 699–705.
- Ciosk, R., Shirayama, M., Shevchenko, A., Tanaka, T., Toth, A., Shevchenko, A., & Nasmyth, K. (2000). Cohesin's binding to chromosomes depends on a separate complex consisting of Scc2 and Scc4 proteins. *Molecular Cell*, *5*(2), 243–254.
- Collins, I., & Newlon, C. S. (1994). Chromosomal DNA replication initiates at the same origins in meiosis and mitosis. *Molecular and Cellular Biology*, *14*(5), 3524–3534.
- Connelly, J. J., Yuan, P., Hsu, H. C., Li, Z., Xu, R. M., & Sternglanz, R. (2006). Structure and function of the *Saccharomyces cerevisiae* Sir3 BAH domain. *Mol Cell Biol*, *26*(8), 3256–3265.
- Cooper, T. J., Garcia, V., & Neale, M. J. (2016). Meiotic DSB patterning: A multifaceted process. *Cell Cycle*, *15*(1), 13–21.
- Corbett, K. D. (2017). Molecular Mechanisms of Spindle Assembly Checkpoint Activation and Silencing. *Progress in Molecular and Subcellular Biology*, *56*, 429–455.
- Coster, G., & Diffley, J. F. X. (2017). Bidirectional eukaryotic DNA replication is established by quasi-symmetrical helicase loading. *Science*, *357*(6348), 314–318.
- Coster, G., Frigola, J., Beuron, F., Morris, E. P., & Diffley, J. F. X. (2014). Origin Licensing Requires ATP Binding and Hydrolysis by the MCM Replicative Helicase. *Molecular Cell*, *55*(5), 666–677.
- Dalal, S., Rosser, M. F. N., Cyr, D. M., & Hanson, P. I. (2004). Distinct Roles for the AAA ATPases NSF and p97 in the Secretory Pathway. *Molecular Biology of the Cell*, *15*(2), 637–648.
- De Ioannes, P., Leon, V. A., Kuang, Z., Wang, M., Boeke, J. D., Hochwagen, A., & Armache, K. J. (2019). Structure and function of the Orc1 BAH-nucleosome complex. *Nature Communications*, *10*(1), 2894.
- De Massy, B. (2013). Spp1 Links Sites of Meiotic DNA Double-Strand Breaks to Chromosome Axes. *Molecular Cell*, *49*(1), 3–5.
- Deegan, T. D., & Diffley, J. F. X. (2016). MCM: One ring to rule them all. *Current Opinion in Structural Biology*, *37*, 145–151.
- DeLaBarre, B., & Brunger, A. T. (2003). Complete structure of p97/valosin-containing protein reveals communication between nucleotide domains. *Nature Structural Biology*, *10*(10), 856–863.
- DePamphilis, M. L. (2005). Cell Cycle Dependent Regulation of the Origin Recognition

- Complex. *Cell Cycle*, 4(1), 70–79.
- Deshong, A. J., Ye, A. L., Lamelza, P., & Bhalla, N. (2014). A Quality Control Mechanism Coordinates Meiotic Prophase Events to Promote Crossover Assurance. *PLoS Genetics*, 10(4), e1004291.
- Diffley, J. F. X. (2011). Quality control in the initiation of eukaryotic DNA replication. *Philosophical Transactions of the Royal Society of London. Series B, Biological Sciences*, 366(1584), 3545–3553.
- Diffley, J. F. X., Cocker, J. H., Dowell, S. J., Harwood, J., & Rowley, A. (1995). Stepwise assembly of initiation complexes at budding yeast replication origins during the cell cycle. *Journal of Cell Science*, (SUPPL. 19), 67–72.
- Diffley, J. F. X., & Labib, K. (2002). The chromosome replication cycle. *Journal of Cell Science*, 115, 869–872.
- Dillin, A., & Rine, J. (1995). On the origin of a silencer. *Trends in Biochemical Sciences*, 20(6), 231–235.
- Dirick, L., Goetsch, L., Ammerer, G., & Byess, B. (1998). Regulation of Meiotic S Phase. *Science*, 281(September), 1854–1857.
- Donovan, S., Harwood, J., Drury, L. S., & Diffley, J. F. X. (1997). Cdc6p-dependent loading of Mcm proteins onto pre-replicative chromatin in budding yeast. *Proceedings of the National Academy of Sciences of the United States of America*, 94(11), 5611–5616.
- Donze, D., Adams, C. R., Rine, J., & Kamakaka, R. T. (1999). The boundaries of the silenced HMR domain in *Saccharomyces cerevisiae*. *Genes and Development*, 13(6), 698–708.
- Donze, D., & Kamakaka, R. T. (2001). RNA polymerase III and RNA polymerase II promoter complexes are heterochromatin barriers in *Saccharomyces cerevisiae*. *The EMBO Journal*, 20(3), 520–531.
- Drury, L. S., Perkins, G., & Diffley, J. F. X. (2000). The cyclin-dependent kinase Cdc28p regulates distinct modes of Cdc6p proteolysis during the budding yeast cell cycle. *Current Biology*, 10(5), 231–240.
- Duan, X., Hall, J. A., Nikaido, H., & Quiocho, F. A. (2001). Crystal structures of the maltodextrin/maltose-binding protein complexed with reduced oligosaccharides: Flexibility of tertiary structure and ligand binding. *Journal of Molecular Biology*, 306(5), 1115–1126.
- Dubey, D. D., Davis, L. R., Greenfeder, S. A., Ong, L. Y., Zhu, J., Broach, J. R., Newlon, C.S., Huberman, J. A. (1991). Evidence suggesting that the ARS elements associated with silencers of the yeast mating-type locus HML do not function as chromosomal

- DNA replication origins. *Molecular and Cellular Biology*, 11(10), 5346–5355.
- Duncker, B. P., Chesnokov, I. N., & McConkey, B. J. (2009). The origin recognition complex protein family. *Genome Biology*, 10(3), 214.
- Duzdevich, D., Warner, M. D., Ticau, S., Ivica, N. A., Bell, S. P., & Greene, E. C. (2015). The Dynamics of Eukaryotic Replication Initiation: Origin Specificity, Licensing, and Firing at the Single-molecule-Level. *Molecular Cell*, 58(3), 483–494.
- Eaton, M. L., Galani, K., Kang, S., Bell, S. P., & MacAlpine, D. M. (2010). Conserved nucleosome positioning defines replication origins. *Genes and Development*, 24(8), 748–753.
- Elsasser, S., Chi, Y., Yang, P., & Campbell, J. L. (1999). Phosphorylation controls timing of Cdc6p destruction: A biochemical analysis. *Molecular Biology of the Cell*, 10(10), 3263–3277.
- Erzberger, J. P., & Berger, J. M. (2006). Evolutionary Relationships and Structural Mechanisms of Aaa+ Proteins. *Annual Review of Biophysics and Biomolecular Structure*, 35(1), 93–114.
- Erzberger, J. P., Mott, M. L., & Berger, J. M. (2006). Structural basis for ATP-dependent DnaA assembly and replication-origin remodeling. *Nature Structural and Molecular Biology*, 13(8), 676–683.
- Fink, R., & Petes, T. (1984). Gene conversion in the absence of reciprocal recombination. *Nature*, 310, 728–729.
- Foss, M., McNally, F. J., Laurenson, P., & Rine, J. (1993). Origin Recognition Complex (ORC) in Transcriptional Silencing and DNA Replication in *S. cerevisiae*. *Science*, 262(5141), 1838–1844.
- Fox, C. A., Ehrenhofer-Murray, A. E., Loo, S., & Rine, J. (1997). The origin recognition complex, SIR1, and the S phase requirement for silencing. *Science*, 276(5318), 1547–1551.
- Fox, C. A., Loo, S., Dillin, A., & Rine, J. (1995). The origin recognition complex has essential functions in transcriptional silencing and chromosomal replication. *Genes and Development*, 9(8), 911–924.
- Freese, E. B., Chu, M. I., & Freese, E. (1982). Initiation of Yeast sporulation by partial carbon, nitrogen, or phosphate deprivation. *Journal of Bacteriology*, 149(3), 840–851.
- Frigola, J., He, J., Kinkelin, K., Pye, V. E., Renault, L., Douglas, M. E., Remus, D., Cherepanov, P., Costa, A., Diffley, J. F. X. (2017). Cdt1 stabilizes an open MCM ring for helicase loading. *Nature Communications*, 8, 1–10.

- Frigola, J., Remus, D., Mehanna, A., & Diffley, J. F. X. (2013). ATPase-dependent quality control of DNA replication origin licensing. *Nature*, *495*(7441), 339–343.
- Fritze, C. E., Verschueren, K., Strich, R., & Esposito, R. E. (1997). Direct evidence for SIR2 modulation of chromatin structure in yeast rDNA. *The EMBO Journal*, *16*(21), 6495–6509.
- Gai, D., Chang, P., & Chen, X. S. (2010). Origin DNA melting and unwinding in DNA replication. *Curr Opin Struct. Biol.*, *20*(6), 756–762.
- Ganley, A. R. D., & Kobayashi, T. (2014). Ribosomal DNA and cellular senescence: new evidence supporting the connection between rDNA and aging. *FEMS Yeast Research*, *14*(1), 49–59.
- Gao, J., & Colaiacovo, M. P. (2018). Zipping and unzipping: protein modifications regulating synaptonemal complex dynamics. *Trends in Genetics*, *34*(3), 232–245.
- Garcia, V., Gray, S., Allison, R. M., Cooper, T. J., & Neale, M. J. (2015). Tel1ATM-mediated interference suppresses clustered meiotic double-strand-break formation. *Nature*, *520*(7545), 114–118.
- Gartenberg, M. R., & Smith, J. S. (2016). The nuts and bolts of transcriptionally silent chromatin in *Saccharomyces cerevisiae*. *Genetics*, *203*(4), 1563–1599.
- Gates, S. N., & Martin, A. (2019). Stairway to translocation: AAA+ motor structures reveal the mechanisms of ATP-dependent substrate translocation. *Protein Science*, 1–13.
- Gaudier, M., Schuwirth, B., Westcott, S., & Wigley, D. (2007). Structural Basis of DNA Replication Origin Recognition by an ORC Protein. *Science*, *317*, 1213–1217.
- Gerton, J. L., DeRisi, J., Shroff, R., Lichten, M., Brown, P. O., & Petes, T. D. (2000). Global mapping of meiotic recombination hotspots and coldspots in the yeast *Saccharomyces cerevisiae*. *Proceedings of the National Academy of Sciences*, *97*(21), 11383–11390.
- Gibson, D. G., Bell, S. P., & Aparicio, O. M. (2006). Cell cycle execution point analysis of ORC function and characterization of the checkpoint response to ORC inactivation in *Saccharomyces cerevisiae*. *Genes to Cells*, *11*(6), 557–573.
- Goni, R., García, P., & Foissac, S. (2009). The qPCR data statistical analysis. *Integromics White Paper*, *1*(September), 1–9.
- Gotta, M., Strahl-Bolsinger, S., Renauld, H., Laroche, T., Kennedy, B. K., Grunstein, M., & Gasser, S. M. (1997). Localization of Sir2p: The nucleolus as a compartment for silent information regulators. *The EMBO Journal*, *16*(11), 3243–3255.
- Gottlieb, S., & Esposito, R. E. (1989). A new role for a yeast transcriptional silencer gene, SIR2, in regulation of recombination in ribosomal DNA. *Cell*, *56*(5), 771–776.

- Granneman, S., & Baserga, S. J. (2005). Crosstalk in gene expression: coupling and co-regulation of rDNA transcription, pre-ribosome assembly and pre-rRNA processing. *Current Opinion in Cell Biology*, 17(3), 281–286.
- Gray, S., & Cohen, P. E. (2016). Control of Meiotic Crossovers: From Double-Strand Break Formation to Designation. *Annual Review of Genetics*, 50, 175–210.
- Grimm, M., Zimniak, T., Kahraman, A., & Herzog, F. (2015). XVis: A web server for the schematic visualization and interpretation of crosslink-derived spatial restraints. *Nucleic Acids Research*, 43(W1), W362–W369.
- Haering, C. H., Farcas, A. M., Arumugam, P., Metson, J., & Nasmyth, K. (2008). The cohesin ring concatenates sister DNA molecules. *Nature*, 454(7202), 297–301.
- Hagstrom, K. A., & Meyer, B. J. (2003). Condensin and cohesin: more than chromosome compactor and glue. *Nature Reviews Genetics*, 4(7), 520–534.
- Hanner, A. S., & Rusche, L. N. (2017). The yeast heterochromatin protein Sir3 experienced functional changes in the AAA+ domain after gene duplication and subfunctionalization. *Genetics*, 207(2), 517–528.
- Hanson, P. I., & Whiteheart, S. W. (2005). AAA+ proteins: Have engine, will work. *Nature Reviews Molecular Cell Biology*, 6(7), 519–529.
- Hartwell, L. H., & Weinert, T. A. (1989). Checkpoints: Controls that ensure the order of cell cycle events. *Science*, 246(4930), 629–634.
- Haruki, H., Nishikawa, J., & Laemmli, U. K. (2008). The Anchor-Away Technique: Rapid, Conditional Establishment of Yeast Mutant Phenotypes. *Molecular Cell*, 31(6), 925–932.
- Hassold, T., & Hunt, P. (2001). To err (meiotically) is human: the genesis of human aneuploidy. *Nature Reviews Genetics*, 2(4), 280–291.
- Hemerly, A. S., Prasanth, S. G., Siddiqui, K., & Stillman, B. (2009). Orc1 controls centriole and centrosome copy number in human cells. *Science*, 323(5915), 789–793.
- Henderson, A. S., Warburton, D., & Atwood, K. C. (1973). Ribosomal DNA connectives between human acrocentric chromosomes. *Nature*, 245(5420), 95–97.
- Henderson, K. A., Kee, K., Maleki, S., Santini, P. A., & Keeney, S. (2006). Cyclin-Dependent Kinase Directly Regulates Initiation of Meiotic Recombination. *Cell*, 125(7), 1321–1332.
- Herruzo, E., Ontoso, D., González-Arranz, S., Caverro, S., Lechuga, A., & San-Segundo, P. A. (2016). The Pch2 AAA+ ATPase promotes phosphorylation of the Hop1 meiotic checkpoint adaptor in response to synaptonemal complex defects. *Nucleic Acids Research*, 44(16), 7722–7741.

- Herruzo, E., Santos, B., Freire, R., Carballo, J. A., & San-Segundo, P. A. (2019). Characterization of Pch2 localization determinants reveals a nucleolar-independent role in the meiotic recombination checkpoint. *Chromosoma*, *128*(3), 297–316.
- Hickman, M. A., Froyd, C. A., & Rusche, L. N. (2011). Reinventing heterochromatin in budding yeasts: Sir2 and the origin recognition complex take center stage. *Eukaryotic Cell*, *10*(9), 1183–1192.
- Hickman, M. A., & Rusche, L. N. (2010). Transcriptional silencing functions of the yeast protein Orc1/Sir3 subfunctionalized after gene duplication. *Proceedings of the National Academy of Sciences*, *107*(45), 19384–19389.
- Ho, H. C., & Burgess, S. M. (2011). Pch2 acts through Xrs2 and Tel1/ATM to modulate interhomolog bias and checkpoint function during meiosis. *PLoS Genetics*, *7*(11).
- Hochwagen, A. (2008). Meiosis. *Current Biology*, *18*(15), 641–645.
- Hochwagen, A., & Amon, A. (2006). Checking your breaks: Surveillance mechanisms of meiotic recombination. *Current Biology*, *16*(6), 217–228.
- Hochwagen, A., Tham, W. H., Brar, G. A., & Amon, A. (2005). The FK506 binding protein Fpr3 counteracts protein phosphatase 1 to maintain meiotic recombination checkpoint activity. *Cell*, *122*(6), 861–873.
- Holding, A. N. (2015). XL-MS: Protein cross-linking coupled with mass spectrometry. *Methods*, *89*, 54–63.
- Hollingsworth, N. M. (2010). Phosphorylation and the creation of interhomolog bias during meiosis in yeast. *Cell Cycle*, *9*(3), 436–437.
- Hollingsworth, N. M., Goetsch, L., & Byers, B. (1990). The HOP1 gene encodes a meiosis-specific component of yeast chromosomes. *Cell*, *61*(1), 73–84.
- Hossain, M., & Stillman, B. (2016). Opposing roles for DNA replication initiator proteins ORC1 and CDC6 in control of Cyclin E gene transcription. *eLife*, *5*(e12785), 1–22.
- Hou, Z., Bernstein, D. A., Fox, C. A., & Keck, J. L. (2005). Structural basis of the Sir1-origin recognition complex interaction in transcriptional silencing. *Proceedings of the National Academy of Sciences*, *102*(24), 8489–8494.
- Huang, J., & Moazed, D. (2003). Association of the RENT complex with nontranscribed and coding regions of rDNA and a regional requirement for the replication fork block protein Fob1 in rDNA silencing. *Genes and Development*, *17*(17), 2162–2176.
- Huang, R. Y., & Kowalski, D. (1993). A DNA unwinding element and an ARS consensus comprise a replication origin within a yeast chromosome. *The EMBO Journal*, *12*(12), 4521–4531.

- Huberman, J. A. (1987). Eukaryotic DNA replication: A complex picture partially clarified. *Cell*, 48(1), 7–8.
- Humphryes, N., & Hochwagen, A. (2014). A Non-Sister Act: Recombination Template Choice During Meiosis. *Exp Cell Res*, 329(1), 53–60.
- Humphryes, N., Leung, W. K., Argunhan, B., Terentyev, Y., Dvorackova, M., & Tsubouchi, H. (2013). The Ecm11-Gmc2 Complex Promotes Synaptonemal Complex Formation through Assembly of Transverse Filaments in Budding Yeast. *PLoS Genetics*, 9(1), e1003194.
- Ide, S., Miyazaki, T., Maki, H., & Kobayashi, T. (2010). Abundance of ribosomal RNA gene copies maintains genome integrity. *Science*, 327(5966), 693–696.
- Iida, T., & Kobayashi, T. (2019). RNA Polymerase I Activators Count and Adjust Ribosomal RNA Gene Copy Number. *Molecular Cell*, 73(4), 645–654.
- Ikemura, T. (1985). Codon usage and tRNA content in unicellular and multicellular organisms. *Molecular Biology and Evolution*, 2(1), 13–34.
- Imai, S. I., Armstrong, C. M., Kaeberlein, M., & Guarente, L. (2000). Transcriptional silencing and longevity protein Sir2 is an NAD-dependent histone deacetylase. *Nature*, 403(6771), 795–800.
- Irniger, S. (2011). The Ime2 protein kinase family in fungi: more duties than just meiosis. *Molecular Microbiology*, 80(1), 1–13.
- Ishiguro, T., Tanaka, K., Sakuno, T., & Watanabe, Y. (2010). Shugoshin-PP2A counteracts casein-kinase-1-dependent cleavage of Rec8 by separase. *Nature Cell Biology*, 12(5), 500–506.
- Joshi, N., Barot, A., Jamison, C., & Börner, G. V. (2009). Pch2 links chromosome axis remodeling at future crossover sites and crossover distribution during yeast meiosis. *PLoS Genetics*, 5(7).
- Joshi, N., Brown, M. S., Bishop, D. K., & Boerner, G. V. (2015). Gradual Implementation of the Meiotic Recombination Program via Checkpoint Pathways Controlled by Global DSB Levels. *Mol Cell*, 57(5), 797–811.
- Joyce, E. F., & Mckim, K. S. (2010). Chromosome axis defects induce a checkpoint-mediated delay and interchromosomal effect on crossing over during drosophila meiosis. *PLoS Genetics*, 6(8).
- Joyce, E. F., & McKim, K. S. (2009). Drosophila PCH2 is required for a pachytene checkpoint that monitors double-strand-break-independent events leading to meiotic crossover formation. *Genetics*, 181(1), 39–51.

- Kang, S., Warner, M. D., & Bell, S. P. (2014). Multiple Functions for Mcm2-7 ATPase Motifs during Replication Initiation. *Molecular Cell*, *55*(5), 655–665.
- Katis, V. L., Lipp, J. J., Imre, R., Bogdanova, A., Okaz, E., Habermann, B., Mechtler, K., Nasmyth, K., Zachariae, W. (2010). Rec8 phosphorylation by casein kinase 1 and Cdc7-Dbf4 kinase regulates cohesin cleavage by separase during meiosis. *Developmental Cell*, *18*(3), 397–409.
- Kawakami, H., Ohashi, E., Kanamoto, S., Tsurimoto, T., & Katayama, T. (2015). Specific binding of eukaryotic ORC to DNA replication origins depends on highly conserved basic residues. *Scientific Reports*, *5*, 14929.
- Keeney, S. (2001). Mechanism and control of meiotic recombination initiation. *Curr. Top. Dev. Biol.*, *52*, 1–53.
- Keeney, S., Giroux, C. N., & Kleckner, N. (1997). Meiosis-specific DNA double-strand breaks are catalyzed by Spo11, a member of a widely conserved protein family. *Cell*, *88*(3), 375–384.
- Keeney, S., & Kleckner, N. (1995). Covalent protein-DNA complexes at the 5' strand termini of meiosis-specific double-strand breaks in yeast. *Proceedings of the National Academy of Sciences of the United States of America*, *92*(24), 11274–11278.
- Keeney, S., Lange, J., & Mohibullah, N. (2014). Self-Organization of Meiotic Recombination Initiation: General Principles and Molecular Pathways. *Annu Rev Genet.*, *38*(3), 319–335.
- Keeney, S., & Neale, M. J. (2006). Initiation of meiotic recombination by formation of DNA double-strand breaks: mechanism and regulation. *Biochemical Society Transactions*, *34*(4), 523–525.
- Kerr, G. W., Sarkar, S., & Arumugam, P. (2012). How to halve ploidy: lessons from budding yeast meiosis. *Cellular and Molecular Life Sciences*, *69*(18), 3037–3051.
- Kim, Y., Rosenberg, S. C., Kugel, C. L., Kostow, N., Rog, O., Davydov, V., Su, T.Y., Dernburg, A.F., Corbett, K. D. (2014). The chromosome axis controls meiotic events through a hierarchical assembly of HORMA domain proteins. *Developmental Cell*, *31*(4), 487–502.
- Kitajima, T. S., Sakuno, T., Ishiguro, K., Iemura, S., Natsume, T., Kawashima, S. A., & Watanabe, Y. (2006). Shugoshin collaborates with protein phosphatase 2A to protect cohesin. *Nature*, *441*(7089), 46–52.
- Klein, F., Mahr, P., Galova, M., Buonomo, S. B. C., Michaelis, C., Nairz, K., & Nasmyth, K. (1999). A Central Role for Cohesins in Sister Chromatid Cohesion, Formation of Axial

- Elements, and Recombination during Yeast Meiosis. *Cell*, 98(1), 91–103.
- Kobayashi, T. (2006). Strategies to maintain the stability of the ribosomal RNA gene repeats - Collaboration of recombination, cohesion, and condensation-. *Genes and Genetic Systems*, 81(3), 155–161.
- Kobayashi, T. (2014). Ribosomal RNA gene repeats, their stability and cellular senescence. *Proceedings of the Japan Academy Series B: Physical and Biological Sciences*, 90(4), 119–129.
- Kobayashi, T., Heck, D. J., Nomura, M., & Horiuchi, T. (1998). Expansion and contraction of ribosomal DNA repeats in *Saccharomyces cerevisiae*: requirement of replication fork blocking (Fob1) protein and the role of RNA polymerase I. *Genes and Development*, 12(24), 3821–3830.
- Kobayashi, T., & Sasaki, M. (2017). Ribosomal DNA stability is supported by many “buffer genes”— introduction to the Yeast rDNA Stability Database. *FEMS Yeast Research*, 17(1).
- Kogut, I., Wang, J., Guacci, V., Mistry, R. K., & Megee, P. C. (2009). The Scc2/Scc4 cohesin loader determines the distribution of cohesin on budding yeast chromosomes. *Genes and Development*, 23(19), 2345–2357.
- Kueng, S., Oppikofer, M., & Gasser, S. M. (2013). SIR Proteins and the Assembly of Silent Chromatin in Budding Yeast. *Annual Review of Genetics*, 47(1), 275–306.
- Kuhl, L.-M. Kinetochores-driven control of meiotic DNA break formation and recombination at centromere-proximal regions. DuEPublico: Duisburg-Essen Publications online, University of Duisburg-Essen, Germany, 2019.
- Kumar, C., & Remus, D. (2016). Eukaryotic replication origins: Strength in flexibility. *Nucleus*, 7(3), 292–300.
- Kuo, A. J., Song, J., Cheung, P., Ishibe-Murakami, Satoko Yamazoe, S., Chen, J. K., Patel, D. J., & Gozani, O. (2012). ORC1 BAH domain links H4K20me2 to DNA replication licensing and Meier-Gorlin syndrome. *Nature*, 484(7392), 115–119.
- Laloraya, S., Guacci, V., & Koshland, D. (2000). Chromosomal addresses of the cohesin component Mcd1p. *The Journal of Cell Biology*, 151(5), 1047–1056.
- Lam, I., & Keeney, S. (2014). Mechanism and Regulation of Meiotic Recombination Initiation. *Cold Spring Harbor Perspectives in Biology*, 7(1), a016634.
- Lam, I., & Keeney, S. (2015). Nonparadoxical evolutionary stability of the recombination initiation landscape in yeast. *Science*, 350(6263), 932–937.
- Lambing, C., Osman, K., Nuntasontorn, K., West, A., Higgins, J. D., Copenhaver, G. P.,

- Yang, J., Armstrong, S., Mechtler, K., Roitinger, E., Franklin, F. C. H. (2015). Arabidopsis PCH2 Mediates Meiotic Chromosome Remodeling and Maturation of Crossovers. *PLoS Genetics*, *11*(7), e1005372.
- Lao, J. P., & Hunter, N. (2010). Trying to avoid your sister. *PLoS Biology*, *8*(10), 1–6.
- Lee, B., & Amon, A. (2001). Meiosis: how to create a specialized cell cycle. *Current Opinion in Cell Biology*, *13*(6), 770–777.
- Leitner, A., Faini, M., Stengel, F., & Aebersold, R. (2016). Crosslinking and Mass Spectrometry: An Integrated Technology to Understand the Structure and Function of Molecular Machines. *Trends in Biochemical Sciences*, *41*(1), 20–32.
- Li, H., & Stillman, B. (2012). The origin recognition complex: a biochemical and structural view. *Subcell Biochem*, *62*, 37–58.
- Li, N., Lam, W. H., Zhai, Y., Cheng, J., Cheng, E., Zhao, Y., Gao, N., Tye, B. K. (2018). Structure of the origin recognition complex bound to DNA replication origin. *Nature*, *559*(7713), 217–222.
- Li, S., Yang, Z., Du, X., Liu, R., Wilkinson, A. W., Gozani, O., Jacobsen, S.E., Patel, D.J., Du, J. (2016). Structural basis for the unique multivalent readout of unmodified H3 tail by Arabidopsis ORC1b BAH-PHD cassette. *Structure*, *24*(3), 486–494.
- Liang, C., & Stillman, B. (1997). Persistent initiation of DNA replication and chromatin-bound MCM proteins during the cell cycle in *cdc6* mutants. *Genes and Development*, *11*(24), 3375–3386.
- Lichten, M., & Goldman, A. S. H. (1995). Meiotic Recombination Hotspots. *Annu. Rev. Genet.*, *29*, 423–444.
- Lipford, J. R., & Bell, S. P. (2001). Nucleosomes positioned by ORC facilitate the initiation of DNA replication. *Molecular Cell*, *7*(1), 21–30.
- Loo, S., Fox, C. A., Rine, J., Kobayashi, R., Stillman, B., & Bell, S. (1995). The origin recognition complex in silencing, cell cycle progression, and DNA replication. *Molecular Biology of the Cell*, *6*(6), 741–756.
- Lucas, I. A., & Raghuraman, M. K. (2003). The Dynamics of Chromosome Replication in Yeast. *Current Topics in Developmental Biology*, *55*, 1–73.
- MacQueen, A. J., & Hochwagen, A. (2011). Checkpoint mechanisms: the puppet masters of meiotic prophase. *Trends in Cell Biology*, *21*(7), 393–400.
- Mao-Draayer, Y., Galbraith, A. M., Pittman, D. L., Cool, M., & Malone, R. E. (1996). Analysis of meiotic recombination pathways in the yeast *Saccharomyces cerevisiae*. *Genetics*, *144*(1), 71–86.

- Marahrens, Y., & Stillman, B. (1992). A yeast chromosomal origin of DNA replication defined by multiple functional elements. *Science*, *255*(5046), 817–823.
- Marston, A. L. (2014). Chromosome segregation in budding yeast: Sister chromatid cohesion and related mechanisms. *Genetics*, *196*(1), 31–63.
- Marston, A. L., & Amon, A. (2004). Meiosis: cell-cycle controls shuffle and deal. *Nature Reviews Molecular Cell Biology*, *5*(12), 983–997.
- Méchali, M., Yoshida, K., Coulombe, P., & Pasero, P. (2013). Genetic and epigenetic determinants of DNA replication origins, position and activation. *Current Opinion in Genetics and Development*, *23*(2), 124–131.
- Meyer, H. (2012). p97 complexes as signal integration hubs. *BMC Biology*, *10*(48).
- Meyer, H., & Weihl, C. C. (2014). The VCP/p97 system at a glance: connecting cellular function to disease pathogenesis. *Journal of Cell Science*, *127*, 3877–3883.
- Miao, C., Tang, D., Zhang, H., Wang, M., Li, Y., Tang, S., Yu, H, Gu, M., Cheng, Z. (2013). Central region component1, a novel synaptonemal complex component, is essential for meiotic recombination initiation in Rice. *The Plant Cell*, *25*(8), 2998–3009.
- Michaelis, C., Ciosk, R., & Nasmyth, K. (1997). Cohesins: Chromosomal proteins that prevent premature separation of sister chromatids. *Cell*, *91*(1), 35–45.
- Mieczkowski, P., Dominska, M., Buck, M. J., Lieb, J. D., & Petes, T. D. (2007). Loss of a histone deacetylase dramatically alters the genomic distribution of Spo11p-catalyzed DNA breaks in *Saccharomyces cerevisiae*. *Proceedings of the National Academy of Sciences of the United States of America*, *104*(10), 3955–3960.
- Miller, T. C. R., Locke, J., Greiwe, J. F., Diffley, J. F. X., & Costa, A. (2019). Mechanism of head-to-head MCM double-hexamers formation revealed by cryo-EM. *Nature*, *575*(7784), 704–710.
- Mitchell, A. P. (1994). Control of meiotic gene expression in *Saccharomyces cerevisiae*. *Microbiological Reviews*, *58*(1), 56–70.
- Mitchison, T. J., & Salmon, E. D. (1992). Poleward kinetochore fiber movement occurs during both metaphase and anaphase-A in newt lung cell mitosis. *Journal of Cell Biology*, *119*(3), 569–581.
- Müller, P., Park, S., Shor, E., Huebert, D. J., Warren, C. L., Ansari, A. Z., Weinreich, M., Eaton, M.L., MacAlpine, D.M., Fox, C. A. (2010). The conserved bromo-adjacent homology domain of yeast Orc1 functions in the selection of DNA replication origins within chromatin. *Genes and Development*, *24*(13), 1418–1433.
- Muniyappa, K., Kshirsagar, R., & Ghodke, I. (2014). The HORMA domain: an evolutionarily

- conserved domain discovered in chromatin-associated proteins, has unanticipated diverse functions. *Gene*, 545(2), 194–197.
- Murakami, H., Borde, V., Shibata, T., Lichten, M., & Ohta, K. (2003). Correlation between premeiotic DNA replication and chromatin transition at yeast recombination initiation sites. *Nucleic Acids Research*, 31(14), 4085–4090.
- Murakami, H., & Keeney, S. (2014). Temporospacial coordination of meiotic dna replication and recombination via DDK recruitment to replisomes. *Cell*, 158(4), 861–873.
- Murray, A. (1994). Cell cycle checkpoints. *Current Opinion in Cell Biology*, 6(6), 872–876.
- Musacchio, A., & Desai, A. (2017). A molecular view of kinetochore assembly and function. *Biology*, 6(1).
- Musacchio, A., & Salmon, E. D. (2007). The spindle-assembly checkpoint in space and time. *Nature Reviews Molecular Cell Biology*, 8(5), 379–393.
- Nasmyth, K. (2001). Disseminating the Genome: Joining, Resolving, and Separating Sister Chromatids During Mitosis and Meiosis. *Annual Review of Genetics*, 35, 673–745.
- Nasmyth, K., & Haering, C. H. (2009). Cohesin: Its Roles and Mechanisms. *Annu. Rev. Genet.*, 43, 525–558.
- Neiman, A. M. (2011). Sporulation in the budding yeast *Saccharomyces cerevisiae*. *Genetics*, 189, 737–765.
- Nelson, C. R., Hwang, T., Chen, P. H., & Bhalla, N. (2015). TRIP13PCH-2 promotes Mad2 localization to unattached kinetochores in the spindle checkpoint response. *Journal of Cell Biology*, 211(3), 503–516.
- Newlon, C. S. (1988). Yeast chromosome replication and segregation. *Microbiological Reviews*, 52(4), 568–601.
- Nguyen, H., Ortega, M. A., Ko, M., Marh, J., & Ward, W. S. (2015). ORC4 surrounds extruded chromatin in female meiosis. *J Cell Biochem.*, 116(5), 778–786.
- Nguyen, V. Q., Co, C., & Li, J. J. (2001). Cyclin-dependent kinases prevent DNA re-replication through multiple mechanisms. *Nature*, 411(6841), 1068–1073.
- Nicklas, R. B. (1988). The forces that move chromosomes in mitosis. *Annual Review of Biophysics and Biophysical Chemistry*, 17(14), 431–449.
- Niu, H., Wan, L., Busygina, V., Kwon, Y., Allen, J. A., Li, X., Kunz, R.C., Kubota, K., Wang, B., Sung, P., Shokat, K.M., Gygi, S.P., Hollingsworth, N. M. (2009). Regulation of meiotic recombination via Mek1-mediated Rad54 phosphorylation. *Molecular Cell*, 36(3), 393–404.
- Ogura, T., Whiteheart, S. W., & Wilkinson, A. J. (2004). Conserved arginine residues

- implicated in ATP hydrolysis, nucleotide-sensing, and inter-subunit interactions in AAA and AAA+ ATPases. *Journal of Structural Biology*, 146(1–2), 106–112.
- Ogura, T., & Wilkinson, A. J. (2001). AAA+ superfamily ATPases: common structure diverse function. *Genes Cells*, 6(7), 575–597.
- Oppikofer, M., Kueng, S., & Gasser, S. M. (2013). SIR-nucleosome interactions: Structure-function relationships in yeast silent chromatin. *Gene*, 527(1), 10–25.
- Oppikofer, M., Kueng, S., Martino, F., Soeroes, S., Hancock, S. M., Chin, J. W., Fischle, W., Gasser, S. M. (2011). A dual role of H4K16 acetylation in the establishment of yeast silent chromatin. *EMBO Journal*, 30(13), 2610–2621.
- Padmore, R., Cao, L., & Kleckner, N. (1991). Temporal comparison of recombination and synaptonemal complex formation during meiosis in *S. cerevisiae*. *Cell*, 66(6), 1239–1256.
- Page, S. L., & Hawley, R. S. (2004). The Genetics and Molecular Biology of the Synaptonemal Complex. *Annual Review of Cell and Developmental Biology*, 20(1), 525–558.
- Pan, D., Brockmeyer, A., Mueller, F., Musacchio, A., & Bange, T. (2018). Simplified Protocol for Cross-linking Mass Spectrometry Using the MS-Cleavable Cross-linker DSBU with Efficient Cross-link Identification. *Analytical Chemistry*, 90(18), 10990–10999.
- Pan, J., Sasaki, M., Kniewel, R., Murakami, H., Blitzblau, H. G., Tischfield, S. E., Zhu, X., Neale, M.J., Jasin, M., Socci, N.D., Hochwagen, A., Keeney, S. (2011). A hierarchical combination of factors shapes the genome-wide topography of yeast meiotic recombination initiation. *Cell*, 144(5), 719–731.
- Panizza, S., Mendoza, M. A., Berlinger, M., Huang, L., Nicolas, A., Shirahige, K., & Klein, F. (2011). Spo11-accessory proteins link double-strand break sites to the chromosome axis in early meiotic recombination. *Cell*, 146(3), 372–383.
- Patel, T. R., Winzor, D. J., & Scott, D. J. (2015). Analytical ultracentrifugation: A versatile tool for the characterisation of macromolecular complexes in solution. *Methods*, 95, 55–61.
- Petes, T. D. (1979). Yeast ribosomal DNA genes are located on chromosome XII. *Proceedings of the National Academy of Sciences of the United States of America*, 76(1), 410–414.
- Petes, T. D. (1980). Unequal meiotic recombination within tandem arrays of yeast ribosomal DNA genes. *Cell*, 19(3), 765–774.

- Petes, T. D. (2001). Meiotic Recombination hot spots and cold spots. *Nature Reviews Genetics*, 2(May), 360–369.
- Petes, T. D., & Botstein, D. (1977). Simple Mendelian inheritance of the reiterated ribosomal DNA of yeast. *Proceedings of the National Academy of Sciences of the United States of America*, 74(11), 5091–5095.
- Petronczki, M., Siomos, M. F., & Nasmyth, K. (2003). Un Menage a Quatre: The Molecular Biology of Chromosome Segregation in Meiosis. *Cell*, 112(4), 423–440.
- Phizicky, D., Berchowitz, L., & Bell, S. P. (2018). Multiple kinases inhibit origin licensing and helicase activation to ensure reductive cell division during meiosis. *eLife*, 7, e33309.
- Plotkin, J. B., & Kudla, G. (2011). Synonymous but not the same: the causes and consequences of codon bias. *Nature Reviews Genetics*, 12(1), 32–42.
- Popova, V. V., Brechalov, A. V., Georgieva, S. G., & Kopytova, D. V. (2018). Nonreplicative Functions of the Origin Recognition Complex. *Nucleus*, 9(1): 460-473.
- Remus, D., Beuron, F., Tolun, G., Griffith, J. D., Morris, E. P., & Diffley, J. F. X. (2009). Concerted Loading of Mcm2-7 Double Hexamers around DNA during DNA Replication Origin Licensing. *Cell*, 139(4), 719–730.
- Remus, D., & Diffley, J. F. X. (2009). Eukaryotic DNA replication control: Lock and load, then fire. *Current Opinion in Cell Biology*, 21(6), 771–777.
- Riedel, C. G., Katis, V. L., Katou, Y., Mori, S., Itoh, T., Helmhart, W., Galova, M., Petronczki, M., Gregan, J., Cetin, B., Mudrak, I., Ogris, E., Mechtler, K., Pelletier, L., Buchholz, F., Shirahige, K., Nasmyth, K. (2006). Protein phosphatase 2A protects centromeric sister chromatid cohesion during meiosis I. *Nature*, 441(7089), 53–61.
- Rieder, C. L., & Salmon, E. D. (1994). Motile kinetochores and polar ejection forces dictate chromosome position on the vertebrate mitotic spindle. *The Journal of Cell Biology*, 124(3), 223–233.
- Robinson, N. P., Dionne, I., Lundgren, M., Marsh, V. L., Bernander, R., & Bell, S. D. (2004). Identification of Two Origins of Replication in the Single Chromosome of the Archaeon *Sulfolobus solfataricus*. *Cell*, 116(1), 25–38.
- Roeder, G. S., & Bailis, J. M. (2000). The pachytene checkpoint. *Trends in Genetics*, 16(9), 395–403.
- Roig, I., Dowdle, J. A., Toth, A., de Rooij, D. G., Jasin, M., & Keeney, S. (2010). Mouse TRIP13/PCH2 is required for recombination and normal higher-order chromosome structure during meiosis. *PLoS Genetics*, 6(8).
- Rosenberg, S. C., & Corbett, K. D. (2015). The multifaceted roles of the HOR MA domain in

- cellular signaling. *Journal of Cell Biology*, 211(4), 745–755.
- Rusche, L. N., Kirchmaier, A. L., & Rine, J. (2003). The Establishment, Inheritance, and Function of Silenced Chromatin in *Saccharomyces cerevisiae*. *Annual Review of Biochemistry*, 72, 481–516.
- Salim, D., Bradford, W. D., Freeland, A., Cady, G., Wang, J., Pruitt, S. C., & Gerton, J. L. (2017). DNA replication stress restricts ribosomal DNA copy number. *PLoS Genetics*, 13(9), e1007006.
- San-Segundo, P. A., & Roeder, G. S. (1999). Pch2 links chromatin silencing to meiotic checkpoint control. *Cell*, 97(3), 313–324.
- Sasaki, M., Lange, J., & Keeney, S. (2010). Genome destabilization by homologous recombination in the germ line. *Nature Reviews Molecular Cell Biology*, 11(3), 182–195.
- Sasanuma, H., Hirota, K., Fukuda, T., Kakusho, N., Kugou, K., Kawasaki, Y., Shibata, T., Masai, H., Ohta, K. (2008). Cdc7-dependent phosphorylation of Mer2 facilitates initiation of yeast meiotic recombination. *Genes and Development*, 22(3), 398–410.
- Schuck, P. (2000). Size-distribution analysis of macromolecules by sedimentation velocity ultracentrifugation and Lamm equation modeling. *Biophysical Journal*, 78(3), 1606–1619.
- Schwacha, A., & Kleckner, N. (1995). Identification of double holliday junctions as intermediates in meiotic recombination. *Cell*, 83(5), 783–791.
- Schwacha, A., & Kleckner, N. (1997). Interhomolog bias during meiotic recombination: Meiotic functions promote a highly differentiated interhomolog-only pathway. *Cell*, 90(6), 1123–1135.
- Schwob, E., Böhm, T., Mendenhall, M. D., & Nasmyth, K. (1994). The B-type cyclin kinase inhibitor p40SIC1 controls the G1 to S transition in *S. cerevisiae*. *Cell*, 79(2), 233–244.
- Sclafani, R. A., & Holzen, T. M. (2007). Cell Cycle Regulation of DNA Replication. *Annu Rev Genet.*, 41, 237–280.
- Serrentino, M. E., & Borde, V. (2012). The spatial regulation of meiotic recombination hotspots: Are all DSB hotspots crossover hotspots? *Experimental Cell Research*, 318(12), 1347–1352.
- Shibata, E., Kiran, M., Shibata, Y., Singh, S., Kiran, S., & Dutta, A. (2016). Two subunits of human ORC are dispensable for DNA replication and proliferation. *eLife*, 5(December 2016), 1–14.
- Shimada, K., & Gasser, S. M. (2007). The Origin Recognition Complex Functions in Sister-Chromatid Cohesion in *Saccharomyces cerevisiae*. *Cell*, 128(1), 85–99.

- Shimada, K., Pasero, P., & Gasser, S. M. (2002). ORC and the intra-S-phase checkpoint: A threshold regulates Rad53p activation in S phase. *Genes and Development*, *16*(24), 3236–3252.
- Shinohara, A., Ogawa, H., & Ogawa, T. (1992). Rad51 protein involved in repair and recombination in *S. cerevisiae* is a RecA-like protein. *Cell*, *69*(3), 457–470.
- Shinohara, M., Hayashihara, K., Grubb, J. T., Bishop, D. K., & Shinohara, A. (2015). DNA damage response clamp 9-1-1 promotes assembly of ZMM proteins for formation of crossovers and synaptonemal complex. *Journal of Cell Science*, *128*(8), 1494–1506.
- Shor, E., Warren, C. L., Tietjen, J., Hou, Z., Müller, U., Alborelli, I., Gohard, F.H., Yemm, A.I., Borisov, L., Broach, J.R., Weinreich, M., Nieduszynski, C.A., Ansari, A.Z., Fox, C. A. (2009). The origin recognition complex interacts with a subset of metabolic genes tightly linked to origins of replication. *PLoS Genetics*, *5*(12).
- Shou, W., Seol, J. H., Shevchenko, A., Baskerville, C., Moazed, D., Susan Chen, Z. W., Jang, J., Shevchenko, A., Charbonneau, H., Deshaies, R. J. (1999). Exit from mitosis is triggered by Tem1-dependent release of the protein phosphatase Cdc14 from nucleolar RENT complex. *Cell*, *97*(2), 233–244.
- Simchen, G. (1974). Are mitotic functions required in meiosis? *Genetics*, *76*(4), 745–753.
- Sinclair, D. A., & Guarente, L. (1997). Extrachromosomal rDNA circles - A cause of aging in yeast. *Cell*, *91*(7), 1033–1042.
- Siow, C. C., Nieduszynska, S. R., Müller, C. A., & Nieduszynski, C. A. (2012). OriDB, the DNA replication origin database updated and extended. *Nucleic Acids Research*, *40*(D1), 682–686.
- Smith, H. E., & Mitchell, A. P. (1989). A transcriptional cascade governs entry into meiosis in *Saccharomyces cerevisiae*. *Molecular and Cellular Biology*, *9*(5), 2142–2152.
- Smith, H. E., Su, S. Y. S., Neigeborn, L., Driscoll, S. E., & Mitchell, A. P. (1990). Role of IME1 expression in regulation of meiosis in *Saccharomyces cerevisiae*. *Molecular and Cellular Biology*, *10*(12), 6103–6113.
- Smith, J. S., & Boeke, J. D. (1997). An unusual form of transcriptional silencing in yeast ribosomal DNA. *Genes and Development*, *11*(2), 241–254.
- Sommermeier, V., Béneut, C., Chaplais, E., Serrentino, M., & Borde, V. (2013). Spp1, a Member of the Set1 Complex, Promotes Meiotic DSB Formation in Promoters by Tethering Histone H3K4 Methylation Sites to Chromosome Axes. *Molecular Cell*, *49*(1), 43–54.
- Speck, C., Chen, Z., Li, H., & Stillman, B. (2005). ATPase-dependent, cooperative binding of

- ORC and Cdc6p to origin DNA. *Nat Struct Mol Biol.*, 12(11), 965–971.
- Srivastava, R., Srivastava, R., & Ahn, S. H. (2016). The Epigenetic Pathways to Ribosomal DNA Silencing. *Microbiology and Molecular Biology Reviews*, 80(3), 545–563.
- Stinchcomb, D. T., Struhl, K., & Davis, R. W. (1979). Isolation and characterisation of a yeast chromosomal replicator. *Nature*, 282, 39–43.
- Storlazzi, A., Tessé, S., Gargano, S., James, F., Kleckner, N., & Zickler, D. (2003). Meiotic double-strand breaks at the interface of chromosome movement, chromosome remodeling, and reductional division. *Genes and Development*, 17(21), 2675–2687.
- Storlazzi, A., Xu, L., Cao, L., & Kleckner, N. (1995). Crossover and noncrossover recombination during meiosis: Timing and pathway relationships. *Proceedings of the National Academy of Sciences of the United States of America*, 92(18), 8512–8516.
- Straight, A. F., Shou, W., Dowd, G. J., Turck, C. W., Deshaies, R. J., Johnson, A. D., & Moazed, D. (1999). Net1, a Sir2-associated nucleolar protein required for rDNA silencing and nucleolar integrity. *Cell*, 97(2), 245–256.
- Stuart, D., & Wittenberg, C. (1998). CLB5 and CLB6 are required for premeiotic DNA replication and activation of the meiotic S/M checkpoint. *Genes and Development*, 12(17), 2698–2710.
- Subramanian, V. V., MacQueen, A. J., Vader, G., Shinohara, M., Sanchez, A., Borde, V., Shinohara, A., Hochwagen, A. (2016). Chromosome Synapsis Alleviates Mek1-Dependent Suppression of Meiotic DNA Repair. *PLoS Biology*, 14(2), e1002369.
- Subramanian, V. V., & Hochwagen, A. (2014). The meiotic checkpoint network: Step-by-step through meiotic prophase. *Cold Spring Harbor Perspectives in Biology*, 6(10).
- Sun, J., Evrin, C., Samel, S., Fernandez-Cid, A., Riera, A., Kawakami, H., Stillman, B., Speck, C., Li, H. (2014). Cryo-EM structure of a helicase loading intermediate containing ORC-Cdc6-Cdt1-MCM2-7 bound to DNA. *Nat Struct Mol Biol.*, 20(8), 944–951.
- Sun, J., Kawakami, H., Zech, J., Speck, C., Stillman, B., & Li, H. (2012). Cdc6-induced Conformational Changes in ORC Bound To Origin DNA Revealed by Cryo-Electron Microscopy. *Structure*, 20(3), 534–544.
- Sun, J. Q., Hatanaka, A., & Oki, M. (2011). Boundaries of transcriptionally silent chromatin in *Saccharomyces cerevisiae*. *Genes and Genetic Systems*, 86(2), 73–81.
- Sun, S. C., & Kim, N. H. (2012). Spindle assembly checkpoint and its regulators in meiosis. *Human Reproduction Update*, 18(1), 60–72.
- Suter, B., Tong, A., Chang, M., Yu, L., Brown, G. W., Boone, C., & Rine, J. (2004). The

- Origin Recognition Complex links replication, sister chromatid cohesion and transcriptional silencing in *Saccharomyces cerevisiae*. *Genetics*, *167*(2), 579–591.
- Sym, M., Sym, M., Engebrecht, J. a, Engebrecht, J., Roeder, G. S., Roeder, G. S., & Haven, N. (1993). ZIP1 Is a synaptonemal complex protein required for meiotic chromosome synapsis. *Cell*, *72*(3), 365–378.
- Thacker, D., & Keeney, S. (2009). PCH'ing together an understanding of crossover control. *PLoS Genetics*, *5*(7), 2–3.
- Thurtle-Schmidt, D. M., Dodson, A. E., & Rine, J. (2016). Histone deacetylases with antagonistic roles in *Saccharomyces cerevisiae* heterochromatin formation. *Genetics*, *204*(1), 177–190.
- Ticau, S., Friedman, L. J., Champasa, K., Correa Jr, I. R., Gelles, J., & Bell, S. . (2017). Mechanism and Timing of Mcm2-7 Ring Closure During DNA Replication Origin Licensing. *Nature Structural and Molecular Biology*, *24*(3), 309–315.
- Ticau, S., Friedman, L. J., Ivica, N. A., Gelles, J., & Bell, S. P. (2015). Single-molecule studies of origin licensing reveal mechanisms ensuring bidirectional helicase loading. *Cell*, *161*(3), 513–525.
- Tipton, A. R., Wang, K., Oladimeji, P., Sufi, S., Gu, Z., & Liu, S. (2012). Identification of novel mitosis regulators through data mining with human centromere/kinetochore proteins as group queries. *BMC Cell Biology*, *13*(15).
- Tischfield, S. E., & Keeney, S. (2012). Scale matters. The spatial correlation of yeast meiotic DNA breaks with histone H3 trimethylation is driven largely by independent colocalization at promoters. *Cell Cycle*, *11*(8), 1496–1503.
- Tocilj, A., On, K. F., Yuan, Z., Sun, J., Elkayam, E., Li, H., Stillman, B., Joshua-Tor, L. (2017). Structure of the active form of human origin recognition complex and its ATPase motor module. *eLife*, *6*, e20818.
- Tóth, A., Rabitsch, K. P., Gálová, M., Schleiffer, A., Buonomo, S. B. C., & Nasmyth, K. (2000). Functional genomics identifies Monopolin: A kinetochore protein required for segregation of homologs during meiosis I. *Cell*, *103*(7), 1155–1168.
- Tran, B. Q., Goodlett, D. R., & Goo, Y. A. (2016). Advances in protein complex analysis by chemical cross-linking coupled with mass spectrometry (CXMS) and bioinformatics. *Biochimica et Biophysica Acta*, *1864*(1), 123–129.
- Triolo, T., & Sternglanz, R. (1996). Role of interactions between the origin recognition complex and SIR1 in transcriptional silencing. *Nature*, *381*(6579), 251–253.
- Tsakraklides, V., & Bell, S. P. (2010). Dynamics of pre-replicative complex assembly.

- Journal of Biological Chemistry*, 285(13), 9437–9443.
- Tucker, P. A., & Sallai, L. (2007). The AAA+ superfamily - a myriad of motions. *Current Opinion in Structural Biology*, 17(6), 641–652.
- Uhlmann, F., & Nasmyth, K. (1998). Cohesion between sister chromatids must be established during DNA replication. *Current Biology*, 8(20), 1095–1101.
- Vader, G. (2015). Pch2 TRIP13: controlling cell division through regulation of HORMA domains. *Chromosoma*, 124(3):333-9.
- Vader, G., Blitzblau, H. G., Tame, M. A., Falk, J. E., Curtin, L., & Hochwagen, A. (2011). Protection of repetitive DNA borders from self-induced meiotic instability. *Nature*, 477(7362), 115–121.
- Van Leeuwen, F., Gafken, P. R., & Gottschling, D. E. (2002). Dot1p modulates silencing in yeast by methylation of the nucleosome core. *Cell*, 109(6), 745–756.
- van Werven, F. J., & Amon, A. (2011). Regulation of entry into gametogenesis. *Philosophical Transactions of the Royal Society B: Biological Sciences*, 366(1584), 3521–3531.
- Vincenten, N., Kuhl, L. M., Lam, I., Oke, A., Kerr, A. R. W., Hochwagen, A., Fung, J., Keeney, S., Vader, G., Marston, A. L. (2015). The kinetochore prevents centromere-proximal crossover recombination during meiosis. *eLife*, 4, e10850.
- Vogelauer, M., Rubbi, L., Lucas, I., Brewer, B. J., & Grunstein, M. (2002). Histone acetylation regulates the time of replication origin firing. *Molecular Cell*, 10(5), 1223–1233.
- Walker, E., Saraste, M., Runswick, M. J., & Gay, N. J. (1982). Distantly related sequences in the a- and B-subunits of ATP synthase, myosin, kinases and other ATP-requiring enzymes and a common nucleotide binding fold. *The EMBO Journal*, 1(8), 945–951.
- Wan, L., Niu, H., Fitcher, B., Zhang, C., Shokat, K. M., Boulton, S. J., & Hollingsworth, N. M. (2008). Cdc28-C1b5 (CDK-S) and Cdc7-Dbf4 (DDK) collaborate to initiate meiotic recombination in yeast. *Genes & Development*, 22: 386–397.
- Wang, X., Connelly, J. J., Wang, C. L., & Sternglanz, R. (2004). Importance of the Sir3 N terminus and its acetylation for yeast transcriptional silencing. *Genetics*, 168(1), 547–551.
- Wang, Y., Mao, Y., Xu, X., Tao, S., & Chen, H. (2015). Codon Usage in Signal Sequences Affects Protein Expression and Secretion Using Baculovirus/Insect Cell Expression System. *PLoS ONE*, 10(12), e0145887.
- Watanabe, Y. (2012). Geometry and force behind kinetochore orientation: lessons from meiosis. *Nature Reviews Molecular Cell Biology*, 13(6), 370–382.

- Weibezahn, J., Schlieker, C., Bukau, B., & Mogk, A. (2003). Characterization of a trap mutant of the AAA+ chaperone ClpB. *The Journal of Biological Chemistry*, 278(35), 32608–32617.
- Weinert, T. (1998). DNA damage checkpoints update: getting molecular. *Current Opinion in Genetics & Development*, 8(2), 185–193.
- Weissmann, F., Petzold, G., VanderLinden, R., Huis in't Veld, P. J., Brown, N. G., Lampert, F., Westermann, S., Stark, H., Schulman, B.A., Peters, J.-M. (2016). biGBac enables rapid gene assembly for the expression of large multisubunit protein complexes. *Proceedings of the National Academy of Sciences*, 113(19), E2564–E2569.
- Wendler, P., Ciniawsky, S., Kock, M., & Kube, S. (2012). Structure and function of the AAA+ nucleotide binding pocket. *Biochimica et Biophysica Acta*, 1823(1), 2–14.
- West, A. M. V., Komives, E. A., & Corbett, K. D. (2018). Conformational dynamics of the Hop1 HORMA domain reveal a common mechanism with the spindle checkpoint protein Mad2. *Nucleic Acids Research*, 46(1), 279–292.
- Whiteheart, S. W., Rossnagel, K., Buhrow, S. A., Brunner, M., Jaenicke, R., & Rothman, J. E. (1994). N-ethylmaleimide-sensitive fusion protein: A trimeric ATPase whose hydrolysis of ATP is required for membrane fusion. *Journal of Cell Biology*, 126(4), 945–954.
- Williamson, D. H., Johnston, L. H., Fennell, D. J., & Simchen, G. (1983). The timing of the S phase and other nuclear events in yeast meiosis. *Experimental Cell Research*, 145(1), 209–217.
- Wojtasz, L., Daniel, K., Roig, I., Bolcun-Filas, E., Xu, H., Boonsanay, V., Eckmann, C.R., Cooke, H.J., Jasin, M., Keeney, S., McKay, M.J., Toth, A. (2009). Mouse HORMAD1 and HORMAD2, two conserved meiotic chromosomal proteins, are depleted from synapsed chromosome axes with the help of TRIP13 AAA-ATPase. *PLoS Genetics*, 5(10).
- Wood, K., Tellier, M., & Murphy, S. (2018). DOT1L and H3K79 methylation in transcription and genomic stability. *Biomolecules*, 8(1), 1–16.
- Wu, H. Y., & Burgess, S. M. (2006). Two Distinct Surveillance Mechanisms Monitor Meiotic Chromosome Metabolism in Budding Yeast. *Current Biology*, 16(24), 2473–2479.
- Yang, D., Fang, Q., Wang, M., Ren, R., Wang, H., He, M., Sun, Y., Yang, N., Xu, R.-M. (2013). Na⁺-acetylated Sir3 stabilizes the conformation of a nucleosome-binding loop in the BAH domain. *Nature Structural and Molecular Biology*, 20(9), 1116–1119.
- Yang, N., & Xu, R.-M. (2013). Structure and function of the BAH domain in chromatin biology. *Critical Reviews in Biochemistry and Molecular Biology*, 48(3), 211–221.

- Yao, N. Y., & Donnell, M. O. (2012). The RFC clamp loader: structure and function. *Subcell Biochem*, 62, 259–279.
- Ye, Q., Kim, D. H., Dereli, I., Rosenberg, S. C., Hagemann, G., Herzog, F., Toth, A., Cleveland, D.W., Corbett, K. D. (2017a). The AAA+ ATPase TRIP13 remodels HORMA domains through N-terminal engagement and unfolding. *The EMBO Journal*, 36(16), 2419–2434.
- Ye, Q., Rosenberg, S. C., Moeller, A., Speir, J. A., Su, T. Y., & Corbett, K. D. (2015). TRIP13 is a protein-remodeling AAA+ ATPase that catalyzes MAD2 conformation switching. *eLife*, 2015(4), 1–44.
- Ye, Y., Meyer, H. H., & Rapoport, T. A. (2003). Function of the p97-Ufd1-Npl4 complex in retrotranslocation from the ER to the cytosol: dual recognition of nonubiquitinated polypeptide segments and polyubiquitin chains. *The Journal of Cell Biology*, 162(1), 71–84.
- Yeeles, J. T. P., Deegan, T. D., Janska, A., Early, A., & Diffley, J. F. X. (2015). Regulated eukaryotic DNA replication origin firing with purified proteins. *Nature*, 519(7544), 431–435.
- Yoshida, K., Bacal, J., Desmarais, D., Padioleau, I., Tsaponina, O., Chabes, A., Pantesco, V., Dubois, E., Parrinello, H., Skrzypczak, M., Ginalski, K., Lengronne, A., Pasero, P. (2014). The Histone Deacetylases Sir2 and Rpd3 Act on Ribosomal DNA to Control the Replication Program in Budding Yeast. *Molecular Cell*, 54(4), 691–697.
- Yoshida, K., Poveda, A., & Pasero, P. (2013). Time to be Versatile: Regulation of the Replication Timing Program in Budding Yeast. *Journal of Molecular Biology*, 425, 4696–4705.
- Yuan, Z., Riera, A., Bai, L., Sun, J., Nandi, S., Spanos, C., Chen, Z.A., Barbon, M., Rappsilber, J., Stillman, B., Speck, C., Li, H. (2017). Structural basis of Mcm2-7 replicative helicase loading by ORC-Cdc6 and Cdt1. *Nature Structural and Molecular Biology*, 24(3), 316–324.
- Zanders, S., & Alani, E. (2009). The pch2 Δ mutation in baker's yeast alters meiotic crossover levels and confers a defect in crossover interference. *PLoS Genetics*, 5(7).
- Zanders, S., Brown, M. S., Chen, C., & Alani, E. (2011). Pch2 modulates chromatid partner choice during meiotic double-strand break repair in *Saccharomyces cerevisiae*. *Genetics*, 188(3), 511–521.
- Zhao, H., Brautigam, C. A., Ghirlando, R., & Schuck, P. (2013). Overview of current methods in sedimentation velocity and sedimentation equilibrium analytical

ultracentrifugation. *Current Protocols in Protein Science*. Chapter 20: Unit 20.12.

Zhao, M., Wu, S., Zhou, Q., Vivona, S., Cipriano, D. J., Cheng, Y., & Brunger, A. T. (2015). Mechanistic insights into the recycling machine of the SNARE complex. *Nature*, *518*(7537), 61–67.

Zickler, D., & Kleckner, N. (1999). Meiotic Chromosomes: Integrating Structure and Function. *Annu. Rev. Genet.*, *33*(1), 603–754.

Acknowledgements

First and foremost, I would like to express my gratitude to my supervisor, Dr. Gerben Vader, for giving me the opportunity to do my Ph.D. in his lab. I really appreciate his continuous guidance and the scientific discussions. He passionately introduced me to the budding yeast genetics and shared his scientific knowledge and enthusiasm with me. I would also like to thank him for helping me in improving my presentation and writing skills over the course of my Ph.D. I would also like to thank the members of my thesis advisory committee, Prof. Dr. Hemmo Meyer and Prof. Dr. Dominik Boos, for the valuable suggestions and inputs throughout the progress of my Ph.D. project. I would like to express my sincere gratitude to Prof. Dr. Andrea Musacchio for being my official Ph.D. supervisor and for providing reagents throughout my Ph.D.

This Ph.D. would not have been possible without the help of present and former members of Department I. Particularly, I owe a very important debt to Dongqing Pan for his help with XL-MS. Moreover, he was always interested on my project and provided me with helpful inputs (and purified protein). Special thanks goes to Andreas Brockmeyer, Tanja Bange and Franziska Müller for their help with the MS/MS analysis. I am also thankful to John Weir, Satyakrishna Pentakota, Alex Faesen, Giuseppe Ciossani, and Valentina Piano for sharing their knowledge about biochemistry, guiding me and helping me troubleshooting whenever I needed it. I also want to thank Arsen Petrovic for performing the AUC analysis and for helping me out with protein purification as well. This work has also benefited from reagents and protocols provided by Prof. Dr. Stephen Bell (MIT Department of Biology) and Dr. John Diffley (Francis Crick Institute), and I am also grateful for that.

All these years in the lab would have been much harder if it was not for the help of Christa Hornemann, Antje Peukert and Lucia Sironi, who are always ready to solve any administrative difficulties. I am particularly grateful to Christa Hornemann for helping me, supporting me and caring for me like a mother would do. Life at the Max Planck Institute has surely been easier thanks to her. I would also like to express my gratitude to the IMPRS-CMB for organizing retreats and symposiums, and providing funding for attending conferences.

My Ph.D. would have been much less enjoyable without the members of the Department I. Special thanks goes to all the former and current members of the Bird and Vader groups. I consider myself lucky to have had such a great company during these years,

not only because of the scientific discussions and inputs in the group meetings, but also for being fantastic lab mates and for the great atmosphere in the lab. I also want to thank Elisabeth Weir and Annika Sarembe for helping me in the lab during a part of my Ph.D. Elisabeth Weir was always a big support outside the lab too, and I have deffinetly missed her the last years. I am deeply grateful to Richard Cardoso da Silva for being a great scientist from whom to learn, and for taking his time to introduce me to many techniques in the lab. He truly helped me with my project. I also thank him for taking the time to proofread my thesis and mostly, for being a good friend outside the lab too. I would also like to thank Lisa Kuhl for being there for me since the beginning of my Ph.D. and for introducing me to the radioactive lab. It was not so much “fun,, to go there without her. I also have to thank her for being so supportive and helping me translating the Summary of this thesis to German. I also would like to thank Vivek B. Raina for his help in the lab and for always trying to make me see the bright side. Shweta Bendre and Divya Singh have also been dearest friends along this way. I want to thank Divya Singh for her warm encouragement, for listening to me and for the free hugs.

I would like to thank all my friends in Spain and in Germany, for encouraging me, for always making me laugh and for cheering me up. I would always be indebted to my family, who supports me whenever I need and whatever I do. I would not have reached where I am now without them. The lab (and the distance) have often kept me apart from them; I have the wish that this will now change. Particularly, I have to thank my parents and siblings for their constant support and their encouragement, even from the distance. My parents have inculcated in me the values that made me being who I am today, and I would never be able to pay this back to them. I thank my mother, for teaching me to be strong, perseverant and to keep faith, and my father for being so caring and for always being there whenever I need someone to listen. Their love and confidence in me have carried me through difficult times. I am also deeply grateful to Flo’s family, who have also become my family here in Germany, with all the implications that this has. They are always interested on how I am doing and they take great care of me, making me feel like at home.

Last but not the least, I would like to thank Flo for patiently taking me by the hand all these years. He has been my support system and a source of strength during good, but also during hard times. He is always there for me and does his best to comfort me. Once again, without him I would not have made it so far.

Curriculum Vitae

The curriculum vitae is not included in the online version for data protection reasons.

Affidavit

Hiermit erkläre ich, *María Ascensión Villar Fernández*, gem. § 7 Abs. (2) d) + f) der Promotionsordnung der Fakultät für Biologie zur Erlangung des Dr. rer. nat., dass ich die vorliegende Dissertation selbstständig verfasst und mich keiner anderen als der angegebenen Hilfsmittel bedient, bei der Abfassung der Dissertation nur die angegebenen Hilfsmittel benutzt und alle wörtlich oder inhaltlich übernommen Stellen als solche gekennzeichnet habe.

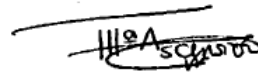
Dortmund, 25.11.19



María-Ascension Villar-Fernandez

Hiermit erkläre ich, *María Ascensión Villar Fernández*, gem. § 7 Abs. (2) e) + g) der Promotionsordnung der Fakultät für Biologie zur Erlangung des Dr. rer. nat., dass ich keine anderen Promotionen bzw. Promotionsversuche in der Vergangenheit durchgeführt habe und dass diese Arbeit von keiner anderen Fakultät/ Fachbereich abgelehnt worden ist.

Dortmund, 25.11.19



María-Ascension Villar-Fernandez

Max-Planck-Institut für molekulare Physiologie

Prof. Dr. Andrea Musacchio



MPI of Molecular Physiology Otto-Hahn-Str. 11 44227 Dortmund

Universität Duisburg-Essen
Fakultät für Biologie
Prof. Dr. Stefan Westermann
Promotionsausschuss
Schützenbahn 70

45127 Essen

Dortmund, 25.11.2019

Erklärung:

Hiermit erkläre ich, gem. § 6 Abs. (2) g) der Promotionsordnung der Fakultät für Biologie zur Erlangung der Dr. rer. nat., dass ich das Arbeitsgebiet, dem das Thema "Biochemical and functional characterization of the Pch2/ORC AAA⁺ assembly in controlling meiotic DNA break formation" zuzuordnen ist, in Forschung und Lehre vertrete und den Antrag von Frau Maria-Ascension Villar-Fernandez befürworte und die Betreuung auch im Falle eines Weggangs, wenn nicht wichtige Gründe dem entgegenstehen, weiterführen werde.

Prof. Dr. Andrea Musacchio

Postfach 50 02 47
44202 Dortmund
dortmund.mpg.de

Otto-Hahn-Str. 11
44227 Dortmund

Telefon *49(0)231/133-2100
Telefax *49(0)231/133-2199
e-mail: andrea.musacchio@mpi-

